JAERI-M
6710

# REACTOR ENGINEERING DIVISION

## ANNUAL REPORT

(April 1, 1975 - March 31, 1976)

September 1976

Division of Reactor Engineering

日本原子力研究所
Japan Atomic Energy Research Institute

JAERI-M 6710

# Reactor Engineering Division Annual Report (April 1, 1975 - March 31, 1976)

Division of Reactor Engineering, Tokai, JAERI

(Received August 19, 1976)

Research activities conducted in Reactor Engineering Division in fiscal 1975 are summarized in this report.

Works in the division are closely related to the development of multi-purpose High-temperature Gas Cooled Reactor, the development of Liquid Metal Fast Breeder Reactor by Power Reactor and Nuclear Fuel Development Corporation, and engineering research of thermonuclear fusion reactor. Many achievements are described concerning nuclear data and group constants, theoretical method and code development, integral experiment and analysis, shielding, heat transfer and fluid dynamics, reactor and nuclear instrumentation, dynamics analysis and control method development, fusion reactor technology and activities of the Committee on Reactor Physics.

---

JAERI－M 6710

# 昭和50年度原子炉工学部年報

日本原子力研究所東海研究所原子炉工学部

（1976年8月19日受理）

本報告書は，原子炉工学部において昭和50年度に行われた研究活動をとりまとめたものである。

原子炉工学部の研究計画は，多目的高温ガス炉の開発，動燃事業団による液体金属高速増殖炉の開発，および核融合炉のための炉工学的研究に密接に関連している。核データと群定数，炉理論とコード開発，積分実験と解析，遮蔽，熱伝達と流動，炉計装と核計装，動特性解析と制御法の開発，核融合炉技術，および炉物理研究委員会の活動の各分野にわたって，多くの成果が述べられている。

# Foreword

This is the annual report of Reactor Engineering Division, Japan Atomic Energy Research Institute, and covers the one year period, April 1975-March 1976. The research activities of the Division extend the broad area of reactor engineering. The major fields are thermal and fast reactor physics, shielding, reactor instrumentation and controls, heat transfer and fluid dynamics, and numerical analysis.

The total number of people working in the Division at the end of the period was 92. Expenditures during the period under review in this report totalled about 0.375 billion yen. In addition to this, a considerable amount of expenditures was covered under research contracts with outside organizations, among which Power Reactor and Nuclear Fuel Development Corporation offered the largest contribution.

The research activities were conducted in eight Laboratories and the Committee on Reactor Physics.

The Laboratories are

Reactor Physics Analytical Laboratory
Fast Reactor Physics Laboratory
Thermal Reactor Physics Laboratory
Reactor Instrumentation Laboratory
Reactor Control Laboratory
Heat Transfer Laboratory
Shielding Laboratory
Numerical Analysis Laboratory.

The major research and development projects, with which some research programmes in the Division are closely associated, are

(1) Development of High Temperature Gas Cooled Reactor (HTGR) for Multi-purpose Use
(2) Development of Liquid Metal Fast Breeder Reactor as a national project conducted by Power Reactor and Nuclear Fuel Development Corporation.
(3) Engineering Research Programme for Thermonuclear Fusion Reactor.

For development of HTGR, a small scale helium-gas loop

and a large scale helium-gas loop have been operated. In the small loop, a study has been made on heat transfer characteristics of turbulence promoters. The large loop has been operated up to 2400 hrs and construction of the secondary hydrogen-gas loop has been started. Measurement of multiple control rod reactivity worth in SHE, development of high-temperature-resistant neutron detector and hybrid simulation of HTGR dynamics have been conducted.

In the field of LMFBR, a critical experiment on the sector-type mockup system for the Prototype Fast Breeder Reactor MONJU has been started following the completion of the enlargement work of FCA. A study of the anisotropic diffusion effect on criticality of plate lattice assemblies and reactivity measurements on far-subcritical systems have been carried out. As for the theoretical work, revision of JAERI-fast set version II, analyses of sodium void worth and Doppler effect, and development of JNDC FP Fast Reactor System Constants have been conducted.

Concerning the fusion reactor technology, an analysis has been progressed on fission rate distributions in lithium and hybrid fusion blanket assemblies. A study on heat transfer of liquid metal in magnetic field, Si(Li) X-ray spectrometry in JFT-2 plasma and analysis of neutral particle transport in torus plasma by Monte Carlo method have been carried out.

As to researches other than those closely related to the projects mentioned above, a series of mockup experiments and analyses for the primary shield repairment of the Nuclear Ship MUTSU have been started using JRR-4 in co-operation with Japan Nuclear Ship Development Agency and Ship Research Institute of Ministry of Transport. In addition, many achievements are reported on the following items; in-situ measurement of environmental gamma-rays by Ge(Li) spectrometer, development of fast response nuclear instrumentation systems for the pulse reactor NSRR, non-destructive measurement of nuclear material, identification of system dynamics of JPDR-II, development of a computer code system for detailed shield calculation, applications of thermoluminescence dosimeter to nuclear heating measurement and the finite element method to the three-

dimensional diffusion equations, and self-similarity analysis of spherical implosion process.

J. Hirota
Division of Reactor
Engineering

# CONTENTS

# 1. Nuclear Data and Group Constants

## 1.1 Evaluation of Neutron Cross Sections of $^{241}Pu$

Y. Kikuchi

Neutron cross sections have been evaluated for $^{241}Pu$ as an activity of Japanese Nuclear Data Committee (JNDC). The evaluated data are stored in the Japanese Evaluated Nuclear Data Library Version - 1 (JENDL-1). The evaluated quantities are the total, elastic and inelastic scattering, fission, capture, (n,2n) and (n,3n) cross sections from the thermal neutron energy up to 15 MeV.

As for the 2200 m/s neutron cross sections, the evaluation by Lemmel[1] was adopted. The cross sections below 1 eV were evaluated by means of available experimental data and resonance calculations.

The cross sections are represented with the resonance parameters between 1 eV and 21.5 keV. The resolved resonance parameters were given up to 100 eV, and were mainly taken from BNL-325, 3rd edition. The cross sections calculated with these parameters agree satisfactorily with the experimental data. The unresolved resonance parameters were given above 100 eV. The parameters were determined so as to represent the available experimental data of the fission and capture cross sections.

Above the resonance region, there are considerable number of experimental data for the fission cross section but exists only one measurement of $\alpha$, i.e., the capture to fission ratio. No experimental data are available for inelastic scattering, (n,2n), (n,3n) and total cross sections.

Evaluation of the fission cross sections was based on the experimental data by Szabo[2] Kaeppeler[3] and Behrens[4]. The data by Kaeppeler and Behrens were given as the ratios to the fission cross section of $^{235}U$, and were renormalized with the evaluated fission cross section of $^{235}U$ by Matsunobu[5]. The fission cross section of $^{241}Pu$ thus renormalized agrees well with the values of absolute measurement by Szabo. The present evaluation is shown in Fig. 1.1.1 with the experimental data as well as the evaluated curve of the ENDF/B-4. The ENDF/B-4 seems to adopt Smith's data above 1 MeV and gives higher values.

The capture cross section was obtained up to 250 keV by means of the

measured α- data by Weston[6]. Above 250 keV, the calculation was carried out with the optical and statistical models. First the (n,2n) and (n,3n) cross sections were calculated approximately with Pearlstein's method. Considering the fission, (n,2n) and (n,3n) reactions as the competing processes, we calculated the capture, elastic and inelastic scattering cross sections with the statistical model, in which the competition with each other is treated adequately[7]. The gamma-ray strength function $\Gamma_\gamma/D$ was adjusted so that the calculated capture cross sections connects smoothly at 250 keV with the value obtained from the experimental α data. The capture cross section thus obtained is shown in Fig. 1.1.2.

References

1) Lemmel, H. D.: Nuclear Cross Section and Technology, Proc. Conf. Washington, D.C., March 3-7, 1975, p.286.
2) Szabo, et al.: Proc. Conf. on Neutron Physics, Kiev, 28 May - 1 June, 1973, Vol. 3, p.27.
3) Kaeppeler, F., Pfletschinger, E.: Nucl. Scie. Eng. 51, 124 (1973).
4) Behrens, J. W., Carlson, C. W.: UCRL-51925 (1975).
5) Matsunobu, H.: Private communication (1975).
6) Weston, L. W., Todd, J. H.: Trans. Am. Nucl. Soc. 15, 480 (1972).
7) Igarasi, S.: J. Nucl. Scie. Technol. 12, 67 (1975).

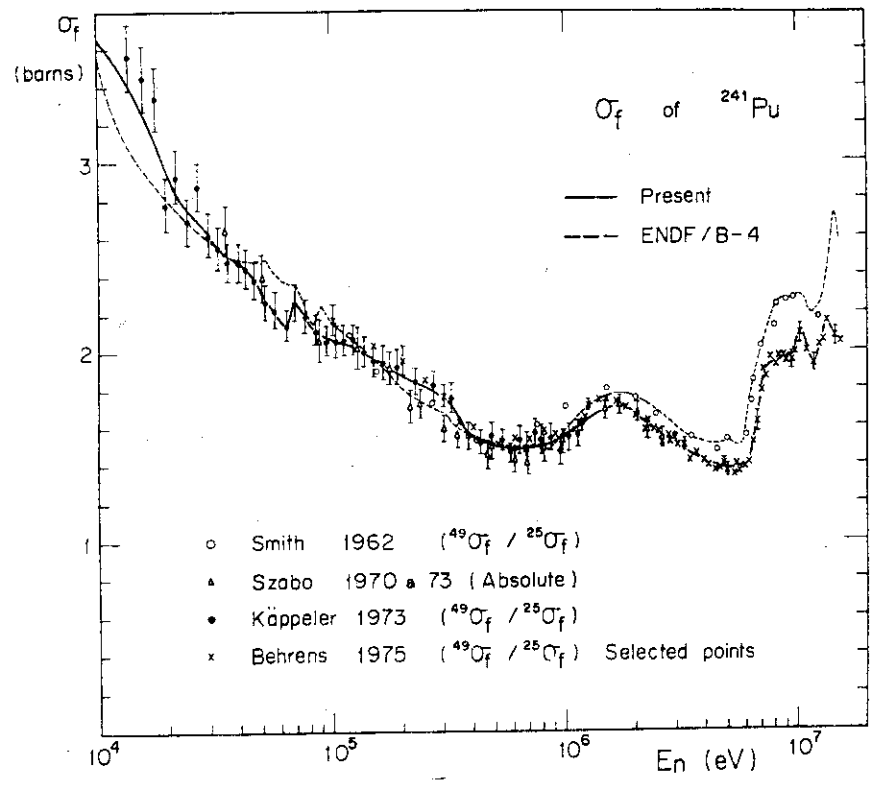


Fig. 1.1.1. Fission cross section of $^{241}$Pu.

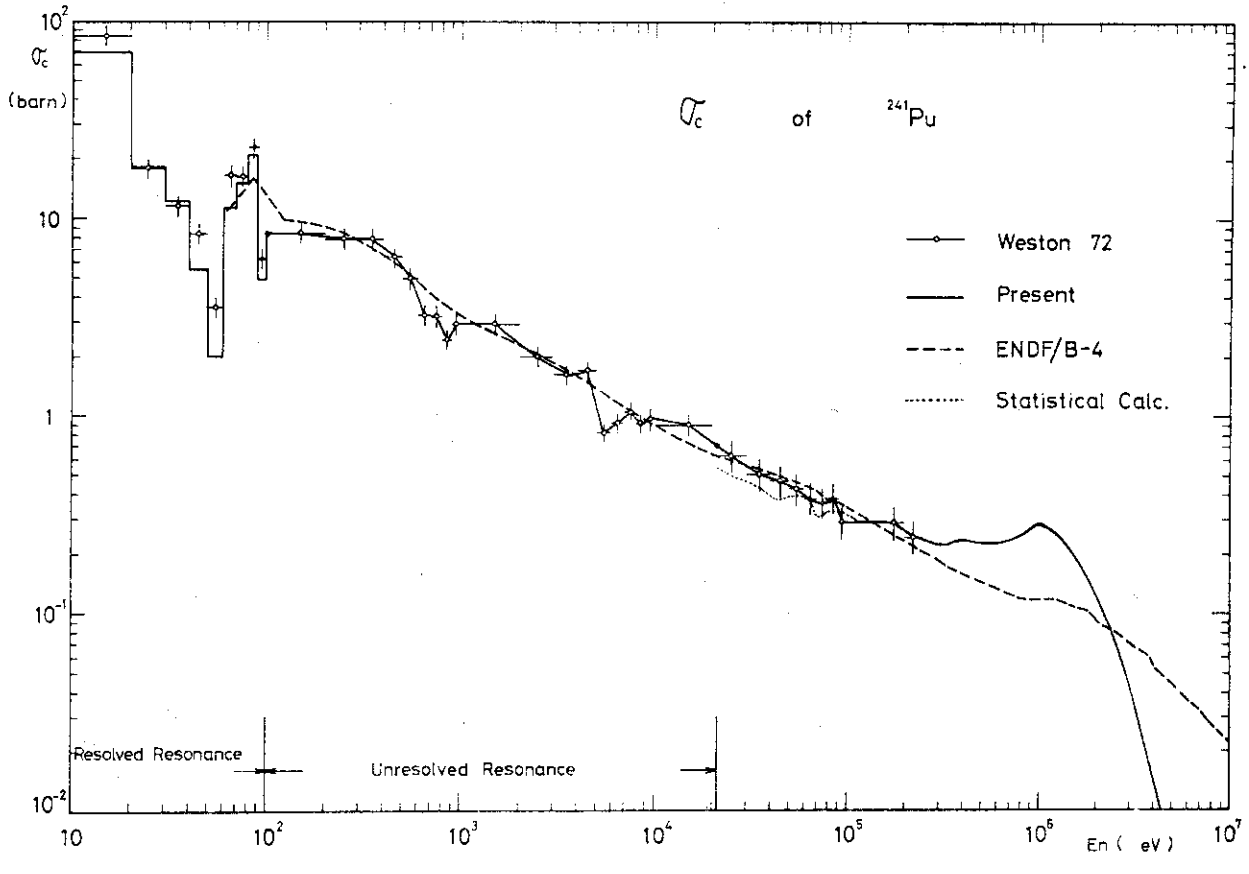


Fig. 1.1.2. Capture cross section of $^{241}$Pu.

## 1.2 Revision of JAERI-Fast Set Version II(1)

(Revision of MeV region fission cross sections for $^{238}U$, $^{235}U$ and $^{239}Pu$, and inelastic scattering cross section for $^{238}U$)

A. Hasegawa, H. Takano and K. Iizima*

In the previous report[1] concerning the analysis of measurements in MZA and MZB based on JAERI-Fast Version I-R set, it was pointed out that the agreements between the experimental and calculational results were fairly good for the majority of the integral quantities such as $k_{eff}$ and central reaction rate ratio, with one notable exception of the central reaction rate ratio of $^{28}\sigma_f/^{25}\sigma_f$.

The cross sections of heavy nuclides contained in the JAERI-Fast Version I-R set were used without change in JAERI-Fast set Version II[2]. Even with this set, the discrepancy of $^{28}\sigma_f/^{25}\sigma_f$ was still observed.

As the probable error sources, we mainly investigated the fission cross sections of heavy nuclides in MeV energy region and inelastic scattering cross section of $^{238}U$.

A simultaneous reevaluation work was performed for $\sigma_f$ of fissile nuclides in MeV range from the microscopic experimental data and evaluated data, since the fission cross sections are often measured as the ratio to those of other fissionable nuclides. From this reevaluation, (1) $\sigma_f$ of $^{238}U$ is slightly reduced, (2) $\sigma_f$ of $^{239}Pu$ is reduced by about 3 % in 2.5 ∿ 6.5 MeV, and (3) $\sigma_f$ of $^{235}U$ is unchanged. This result is against the requests from the integral experiments, and C/E value will become worse yet. Nevertheless we have accepted these revisions and concluded that the error source is not attributed to the fission cross sections.

Inelastic scattering cross section is very important for the formation of energy spectrum in MeV range, but the experimental data are scarce and their accuracy is very poor, say about 30 % or worse. So we performed sensitivity calculations for this reaction using 21 critical assemblies in the world including the international benchmark test assemblies. We varied $\sigma_{in}^{t}$ value from 0 % to -30 % with 10 % step without changing the transfer probability and analyzed several integral quantities. The results are given in Table 1.2.1, where average quantities are shown. We have estimated the best value of $^{28}\sigma_{in}$ for each integral quantities using the least squares method as : 1 for $k_{eff}$, 10 % reduction of the values

---

* Japan Information Service Co. Ltd.

in JAERI-Fast-II, 2 for $^{28}\sigma_f/^{25}\sigma_f$, 7 % reduction. The $^{28}\sigma_{in}$ in JAERI-Fast-II is based on the UKNDL-68. Replacing these data by the ENDF/B-IV value, we had the results fairly close to the 10 % reduction value in Table 1.2.1. Therefore we have recommended the ENDF/B-IV data for this cross section.

With these revisions, the agreements between the experimental and calculational values of the central reaction rate ratio for $^{28}\sigma_f/^{25}\sigma_f$ are greatly improved (C/E value from 0.90 to 0.96 in MZA).

References

1) Nakagawa, M., Hasegawa, A., Kikuchi, Y. and Kasturagi, S.: Reactor Engineering Annual Report (April 1, 1974 to March 31, 1975). p.77.
2) Hasegawa, A. et al.: to be published.
3) Norton, D. S.: "The UKAEA Nuclear Data Library", AEEW-M824 (1968).

Table 1.2.1 Results from sensitivity analysis for $^{238}U\sigma_{in}$ cross section

| Integral Data | | | Variation of U-238$\sigma_{in}$ | | | | |
|---|---|---|---|---|---|---|---|
| | Set name | | 0 % | -10 % | -20 % | -30 % | ENDF/B-IV |
| | | | LTFR901 | LTFR901P1 | LTFR901P2 | LTFR901P3 | LTRF901B4 |
| $k_{eff}$ | $\overline{k_i}$ | a | 0.99460 | 0.99677 | 0.99929 | 1.00229 | 0.99853 |
| | $\overline{\lvert 1-k_i \rvert}$ | b | 0.01018 | 0.00908 | 0.00958 | 0.01166 | 0.00939 |
| | S.T.D | c | 0.01391 | 0.01402 | 0.01477 | 0.01619 | 0.01450 |
| $\frac{^{238}U\sigma_f}{^{235}U\sigma_f}$ | $\overline{C/E}$ | a | 0.98140 | 1.01417 | 1.04976 | 1.08855 | 1.02384 |
| | $\overline{\lvert 1-C/E \rvert}$ | b | 0.07879 | 0.07215 | 0.07657 | 0.09900 | 0.07211 |
| | S.T.D | c | 0.09210 | 0.08544 | 0.08164 | 0.08311 | 0.08405 |
| $\frac{^{239}Pu\sigma_f}{^{235}U\sigma_f}$ | $\overline{C/E}$ | a | 0.98047 | 0.98500 | 0.98981 | 0.99493 | 0.98418 |
| | $\overline{\lvert 1-C/E \rvert}$ | b | 0.03576 | 0.03216 | 0.02930 | 0.02879 | 0.03303 |
| | S.T.D | c | 0.03662 | 0.03641 | 0.03833 | 0.03644 | 0.03637 |
| $\frac{^{240}Pu\sigma_f}{^{235}U\sigma_f}$ | $\overline{C/E}$ | a | 1.03954 | 1.06153 | 1.08528 | 1.11100 | 1.06681 |
| | $\overline{\lvert 1-C/E \rvert}$ | b | 0.08338 | 0.09225 | 0.10838 | 0.12876 | 0.09496 |
| | S.T.D | c | 0.10512 | 0.10409 | 0.10447 | 0.10697 | 0.10564 |
| $\frac{^{238}U\sigma_c}{^{235}U\sigma_f}$ | $\overline{C/E}$ | a | 0.99125 | 0.98617 | 0.98079 | 0.97508 | 0.98164 |
| | $\overline{\lvert 1-C/E \rvert}$ | b | 0.02193 | 0.02402 | 0.02643 | 0.03007 | 0.02358 |
| | S.T.D | c | 0.02364 | 0.02369 | 0.02403 | 0.02475 | 0.02389 |
| $\frac{^{238}U\sigma_c}{^{239}Pu\sigma_f}$ | $\overline{C/E}$ | a | 1.00928 | 0.99895 | 0.98811 | 0.97673 | 0.99976 |
| | $\overline{\lvert 1-C/E \rvert}$ | b | 0.04126 | 0.03967 | 0.04177 | 0.04431 | 0.04081 |
| | S.T.D | c | 0.04779 | 0.04584 | 0.04631 | 0.04632 | 0.04726 |

* S.T.D Standard deviation

## 1.3 JNDC FP Fast Reactor Constants System

Y. Kikuchi, A. Hasegawa, H. Nishimura and K. Tasaka

Japanese Nuclear Data Committee (JNDC) revised the evaluated data of 28 important fission products[1] with applying more sophisticated models and taking account of the resonance structure. According to this revision work, the group constants of these nuclides were also revised. Considering the situation that the number of FP nuclides evaluated by JNDC will become 100 in a year, we have developed a system in which the lumped group constants can be produced rather automatically from the nuclear data file contained in the Japanese Evaluated Nuclear Data Library (JENDL) with the ENDF/B-4 format. This system is called "JNDC FP Fast Reactor Constants System". The detail of the system is described in Ref. 2.

The reliability of the group constants based on the revised JNDC data was tested with the integral data measured at RCN, Petten, the Netherlands[3]. The reactivity worths of separated FP isotopes were calculated for 5 STEK cores with four FP constants sets, i.e., the present set (JNDC set), the preliminary JNDC set[4] (JNDC-P set), the constants based on Cook's evaluation (Cook set) and those on the ENDF/B-4 (ENDF/B-4 set). The calculated worths were compared with each other and with the experimental values. The results are shown in Fig. 1.3.1 as the C/E ratios. The detailed discussion are given in Ref. 2. Followings can be pointed out from the comparison:

1) The JNDC set gives satisfactory results for

$^{93}Zr$, $^{95}Mo$, $^{97}Mo$, $^{101}Ru$, $^{103}Rh$, $^{109}Ag$, $^{129}I$, $^{133}Cs$, $^{143}Nd$ and $^{147}Sm$. (Category 1)

2) The results with the JNDC set deviate from the experiments, but give the best or one of the best agreement with the expeirments for

$^{102}Ru$, $^{104}Ru$, $^{144}Nd$, $^{145}Nd$, $^{149}Sm$, $^{151}Sm$ and $^{153}Eu$. (Category 2)

3) The JNDC-P set might give the best agreement with the experimental data for

$^{99}Tc$, $^{105}Pd$, $^{107}Pd$ and $^{147}Pm$. (Category 3)

4) The Cook set often shows the extreme values, for example, for $^{101}Ru$, $^{102}Ru$, $^{105}Pd$, $^{144}Nd$, $^{153}Eu$ and $^{151}Sm$.

5) The ENDF/B-4 set gives slightly better results than the JNDC set for $^{103}Rh$, $^{105}Pd$ and $^{147}Pm$ but gives much worse results for $^{101}Ru$ and $^{149}Sm$.

As a conclusion, it can be said that the JNDC set is the most reliable set among the four sets compared here. Further investigation should be required for the nuclides of categories 2 and 3. Especially we are checking the cases of $^{105}Pd$, $^{107}Pd$ and $^{147}Pm$ for which the JNDC-P set gives better results and no differential experimental data exist above 1 keV.

References

1) Iijima, S., et al.: to be published in J. Nucl. Scie. Technol.
2) Kikuchi, Y., et al.: JAERI-1248 (1976).
3) Bustraan, M., et al.: Proc. International Symp. on Physics of Fast Reactors, Tokyo, Oct. 1973, Paper B-26.
4) Kikuchi, Y., et al.: "JNDC Fission Product Group Constants (Preliminary Version)", JAERI-M 6001 (1975).
5) Kikuchi, Y., et al.: "Production of FP Group Constants for Fast Reactors with Cook's Evaluated Data", JAERI-M 5492 (1973).

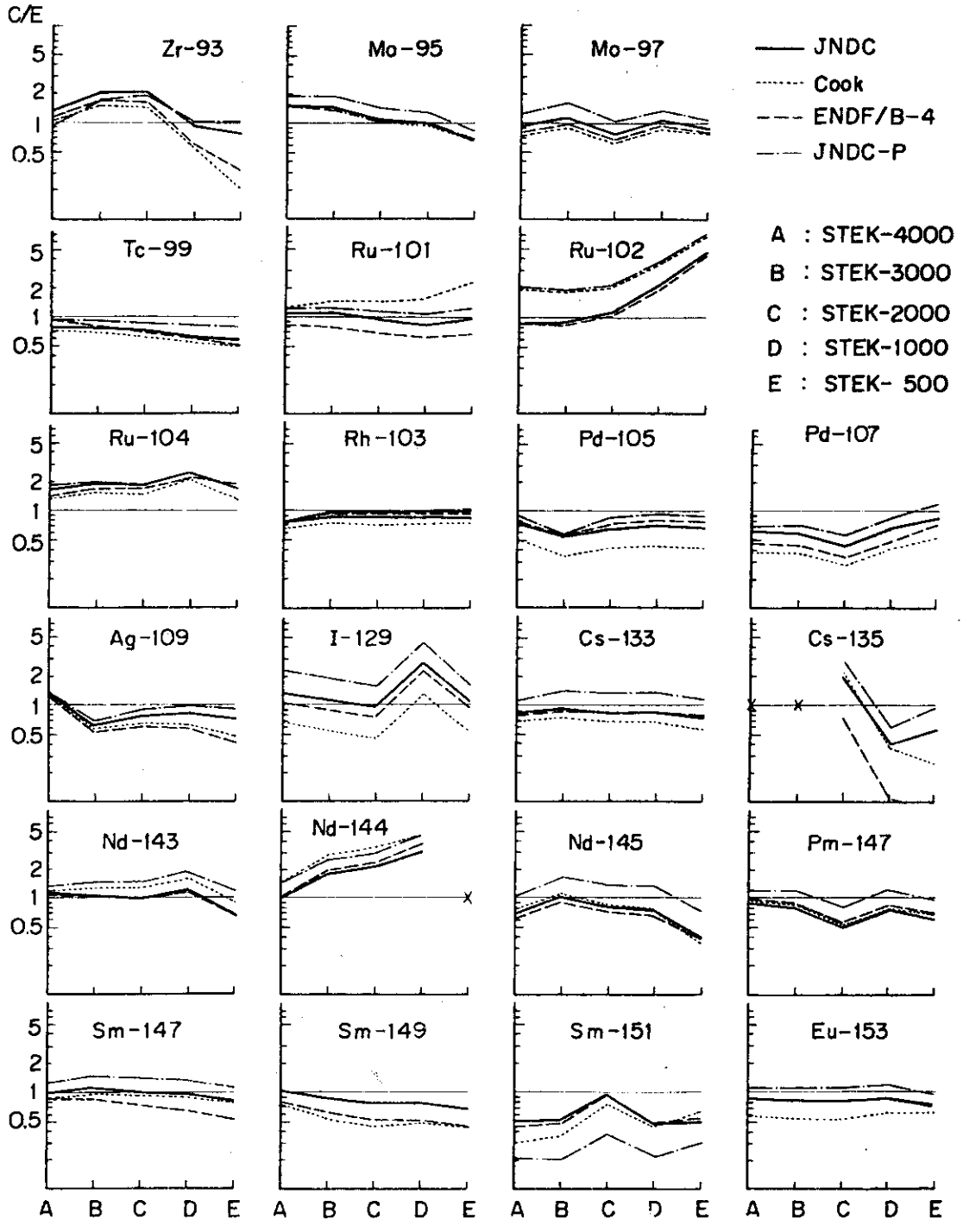


Fig.1.3.1. C/E ratio of the central reactivity worths of FP isotopes in various STEK cores.

## 1.4 Twenty-five-Group Constants of Tritium

K. Koyama and H. Kuroi

ABBN type's 25-group constants of tritium were generated from Stewart's recommended data evaluated from several experimental cross section data for tritium and for Helium-3. The cross sections of elastic scattering were expanded up to P5 order of Legendre polynomials. It is assumed that the angular dependence of the elastic scattering cross section $\sigma(E,\mu)$ in the center-of-mass system is represented in the form

$$\sigma(E,\mu) = \frac{\sigma_s(E)}{2\pi} \sum_{\ell=0}^{5} \frac{(2\ell+1)}{2} B_\ell(E) P_\ell(\mu) ,$$

where

$$\sigma_s(E) = \int_{-1}^{1} \sigma(E,\mu) d\mu ,$$

$\mu$ : cosine of the elastic scattering angle in the center-of-mass system,

$P_\ell(\mu)$ : $\ell$-th Legendre polynomial,

$B_\ell(E)$ : expansion coefficient ($B_0(E)=1$).

The number of energy points for calculating $B_\ell(E)$ are 12 points in the range of 0.5 to 19.4 Mev. The values of $B_\ell(E)$ determined from these data are shown in reference 9.

The 1/E neutron spectrum was used as a weighting function. The group constants obtained are given in Tables 1.4.1. and 1.4.2. The non elastic cross sections of (n,2n) reaction are added to the total cross sections. Moreover, an empirical formula for elastic scattering is obtained from experimental data by mean of least square method; the following formula

is recomended:

$$\sigma_e(E) = 1.13555 + 0.72775E - 0.14092E^2 + 0.00875E^3 - 0.00018E^4,$$

where E is the neutron energy in Mev.

As shown in Fig. 1.4.1, the formula can represent the cross section fairly well.

References


1) Stewart, L.: LA-3270 (1965).

2) Seagrave, J.D., et al.: Phys. Rev. 119, 1981 (1960).

3) Brolley, J.E. Jr., et al.: Phys, Rev. 117, 1307 (1960).

4) Clegg, T.B., et al.: Nucl. Phys. 50, 621 (1964).

5) Lovberg, R.H.: Phys. Rev, 103, 1393 (1956).

6) Los Alamos Physics and Cryogenics Groups, Nucl. Phys.12, 291 (1959).

7) McDonald, D.G., et al.: Phys. Rev. 133, B1178 (1964).

8) Coon, J.H., et al.: Phys. Rev. 81, 33 (1951).

9) Kim, Jung-Do., Koyama, K and Kuroi, H.: JAERI-M 6494 (1967).


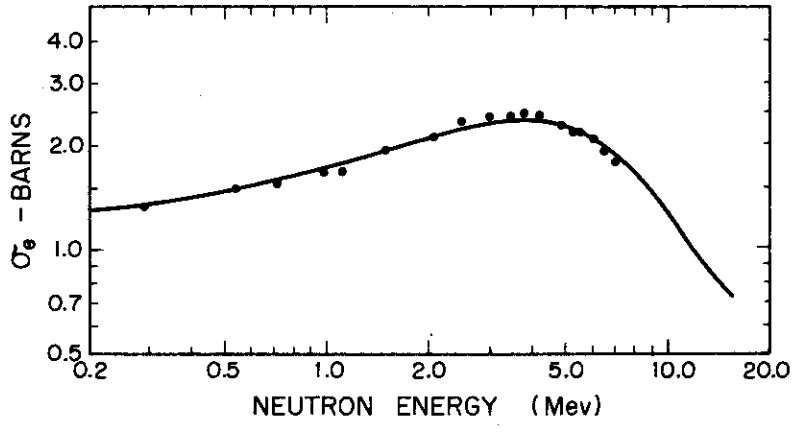


Fig. 1.4.1 Comparison of calculated n-T elastic scatering cross section with the experimental data

Table 1.4.1 Group constants for tritium

| Group | Energy Range | $\sigma_t$ | $\sigma_c$ | $\sigma_{in}$ | $\sigma_e$ | $\mu_e$ | $\sigma_s(e)$ |
|---|---|---|---|---|---|---|---|
| 1 | 6.5 ∿ 10.5MeV | 1.588 | 0.0 | 0.011 | 1.577 | 0.575 | 0.846 |
| 2 | 4.0 ∿ 6.5 | 2.214 | ↑ | 0.000 | 2.214 | 0.482 | 1.254 |
| 3 | 2.5 ∿ 4.0 | 2.396 | ↑ | ↑ | 2.396 | 0.323 | 1.557 |
| 4 | 1.4 ∿ 2.5 | 2.068 | ↑ | ↑ | 2.068 | 0.108 | 1.584 |
| 5 | 0.8 ∿ 1.4 | 1.718 | ↑ | ↑ | 1.718 | 0.023 | 1.454 |
| 6 | 0.4 ∿ 0.8 | 1.488 | ↑ | ↑ | 1.343 | 0.121 | 1.119 |
| 7 | 0.2 ∿ 0.4 | 1.343 | ↑ | ↑ | 1.343 | 0.198 | 0.955 |
| 8 | 0.1 ∿ 0.2 | 1.301 | ↑ | ↑ | 1.301 | 0.218 | 0.931 |
| 9 | 46.5 ∿ 100 KeV | 1.300 | ↑ | ↑ | 1.300 | 0.222 | 0.930 |
| 10 | 21.5 ∿ 46.5 | 1.300 | ↑ | ↑ | 1.300 | 0.222 | 0.930 |
| 11 | 10.5 ∿ 21.5 | 1.300 | ↑ | ↑ | 1.300 | 0.222 | 0.930 |
| 12 | 4.65 ∿ 10.0 | 1.300 | ↑ | ↑ | 1.300 | 0.222 | 0.930 |
| 13 | 2.15 ∿ 4.65 | 1.300 | ↑ | ↑ | 1.300 | 0.222 | 0.930 |
| 14 | 1.0 ∿ 2.15 | 1.300 | ↑ | ↑ | 1.300 | 0.222 | 0.930 |
| 15 | 465 ∿ 1000 eV | 1.300 | ↑ | ↑ | 1.300 | 0.222 | 0.930 |
| 16 | 215 ∿ 465 | 1.300 | ↑ | ↑ | 1.300 | 0.222 | 0.930 |
| 17 | 100 ∿ 215 | 1.300 | ↑ | ↑ | 1.300 | 0.222 | 0.930 |
| 18 | 46.5 ∿ 100 | 1.300 | ↑ | ↑ | 1.300 | 0.222 | 0.930 |
| 19 | 21.5 ∿ 46.5 | 1.300 | ↑ | ↑ | 1.300 | 0.222 | 0.930 |
| 20 | 10.0 ∿ 21.5 | 1.300 | ↑ | ↑ | 1.300 | 0.222 | 0.930 |
| 21 | 4.65 ∿ 10.0 | 1.300 | ↑ | ↑ | 1.300 | 0.222 | 0.930 |
| 22 | 2.15 ∿ 4.65 | 1.300 | ↑ | ↑ | 1.300 | 0.222 | 0.930 |
| 23 | 1.0 ∿ 2.15 | 1.300 | ↑ | ↑ | 1.300 | 0.222 | 0.930 |
| 24 | 0.465 ∿ 1.0 | 1.300 | ↑ | ↑ | 1.300 | 0.222 | 0.930 |
| 25 | 0.215 ∿ 0.465 | 1.300 | 0.0 | 0.000 | 1.300 | 0.222 | |

Table 1.4.2 Elastic scattering transfer matrix for tritium

| i \ K | $\sigma_e(i,i+k)$ at k equal to | | | |
|---|---|---|---|---|
| | 0 | 1 | 2 | 3 |
| 1 | 0.731 | 0.546 | 0.158 | 0.142 |
| 2 | 0.960 | 0.637 | 0.430 | 0.187 |
| 3 | 0.839 | 0.714 | 0.713 | 0.130 |
| 4 | 0.484 | 0.670 | 0.887 | 0.027 |
| 5 | 0.264 | 0.842 | 0.612 | —— |
| 6 | 0.369 | 0.760 | 0.359 | |
| 7 | 0.388 | 0.677 | 0.278 | |
| 8 | 0.370 | 0.702 | 0.229 | |
| 9 | 0.370 | 0.702 | 0.228 | |
| 10 | 0.370 | 0.702 | 0.228 | |
| 11 | 0.370 | 0.702 | 0.228 | |
| 12 | 0.370 | 0.702 | 0.228 | |
| 13 | 0.370 | 0.702 | 0.228 | |
| 14 | 0.370 | 0.702 | 0.228 | |
| 15 | 0.370 | 0.702 | 0.228 | |
| 16 | 0.370 | 0.702 | 0.228 | |
| 17 | 0.370 | 0.702 | 0.228 | |
| 18 | 0.370 | 0.702 | 0.228 | |
| 19 | 0.370 | 0.702 | 0.228 | |
| 20 | 0.370 | 0.702 | 0.228 | |
| 21 | 0.370 | 0.702 | 0.228 | |
| 22 | 0.370 | 0.702 | 0.228 | |
| 23 | 0.370 | 0.702 | 0.228 | |
| 24 | 0.370 | 0.930 | —— | |
| 25 | 1.300 | —— | —— | |

| i \ K | $\mu_e(i,i+k)$ at k equal to | | | |
|---|---|---|---|---|
| | 0 | 1 | 2 | 3 |
| 1 | 0.872 | 0.422 | -0.404 | -0.680 |
| 2 | 0.869 | 0.396 | -0.437 | -0.403 |
| 3 | 0.863 | 0.282 | -0.594 | -0.179 |
| 4 | 0.823 | 0.172 | -0.622 | 0.189 |
| 5 | 0.791 | 0.096 | -0.700 | —— |
| 6 | 0.736 | 0.026 | -0.561 | |
| 7 | 0.747 | 0.041 | -0.598 | |
| 8 | 0.757 | 0.025 | -0.474 | |
| 9 | 0.757 | 0.025 | -0.474 | |
| 10 | 0.757 | 0.025 | -0.474 | |
| 11 | 0.757 | 0.025 | -0.474 | |
| 12 | 0.757 | 0.025 | -0.474 | |
| 13 | 0.757 | 0.025 | -0.474 | |
| 14 | 0.757 | 0.025 | -0.474 | |
| 15 | 0.757 | 0.025 | -0.474 | |
| 16 | 0.757 | 0.025 | -0.474 | |
| 17 | 0.757 | 0.025 | -0.474 | |
| 18 | 0.757 | 0.025 | -0.474 | |
| 19 | 0.757 | 0.025 | -0.474 | |
| 20 | 0.757 | 0.025 | -0.474 | |
| 21 | 0.757 | 0.025 | -0.474 | |
| 22 | 0.757 | 0.025 | -0.474 | |
| 23 | 0.757 | 0.025 | -0.474 | |
| 24 | 0.757 | -0.097 | —— | |
| 25 | 0.146 | —— | —— | |

## 1.5 Japanese Evaluated Nuclear Data Library, Version-1 (JENDL-1)

JENDL-1 Compilation Group*

The Japanese Evaluated Nuclear Data Library has been developed by Nuclear Data Center, JAERI in cooperation with the members of Japanese Nuclear Data Committee (JNDC). The final goal of this work is to provide the standard nuclear data library in Japan. The data adopted in this library should be evaluated by Japanese evaluators so that their detail is clearly known. The version-1 (JENDL-1) is mainly aimed at providing the data needed for calculation of fast reactors. Its compilation was started early in 1974 and was completed in April, 1976.

JENDL-1 contains the data of the following nuclides in the ENDF/B-4 format;

H, $^{6}$Li, $^{7}$Li, $^{10}$B, $^{11}$B, $^{12}$C, $^{16}$O, $^{23}$Na, $^{27}$Al, Si, Cr, $^{55}$Mn, Fe, Ni, Cu, Mo, $^{181}$Ta, $^{232}$Th, $^{233}$Pa, $^{234}$U, $^{235}$U, $^{238}$U, $^{239}$Np, $^{239}$Pu, $^{240}$Pu, $^{241}$Pu, $^{241}$Am and 28 FP nuclides.

For Si, Cr, Fe, Ni, Cu and Mo, the data of each isotope are also compiled as well as those of the natural elements.

The present status of the experimental data and of the evaluated data has been examined for those nuclides mentioned above. The data already evaluated as the activities of JNDC were mainly adopted for $^{12}$C, Fe, $^{181}$Ta, $^{235}$U, $^{238}$U, $^{239}$Pu, $^{240}$Pu, $^{241}$Pu and FP nuclides. New evaluation was carried out with the aid of the Japanese evaluators in various organizations for H, $^{6}$Li, $^{10}$B, $^{23}$Na, $^{27}$Al, Si, Cr, $^{55}$Mn, Ni, Cu, Mo, $^{233}$Pa, $^{232}$Th, $^{234}$U, $^{239}$Np and $^{241}$Am. For $^{7}$Li, $^{11}$B and $^{16}$O, the data contained in the ENDF/B-4 were adopted according to the recommendation of the Japanese evaluations.

In order to examine the reliability of JENDL-1, the multi-group cross sections of the JAERI-Fast set type were produced with the PROF-GROUCH-G-II[1] and ETOX[2] system. Various benchmark tests are now in progress with using more than 30 critical assemblies including the international benchmark assemblies and some FCA assemblies.

(Reported by Y. Kikuchi)

---

* The members of the group are S. Igarasi (Head), T. Asami, Y. Kikuchi, T. Nakagawa and T. Narita.

References

1) Hasegawa, A., Katsuragi, S.: to be published.

2) Schenber, R. E., Baker, J. L., Kidman, R. B.: BNWL-1002 (1969).

# 2. Theoretical Method and Code Development

## 2.1 Application of the Finite Element Method to the Three-Dimensional Neutron Diffusion Equation

T. Ise, T. Fuzimura, T. Yamazaki*, Y. Ohkawa**,
Y. Nakahara, T. Ohnishi*** and T. Asaoka

We have applied the finite element method (FEM) to solve the three-dimensional neutron diffusion equation, in order to get a profit from the fact that the FEM should have the geometrical flexibility[1] and offer an attractive solution procedure for practical problems[2]. A computer code FEM-BABEL has been developed on the basis of the formalism in the Galerkin approximation[3]. In order to challenge the computer limitation such as the storage capacity and the computation time required to the three-dimensional problems, the FEM-BABEL code has been equipped with the following several characteristics.

(i) Combination of the prism-formed (triangles in x-y plane) and the box-formed (rectangles in x-y plane) elements is adopted for the geometrical generocity. Use of both the elements will give more applicable geometrical symmetry to the system and then save the storage capacity because the number of node points can be reduced.

(ii) The iteration solution method (point SOR) is adopted because the system equation has a large and sparse

* Hiratsuka Research Laboratory, Sumitomo Ship Building & Machinery Co. Ltd.

** Sumitomo Atomic Energy Industries, Ltd.

*** Atomic Energy Research Laboratory, Hitachi Ltd.

coefficient matrix. Taking advantage of the above-mentioned characteristics (i), the point SOR is applied successively to x-y plane as unit and moreover the symmetric SOR is used as the plane matrices are banded and symmetric.

(iii) Acceleration based on the SOR is adopted for both the inner and outer iterations, and the coarse mesh rebalancing technique is used for improving the flux guess at the beggining of the inner iteration.

(iv) Automatic mesh generation routine built-in for the system composed of only the prism- or box-formed element, the input format in FIDO, various restarting procedures and so on will give users a help to prepare the input data more easily.

We are now developing a solution procedure for the system equation with an irregular sparse matrix and an automatic mesh generation technique to make the present FEM-BABEL more efficient for most practical problems.

References

1) Ohnishi, T.: "Application of Finite Element Solution Technique to Neutron Diffusion and Transport Equations", CONF-710302 (1971), p.723.

2) Hageman, L. A.: "The Solution of Linear Equations Resulting from Finite Element Discretizations of Multi-Dimensional Boundary Value Problems, WAPD-TM-1209 (1975).

3) Kaper, H. G., Leaf, G. K., Lindeman, K. J.: "Application of Finite Element Methods in Reactor Mathematics: Numerical

Solution of the Neutron Diffusion Equation", ANL-7925 (1972).

4) Jones, R. E.: "QMESH: A Self-Organizing Mesh Generation Program", SLA-73-1088 (1974).

## 2.2 Benchmark Evaluations of Space-Dependent Neutron Kinetics Codes

T. Ise, T. Tsutsui, K. Horikami and K. Kobayashi

As reactor kinetics calculations have become more necessary for optimal design and safety analyses, we have a plan of benchmark tests for available space-dependent reactor kinetics computer codes[1,2]. The review study given here describes the present status of algorithms and numerical tests of several neutron transport kinetics codes (except the Monte Carlo method)[3].

At present, being compared with the diffusion kinetics codes, there are a few transport kinetics code available: TDA, TASK, TIMEX and TDT for one-dimensional problems and only one TRANZIT code for the two-dimensional problems. The TDA, TIMEX and TRANZIT are the time-dependent multi-group codes based on diamond difference. What is known as the response matrix method is applied to TASK and TDT codes.

In TDA code, numerical results are compared with those from the diffusion theory. The effects of rebalancing technique and exponential extrapolation are discussed in TIMEX code. A comparison between calculation and experiment is made in TASK code. Numerical comparisons between TDA and TDT are performed and moreover TDA is compared to the Monte Carlo Method[4]. The TRANZIT is also compared to the Monte Carlo method. However, these discussions are made only for simple geometry such as a sphere.

The TRASCAL code based on the transfer matrix method is

discussed comparing to the diffusion theory code of the same method. Although the algorithm on the transfer matrix method is appropriate to complex geometries, much computing time is needed because the calculation of the transfer matrix is laborious.

Generally, neutron transport kinetics code gives more accurate results than the diffusion theory code, but it is much expensive in computation. Consequently, it is recommended that transport codes are to be used for source problems, pulse neutron experiments, neutron wave propagations and deep penetration problems rather than for eigenvalue problems.

References

1) Asaoka, T., et al.: "Status of Benchmark Tests on Neutron and Gamma-Ray Transport and Reactor Kinetics Computer Codes", JAERI-M 5557 (1974) (in Japanese).

2) Nakahara, Y., et al.: "A Direct Method for Numerical Solution of a Class of Nonlinear Volterra Integro-Differential Equations and its Application to the Non-linear Fission and Fusion Reactor Kinetics", JAERI-M 6351 (1975).

3) Ise, T., Horikami, K., Kobayashi, K.: "Present Status on Algorithms and Benchmark Tests for Numerical Solution of the Time-Dependent Neutron Transport Equation (Benchmark Test on the Space-Dependent Neutron Kinetics Codes·1)", JAERI-M 6373 (1975) (in Japanese).

4) McGregor, B., Harrington, B.: "Comparison of Calculations Made with Three Time-Dependent Neutron Codes TDA, MORSE and POW", AAEC/E 336 (1974).

## 2.3 Analysis of Control Rod Worth by Correlated Sampling Monte Carlo Method

M. Nakagawa and T. Asaoka

The correlated Monte Carlo technique[1] has been applied to calculations of the reactivity perturbation through the development of the similar flight path method to evaluate also the second order change of the reactivity. The reactivity change can be obtained from the following formula:

$$\delta k = k^{P}_{eff} - k_{eff}$$

$$= \frac{1}{\int Q(x)dx} \{ \int\int (P^{P}(x' \to x) - P(x' \to x)) Q(x) dx' dx$$

$$+ \int\int P^{P}(x' \to x)\ Q(x) dx' dx$$

$$- \frac{\int \delta Q(x) dx}{\int Q(x) dx} \int\int P^{P}(x' \to x) Q(x') dx' dx \} \quad , \qquad (1)$$

where x stands for space and energy variable, Q(x) is fission source distribution and $P(x' \to x)$ is transport kernel for neutron multiplication. This algorithm has been introduced to the general purpose Monte Carlo code MORSE[2].

As a sample problem, the control rod worths measured in the FCA assembly V-3[3] have been analysed. The geometry of the assembly and the control rod positions are illustrated in Fig. 2.3.1.

The nuclear cross sections of the core were obtained through the cell calculation for the plate lattice and those of the control rods were obtained through a 7 rods cluster calculation with using the collision probability method. These 70-group cross sections based on the JAERI-Fast set, version 1-R, are collapsed into 8 groups.

The rod worths were measured for the fully inserted central rod and off-central five rods, and also for the partially inserted rod at the off-center. For the partial insertion of one rod, the worths were measured at 15 cm, 30 cm, 45 cm and 60 cm (full) of insertion.

The Monte Carlo game is performed as follows. The number of neutron histories is taken as 1000 per batch. The 10 batch source calculations are performed to obtain the converged neutron source distribution. In the following batches, the correlated sampling is carried out for unperturbed and perturbed systems. Each neutron entering the region to be purturbed is marked in the course of the calculation of unperturbed system.

Then, the marked neutrons are followed again for the perturbed system with the same random number chain as for the unperturbed case. The second order effect described by the second and third terms on the right hand side of Eq. (1) is obtained by following secondary fission neutrons produced by the marked neutrons in the unperturbed and perturbed systems.

The result for five batch calculations is presented in Table 2.3.1. All the cases are in a good agreement within one standard deviation. The central rod worth agrees very nicely with the $S_8$ calculation by the TWOTRAN code. The second order correction amounts to about 30 %.

The five control rod worth also shows a good agreement with the measurement. However, the second order correction has a large standard deviation.

In the partially inserted rod case, the first order calculations seem to be sufficiently accurate but the second order corrections bring rather large standard deviations.

References

1) Asaoka, T., et al.: "Analysis of Reactivity Perturbation by Correlated Sampling Monte Carlo Method", in "Reactor Engineering Division Annual Report", JAERI-M 6320, 35 (1975).

2) Straker, E. A., et al.: "Ther MORSE Code - A Multigroup Neutron and Gamma-Ray Monte Carlo Transport Code", ORNL-4585 (1970).

3) Mizoo, N., et al.: "Experiment and Analysis of $B_4C$ Simulating Control Rod on FCA V-3 Assembly, 1", JAERI-M 5867 (1974).

Table 2.3.1 Comparison of control rod worths between calculations and measurements (%Δk/k)

| Rod position | Exp. | 1st order | 2nd order | Total | Average sample number |
|---|---|---|---|---|---|
| center 1 rod | -2.52 ±0.04 | -2.144 ±0.098 | -0.577 ±0.154 | -2.72* ±0.25 | 143 |
| off-center 5 rods | -5.87 ±0.10 | -6.153 ±0.362 | 0.091 ±0.528 | -6.06 ±0.89 | 459 |
| 15 cm | -0.265 | -0.269 ±0.019 | -0.032 ±0.114 | -0.292 ±0.133 | 30 |
| 30 cm | -0.681 | -0.682 ±0.030 | 0.016 ±0.125 | -0.666 ±0.155 | 67 |
| 45 cm | -1.11 | -1.030 ±0.078 | -0.248 ±0.096 | -1.27 ±0.174 | 94 |
| 60 cm | -1.29 | -1.31 ±0.056 | 0.188 ±0.253 | -1.12 ±0.31 | 117 |

* Homogenized control rod cross section is used and corrected value for heterogeneity effect is -2.54.
($2D \cdot S_8$ calculation gives -2.68)

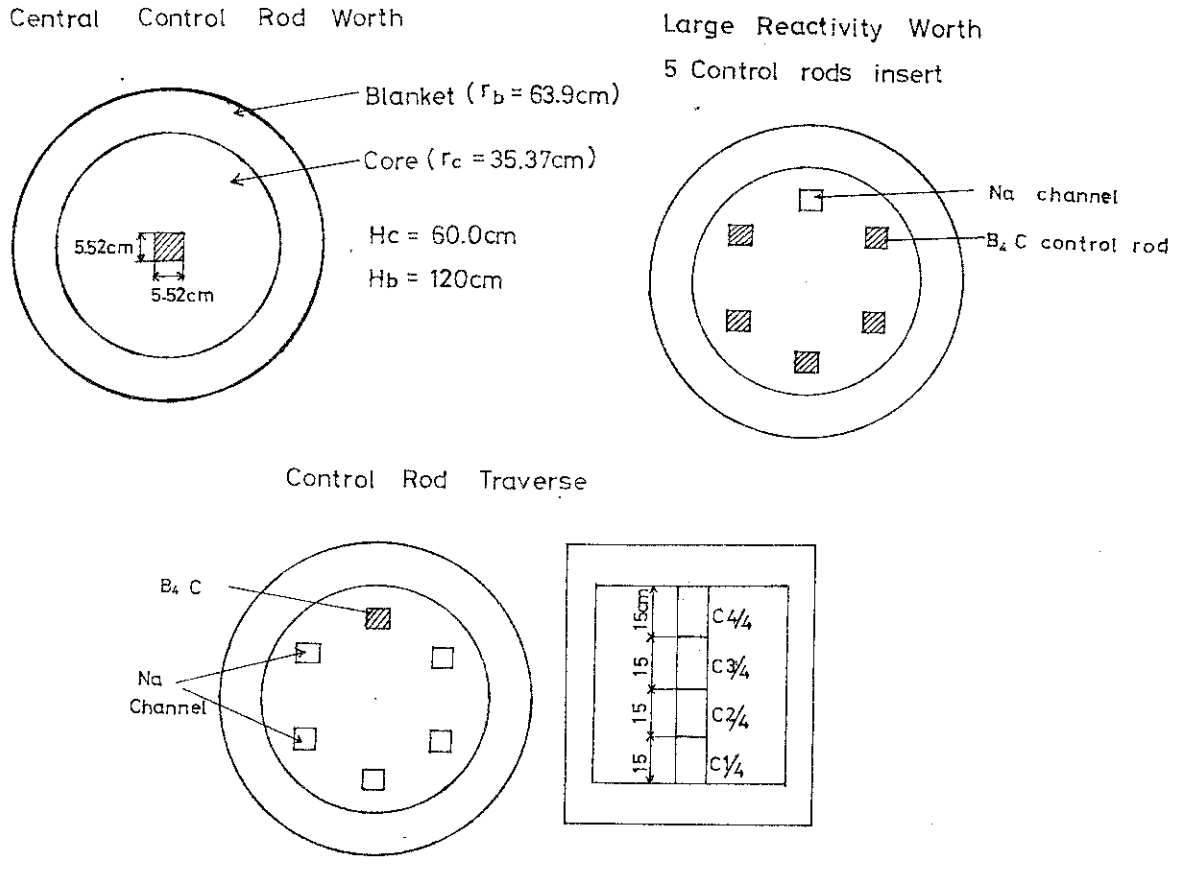


Fig.2.3.1. Configuration of control rods.

## 2.4 Computer Simulation of Atomic-Displacement Cascades in Cu by CASCADE/CLUSTER Code

T. Asaoka, M. Nakagawa, Y. Taji, T. Tsutsui, Y. Nakahara and T. Nishida

For a detailed analysis of the damage produced by primary recoil atoms of various energies, several computer programs have been developed to simulate atomic-displacement cascades by using the binary collision approximation which is especially useful at high energies. Two computer programs of this sort are presently available; one is CASCADE/CLUSTER[1] and the other is MARLOWE[2]. The CASCADE/CLUSTER code deals with a body-centered cubic or face-centered cubic crystal structure at absolute zero temperature neglecting the energy loss by electron excitation. On the other hand, MARLOWE can take into account the inelastic energy loss as well as the thermal vibration of target atoms. Table 2.4.1 summarizes the main difference in the physical model adopted for these two codes.

In order to see the effect of the difference on displacement cascades, we have calculated with the use of CASCADE/CLUSTER the distribution functions of the number of Frenkel pairs produced in Cu for three different primary recoil energies, 1, 5 and 10 keV. In each case, 240 primary recoil directions are taken as distributed uniformly over 1/48 of the unit sphere. Figure 2.4.1 shows the results for 5 keV and compares them with the MARLOWE results[2] of 1,000 cascades. Due to the neglect of inelastic energy losses in CASCADE/CLUSTER, the distribution function shifts towards the high defect-number side of the histogram. In addition, a pronounced tail due to the channeling seen on the low defect-number side of the MARLOWE results is not observed in CASCADE/CLUSTER.

Table 2.4.2 summarizes the defect statistics for the three primary recoil energies and for 20 keV of 48 directions (instead of 240 for saving the computation time) distributed uniformly over 1/48 of the unit sphere. The displacement efficiency $\kappa$ based on the Kinchin-Pease model with $E_d$ = 25 eV is about 0.8 though it decreases as the primary energy increases. This shows that the displacement model used in CASCADE/CLUSTER corresponds to $E_d$ = 25 eV for permanent displacement as adopted for MARLOWE. On the other hand, the displacement efficiency calculated by taking into account inelastic energy losses based on the theory of Lindhard et al.[4] is fairly constant though it is larger than 1. The ratio of the displacement to replacement

threshold energy is around 1.3 which is near to about 2 calculated by Thompson but different from 10 suggested by Kinchin and Pease.

References

1) Besco, D. G., Baumgardt, N. R.: "CASCADE and CLUSTER", GEMP-356 (1965).
2) Robinson, M. T., Torrens, I. M.: Phys. Rev. B, 9, 5008 (1974).
3) Gibson, J. B., et al.: Phys. Rev., 120, 1229 (1960).
4) Lindhard, J., et al.: Mat. Fys. Medd. Dan. Vid. Selsk., 33, No.10 (1963).
5) Dienes, G. J., Vineyard, G. H.: "Radiation Effects in Solids", Interscience Publishers, Inc., New York (1957).

Table 2.4.1 Comparison between physical models adopted in CASCADE/CLUSTER and MARLOWE codes

| Computer code | CASCADE/CLUSTER | MARLOWE |
|---|---|---|
| Atomic potential | Bohr | Moliere |
| Inelastic energy loss | None | Firsov model |
| Thermal vibration | None | Yes |
| $E_d = E_b = E_c^*$ for Cu[3] | 7 eV | 25 eV |
| Recombination radius for Cu | $\sim\sqrt{5}\ a_o/2$** (nonspherical) | 0 |

* $E_d$ = displacement threshold energy,
$E_b$ = binding energy of target atom, and
$E_c$ = cut-off energy below which atoms are not followed.

** $a_o$ = lattice constant.

Table 2.4.2 CASCADE/CLUSTER defect statics of displacement cascades in Cu for 4 primary recoil energies

| Primary recoil energy T | | 1 keV | 5 keV | 10 keV | 20 keV |
|---|---|---|---|---|---|
| Number of replacement $\bar{\mu}$ | | 22.28 | 114.8 | 228.4 | 457.0 |
| Number of Frenkel pairs $\bar{\nu}$ | | 17.43 | 82.4 | 159.4 | 307.4 |
| Scaled variance $(\bar{\nu}^2-\bar{\nu}^2)/\bar{\nu}$ | | 0.301 | 0.365 | 0.501 | 0.666 |
| Displacement efficiency $\kappa$ | Kinchin-Pease* | 0.872 | 0.824 | 0.797 | 0.769 |
| | Lindhard et al.** | 1.063 | 1.065 | 1.064 | 1.064 |
| Ratio of $E_d/E_r$*** | | 1.19 | 1.28 | 1.31 | 1.35 |

* $\bar{\nu}(T) = \kappa T/(2E_d)$ with $E_d = 25$ eV.

** $\bar{\nu}(T) = \kappa(T-T_{in})/(2E_d)$ where $T-T_{in} = T/[1+kg(\varepsilon)]$ [4].

*** $\bar{\mu}/\bar{\nu} = 1.614\ell n(E_d/E_r)+1$ where $E_r$ = replacement threshold energy[5].

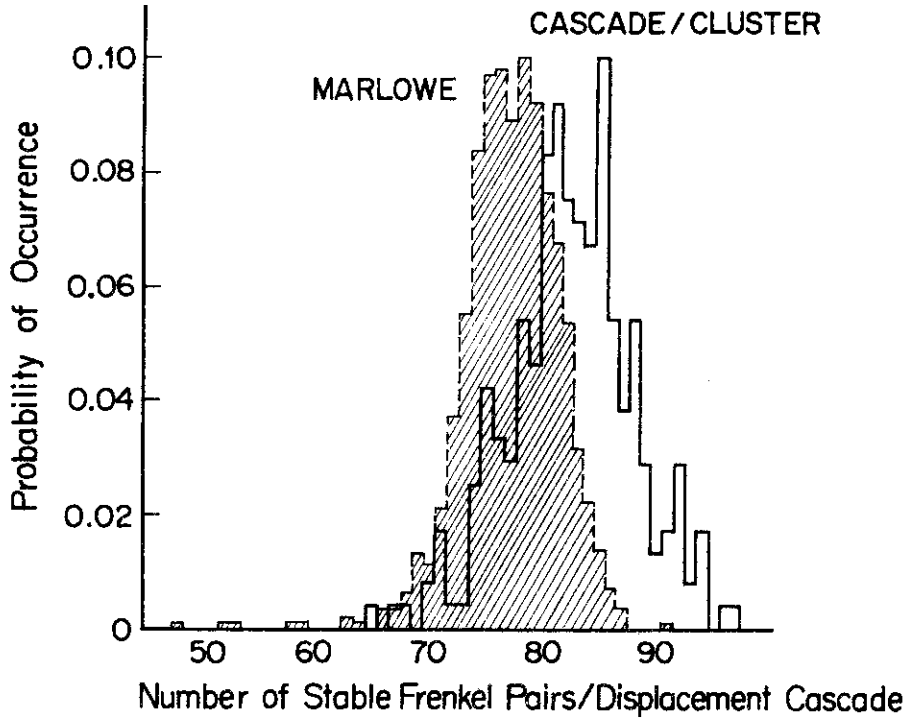


Fig. 2.4.1 Comparison of the distribution function of the number of Frenkel pairs produced in Cu for 5 keV primary recoil energy with the MARLOWE result

## 2.5 Localization of Electron Current Density and its Effect on Damage Production in a Germanium Crystal

T. Nishida and K. Izui

In a research field of radiation damage, it is of primary importance to estimate accurately the damage production rate due to high energy particle bombardment. In this work we are concerned with the localization of total current density $J^T$ which is a result of the interference of all Bloch waves. The calculations are made on the three-dimensional distribution of electron current density in a germanium crystal for the axial cases, using the many-beam theory. Combining the classical picture of knock-on process with the localized current density, we present a model to estimate an "effective current density" for atomic displacement. The current density in the <HKL> direction is given by

$$J^T_{<HKL>}(r) = \frac{h}{2im} [\Psi^*(r)\,\mathrm{grad}\,\Psi(r) - \Psi(r)\,\mathrm{grad}\,\Psi^*(r)],$$

where $\Psi(r)$ is Bloch wave and m electron mass and h Plank constant.

The main quantities calculated here are the profiles of $J^T(0,0,u_3)$ along the <100> direction of incidence, two-dimensional distribution of both $J^T(u_1,u_2,u_3)$ and the diagonal total current $J^{DT}(u_1,u_2)$ displayed as contour-maps in the transverse planes perpendicular to the incident direction of some principal zone axes, where $J^{DT}$ is the average of $J^T$ over $u_3$ and co-ordinate system $(u_1,u_2,u_3)$ is illustrated in Fig. 2.5.1. "Effective current ratio" $J_{eff}$ is defined as the ratio of the localized diagonal total current density at the atomic position to the mean current density and calculated for the <100>, <110> and <111> axial cases. The effect of the number of beams used in the calculation was examined in some cases, and then 61-beams were used for most cases except for the contour-maps of $J^T(u_1,u_2,u_3)$ and $J^{DT}(u_1,u_2)$, which were obtained by 13 beams or so. As for the atomic scattering factors, use was made of the Smith and Burge's analytical expressions[1]. The effect of electron absorption was not taken into account in the present work. The computation were carried out by modifying the Program System MSCOPE-I which was developed for FACOM-230-60 computer in JAERI.

The main results are summarized as follows:

(a) The distribution of $J^T(u_1,u_2,u_3)$ in the transverse plane is found to

oscillate periodically with depth. That is, in the axial case a highly localized distribution and a nearly flat distribution of current density appear alternatively with a definite period of the depth. This period may be called as a "localization period of electron current" (see Fig. 2.5.2). In the slightly off-axis case the period becomes somewhat irregular.

(b) The two-dimensional, transverse distributions of $J^{DT}(u_1,u_2,u_3)$ are examined for the <100>, <110>, <111> and <120> axial cases (see Fig. 2.5.3). From the profiles of $J^{DT}$ (see Fig. 2.5.4), $J_{eff}$ were estimated for 1 MeV electrons to be about 6, 5 and 4 in the <100>, <111> and <110> axial cases, respectively.

(c) The energy dependence of the localization of $J^{DT}$ is examined and $J_{eff}$'s are found to decrease slightly with increasing the energy of incident electrons. It is also confirmed that the increase in the localized current density in the interspace among the atomic rows is caused by growing of sub-peaks there with the increase of the energy. (see Fig. 2.5.5)

References

1) Smith G. H., Burge, R. E.: Acta Cryst., 15, 182 (1962).

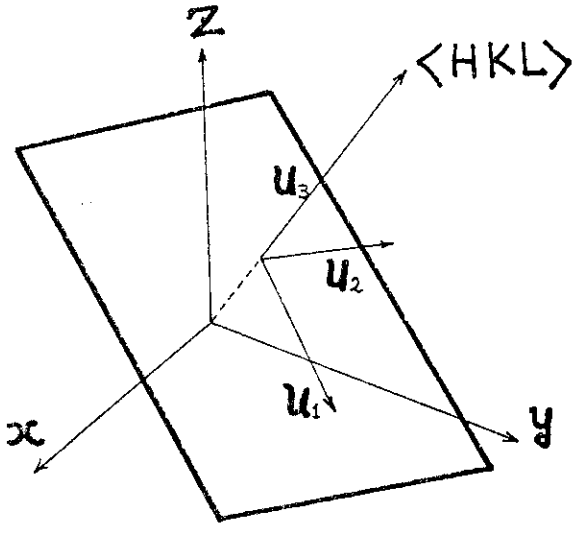


Fig. 2.5.1 Coordinate system in the calculation. x,y and z axes are taken to coincide with the cube edges of the unit cell of Ge, $u_1$ and $u_2$ axes lie on the (HKL) plane and $u_3$ axis is normal to the (HKL) plane.

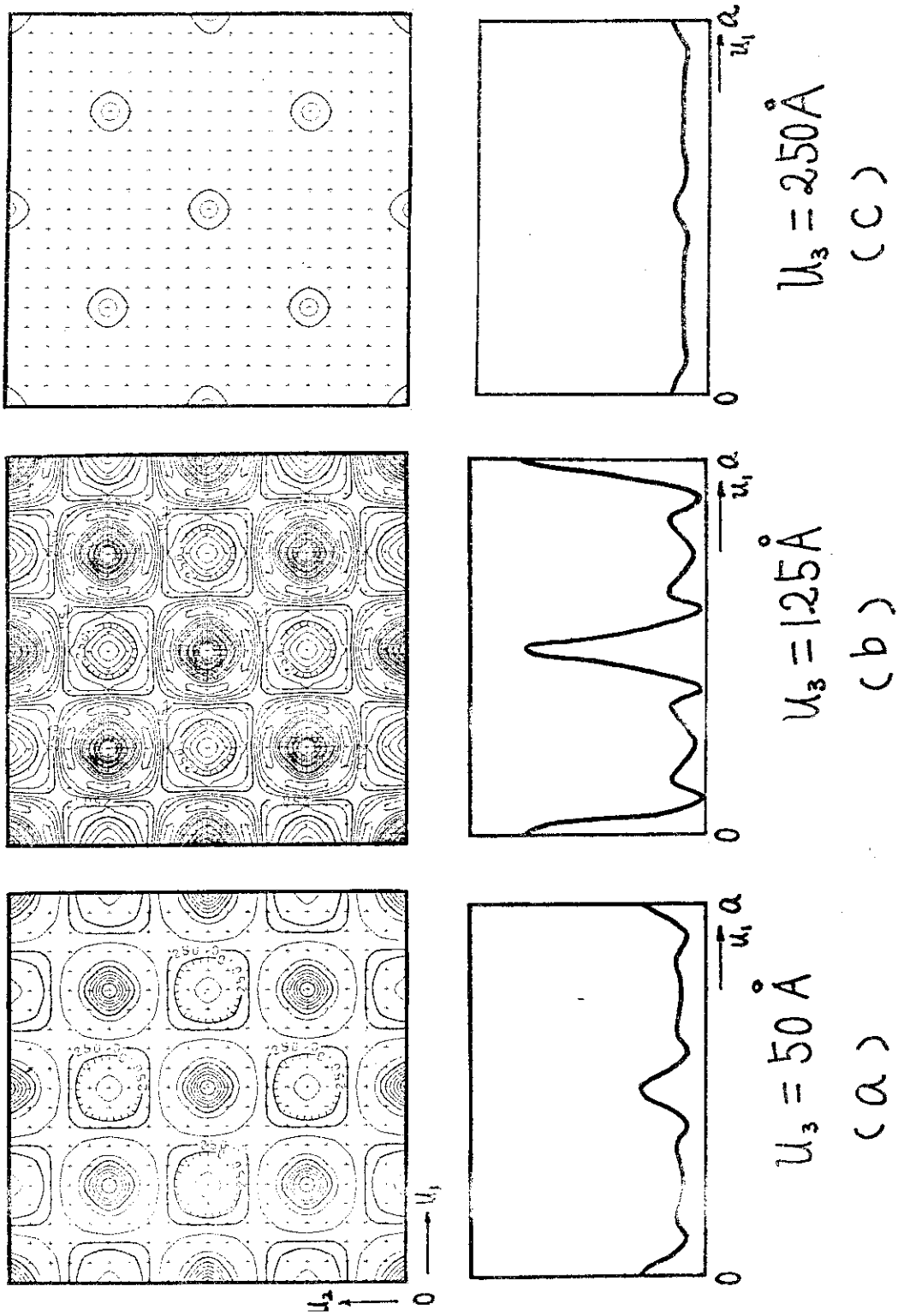


Fig. 2.5.2 Distributions of the total current density in the transverse plane at the depths of 50 Å, 125 Å and 250 Å for the <100> directions of incidence. The curves in the lower part are the profiles at $u_2 = 0$ along $u_1$.

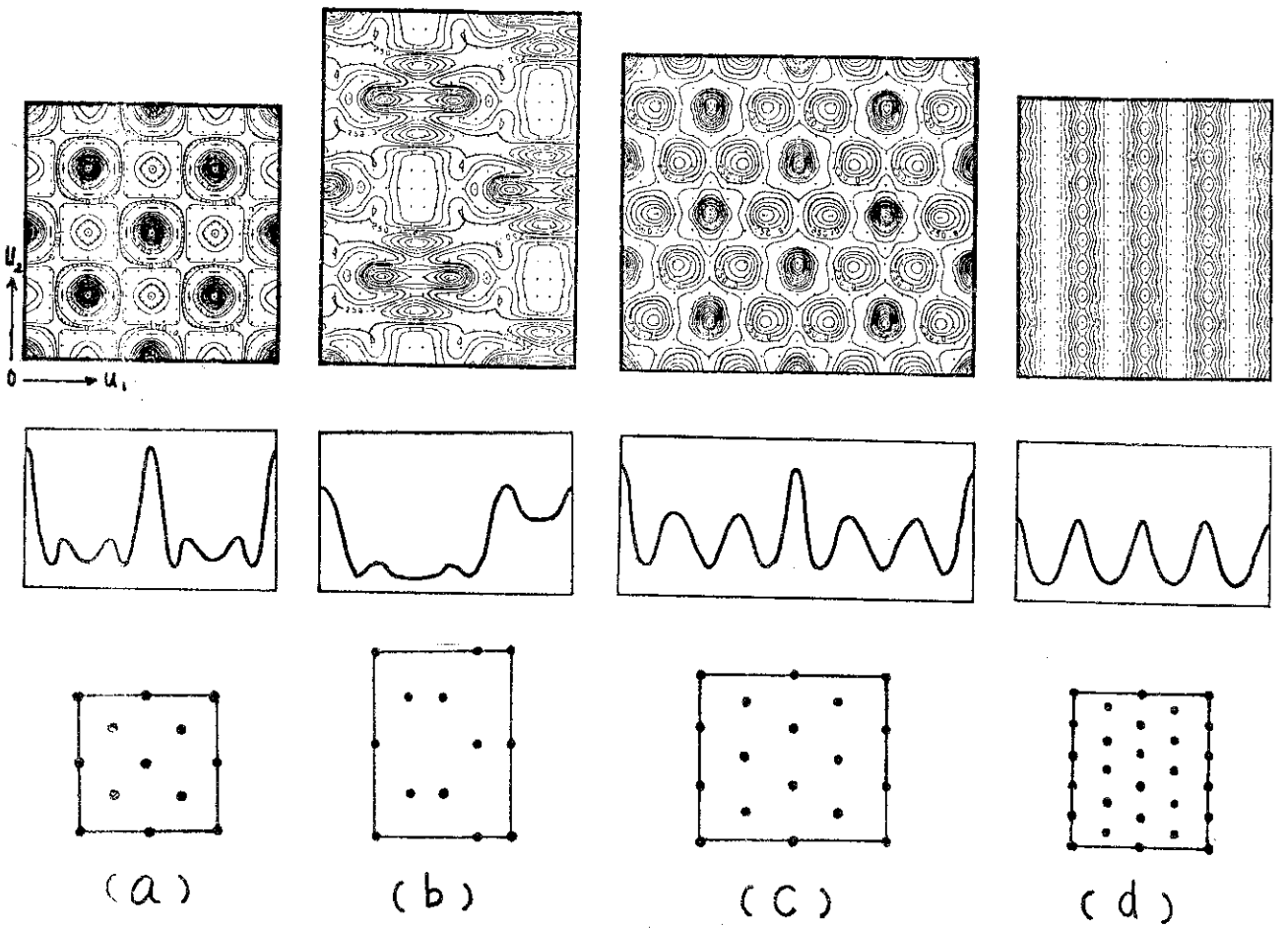


Fig. 2.5.3 The directional dependence of the two-dimensional distributions and the profiles of diagonal current density in the transverse plane, and the projected positions of atoms on the transverse planes are also schematically shown in (a), (b), (c) and (d) for the <100>, <110>, <111> and <120> directions of incidence respectively.

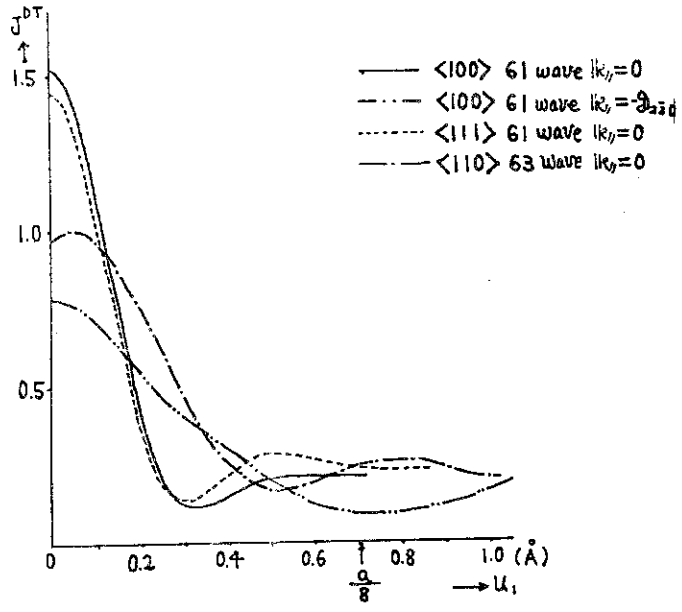


Fig. 2.5.4 Directional dependence of the profiles of the diagonal total current density obtained by 61- and 63- beam calculations for the <100>, <111> and <110> axial directions and for the slightly off axis case.

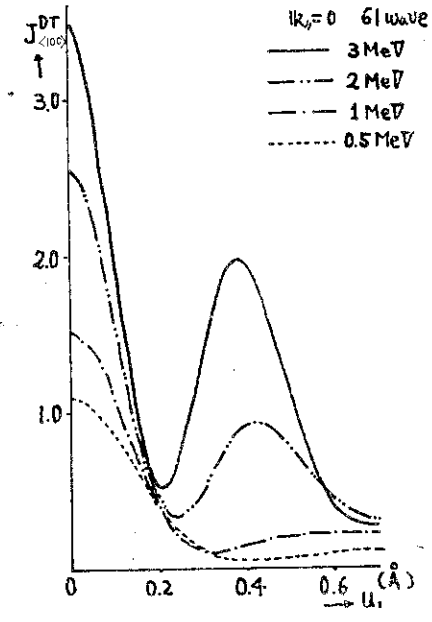


Fig. 2.5.5 The variation of the profiles of the diagonal total current density with the increase of the energy of 0.5 MeV to 3 MeV for the <100> axial case, obtained by 61- beam calculation. The characteristic sub-peak occurs at about 0.4 Å from the position of an atomic nucleus above ∿2 MeV.

## 2.6 Build-up and Decay of Fuel Actinides in the Fuel Cycle of Nuclear Reactors

K. Tasaka, Y. Kikuchi, R. Shindo, H. Yoshida and S. Yasukawa

Build-up and decay of fuel actinides have been studied for BWR, PWR, HWR, HTGR and LMFBR, which are fueled with uranium-oxide or mixed-oxide, and produce an electric power of 1000 MW. The following items were examined by using the evaluated nuclear data[1] and DCHAIN program[2),3)];

(1) quantities of plutonium and other fuel actinides built up in the reactor,
(2) cooling behaviors of fuel actinides in the spent fuels,
(3) activity of fuel actinides in the reprocessed plutonium and in the high-level reprecessing wastes as a function of storage time, and
(4) variation of plutonium composition under long-term irradiation.

From the calculated results the following have been revealed;

(1)-1. a uranium fueled thermal reactor produces about 300 kg of plutonium a year, 60 ∿ 74 % of which are $^{239}$Pu and $^{241}$Pu,
(1)-2. a mixed-oxide fueled thermal reactor produces about 68% of initial inventory of $^{239}$Pu and $^{241}$Pu per one fuel cycle,
(1)-3. a fast breeder reactor has a large internal breeding ratio and produces about 84% of $^{239}$Pu and $^{241}$Pu per one fuel cycle in the core,
(1)-4. activities of $^{238}$Pu and americium and curium isotopes produced in a LMFBR, especially in a blanket-plutonium fueled one, are much less than those in a mixed-oxide fueled thermal reactor,
(2)-1. α-activities are mainly contributed by $^{242}$Cm at short cooling times, by $^{241}$Am, $^{238}$Pu and $^{244}$Cm at more than one year, and by $^{237}$Np, $^{243}$Am, $^{236}$U and $^{238}$U at more than 10,000 years,
(2)-2. β-activities are mainly contributed by $^{241}$Pu and $^{237}$U at short cooling times, and by $^{239}$Np and $^{242}$Am at more than 100 years,
(3)-1. in the reprocessed plutonium, $^{238}$Pu, $^{239}$Pu, $^{240}$Pu and $^{241}$Am are principal α emitters, and $^{241}$Am build up strongly with storage time,
(3)-2. in the reprocessed plutonium, $^{241}$Pu is the only β emitter,
(3)-3. in the high-level reprocessing wastes the activity of each plutonium isotope increases markedly with storage time by the decay of each mother nuclide,
(4)-1. the activity of $^{238}$Pu increases rapidly with irradiation time in a

mixed-oxide fueled thermal reactor, that makes it difficult to utilize plutonium in a thermal reactor for many cycles, and

(4)-2. in a BWR-plutonium fueled LMFBR the content of $^{238}Pu$ saturates at the value lower than the initial amount for long-term irradiation.

It is concluded from the above results that for easy reprocessing and high-level waste management, as well as effective utilization of uranium resources, a thermal reactor should be fueled with uranium; the plutonium produced in a thermal reactor should be used in a fast reactor; and plutonium produced in the blanket of a fast reactor is more appropriate for a fast reactor than that from a thermal reactor.

References

1) Tasaka, K., et al.: JAERI-M 6541 (1976) (in Japanese).
2) Tasaka, K., Sasamoto, N.: "FP-S: Program for Calculation of Atomic Density of Each Fission Product Nuclide," JAERI-1198 (1971).
3) Tasaka, K.: to be published.

## 2.7 On Feasibility of Actinide Burning Fast Reactor in Reactor Physics Standpoint

H. Kuroi, K. Koyama, M. Obu and H. Mitani

The disposal of the long-lived radioactive waste produced in the nuclear fuel cycle is a problem that must be solved in any plan to introduce fission energy. As well as the fission products, the reactor produces numerous actinide isotope, about 90kg / 1000MWe / year, by neutron capture. Whereas the great majority of fission products decay to harmless elements in a relatively short time scale of 1000 years, time scale of greater than $10^5$ years must be considered for actinides. Geological stability can be reasonably assured over 1000 years so that adequate deep underground storage may be feasible to contain most fission product safely. However, there is no reliable way to ensure containment for the more than $10^5$ years necessary for actinides to decay to harmless levels.

Many suggestion are being considered for dealing with these actinide wastes, for example, outer space disposal, recycling in fast reactor or transmutation by fussion neutrons. From the viewpoint of waste disposal, neutron induced fission is one of the most suitable condidates for transmutation of actinides. Many of actinide has threshold type fission cross section, so that the harder neutron spectrum, the better for transmutation of actinide by the fission process.

As shown in Table 2.7.1, the average fission to capture rate ratios indicate that the neutron spectrum in typical LMFBR is rather soft for the transmutation of actinide. Consequently, the actinide distruction rate may not be sufficient in recycling concept using LMFBR, so that specially designed harder neutron spectrum reactor is necessary for efficient destruction of actinide waste. Taking into consideration of neutron economy and high destruction rate, we investigate feasibility and performance of an actinide burning fast reactor (ABFR) fueled with only actinide mixture contained in the waste from fuel reprocessing plant.

According to the report presented by Harries[1], a typical weight of actinide in the waste from reprocessing of fast reactor fuel is given in the Table 2.7.2. The uranium and plutonium recovery process has been assumed to be 99.5% efficient, so that the quantities in the table correspond to 0.5% of uranium and plutonium content of discharged fuel. When only the actinide waste is considered as reactor fuel, it is necessary to separate $^{238}U$ from

the other actinides given in Table 2.7.2, because large amount of $^{238}U$ in the actinide mixture is not favorable in the viewpoint of criticality and hard neutron spectrum required for the actinide burning reactor. Here, we use all actinides given in the table as reactor fuel, except uranium. The reactor type is assumed to be sodium cooled oxide fuel type and the volume % of reactor core is assumed to be Fuel / Structure / Coolant = 40/30/30.

The cross section data[2] used for the study are 25 group constants based on ENDFB/IV except $^{242}Cm$. The evaluated data by Henkelman[3] are used for obtaining the 25 group constants of $^{242}Cm$. The 25 group constant of $^{240}Pu$ or $^{241}Pu$ are employed instead of cross section data absent in ENDFB/IV data file.

Criticality of reactor was investigated by means of 25 energy group Sn approximation. The $K_\infty$ of the core was found to be 1.85 and critical radius in spherical bare geometry was about 30cm. The mass coefficient was found to be 2.2%$\Delta$k/k/cm. The fission and capture rate ratio in the ABFR core is also given in Table 2.7.1, together with those in LMFBR and JEZEBEL. The ratio of actinide reactivity worth to the $^{239}Pu$ reactivity worth in ABFR is given in Table 2.7.3. Owing to hard neutron spectrum achieved in ABFR, fairly large reactivity worth is obtained, even for the actinide whose fission cross section is a threshold type. From these results, it is found that the reactor has sufficient reactivity for power operation at the beginning of core life.

Then we have performed burn-up analysis of the reactor using the computer code ORIGEN[4] in order to check an abnormal reactivity reduction due to selective burning occurred in certain nuclides. For this purpose, readymade cross section data library in ORIGEN provided for LMFBR burn-up analysis is replaced with one-group cross sections newly obtained using neutron spectrum in the ABFR as an weighting function. Typical results are summarized in Table 2.7.4. In this table, concentration change in each nuclide corresponding to reactor operation of 14000 MWd total power output is given in % change and also in kg. The reactivity change due to above concentration change was found to be about -3.5%$\Delta$k/k. As seen in the table, fairly large amount of actinide nuclides other than $^{239}Pu$ was destructed to fission product. Since the ratio of the per cent reactivity reduction to the per cent fuel depletion is about 1, reactivity adjustment during power operation seems to be well manageable. Insofar as the present nuclear data are concerned, the ABFR concept seems to be feasible in reactor physics point of view.

References

1) Harries, J.R.: The Transmutation of Radioactive Reactor Waste, Australian Atomic Energy Commision, (1972).

2) Kikuchi, Y.: Private Communication

3) Hinkelman, B.: KFK-1186, (1970).

4) Bell, M.J.: ORNL-4628, (1973).

Table 2.7.1 Average fission to capture rate ratios in various reactor spectrum

| Nuclide | LMFBR | ABFR | JEZEBEL |
|---|---|---|---|
| $^{237}Np$ | 0.264 | 1.00 | 4.47 |
| $^{238}Pu$ | 2.98 | 9.78 | 32.1 |
| $^{239}Pu$ | 3.84 | 8.57 | 20.3 |
| $^{240}Pu$ | 0.434 | 1.68 | 5.55 |
| $^{241}Pu$ | 6.29 | 9.60 | 18.2 |
| $^{242}Pu$ | 0.84 | 3.73 | 14.1 |
| $^{241}Am$ | 0.42 | 1.43 | 9.71 |
| $^{242}Am$ | 7.45 | 13.1 | 22.0 |
| $^{243}Am$ | 0.28 | 1.34 | 7.9 |
| $^{243}Cm$ | 5.34 | 10.6 | 26.4 |
| $^{244}Cm$ | 1.28 | 5.60 | 17.6 |

Table 2.7.2 Actinide waste from LMFBR per 1000 MWd

| Nuclide | Waste (g) |
|---|---|
| $^{235}U$ | 0.215 |
| $^{236}U$ | 0.0057 |
| $^{238}U$ | 133.0 |
| $^{237}Np$ | 3.82 |
| $^{238}Pu$ | 0.101 |
| $^{239}Pu$ | 8.83 |
| $^{240}Pu$ | 2.92 |
| $^{241}Pu$ | 0.797 |
| $^{242}Pu$ | 0.494 |
| $^{241}Am$ | 14.7 |
| $^{243}Am$ | 7.72 |
| $^{242}Cm$ | 0.600 |
| $^{244}Cm$ | 0.564 |

Table 2.7.3 Ratio of sample reactivity worth of threshold fission type nuclide to that of $^{239}Pu$

| Nuclide | $\Delta\rho$ / $\Delta\rho$ ($^{239}Pu$) |
|---|---|
| $^{237}Np$ | 0.170 |
| $^{240}Pu$ | 0.226 |
| $^{242}Pu$ | 0.170 |
| $^{241}Am$ | 0.191 |
| $^{243}Am$ | 0.107 |

Table 2.7.4 Burn-up performance of ABFR ( 14000 MWd )

| Nuclide | depletion in % | depletion in kg |
|---|---|---|
| $^{237}Np$ | -4.5 | -1.75 |
| $^{238}Pu$ | +190.0 | +2.02 |
| $^{239}Pu$ | -7.8 | -7.17 |
| $^{240}Pu$ | -0.7 | -0.22 |
| $^{241}Pu$ | -8.2 | -0.7 |
| $^{242}Pu$ | +5.0 | +1.1 |
| $^{241}Am$ | -3.6 | -5.5 |
| $^{243}Am$ | -3.0 | -2.4 |
| $^{243}Cm$ | -22.0 | -0.7 |
| $^{244}Cm$ | +14.0 | +0.4 |
| the other actinide | | +0.8 |

## 2.8 Topics of Scientific Subroutine Library and Numerical Evaluations of Algorithms for Interpolations and Least-Squares

T. Ise, T. Fuzimura, T. Nishida, T. Suzuki and T. Tsutsui

Some programs have been added to our SSL (Scientific Subroutine Library): a fast Fourier transformation, a Gaussian quadrature and a plotting routine, in addition to a conversion program of binary mode from CDC to FACOM computer. Furthermore, algorithms and computer programs are evaluated on the interpolations[1] and the least-squares[2].

We have recognized that the interpolation using rational function is more exact approximation than that using polynomials, though the former is a little laboured. Stoer, Krogh and Guftafson have developed the algorithms based on them and the methods due to Krogh and Guftafson are more precise. The spline interpolation gives a good smooth form but the curve fitted by the interpolation is not necessarily valid. Cline and Akima, separately, have got success in developing the new algorithm, what is known as the spline under tension, eliminating these unnatural wiggles. Lagerlöf's interpolation using spline-like the rounded ramp function is valuable, too.

Useful algorithms are also found in the least-squares. The algorithms due to Reinsch, Schumaker and Ichida belong to the smoothing method based on piece-wise polynomials. Many programs have been developed for analyzing the gamma-ray spectrum. New algorithms about the non-linear least-squares have been found, in addition to the conventional Marquardt's

method. They are Brown's algorithm which is an extension of the method without using derivative and Keller's one based on the projection method.

The above-mentioned algorithms will give a help to enlarge the SSL, since they have clear mathematical bases and many of them programmed as computer subroutines.

References

1) Ise, T., Fuzimura, T.: "Recent Algorithms and Computer Programs for Interpolation", J. Information Processing Soc. Japan, 17, 417 (1976) (in Japanese).

2) Ise, T., Nishida, T., Suzuki, T.: "Recent Computer Programs for Least-Squares Problems", J. Atomic Energy Soc. Japan, 18, 89 (1976) (in Japanese).

# 3. Integral Experiment and Analysis

## 3.1 Critical Experiment on the Sector Mockup System for Prototype Fast Breeder Reactor MONJU (FCA Assembly VII-1)

T. Iijima, N. Mizoo, M. Nakano, K. Shirakata, T. Nakamura, K. Ogura*, H. Mitani, S. Fujisaki, H. Ogawa, K. Yamagishi, J. Yamamoto**, J. Yang***, T. Mukaiyama and J. Hirota

FCA Assembly VII-1 is a sector type mockup of MONJU, in which, for the reason of the limited amount of Pu fuel inventry, the core consists of Pu-fueled sector test regions simulating the MONJU core compositions and U-235-fueled driver regions (Fig. 3.1.1). The critical experiment was started after the completion of enlargement of the FCA matrix assembly from 35x35 to 51x51, and went critical on July 18th, 1975.

Previous to the experiment, determination of optimun driver composition, applicability or limit of sector type mockup, simulating accuracy of the quantities of the full mockup system by the sector system, and possible experiments in the sector mockup system were intensively studied.[1] The compositions of driver regions were so determined as to match the characteristics between driver and test regions; the three quantities, (i) fundamental mode spectrum $\phi_m(E)$, (ii) material buckling $B_m^2$, and (iii) diffusion coefficient $\overline{D}$ of the drivers were equalised to those of the corresponding test regions. Calculated distribution properties of the sector system were compared with the full mockup system and it was made clear that the deviation of the neutron spectrum, the reaction rate distribution, and the reactivity worth distribution in the test region from the full mockup system are very small.

The critical mass for the full mockup system, i.e., the system fully composed of test regions was determined as 718 $\pm$ 6 kg of Pu-fissile by substitution reactivity measurements between driver and test regions. By the fuel density coefficient method, the reactivity scale for the full mockup system was also determined.

In order to investigate experimentally the applicability of sector type mockup, radial distributions of fission rates (U-235, U-238 and Pu-239) and sample worths (U-235, $B_4C$ and Cf-252) were measured by changing the sector

* Nagoya University,
** Osaka University,
*** Korea Atomic Energy Research Institute

The work performed under contract between PNC and JAERI

angle. The results indicate that quantities such as power distribution and reactivity worth of the full mockup system can be obtained by the measurements with the sector system. This means that the experimental results in the sector system can be analysed on the model of full mockup system.

Various experiments to support the design of MONJU, i.e., power distribution, density coefficients, control rod effects, etc., have been measured (cf. §3.2, 3.5, and 3.6). The neutron streaming effect in plate lattice cells has also been investigated (cf. §3.3 and 3.4).

Reference

1) Iijima, T., et al.: "A Study of the Sector Mockup System for Prototype Fast Breeder Reactor MONJU," Reactor Engineering Division Annual Report (April 1, 1974～March 31, 1975), pp. 68-70 (§3.4), JAERI-M 6320 (1975).

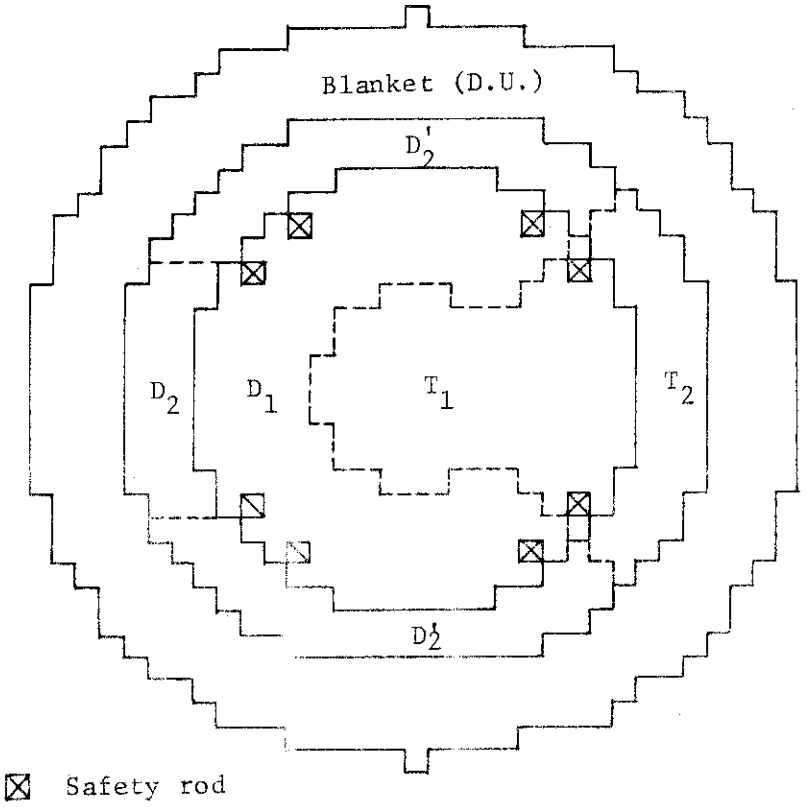


⊠ Safety rod

⊠ Control rod

$T_1$, $T_2$ : Test region

$D_1$, $D_2$, $D_2'$ : Driver

Fig. 3.1.1 Loading pattern of FCA Assembly VII-1

## 3.2 Application of the Density Coefficient Method to Two-Zone Core Fast Reactors

T. Iijima, K. Shirakata and K. Ogura*

In large fast power reactors, the core is usually two-zone type with high enrichment region in outer core for flattening of the power distribution. The Density Coefficient Method (D.C.M.)[1)~5)], which enables to predict experimentally the criticality of an unknown reactor with high accuracy, is already well established for one-region core. The applicability of the method for two-zone core has been intensively studied in connection with Prototype Fast Breeder Reactor MONJU.

In mockup experiments, it is difficult to build the same core composition and volume as a given reactor. Then, D.C.M. was developed for an experimental determination of the reactivity change between the mockup and the given reactor. Fig. 3.2.1 shows the procedure of D.C.M.. The criticality of the given reactor is determined by two steps; (1) extrapolation in composition and (2) extrapolation in volume.

The composition extrapolation consists of measuring the density coefficient Cm for each core constituent material in the mockup system and determining, by an extrapolation, the reactivity effect due to the composition difference, $\Delta\rho = \sum_m Cm \cdot \Delta Nm$. However, such a linear extrapolation is not applicable for a large composition difference because the density coefficient changes with the density. A modified extrapolation is adopted in D.C.M.. According to the exact perturbation theory, the reactivity change is expressed as

$$\Delta\rho_{1\to 2} = \frac{\frac{1}{k'} < \phi_1^+ \Delta F \phi' > - < \phi_1^+ \Delta A \phi' >}{< \phi_1^+ F \phi' >} \quad , \qquad (1)$$

where $\Delta F$ and $\Delta A$ are the changes in the fission source and removal pperators, and $< >$ means the energy and space integral over the reactor. Approximating $\phi'$ by $\phi_1$, the effective density coefficients between the composition 1 and 2 are given as

$$\bar{C}_m = C_{m1} \cdot \left( \frac{\overline{\nu\sigma}_f}{k'} - \bar{\sigma}_a \right) \Big/ \left( \frac{\overline{\nu\sigma}_f}{k_1} - \bar{\sigma}_a \right) \qquad (2)$$

for fissile material, $\bar{C}m = Cm_1$ for absorbing material, and $\bar{C}m = Cm_1 \cdot \bar{D}_2/\bar{D}_1$ for scattering material, where $\overline{\nu\sigma}_f$ and $\bar{\sigma}_a$ are the bilinear average by $\phi_1$ and $\phi_1^+$, and $\bar{D}$'s are the one-group diffusion coefficient. Then, the reactivity

* Nagoya University

change is obtained by $\Delta\rho_{1\to 2} = \sum_m \bar{C}_m \cdot \Delta N_m$.

The volume extrapolation is to obtain the reactivity change due to the core volume change. To perform this accurately even for a large volume change, a calculated "k-ratio", $k_2/k'$ is used. The k-ratio is usually accurate quantity because errors in cross-section are almost cancelled out, i.e., only non-leakage probability is contained in it:

$$\frac{k_2}{k'} = \frac{k_{\infty 2} \cdot P(V_2)}{k_{\infty 2} \cdot P(V_1)} = \frac{P(V_2)}{P(V_1)} \quad . \tag{3}$$

The "experimental" $k_2$ value for $V_2$ is obtained by multiplying the k-ratio to the "experimental" k'-value obtained by composition extrapolation.

In FCA Assembly VII-1 (cf. §3.1), the density coefficient measurements were performed with the sector test region. The density coefficients were obtained by reactivity traverse measurements with "Sample drawer" and their volume integration over the inner or outer core. The reactivity scale for the full mockup system was adopted (cf. §3.1). Results are given in Table 3.2.1 together with calculated density coefficients by perturbation code SIMPLE-D using three cross-section sets.

In order to investigate the applicability of the D.C.M. for two-zone core, the criticality of equilibrium core of MONJU was estimated. The results are given in Table 3.2.1 and 3.2.2. The comparison of k'-values between the direct diffusion calculation (direct-k) and the D.C.M. using three different cross-section sets shows that composition extrapolation is very accurate even for the large composition change ($\sum_m |\Delta\rho_m| = 33\%\Delta k/k$, in spite of $\sum_m \Delta\rho_m = 0.83\%\Delta k/k$). The accuracy of volume extrapolation is also good. The overall accuracy is estimated as $< \pm 0.4\%\Delta k/k$. On the other hand, the prediction accuracy of k-value of MONJU equilibrium core by the present cross-section sets is, as seen in Table 3.2.1, $\sim \pm 2\%\Delta k/k$, in which the effects of Pu higher isotopes take the major part. Present results shows the usefulness of D.C.M. for large fast reactors.

References

1) Iijima, T., et al.: Measurement and Analysis of Density Coefficient on FCA V, JAERI-M 5890 (1974) (in Japanese).

2) Iijima, T., et al.: Density Coefficient Measurements in FCA Assembly VI-1, JAERI-M 6062 (1975) (in Japanese).

3) Iijima, T.: Application of the Density Coefficient Method for Large Fast Reactors, JAERI-M 6063 (1975) (in Japanese).

4) Hirota, J., et al.: "Recent Progress in Fast Integral Experiment and Analysis at FCA," Proc. International Symp. on Physics of Fast Reactors, Vol. I, p.506 (1973).

5) Iijima, T., Hirota, J.: "Density Coefficient Method and its Application," Reactor Engineering Division Annual Repor (April 1, 1973 to March 31, 1974), pp70-73, JAERI-M 5995 (1975).

Table 3.2.1 Density coefficients of FCA VII-1 core

( $\Delta k/k$ / $10^{24}$atoms/cm$^3$ )

| | Material | Experiment | Calculation | | |
|---|---|---|---|---|---|
| | | | JAERI-F/II | RCBN | ABBN |
| Inner core | Pu-239 | 343.2 ± 3.4 | 345.1 | 343.6 | 348.5 |
| | -240 | 33.5 ± 1.2 | 43.4 | 37.8 | 11.0 |
| | -241 | 524.0 ± 6.6 | 615.2 | 541.9 | 548.4 |
| | U-235 | 271.0 ± 2.7 | 267.5 | 275.0 | 263.8 |
| | -238 | -16.73 ± 0.17 | -15.80 | -16.73 | -13.51 |
| | O | 0.385 ± 0.006 | 0.1238 | 0.8509 | 0.6658 |
| | Na | -0.088 ± 0.002 | 0.7400 | 1.2376 | 0.7350 |
| | Al | -0.366 ± 0.008 | -0.2619 | 0.0147 | 0.0102 |
| | SUS | -0.768 ± 0.009 | -1.0052 | -0.7242 | -0.3635 |
| | Mo | ——— | -22.91 | -42.96 | -12.10 |
| | Pu-242 | ——— | ——— | 30.14 | 13.46 |
| Outer core | Pu-239 | 102.9 ± 1.0 | 100.5 | 96.8 | 98.2 |
| | -240 | 19.7 ± 0.9 | 17.7 | 16.3 | 9.4 |
| | -241 | 145.1 ± 3.4 | 170.6 | 144.4 | 142.7 |
| | U-235 | 85.5 ± 0.9 | 75.6 | 76.1 | 72.6 |
| | -238 | -2.62 ± 0.03 | -2.20 | -2.31 | -1.58 |
| | O | 0.693 ± 0.008 | 0.5978 | 0.8313 | 0.7947 |
| | Na | 0.574 ± 0.006 | 0.7847 | 1.0309 | 0.8918 |
| | Al | 0.553 ± 0.010 | 0.5547 | 0.6087 | 0.6075 |
| | SUS | 0.431 ± 0.006 | 0.3959 | 0.5454 | 0.5371 |
| | Mo | ——— | -3.73 | -7.06 | -1.56 |
| | Pu-242 | ——— | ——— | 13.56 | 9.01 |

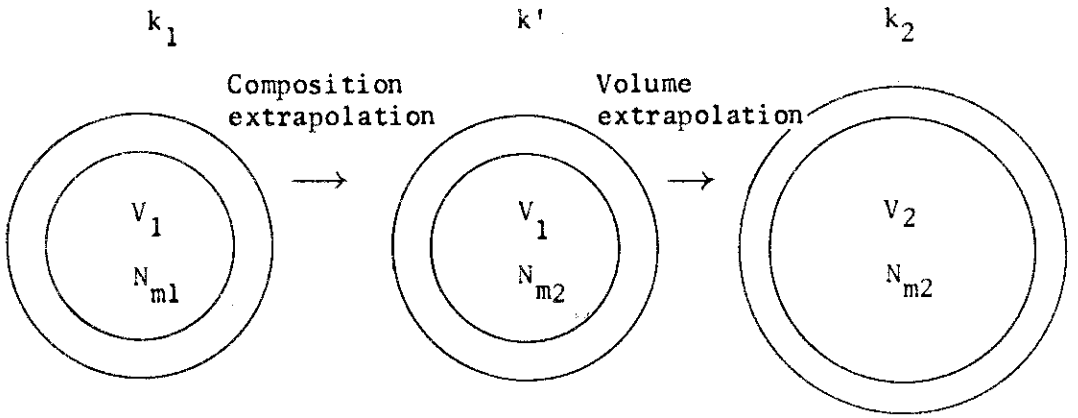


Fig. 3.2.1 Procedure of the Density Coefficient Method

Table 3.2.2 Summary of criticality estimation of MONJU

| | Composition extrapolation ($N_m$(VI-1) → $N_m$(MONJU)) | | | | Volume extrapolation* ($V_1 \rightarrow V_2$, $N_m$(MONJU)) | |
|---|---|---|---|---|---|---|
| | $k_1$ Direkt-k | $k'$ Direct-k | $k'$ D.C.M. | ($\Delta\rho$(%$\Delta$k/k)) | $k_2$ Direct-k | ($k_2/k'$) |
| Calculation JAERI-F/II | 0.997 | 1.025 | 1.025 | (2.745) | 1.072 | (1.046) |
| RCBN | 0.983 | 0.987 | 0.984 | (0.097) | 1.035 | (1.048) |
| ABBN | 1.038 | 1.034 | 1.036 | (-0.145) | 1.085 | (1.049) |
| Experiment** | 1.000 | —— | 1.008 ±0.001 | (0.83 ±0.1) | 1.055 ±0.001 | (1.046) |

* $V_1$=1414 ℓ, $V_2$=2336 ℓ

**The error due to the experimental errors in density coefficients

Table 3.2.2 Reactivity contributions

| | Material m | Correction factor $f_m$* | $\Delta\rho_m$(%$\Delta$k/k) |
|---|---|---|---|
| Inner core | Pu-239 | 0.987 | -9.81 |
| | Pu-240 | 0.977 | 0.89 |
| | Pu-241 | 0.988 | 8.99 |
| | U-235 | 0.984 | -0.10 |
| | U-238 | 1.007 | 2.04 |
| | O | 1.063 | -0.13 |
| | Na | " | -0.01 |
| | Al | " | 0.09 |
| | SUS | " | -0.28 |
| | Mo** | " | -0.40** |
| Outer core | Pu-239 | 0.987 | -5.04 |
| | Pu-240 | 0.983 | 0.73 |
| | Pu-241 | 0.988 | 3.48 |
| | U-235 | 0.985 | -0.04 |
| | U-238 | 1.016 | 0.46 |
| | O | 1.043 | -0.11 |
| | Na | " | 0.07 |
| | Al | " | -0.08 |
| | SUS | " | 0.12 |
| | Mo** | " | -0.05** |
| | $\Sigma_m \Delta\rho_m$ | 0.83 ± 0.11 | |
| | k' | 1.0083 ± 0.0011*** | |

* Calculated value by JAERI-F/II, $f_m = \bar{C}_m / C_{mi}$

** Calculated by ABBN,

*** k'=1.0083 ± 0.0011 by $f_m$(RCBN)
k'=1.0075 ± 0.0011 by $f_m$(ABBN)

## 3.3 Measurement of the Anisotropy of Diffusion Coefficient in Plate Cell[1)]

K. Shirakata, T. Iijima and K. Yamagishi

In most fast critical assemblies the reactor core is composed of plate type fuel and other materials. The neutron diffusion in such a plate lattice is anisotropic ; the diffusion coefficient for parallel direction to lattice plate is usually several percent larger than that for perpendicular direction. The diffusion coefficient anisotropy affects the criticality, sodium void effect and other reactor properties.

In the FCA VII-1 core, the parallel to perpendicular ratio of diffusion coefficients $\tilde{D}_{\parallel}/\tilde{D}_{\perp}$ was determined from the reactivity change due to 90° turning of plate direction in the core and compared with cell calculation by Benoist's formula[2)].

The method of determination of $\tilde{D}_{\parallel}/\tilde{D}_{\perp}$ is based on the relation between the change in diffusion coefficient and the induced reactivity change. As shown in Fig. 3.3.1, the plate direction of the test region V is turned by 90 degrees from vertical to horizontal, and the induced reactivity change $\Delta\rho$ is measured.

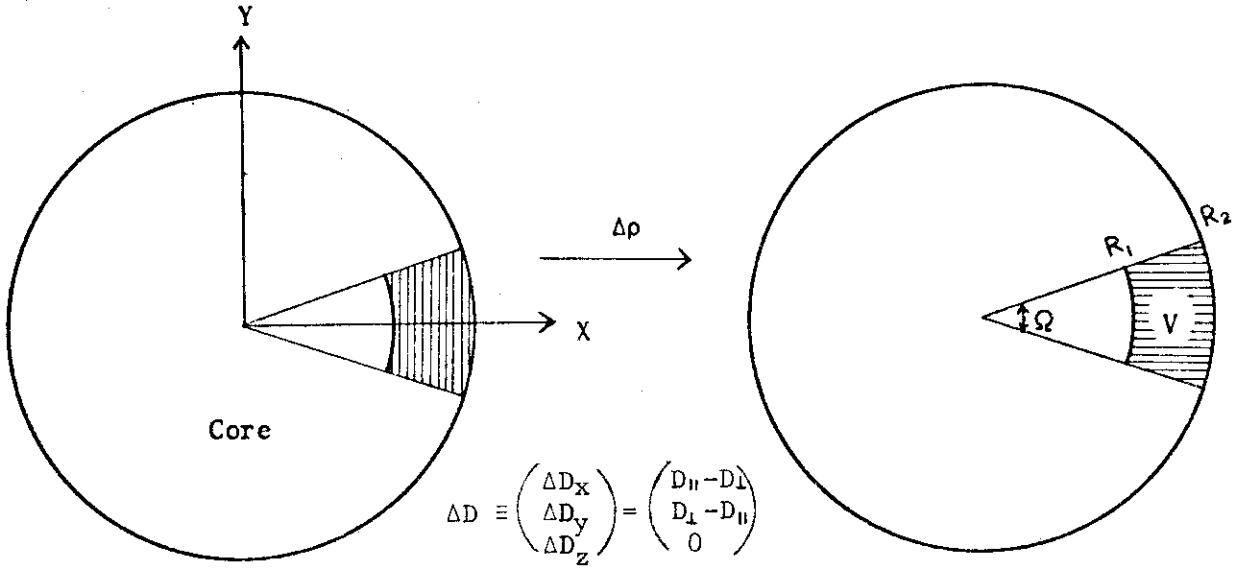


Fig. 3.3.1 Measurement of diffusion coefficient anisotropy

The change of the directional diffusion coefficients of the test region, $\Delta D$ results in the reactivity change $\Delta\rho$ ;

$$\Delta\rho = - \frac{<\mathrm{grad}\,\phi^{+}\cdot\Delta D\,\mathrm{grad}\,\phi>_{V}}{<\phi^{+}F\phi>_{\mathrm{reactor}}}$$

$$= - \frac{1}{<\phi^{+}F\phi>_{r}} \int\int\int_{V}\int_{0}^{\infty} \left(\Delta D_{x}\frac{\partial\phi^{+}}{\partial x}\frac{\partial\phi}{\partial x} + \Delta D_{y}\frac{\partial\phi^{+}}{\partial y}\frac{\partial\phi}{\partial y}\right) dE\cdot dx\cdot dy\cdot dz \qquad (1)$$

by the perturbation theory, where $<\ >$ means energy and space integrations and the z component is omitted on account of $\Delta D_z = 0$. Using general relations between the x, y and the r, $\theta$ coordinates as

$$\frac{\partial}{\partial x} = \cos\theta\frac{\partial}{\partial r} - \frac{\sin\theta}{r}\frac{\partial}{\partial\theta} \quad , \qquad \frac{\partial}{\partial y} = \sin\theta\frac{\partial}{\partial r} + \frac{\cos\theta}{r}\frac{\partial}{\partial\theta} \quad , \qquad (2)$$

with the assumption $\frac{\partial\phi}{r\partial\theta} << \frac{\partial\phi}{\partial r}$ and $\frac{\partial\phi^{+}}{r\partial\theta} << \frac{\partial\phi^{+}}{\partial r}$, Eq.(2) leads to

$$\Delta\rho = - \frac{1}{<\phi^{+}F\phi>_{r}} \int_{0}^{H}\int_{R_1-\frac{\Omega}{2}}^{R_2+\frac{\Omega}{2}}\int_{0}^{\infty} \left\{\frac{\partial\phi^{+}}{\partial r}\frac{\partial\phi}{\partial r}\left(\Delta D_{x}\cos^{2}\theta + \Delta D_{y}\sin^{2}\theta\right)\right\} dE\cdot d\theta\cdot r dr\cdot dz$$

$$= - \frac{<\frac{\partial\phi^{+}}{\partial r}\cdot D_{\perp}\frac{\partial\phi}{\partial r}>_{V}}{<\phi^{+}F\phi>_{r}} \cdot \frac{\sin\Omega}{\Omega} \cdot \frac{\tilde{D}_{\parallel}-\tilde{D}_{\perp}}{\tilde{D}_{\perp}} \equiv f\cdot\left(\frac{\tilde{D}_{\parallel}}{\tilde{D}_{\perp}} - 1\right) \quad , \qquad (3)$$

where $\tilde{D}_i$ means the effective (one-group) diffusion coefficient, i. e., flux weighted average over energy and space. Since it is known by calculational studies that the conventional isotropic diffusion coefficient in a plate cell is nearly equall to the perpendicular coefficient $D_\perp$, the sensitivity factor f by the isotropic coefficient $D_h$,

$$f = - \frac{<\frac{\partial\phi^{+}}{\partial r}\cdot D_{h}\frac{\partial\phi}{\partial r}>_{V}}{<\phi^{+}F\phi>_{\mathrm{reactor}}} \cdot \frac{\sin\Omega}{\Omega} \qquad (4)$$

can be used with accuracy. The value of f can be obtained by the conventional diffusion calculation. By Eq.(3), the reactivity change is straightforwardly related to the anisotropy.

Measurements were made using the sector region of FCA Assembly VII-1, a mockup for the Prototype Fast Breeder Reactor MONJU. Using the relation

$\Delta\rho = (\tilde{D}_{//}/\tilde{D}_{\perp}-1)\cdot f$, the anisotropy $\tilde{D}_{//}/\tilde{D}_{\perp}$ was determined from the measured reactivity change due to changing of the plate direction. Experiments were performed for several cell patterns ; standard cells and sodium voided cells in the inner-and outer-core regions. The results are given in Table 3.3.1.

Directional diffusion coefficients, $D_{//}$ and $D_{\perp}$ were also calculated by the code LAMP-B[3] using 70-group constants AGLI-70. The cell calculation is based on the collision probability method. The cell model is infinite slab geometry. It has been found that the $D_{//}$ is very sensitive to the cell model, e. g., to the way of smearing of the structural stainless steel into the cell, while the $D_{\perp}$ is insensitive to the cell model and nearly equal to the conventional diffusion coefficient $D_h$. The effective (one-group) diffusion coefficients $\tilde{D}_{//}$ and $\tilde{D}_{\perp}$, hence $\tilde{D}_{//}/\tilde{D}_{\perp}$, were obtained by averaging over the fundamental mode spectrum. The results are shown in Table 3.3.1. It should be noted that the experimental $\tilde{D}_{//}/\tilde{D}_{\perp}$ is not for the fundamental mode spectrum, but for the spectrum of the reactor core. However, the ratio $\tilde{D}_{//}/\tilde{D}_{\perp}$ is very insensitive to the neutron spectrum.

Table 3.3.1 Anisotropy $\tilde{D}_{//}/\tilde{D}_{\perp}$ of FCA VII-1 cells

| Cell | | Experiment | Calculation (Benoist) |
|---|---|---|---|
| Outer core | Normal cell | 1.032 ± 0.001 | 1.029 |
| | Na-voided cell | 1.056 ± 0.001 | 1.063 |
| Inner core | Normal cell | 1.027 ± 0.005 | 1.030 |
| | Na-voided cell | 1.045 ± 0.004 | 1.064 |

References

1) Shirakata, K., Iijima, T., Yamagishi, K.: NEACRP-A-260 (1976).

2) Benoist, P.: CEA R-2278 (1964).

3) Tsuchihashi, K.: JAERI, to be published.

## 3.4 A Study of the Anisotropic Diffusion Effect on the Criticality of Plate Lattice Assembly [1)]

T. Iijima and K. Shirakata

The core structure of FCA type loading with plate lattice cell is essentially three-dimensional, whose reactor calculation requires 3D anisotropic diffusion equation taking into account the anisotropic diffusion coefficients. A more practical treatment for the effect has been proposed, in which a correction term for the anisotropy is applied to the conventional k-value and required calculations are the conventional isotropic diffusion calculation and the cell calculation of anisotropy.

From the analogy to Eq.(3) of the previous section (§3.3), the correction term to be applied to the k-value of isotropic calculation is assumed as

$$\Delta\rho = f_x \cdot \frac{\Delta\tilde{D}_x}{\tilde{D}_h} + f_y \cdot \frac{\Delta\tilde{D}_y}{\tilde{D}_h} + f_z \cdot \frac{\Delta\tilde{D}_z}{\tilde{D}_h} \quad , \tag{1}$$

where $\Delta\tilde{D}_i/\tilde{D}_h = (\tilde{D}_i - \tilde{D}_h)/\tilde{D}_h$ and $f_i$'s are the sensitivity factor. If the core is multi-regions, the correction term is the summation of Eq.(1) for each region.

The reactivity change from the isotropic system to the actual (anisotropic) system is, according to the perturbation theory,

$$\Delta\rho = -\frac{\langle \mathrm{grad}\,\phi^+ \cdot \Delta D \,\mathrm{grad}\,\phi \rangle_{\mathrm{reactor}}}{\langle \phi^+ F \phi \rangle_{\mathrm{reactor}}}$$

$$= -\frac{1}{\langle \phi^+ F \phi \rangle_r} \int_0^{HR} \int_{0}^{0} \int_{-\Pi}^{\Pi} \int_0^{\infty} \left\{ \frac{\partial \phi^+}{\partial r}\frac{\partial \phi}{\partial r}(\Delta D_x \cos^2\theta + \Delta D_y \sin^2\theta) + \frac{\partial \phi^+}{\partial z}\frac{\partial \phi}{\partial z}\Delta D_z \right\} dE \cdot d\theta \cdot r dr \cdot dz$$

$$= -\frac{1}{2}\frac{\left\langle \frac{\partial \phi^+}{\partial r} \cdot D_h \frac{\partial \phi}{\partial r} \right\rangle_{\mathrm{core}}}{\langle \phi^+ F \phi \rangle_{\mathrm{reactor}}} \left\{ \frac{\Delta\tilde{D}_x}{\tilde{D}_h} + \frac{\Delta\tilde{D}_y}{\tilde{D}_h} \right\} - \frac{\left\langle \frac{\partial \phi^+}{\partial z} \cdot D_h \frac{\partial \phi}{\partial z} \right\rangle_{\mathrm{core}}}{\langle \phi^+ F \phi \rangle_{\mathrm{reactor}}} \cdot \frac{\Delta\tilde{D}_z}{\tilde{D}_h} \quad . \tag{2}$$

Hence, the sensitivity factors are

$$f_x = f_y = -\frac{1}{2}\frac{<\frac{\partial\phi^+}{\partial r}\cdot D_h\frac{\partial\phi}{\partial r}>_{core}}{<\phi^+F\phi>_{reactor}} \quad \text{and} \quad f_z = -\frac{<\frac{\partial\phi^+}{\partial z}\cdot D_h\frac{\partial\phi}{\partial z}>_{core}}{<\phi^+F\phi>_{reactor}}, \tag{3}$$

which can be calculated by the conventional isotropic diffusion calculation. The values of the correction term in FCA VII-1 core are given in Table 3.4.1. In the table, the experimental values are obtained using the measured $\Delta\tilde{D}/\tilde{D}$, i.e., with the assumption $\tilde{D}_h=\tilde{D}_\perp$, and the calculational ones are obtained from the $\Delta\tilde{D}_i/\tilde{D}_h$ values by cell calculation.

As shown in the Table, the amount of anisotropy correction is fairly large, especially in sodium-voided core. The results indicate the importance of anisotropic diffusion problem.

Table 3.4.1 Anisotropy correction on FCA VII-1 criticality

| Core | Correction term (%Δk/k) | |
|---|---|---|
| | Experimental | Calculation |
| Normal | -0.42 ± 0.05 | -0.47 |
| Na-voided | -0.81 ± 0.05 | -1.24 |

Reference

1) Shirakata, K., Iijima, T., Yamagishi, K.: NEACRP-A-260 (1976).

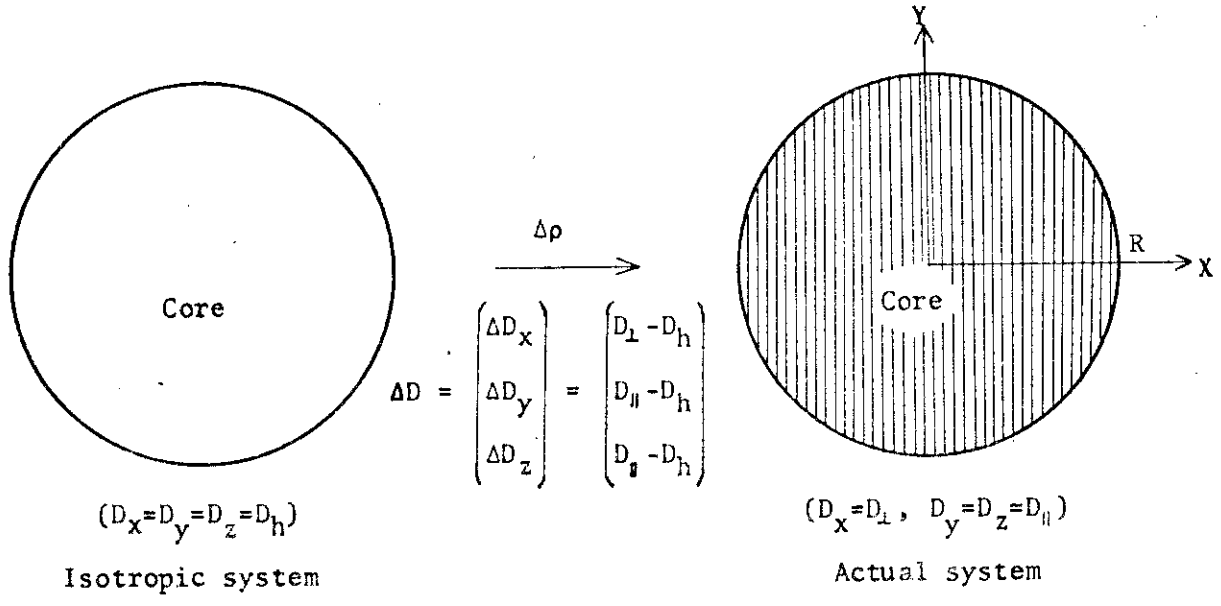


Fig. 3.4.1 Criticality correction for anisotropy

## 3.5 Subcriticality Measurement by Neutron Source Multiplication Method on Fast System with Non-uniform Source Distribution

N. Mizoo and M. Nakano

The accurate and reliable estimation of the subcritical reactivity of a reactor is required to preclude the possibility of accidental criticality or supercriticality during reactor maintenance and refueling operations. Neutron source multiplication technique(SM) is regarded as a principal method for measuring the subcriticality in an LMFBR. Non-uniform source distribution is likely to occur during refueling, because the neutron source is expected from the spontaneous fission of Pu fuel. Investigations have been made on the trends of the observed reactivities in the non-uniform source distributed systems, assemblies VII-1/90Z and VII-1/90B-10D of FCA.

Modelized cross sections of the assemblies VII-1/90Z and VII-1/90B-10D, together with the detector positions I,II and III, are shown in Fig.3.5.1 and 3.6.1, where T1, T2 and D2* regions are loaded with Pu fuel. These assemblies are modified versions of the assembly VII-1/90B.[1] Loading change had been made for outer core of the assembly VII-1/90B, of which D2 region was replaced with Pu fueld D2*. Modification of the inner core had also been introduced, providing cylindrical zone of T1 for the assembly VII-1/90Z. Det. I and Det.III were located on the vertical center line of the assembly and were apart from the neutron source. Det.II was placed at the point immediately adjoining T2 region, consequently its count rates might be contamined by the neutrons coming from the source directly.

Ten detectors, including three detectors above mentioned, were placed in and around the assemblies, and the weighted averages( $\bar{\rho}$ ) of the reactivities observed by them are reliable in the preliminary stages[2]. Several features can be pointed out through the comparison of the reactivities obtained by Det.I, II and III, as follows.

1) A $B_4C$ mock-up control rod with 3.2 Kg $B_4C$(73% enriched) was inserted at the core center in both assemblies and the subcritical reactivities were measured. The results are shown in Table 3.5.1, where the fractional deviations $\Delta_i$ ( $=(\rho_i - \bar{\rho})/\bar{\rho}$) of the observed reactivities( $\rho_i$) from the weighted averages ( $\bar{\rho}$ ) are indicated. The table showes that Det.I observes the systems more subcritical and Det.II does opposite due to the neutron source in the vicinity, measured reactivities of Det.II being lowered by 8~13%. Changes in the

neutron source distribution affect $\Delta_i$ more significantly for Det.I, which has no neutron source in the neiborhood.

2) The reactivities were measured on the assembly VII-1/90Z with a $B_4C$ mock-up control rod located at the core center, where the content and the enrichment of $B_4C$ were varied in several kinds. The fractional deviations $\Delta_i$'s are illustrated in Fig. 3.5.2, where the different tendencies are exhibited by Det.I and II. The overestimating trend of Det.I is pronounced as the subcriticality increases, while the saturation of the fractional deviations is suggested with Det.II .

3) Up to five $B_4C$ mock-up control rods with the same specification as the one in 1) were symmetrically distributed in T1 zone of the assembly VII-1/90Z, and the results are shown in Table 3.5.2 . $\Delta_i$'s begin to be widely apart from unity for opposite directions by the two detectors as the system becomes more subcritical, where more rapid change is displayed by Det.I .

4) The measurements in which a $B_4C$ rod was inserted at some points on X (horizontal center line) or Y(vertical one) axis of the assembly VII-1/90B-10D, were carried out to obtain $\Delta_i$'s of the detector on each axis. The results of the measurements are shown in Table 3.5.3 , where the positions of the $B_4C$ rod are indicated as the distance from the core center, the positive numbers standing for the detector side. $\Delta_i$'s have in all cases decreasing trends from positive to negative, according as the $B_4C$ rod is placed at further point from the detector. The variation in the fractional deviations of Det.II is small in the negative range of the rod position.

Thus, changes in the neutron source distribution fairly affect the observed reactivities of a detector. Care must be made on the measurement by the detector in the vicinity of neutron source, because its trends of the observed values are complex.

References

1) Iijima, T., et al.: 3.1 of this report.

2) Mizoo, N., et al.: "Reactivity Measurement on Far-subcritical Fast System," Proceedings of Specialists Meeting on Control Rod Measurement Techniques, Cadarache, April 21-22, 1976(to be published).

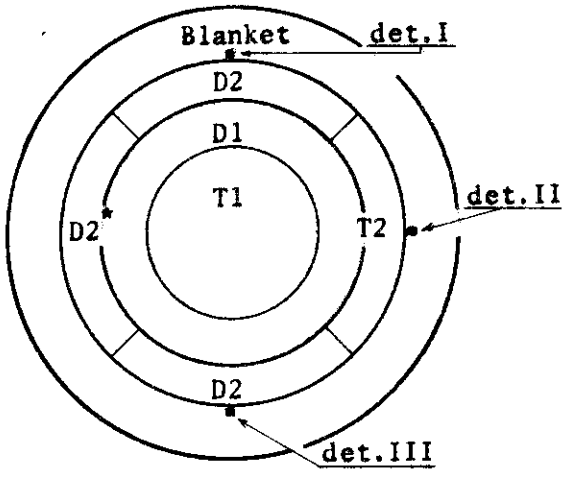


Fig. 3.5.1 Model of assembly VII-1/90Z

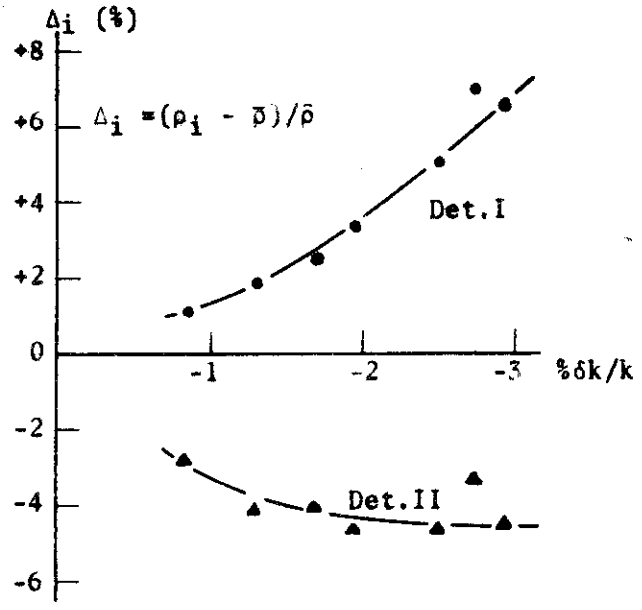


Fig. 3.5.2 Fractional deviations with $B_4C$ rod at core center

Table 3.5.1 Changes in the fractional deviations $\Delta_i$ by the neutron source distribution (in %)

| Sys. | Det.I | Det.II | Det.III |
|---|---|---|---|
| VII-1/90Z | +3.4 | -4.7 | +3.3 |
| VII-1/90B-10D | +6.4 | -6.3 | +7.3 |

$\bar{\rho}$ = -1.9 %δk/k, $\Delta_i = (\rho_i - \bar{\rho})/\bar{\rho}$ .
A $B_4C$ mock-up control rod is inserted at core center.

Table 3.5.2 Trends of the fractional deviations $\Delta_i$ with $B_4C$ rods distributed symmetrically in assembly VII-1/90Z

| $-\bar{\rho}$ (%δk/k) | Det.I(%) | Det.II(%) |
|---|---|---|
| 1.77 | +3.0 | -4.1 |
| 3.23 | +5.9 | -5.8 |
| 5.74 | +12.6 | -9.5 |
| 6.52 | +14.8 | -10.5 |

Table 3.5.3 Variations of the fractional deviations $\Delta_i$ by the $B_4C$ mock-up control rod positions in assembly VII-1/90B-10D

| Pos. (cm) | 60.7 | 44.2 | 22.1 | 0 | -44.2 |
|---|---|---|---|---|---|
| Det.I (%) | - | +37 | - | +6.4 | -5.0 |
| Det.II (%) | +42 | - | +1.7 | -6.3 | -9.5 |

## 3.6 Subcriticality Measurement by Inverse-Kinetic Rod Drop Method on FCA

N. Mizoo and M. Nakano

Inverse kinetic rod drop (IKRD) method was employed for the subcritical reactivity measurements on FCA assembly VII-1/90B-10D. Investigations have been made on the trends of the observed reactivities, which may be affected by the positions of the detectors, the singularities, the neutron source distribution and the subcriticality of the system.

The principle of IKRD method is based on the kinetic equations;

$$\dot{N} = (\rho-\beta)N/\Lambda + \sum_i \lambda_i C_i + S \ , \qquad \dot{C}_i = \beta_i N/\Lambda - \lambda_i C_i \qquad (1)$$

where the notations are as usual. Power history of a system N(t) being measured, the unknown variables in the above equations are $\rho$ and S, which must be constant after rod-drop. Then, $\rho$ (and S) can be obtained by means of least square fitting with measured N=N(t). Hence the method has an essential advantage of not requiring reactivity caliblation. While, a major disadvantage of the IKRD technique is the loss of dynamic range in the measurement as the system becomes far subcritical, which will result in highly imprecise estimates of $\rho$.

The assembly VII-1/90B-10D is a slightly modified version of the assembly VII-1/90B[1]. Cylindrically modelized cross section of the system is shown in Fig. 3.6.1. The spontaneous fission neutrons from Pu fuels loaded in T1, T2 and D2* regions were utilized as the neutron source. Time-dependent count rates were accumulated in 2000 ∿ 3000 channels with the dwell time of 0.1 sec. The rod-drop was carried out at the core center point O.

The observed reactivities of four detectors both by the IKRD and by the neutron source multiplication (SM) methods are shown in Table 3.6.1. The weighted averages of the observed reactivities with the SM method obtained by 10 detectors in and around the core are also indicated in the

first column of the table. Det.VI was located far from the core center (∿6M). Resultant reactivities through the rod-drop for the system denoted NOB are listed in the table, where initial state was -0.46$ subcritical. A $B_4C$ mock-up control rod was placed at the point B for 1BI and 1BO systems, each meaning the state before and after the rod-drop, respectively.

It is clarified that the observed reactivities of the IKRD method where the rod-drop's are carried out at the core center, show little position dependence compared with those of the SM method. The $B_4C$ mock-up control rod at the position B does not so affect the observed reactivities of Det.III in the case of the IKRD method. While Det.II has the trends of observing a system more reactive ( of smaller subcritical reactivity ) with the SM method caused by the neutron source in the vicinity of the detector[2], the IKRD technique does not validate such tendency. The indicated errors of the observed reactivities, by which the applicable range of the IKRD method is bounded, are mainly decided by the reactivity of the initial state and by the magnitude of the reactivity gap.

References

1) Iijima, T., et al.: §3.1 of this report.

2) Mizoo, N., Nakano, M.: § 3.5 of this report.

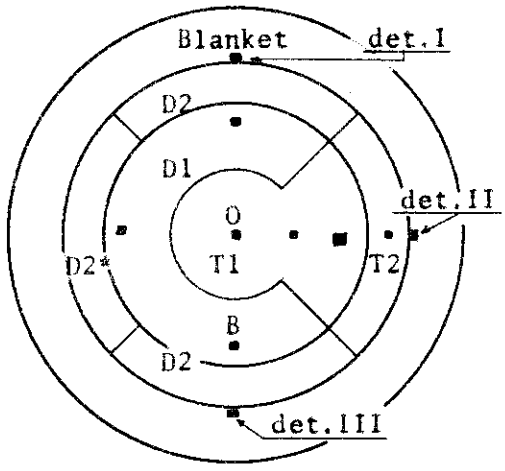


Fig. 3.6.1 Model of assembly VII-1/90B-10D

Table 3.6.1 Measured reactivities -ρ

( $ unit )

| Sys. | Det. | IKRD | SM |
|---|---|---|---|
| NOB 2.68[a] | I | 2.73 ± 0.07 | 2.81 ± 0.01 |
| | II | 2.67 ± 0.05 | 2.58 ± 0.01 |
| | III | 2.80 ± 0.04 | 2.92 ± 0.06 |
| | VI | 2.70 ± 0.05 | 2.65 ± 0.01 |
| 1BO 4.01[a] | I | 3.91 ± 0.80 | 3.94 ± 0.01 |
| | II | 3.86 ± 0.58 | 3.64 ± 0.01 |
| | III | 4.05 ± 0.29 | 5.92 ± 0.12 |
| | VI | 4.12 ± 0.58 | 3.92 ± 0.01 |
| 1BI 1.89[a] | I | 1.82 ± 0.30 | 1.78 ± 0.01 |
| | II | 1.89 ± 0.18 | 1.77 ± 0.01 |

a ; Weighted averages of SM values.

## 3.7 Development of On-line Subcriticality Measurement System by Neutron Source Multiplication Method

K. Yamagishi, N. Mizoo and K. Ogura*

Neutron source multiplication (SM) method is a principal technique of subcritical reactivity measurement for fast neutron systems. The method is often employed for the control rod worth measurements of engineering mock-up critical experiment (EMC). On-line system of SM measurement was constructed and is successfully operating in FCA by the use of small computer PDP-9[1].

The observed reactivity $\rho_i$ of the detector i located in or around the system is determined, in SM method, as $\rho_i = A_i/N_i$, where $N_i$ and $A_i$ are the count rate and the constant of the detector i, respectively.

Some essential features of our system are descrived as follows.

1) The hardware description of the data acquisition system

The neutron pulses from the detectors are counted and accumulated by universal scalers (NIM module model 146), of which digital data are transfered into PDP-9 core memory at the end of preset time via NL-01 (special interface of the computer). The content of a model 146 is divided into two parts (2 digits of MSB and 4 digits of LSB), and the transfer is carried out for each part, because of 18-bit memory of PDP-9.

2) The software programming

FOCAL[2] (Formula Calculator), an interactive service program of PDP-9, was utilized for the sytem software, together with the user's programs USIF and FNEW. The control of the whole system is executed by the code USIF written in FOCAL language. User-defined two functions in assembly language, FNLC and FCNV are incorporated into FNEW, which, when reassembled by MACRO, can be load with FOCAL. FNLC has a function to control interface NL-01 and FCNV performs code conversion. Communications between the computer and experimenter are established by means of TTY. Instantaneous interruption and/or change of program sequence, temporary change and/or edit of index and variables, and the additional arithmetic operations between variables are acceptable at any time with corresponding imperative statements via TTY.

3) Data analysis

The dead time corrections, evaluation of averages and standard

---

* Nagoya University

deviations, and other arithmetic operations are performed with floating point numbers by FOCAL. The results are immediately output on TTY, and the computer is waiting for the decision of experimenter, who can judge by the results on TTY, for example, to continue or to terminate the measurement.

4) Program loading

The program loading must be done every day of experiments. Therefore, it should be symple in operation and should not be time consuming. Both FOCAL and FNEW codes are built into the Keyboad-Monitor System Tape (magnetic tape) of PDP-9, and USIF code is in the form of paper tape. Consequently, the program loading requires less than five minutes.

5) Device for trouble shooting

The user's program FNEW is so coded that only the instructions in the program is executed during the measurement. Having the full knowlege about FNEW, by checking instruction by instruction of the program, we can make quick diagnostic on the system including the interface at the occurence of troubles.

All of the above mentioned items can be regarded as fundamental specifications which must be satisfied by on-line measurement systems. A typical output example of USIF is shown in Fig. 3.7.1. Six detectors are employed in the measurement.

References

1) Digital Equipment Corporation : PDP-9 User Handbook (1968).
2) Digital Equipment Corporation : PDP-15 FOCAL Programming Manual, DEC-15-KJZA-D (1969).

```
TITLE OF THIS BRANCH:RD-41  DD'-IN A-0 PATTERN 1 ROD CRP=30-26


          MEASURE A/N (YES/NO):NO
          THE NUMBER OF A =:1
 RX =:8

        *** UNCORRECTED RAW DATA ***

      80   188146    66520    87797   106387    42533    24049
      80   186896    66849    87804   105647    42725    24089
      80   187390    66869    87691   106719    42942    24091
      80   188184    66516    87884   106222    43208    23977
      80   187502    66373    88071   106147    43030    24062
      80   187708    67131    88047   106196    43308    24071
      80   187911    66515    87589   106528    42772    24195
      80   188060    67019    87933   106534    43020    24051

          CHANGE TO RIGHT DATA? (YES/NO):NO

        *** CORRECTED RAW DATA ***

      2423       834       1102       1337       533       351
      2407       838       1102       1328       535       321
      2420       838       1101       1341       538       304
      2424       834       1103       1335       541       300
      2415       832       1105       1334       539       301
      2417       841       1105       1335       542       302
      2420       834       1099       1339       536       303
      2422       842       1104       1339       539       301
 AV & SD
      2419       836       1103       1336       538       302

      1.99      1.21       0.74       1.46      1.14      0.46

          CONTINUE/RETURN (YES/NO):YES

REACTIVITY & SD
      33.7151          0.0471
      34.1312          0.0566
      34.1339          0.0343
      32.4027          0.0469
      33.4263          0.0743
      34.9563          0.0583
          NORMALIZATION CHANNEL =:2
   1.25159    1.00000    1.00000    0.94936    0.97876    1.02417


NEXT PATTERN ?  (YES/NO):YES
```

Fig. 3.7.1 An output example of USIF

## 3.8 A Method for Estimating Multiple-rod Worth by Single-rod Experiment[1)]

M. Nakano

A method has been proposed to estimate experimentally the reactivity worth of multiple control rods by single-rod experiment.

Suppose two absorber rods are simultaneously introduced at positions i and j in a reactor. On the basis of the exact perturbation theory, reactivity worth of the two rods $\Delta\rho_{ij}$ can be written as

$$\Delta\rho_{ij} = f_i(j)\cdot\Delta\rho_i + f_j(i)\cdot\Delta\rho_j \qquad (1)$$

where $\Delta\rho_i$ and $\Delta\rho_j$ are the worth of individual rod i and j respectively. The correction factor $f_i(j)$ can be given by the disturbance parameter $A_i(j)$ defined as

$$A_i(j) = \frac{\langle\phi_0^+ P_i \phi_j\rangle}{\langle\phi_0^+ M\phi_j\rangle} \Big/ \frac{\langle\phi_0^+ P_i \phi_0\rangle}{\langle\phi_0^+ M\phi_0\rangle} \quad , \qquad (2)$$

where M is the fission operator of a reactor, $P_i$ the perturbation operator for the insertion of rod i, $\phi_0^+$ and $\phi_j$ the adjoint flux in the unperturbed system and the normal flux in the system with a single-rod j respectively, and $\langle\ \rangle$ means the energy and space integral over the reactor. The parameter $A_i(j)$ represents the effective change in the flux at position i caused by a single-rod j. The assumption adopted in the above is that the disturbance parameter for a multiple insertion can be factorized into the individual disturbance parameter[2)].

Under the similar assumption of factorization on the effective disturbance in the importance, the correction factor $f_i(j)$ can also be given by the disturbance parameter in the importance $A_i^+(j)$, which is defined as

$$A_i^+(j) = \frac{\langle\phi_j^+ P_i \phi_0\rangle}{\langle\phi_j^+ M\phi_0\rangle} \Big/ \frac{\langle\phi_0^+ P_i \phi_0\rangle}{\langle\phi_0^+ M\phi_0\rangle} \qquad (3)$$

The correction factor is then expressed as

$$[f_i(j)]^2 = A_i^+(j)\ A_i(j) \approx \frac{\langle\phi_j^+ P_i \phi_0\rangle}{\langle\phi_j^+ M\phi_j\rangle} \Big/ \frac{\langle\phi_0^+ P_i \phi_0\rangle}{\langle\phi_0^+ M\phi_0\rangle} \qquad (4)$$

The right-hand side of Eq. (4) is derived by ignoring the higher order terms of disturbances in the adjoint and normal fluxes than the first one. Therefore, the value of $f_i(j)$ may be estimated by the square root of the ratio

of sample worths measured at positon i in the systems with and without the rod j, if a sample material is selected to be similar in nuclear property to the rod concerned. A large sample can be used if the selfshielding effect of the sample at position i is not affected by insertion of the rod j. In the case of a multiple insertion, the correction factor to a single-rod worth is factorized into those from the individual rod, each of which may be estimated from the ratio of the sample worths.

To examine the validity of the method, a numerical study was made with the reactor model shown in Fig. 3.8.1, which is a modification of FCA Assembly VII-1. Natural and 90% enriched $B_4C$ rods are introduced at positions R and S respectively, the worth of the individual rod ranging from -0.4%$\Delta$k/k(R4) to -1.9%$\Delta$k/k(S0). There is no significant difference in the multiple-rod worth calculated by the present method either a small or a large $B_4C$ sample is used. The results for several rod patterns are compared in Table 3.8.1 with those obtained by the conventional k-calculation. Agreement is good, the discrepancy being 1.0% at most when half $B_4C$ of the respective rod is used as the sample. Consequently, the method proposed is usefull in estimating the 'experimental' value of a multiple-rod worth, in which only measurements are necessary of the single-rod worths and sample worths in the systems with and without an individual rod.

References

1) Nakano, M.: JAERI-M 6504 (1976) (in Japanese).
2) Konishi, T., Yamamoto, M.: J. Nucl. Sci. Technol., 12, 336 (1975).

Table 3.8.1 Comparison of multiple-rod worth

| Rod pattern | Rod worth $-\Delta\rho$ (%Δk/k) | | Ratio Present/Direct-k | Interaction[c] effect (%) |
|---|---|---|---|---|
| | Present[a] | Direct-k[b] | | |
| S0*S2 | 2.932 | 2.925 | 1.002 | +0.7 |
| S1*S2 | 2.131 | 2.147 | 0.993 | +11.4 |
| S0*S1*S2 | 3.989 | 4.030 | 0.990 | +6.9 |
| R1*R3 | 1.415 | 1.415 | 1.000 | +2.7 |
| R1*R4 | 1.033 | 1.034 | 0.999 | -5.7 |
| S1*R4 | 1.159 | 1.164 | 0.996 | -9.5 |
| S1*R1*R4 | 1.660 | 1.672 | 0.993 | -14.4 |
| S1*R1*R2*R4 | 2.076 | 2.091 | 0.993 | -19.0 |

(a) Half $B_4C$ of the respective rod is used as the sample.

(b) $\Delta\rho_{ij\ldots\ell} = (1/k_{eff})_o - (1/k_{eff})_{ij\ldots\ell}$

(c) Interaction effect = $\left[\frac{\Delta\rho_{ij\ldots\ell}}{\Delta\rho_i+\Delta\rho_j+\ldots+\Delta\rho_\ell} - 1\right]$ (Direct-k calc.)

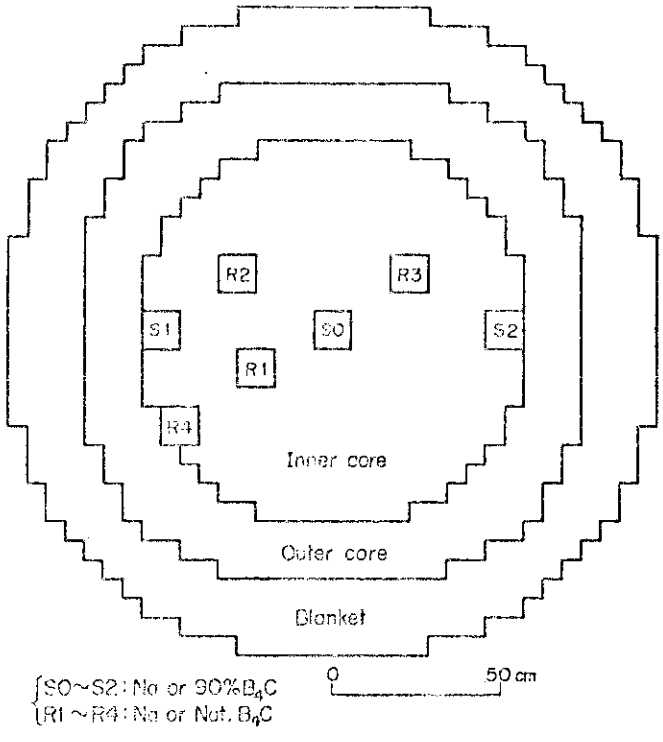


Fig. 3.8.1 Reactor model

## 3.9 An Estimation of the Multiple Control Rod Worth by Means of the Higher Order Perturbation Method

H. Mitani

In the design of large fast reactors, a number of control rods are used to operate the reactors functionally and with safety. Therefore, to estimate exactly multiple control rod worths is one of the most important design problems. It is, however, reported that the interaction effect between multiple control rods is very large and it also affects strongly the power distribution of the reactor. To obtain an optimal control rod programming for such a large fast reactor, it is necessary to understand and grasp the problem of strong interaction effect in detail.

For this purpose, a method of estimating the multiple control rod worth was developed by using the higher order perturbation technique[1]. In the method, the worth of N control rods up to the third order can be expressed as

$$\rho_{1+\ldots+N} = \sum_{i=1}^{N} \rho_i + \sum_{i=1}^{N-1} \sum_{j=i+1}^{N} \left( \sum_{p(2,2)} \rho_{ij}^{(2)} \right) + \sum_{i=1}^{N-1} \sum_{j=i+1}^{N} \left( \sum_{p(3,2)} \rho_{iij}^{(3)} \right) + \sum_{i=1}^{N-2} \sum_{j=i+1}^{N-1} \sum_{k=j+1}^{N} \left( \sum_{p(3,3)} \rho_{ijk}^{(3)} \right) + O(\delta^4) , \quad (1)$$

where $\left( \sum_{p(m,n)} \right)$ is the summation of all the terms $\rho_{ij\ldots j}^{(m)}$, ... belonging to the permutation p(m,n) which represents the number of arrangements of n kinds of objects in m places, permitting to take the same object repeatedly. In Eq. (1), for example, the value of $\rho_{ijk}^{(3)}$ is the third order reactivity worth of the control rod i which is affected by the absorptions of control rods j and k.

Similarly, the worth of two control rods i and j and also that of three control rods i, j and k are given by

$$\rho_{i+j} = \rho_i + \rho_j + \sum_{p(2,2)} \rho_{ij}^{(2)} + \sum_{p(3,2)} \rho_{iij}^{(3)} + O(\delta^4) , \quad (2)$$

$$\rho_{i+j+k} = \rho_i + \rho_j + \rho_k + \sum_{p(2,2)} \rho_{ij}^{(2)} + \sum_{p(2,2)} \rho_{jk}^{(2)} + \sum_{p(2,2)} \rho_{ki}^{(2)}$$

$$+ \sum_{p(3,2)} \rho_{iij}^{(3)} + \sum_{p(3,2)} \rho_{jjk}^{(3)} + \sum_{p(3,2)} \rho_{kki}^{(3)} + \sum_{p(3,2)} \rho_{ijk}^{(3)}$$

$$+ O(\delta^4) \quad . \tag{3}$$

We consider only up to the second order terms in both Eqs. (1) and (2). Then, substituting Eq. (2) into Eq. (1), we have

$$\rho_{1+2+\ldots+N} = \sum_{i=1}^{N} \rho_i + \sum_{i=1}^{N-1} \sum_{j=i+1}^{N} (\rho_{i+j} - \rho_i - \rho_j) + O(\delta^3) \quad . \tag{4}$$

In this equation, the interaction effect between multiple control rods is expressed by the combination of those between two control rods selected out of N control rods.

When the interaction effect between multiple control rods is slightly strong, it can be expressed by the combination of those between three control rods selected out of N control rods. That is,

$$\rho_{1+2+\ldots+N} = \sum_{i=1}^{N} \rho_i - (N-3) \sum_{i=1}^{N-1} \sum_{j=i+1}^{N} (\rho_{i+j} - \rho_i - \rho_j)$$

$$+ \sum_{i=1}^{N-2} \sum_{j=i+1}^{N-1} \sum_{k=j+1}^{N} (\rho_{i+j+k} - \rho_i - \rho_j - \rho_k) + \Delta O(\delta^4) \quad . \tag{5}$$

Validity of the present method was examined by using the experimental data of the PHENIX[2] where six control rods are arranged in a hexagonal pattern. Experimental data of the PHENIX and the worth estimated by Eq. (4) are given in Table 3.9.1, in which the estimated worth agrees well with the measured one within experimental error. Numerical examinations for modified MONJU also show that the interaction effect between multiple control rods can be estimated from the combination of those between two control rods. Further examinations for a 1000 MWe fast reactor will be discussed in a coming paper[3].

References

1) Mitani, H.: Nucl. Sci. Eng., 51, 180 (1973).

2) Clauzon, M. M., et al.: NEACRP-17, (1974).

3) Mitani, H.: to be published in J. Nucl. Sci. Technol., (1976).

Table 3.9.1 Estimation of six control rod worths in PHENIX

| Experimental data of PHENIX | | | Estimated by the present method | |
|---|---|---|---|---|
| Rods | Rod worth* | Interaction effect (%) | Terms | Reactivity worth * |
| rod (1) | 830 ± 20 | ——— | $6\rho_1$ | 4980 |
| rods (1+2) | 1620 ± 100 | 2.4 ± 8 | $6(\rho_{1+2} - \rho_1 - \rho_2)$ | -240 |
| rods (1+3) | 1700 ± 80 | 2.4 ± 7 | $6(\rho_{1+3} - \rho_1 - \rho_3)$ | +240 |
| rods (1+4) | 1800 ± 100 | 8.4 ± 7 | $3(\rho_{1+4} - \rho_1 - \rho_4)$ | +420 |
| 6 rods | 5800 ± 800 | 16.5 ± 16 | $\rho_{1+2+.....+6}$ | 5400 |

* $10^{-5}\Delta K/K$

## 3.10 Critical Experiment on 20 % Enriched Uranium and Thorium Loaded and Graphite-Moderated Core (SHE-T1) for Very High Temperature Gas Cooled Reactor

Y. Kaneko, F. Akino, H. Yasuda, K. Kitadate, R. Kurokawa and M. Takeuchi

Critical experiments to support the core design of Very High Temperature Gas Cooled Reactor have been done at Semi-Homogeneous Critical Assembly. Since January 1970, 20 % enriched uranium and thorium oxide fuels loaded core ($C/^{235}U$ = 6628, $C/^{232}Th$ = 2560) in shape of cylinder reflected with graphite has been built there. Critical mass, neutron generation time, reactivity worths of the experimental control rods and also their effects on the spatial distribution were measured, and compared with calculation. For example, the spatial distributions of the induced activity of the copper pins are illustrated in Fig. 3.10.1.

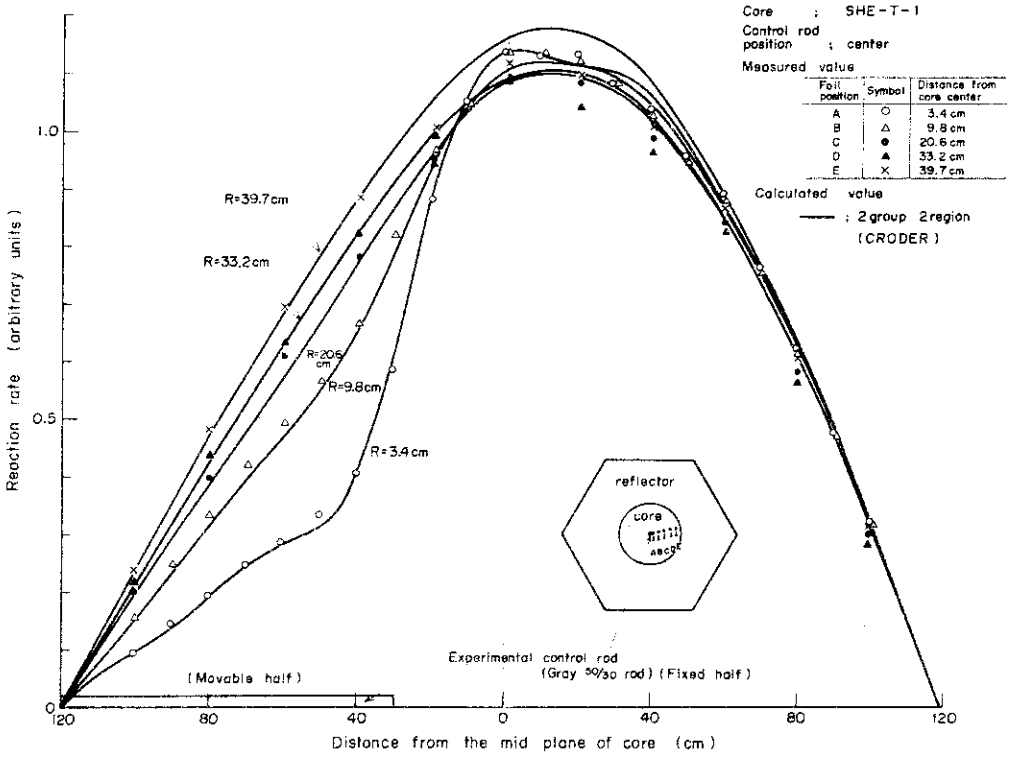


Fig. 3.10.1 Spatial distributions of reaction rate of copper pins in control rod inserted core of SHE-T1.

## 3.11 Measurement and Analysis of Critical Masses of Graphite Moderated 20 % Enriched Uranium Loaded Core

F. Akino, Y. Kaneko, K. Kitadate, R. Kurokawa, H. Yasuda and M. Takeuchi

The critical masses of 20 % enriched graphite moderated SHE assembly[1] were measured for the seven cores of the different core configurations. The C/$^{235}$U atomic ratio in the core region was varied from 2226 to 6628 by changing the combination of fuel and graphite disks. The six cores among them were in shape of cylinder surrounded with radial graphite reflector, and slightly loaded with thorium oxide fuels in core region. The other one was in shape of annular with inner as well as the outer radial graphite reflectors.

The physical properties of the different core configurations of SHE are summarized in Table 3.11.1.

The calculations of critical masses were made with the use of a 34 group one-dimensional diffusion computer code TUD. The computer inputs were prepared as follows. The group constants for thermal neutrons were determined through a conventional procedure taking into account of the spatial dependence of neutron thermalizition with use made of Young and Koppel's[2] scattering kernel (ENDF/A)[3] for graphite. For this procedure, computer codes PIXSE[4] and TUD were used. The absorption and fission cross sections for $^{235}$U, $^{238}$U and C were taken from ENDF/B-II file[5]. On the other hand, the epithermal energy interval from 10 MeV to 0.683 eV was divided into 33 groups. These epithermal cross sections for each group were calculated by use of FAXSE code from GAM-I file[6]. The resonance absorption and fission integrals of $^{235}$U and $^{238}$U were calculated by use of RICM code[7].

The calculated and measured values of critical masses for the seven core configurations of SHE are listed in Table 3.11.1 and are shown graphically in Fig. 3.11.1.

Experiment agrees well with calculation. Discrepancies between calculated and measured critical masses are only 2.6 % on the average and 4.4 % at the maximum. Accordingly, we can conclude that the calculational technique is established to

predict the critical mass for graphite moderated 20 % enriched uranium homogeneously loaded core.

References

1) Inoue, K. et al. : JAERI-1032 (1962)
2) Young, J.A. and Koppel, J.U. : J. Che. Phy. Vol.42, No.1, p.357 (1965)
3) Honeck, H.C. : BNL-8381 (1965)
4) Macdougall, J.D. : AEEW-M318 (1963)
5) Honeck, H.C. : BNL-50066(T-467) (1966)
6) Joanou, G.D. and Dudek, J.S. : GA-1850 (1961)
7) Mizuta, H. et al. : JAERI-1134 (1967)

Table 3.11.1 Physical properties of the different core configurations of SHE

| Configuration | $C/^{235}U$ | Number of fuel rods at critical | | Critical mass in $^{235}U$ (kg) | | Inner reflector $R_1$ (cm) | Core radius $R_2$ (cm) | | Core length $H_1$ (cm) | Axial reflector thickness $H_2$ (cm) |
|---|---|---|---|---|---|---|---|---|---|---|
| | | exp. | cal | exp. | cal | | exp | cal | | |
| SHE-5 | 5378 | 211.6 | 210.3 | 5.12 | 5.09 | 0 | 35.13 | 35.02 | 240 | 0 |
| SHE-6 | 4328 | 189.0 | 180.9 | 5.74 | 5.49 | 0 | 33.20 | 32.48 | 240 | 0 |
| SHE-7 | 3276 | 165.5 | 160.1 | 6.68 | 6.46 | 0 | 31.07 | 30.55 | 240 | 0 |
| SHE-8 | 2226 | 141.5 | 143.4 | 8.61 | 8.73 | 0 | 28.73 | 28.92 | 240 | 0 |
| SHE-12 | 6628 | 79.45 | 77.52 | 4.83 | 4.71 | 0 | 37.28 | 36.83 | 240 | 0 |
| SHE-T-1 | 6624 ($C/^{232}Th$ =2558) | 92.77 | 96.57 | 5.65 | 5.88 | 0 | 40.29 | 41.11 | 240 | 0 |
| SHE-9-A7 | 5378 | 286.4 | 279.7 | 6.93 | 6.77 | 46.55 | 61.95 | 61.63 | 240 | 0 |

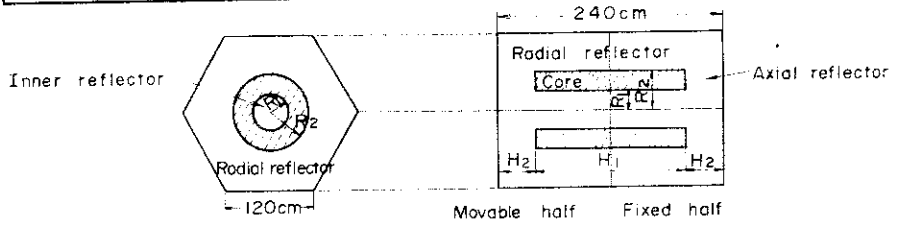


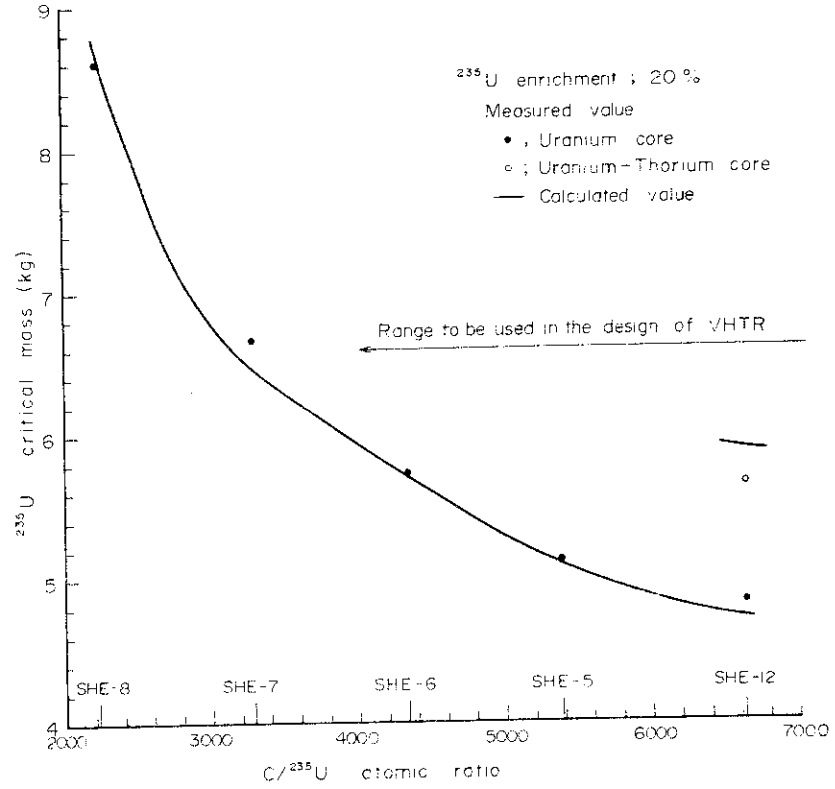


Fig. 3.11.1 Critical masses of the various SHE cores

## 3.12 Measurement of Multiple Control Rods Reactivity Worths in Semi-Homogeneous Critical Assembly

Y. Kaneko, F. Akino, H. Yasuda, R. Kurokawa, K. Kitadate and M. Takeuchi

Experimental and theoretical works are described which have been made to obtain the experimental techniques of determining large negative reactivity worths as accurately as practicable.

Measurements are first made on reactivity effect of the experimental multiple control rods arranged in ring by the pulsed neutron method in the Semi-Homogeneous Critical Assembly, a heavily reflected graphite-moderated 20 % enriched multiplying system. The atomic ratios of C to $^{235}U$ in the core region are 2226 and 6628 in the SHE-8 and SHE-T-1 cores respectively. Subcriticality is determined in the static reactivity from the measured prompt neutron decay constants by making resonable, large correction to the well-known King-Simmons formula due to change of the neutron generation time estimated by calculation. Measured reactivity worths of the multiple control rods thus obtained are in good agreement with those by two-group diffusion calculation.

New multi-point type formulas are then given which replace the single-point type expressions for methods of "area-type" pulsed-neutron, source multiplication, and rod drop. In the formulas, the reactivity value is derived by integrating all the neutron counting data from every part of the reactor core to sweep out effects of the kinetic distortion and the spatial harmonics. Experiments made for SHE-T-1 are to examine the proposed integral versions and to confirm validity of the King-Simmons formula with large correction for the change of neutron generation time. The numbers of measuring points in each core are 16 and 48 for the pulsed neutron and the rod drop method, and for the source multiplication method, respectively. Consequently, space dependence of the reactivity value obtained by the single-point type formulas is up to ∿40 % for each of the experimental methods.

Discrepancies among the different experimental methods are reduced within ∿5 % down to ∿35 $, once the spatial averages of the space-dependent experimental values are done with use of the new multi-point type formulas.

## 3.13 Polarity Correlation Experiment for Large Negative Reactivity Measurement

H. Yasuda and M. Takeuchi

The polarity correlation method is applied to an experiment to measure the prompt neutron decay constant or the subcriticality in a graphite moderated and reflected reactor SHE-T-1 with the reactivity ranging widely from critical to almost shut down state (-12 dollars) without external disturbance such as pulsed neutron source.

A polarity correlation function is defined as a correlation function of the polarity signal.

$$\phi_{p(\tau)} = \lim_{T\to\infty} \frac{1}{2T} \int_{-T}^{T} \operatorname{sgn} x_1(t) \cdot \operatorname{sgn} x_2(t+\tau)dt \ . \qquad (1)$$

When the statistical property of count rate x is approximated to obey a two demensional Gaussian distribution, and the reactor kinetics is approximated by one-point model, the polarity correlation function becomes,

$$\phi_{p(\tau)} = \frac{2A}{\pi} e^{-\alpha|\tau|} \ . \qquad (2)$$

Eq. (2) is used to analyze the experimental data.

In SHE-T-1 core, the polarity correlation method is applied to the experiment for measuring the safety rod reactivity worth. The pulsed neutron and rod drop experiments are also performed for the purpose of comparison.

A large volume $BF_3$ proportional counter (84EB 45/50G, O.D. = 5 cm, L = 100 cm) is placed on the axis of cylindrical core to get a sufficient detection efficiency. In Fig. 3.13.1 are drawn the decay curves of polarity correlation function against delay time for the various number of safety rods inserted.

The reactivity worth is calculated from the prompt neutron decay constant using the original King-Simmon's formula,

$$\frac{\rho}{\beta} = \frac{\alpha-\alpha_c}{\alpha} \qquad (3)$$

in both cases of polarity correlation and pulsed neutron experiments, while in case of rod drop experiment, the reactivity worth is calculated using the well-known formula for $^{235}U$ loaded core:

$$\rho/\beta_{eff} = (\text{count rate before rod drop/integrated counts after rod drop}) \times 13.01 \quad (4)$$

The resultant values of reactivity worth are plotted against the number of safety rods inserted into the critical core and shown in Fig. 3.13.2.

The reactivity worths obtained from the prompt neutron decay constant using the original King-Simmon's formula showed fairly good agreements between polarity correlation and pulsed neutron experiment involving 4 % discrepancies and agreed also with that obtained from rod drop experiment involving 7 % discrepancies at most.

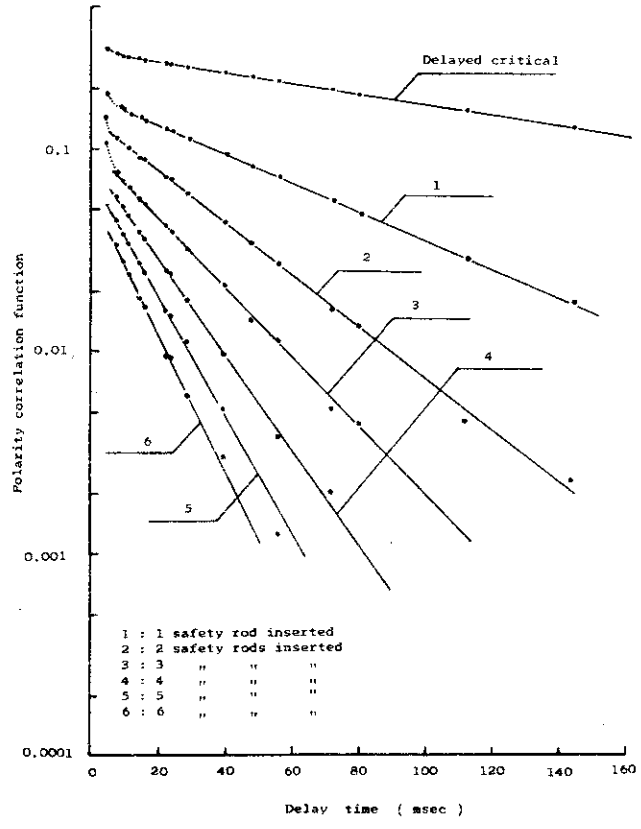


Fig.3.13.1 Decay curves of polarity correlation function against delay time for the various number of safety rods inserted.

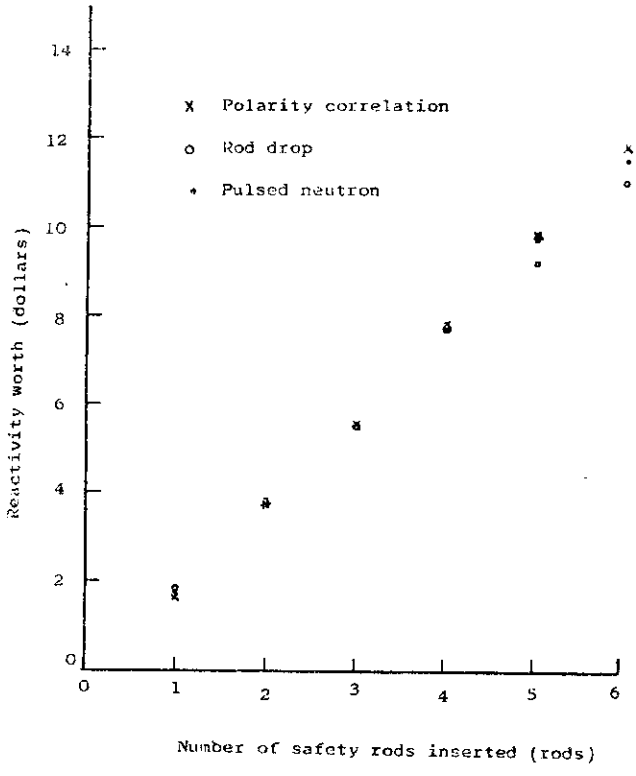


Fig.3.13.2 Reactivity worths plotted against the number of safety rods inserted.

## 3.14 Analysis of Sodium Void Worth in Phase 3 Core of ZPPR Assembly 3

M. Nakagawa and Y. Tokuno*

The Analysis of sodium void worth measurements in the phase 3 core of ZPPR assembly 3[1] has been performed with the use of the JAERI Fast set Version 2.

The ZPPR assembly 3 is a engineering mock up of the proto type fast reactor. The phase 3 core, representing a beginning-of-cycle configuration, had nine control rods filled with $B_4C$-Sodium-SUS. The remaining ten control rod positions were filled with Sodium-SUS. Voiding zones were of ± 12 inch axially and varied radially from 4 central drawers to 632 drawers. The later core was the most reactive core determined experimentally. Seventeen additional voiding steps were measured in between these two configurations. The pattern of void stages is provided in Fig.3.14.1.

The analysis is based on the 70 group JAERI Fast set version 2. The unit cell heterogeniety calculations were performed by the SLAROM[2] code and the cell averaged cross sections were collapsed into 18 groups through the one dimensional diffusion calculations. The criticality calculations were carried out in X-Y-Z geometry based on the diffusion model. The two dimensional r-z calculation underestimates the eigenvalue about 3-4 percents due to the cylindricalized equi-volume model of control rods. Therefore it is necessary to use the three dimensional calculations.

The contribution from the anisotropic leakages were considered in the perturbation calculation by using the Benoist model.

The comparison between calculations and measurements is presented in Table 3.14.1. The table shows the cumulative worths for progressive voiding zones. The VP calculations in the table use the adjoint flux in the normal core and the neutron flux in the voided inner core.

The C/E values are gradually reduced with increasing the voiding zones for the both of FOP (first order perturbation) and VP calculations. The VP calculations nicely agree with measurements in the inner core region. In the outer core region, if the exact perturbation calculation is performed, the agreement will become well.

---

The Wash performed under Contract between PNC and JAERI.

* JAPAN INFORMATION SERVICE, TOKYO

References

1) Lineberry, M.J., et al. : Trans Am. Nuc. Soc. 17, P.456 (1973)

2) Nakagawa, M., Tsuchihashi, K. : "SLAROM", JAERI-M 5916 (1974)

Table 3.14.1 Comparison of Calculation and Measurement of Progressive Sodium Voiding Worth of ZPPR 3-Phase 3 ($10^{-4}$ $\Delta$ k/k unit)

| Voiding Stage | Exp. | FOP | | | VP | | |
|---|---|---|---|---|---|---|---|
| | | Calc. | C/E | (C-E)/kg | Calc. | C/E | (C-E)/kg |
| CRP #1 | 0.9188 | 0.780 | 0.85 | -0.026 | 1.225 | 1.33 | 0.058 |
| A4 | 9.237 | 7.734 | 0.84 | -0.049 | 8.524 | 0.92 | -0.023 |
| B3.1 | 13.53 | 10.56 | 0.78 | -0.070 | 11.93 | 0.88 | -0.038 |
| B3.2 | 21.85 | 16.13 | 0.74 | -0.083 | 19.03 | 0.87 | -0.041 |
| B3.3 | 33.11 | 23.97 | 0.72 | -0.083 | 30.41 | 0.92 | -0.024 |
| B3.4 | 41.88 | 30.17 | 0.72 | -0.085 | 37.85 | 0.90 | -0.029 |
| B3.5 | 49.83 | 35.38 | 0.71 | -0.088 | 44.08 | 0.88 | -0.035 |
| B3.6 | 57.27 | 39.90 | 0.70 | -0.088 | 49.85 | 0.87 | -0.038 |
| B3.7 | 62.63 | 42.79 | 0.68 | -0.086 | 54.35 | 0.87 | -0.036 |
| B3.8 | 66.73 | 44.62 | 0.67 | -0.087 | 56.97 | 0.85 | -0.039 |
| B3.8a | 66.19 | 42.47 | 0.64 | -0.091 | 55.49 | 0.84 | -0.041 |
| B3.9 | 68.17 | 41.14 | 0.60 | -0.091 | 57.67 | 0.85 | -0.035 |
| | | | | | (57.17)* | (0.84)* | (-0.037) |
| B3.10 A | 72.07 | 44.29 | 0.61 | -0.090 | 61.56 | 0.85 | -0.034 |
| B3.11 B | 75.85 | 44.52 | 0.59 | -0.092 | 63.44 | 0.84 | -0.037 |
| B3.12 C | 76.69 | 44.10 | 0.58 | -0.093 | 63.51 | 0.83 | -0.038 |
| B3.13 D | 77.72 | 43.17 | 0.56 | -0.094 | 63.01 | 0.81 | -0.040 |
| B3.14 E | 77.98 | 42.38 | 0.54 | -0.094 | 62.45 | 0.80 | -0.041 |
| B3.15 F | 78.80 | 41.37 | 0.53 | -0.095 | 61.81 | 0.78 | -0.043 |
| B3.16 G | 80.50 | 41.52 | 0.52 | -0.096 | 62.11 | 0.77 | -0.045 |
| B3.17 H | 79.48 | 38.82 | 0.49 | -0.096 | 59.60 | 0.75 | -0.047 |
| B3.18 I | 79.64 | 38.00 | 0.48 | -0.095 | 58.77 | 0.74 | -0.048 |

* Exact perturbation with $\Phi'$ and $\Phi^*$

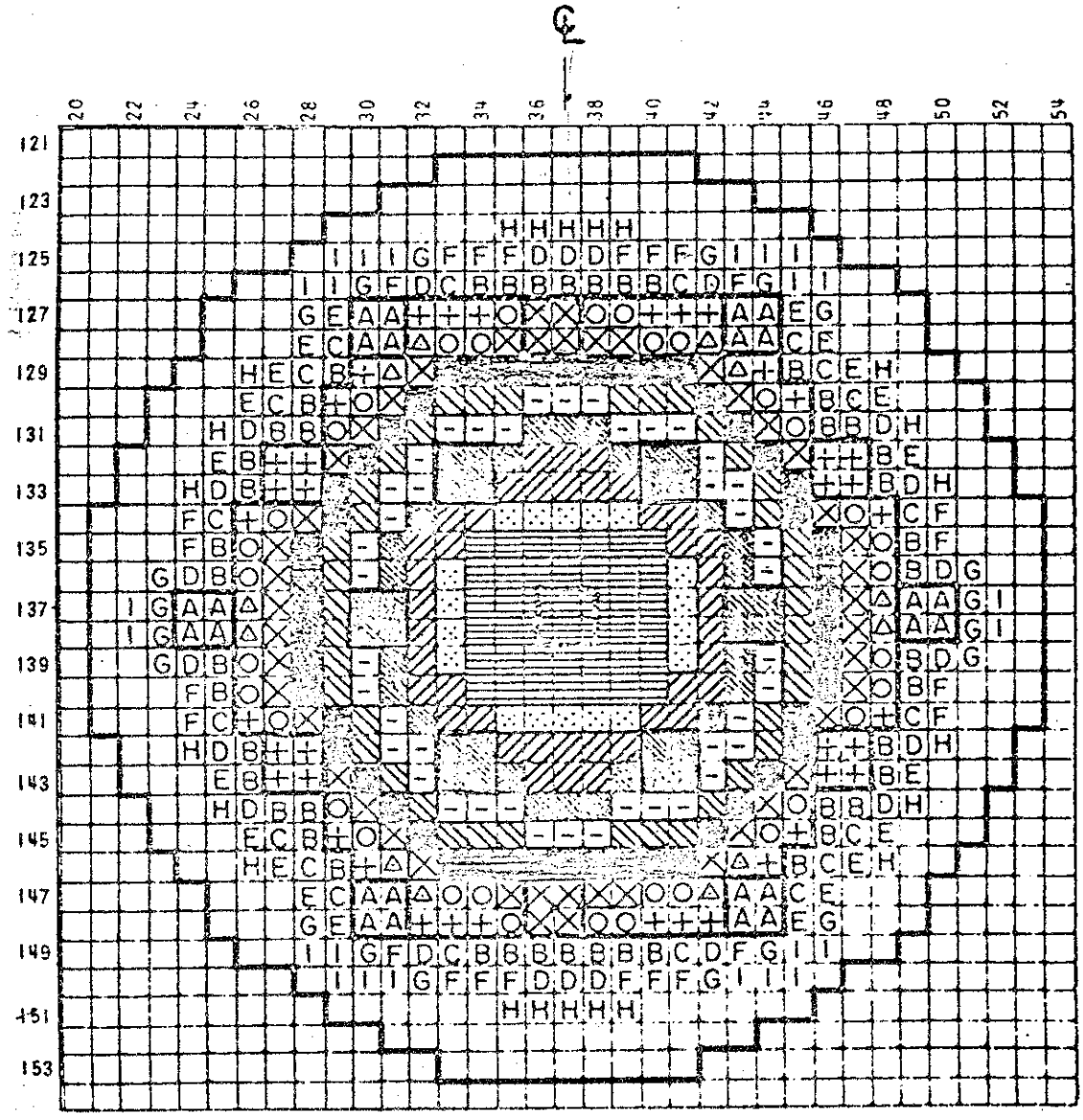

Fig. 3.14.1. Stages of the sodium voiding experiment in the phase-3 core of ZPPR assembly 3.

## 3.15 Analysis of Doppler Effect with the JAERI-Fast Set Version-II

H. Takano and Y. Matsui*

The JAERI-Fast Set Version II[1] has been produced on the basis of the benchmark test[2], the adjustment[3] and the evaluation[4),5] for group cross sections. The temperature dependence of group cross sections in the JAERI-Fast Set Version II was tested from the analyses of Doppler experiments performed with different methods. One is the Doppler reactivity measurement for the whole core of SEFOR assembly[6]. Another is the sample Doppler reactivity measurement for the natural $UO_2$ in FCA assemblies V-1, V-2, VI-1 and VI-2[7], and ZPPR assembly 2[8].

The isothermal Doppler coefficient of SEFOR was calculated with the use of the benchmark specification provided by Hutching et al[6]. We adopted the proposed one-dimensional spherical model and two-dimensional R-Z model. The 70-group cross sections of Be were produced with the PROF-GROUCHG-II code[9] using the cross section data in the ENDF/B-IV file. The two-dimensional R-Z diffusion calculation was performed with 25 energy groups collapsed from 70 groups with the use of the one-dimensional diffusion spectrum. Table 3.15.1 shows the comparisons between the calculated and experimental results. The corrections were taken from the benchmark description. The calculated Doppler coefficients are in good agreement with the experimental values.

The sample Doppler reactivity worths of FCA assemblies V-1, V-2, VI-1 and VI-2[7], and of ZPPR assembly 2[8] have been measured by heating the sample located at the center of the inner core. The samples are electrically heated from room temperature ($\sim$300°K) up to $\sim$1100°K. The calculations of Doppler effect were performed with one- and two-dimensional first order perturbation theory.

The calculated values are compared with the experimental values of FCA assemblies V-1, V-2, VI-1 and VI-2 in Table 3.15.2. The heterogeneity effect was considered by the usual equivalent relation $\sigma_e = a(1-c)/N\ell$, where $a(1-c) = 1.35$ and $\ell = 2.5$ cm were assumed. The results are in good agreement with the experiments except for FCA V-1 and -2 which have relatively hard core spectra.

Tables 3.15.3 and 3.15.4 show the comparisons of the calculated values with the experimental values in the normal and Na-voided core of ZPPR

* Nippon Information Service Co., Ltd.

assembly 2. The values of the rod/plate experimental ratios are also compared with the calculated homo/plate ratios. Two calculating models were used: the flux-depressions of the Doppler region were calculated by considering only the sample rod for the model-1, and the sample rod and the surrounded SUS region for the model-2. The calculated results with the model-2 are in very good agreement with the experimental values. The effect of the heterogeneity on the Doppler reactivity coefficient of $^{238}U$ is well evaluated.

We conclude that the JAERI-Fast Set Version II gives C/E-values which are always near to unity for the analyses of the whole core and $NUO_2$ sample Doppler experiments.

References

1) "JAERI-Fast Set Version-II", N241, 75-19 (1975).
2) TAKANO, H., HASEGAWA, A., KATSURAGI, S.: "An analysis of fast critical experiments and a revision of the JAERI-Fast set", JAERI-M4215 (1971) (in Japanese).
3) TAKANO, H., HASEGAWA, A., KATSURAGI, S.: unpublished work (1974).
4) TAKANO, H., KATSURAGI, S.: unpublished work (1975).
5) HASEGAWA, A., KATSURAGI, S.: unpublished work (1975).
6) HUTCHING, B. A., et al.: "SEFOR Doppler Benchmark Problem" unpublished work
7) IIJIMA, T., MUKAIYAMA, T.: unpublished work (1971).
8) DAVEY, W. G., et al.: Nucl. Sci. Eng., 51, 415 (1973).
9) HASEGAWA, A., et al.: to be published.

Table 3.15.1 Analysis of SEFOR Doppler experiment

| | | Spherical model | R-Z model |
|---|---|---|---|
| $k_{eff}$ | Calculation | 1.02186 | 0.996834 |
| | Correction | -0.00149 | -0.00149 |
| | Corrected | 1.02037 | 0.995344 |
| $T\frac{dk}{dt}$ | Experiment | -0.0081±0.001 | -0.0081±0.001 |
| | Calculation | -0.00781* | -0.007753** |
| | Correction | -0.00065 | -0.00065 |
| | Corrected | -0.00846 | -0.008403 |
| | C/E | 1.044 | 1.037 |

* first order perturbation calculation
** exact perturbation calculation

Table 3.15.2 Comparison of $NUO_2$ Doppler effect in FCA assemblies
(One-dimensional first order perturbation calculation)

| T(°K) | Doppler effect ($\times 10^6$ $\Delta k/k$) | | | | | | | | | | | |
|---|---|---|---|---|---|---|---|---|---|---|---|---|
| | FCA V-1 | | | FCA V-2 | | | FCA VI-1 | | | FCA VI-2 | | |
| | EXP. | HOM | HET | EXP. | HOM | HET | EXP. | HOM | HET | EXP. | HOM | HET |
| 300-600 | -4.66±0.1 | -4.89 (1.05) | -3.76 (0.81) | | | | | | | | | |
| 300-650 | | | | | | | -5.19±0.34 | -5.40 (1.04) | -4.96 (0.96) | | | |
| 300-850 | -7.12±0.1 | -7.69 (1.08) | -5.92 (0.83) | | | | -7.51±0.33 | -7.66 (1.02) | -7.02 (0.93) | -6.83±0.1 | -6.31 (0.92) | -6.20 (0.91) |
| 300-1100 | -9.18±0.2 | -9.68 (1.05) | -7.44 (0.81) | -10.65 ±0.13 | -9.14 (0.86) | -7.38 (0.69) | -9.38±0.4 | -9.84 (1.05) | -9.01 (0.96) | -8.78±0.1 | -8.18 (0.93) | -8.02 (0.91) |
| Cold worth | -121.±2 | -127 (1.05) | -137 (1.13) | -103±1 | -106 (1.03) | -116 (1.13) | -132.5 ±0.13 | -157.6 (1.18) | -169 (1.28) | | | |

C/E-values are presented in the parentheses.
HOM and HET mean homogeneous and heterogeneous calculations, respectively.

Table 3.15.3 Comparison of natural $UO_2$ Doppler effects in the normal inner core plate of ZPPR assembly 2
(2-dimensional R-Z 1-st order perturbation calculation)

| Temperature (°K) | Doppler effect, $\Delta k/k \times 10^6$ | | | | | | | | |
|---|---|---|---|---|---|---|---|---|---|
| | Exp. | | | Calculation | | | | | |
| | | | | Plate-Homo | | Plate-Hetero | | Homo/Hetero | |
| | rod | plate | rod/plate | model-1 | model-2 | model-1 | model-2 | model-1 | model-2 |
| 300 | -71.9 | -72.62±0.22 | 0.990 | -80.12<br>(1.11) | -78.61<br>(1.09) | -76.32<br>(1.05) | -82.79<br>(1.18) | 1.05<br>(1.06) | 0.950<br>(0.96) |
| 500 | -2.11±0.1 | -2.41±0.09 | 0.876 | -1.83<br>(0.87) | -2.03<br>(0.96) | -1.95<br>(0.81) | -2.24<br>(0.93) | 0.938<br>(1.07) | 0.906<br>(1.03) |
| 800 | -4.55±0.1 | -4.93±0.1 | 0.923 | -3.65<br>(0.80) | -4.18<br>(0.92) | -4.02<br>(0.82) | -4.62<br>(0.94) | 0.908<br>(0.984) | 0.906<br>(0.982) |
| 1100 | -6.00±0.1 | -6.76±0.1 | 0.888 | -4.94<br>(0.82) | -5.73<br>(0.95) | -5.52<br>(0.82) | -6.36<br>(0.94) | 0.895<br>(1.01) | 0.901<br>(1.01) |

C/E-values are presented in the parentheses.

Ih/% $\Delta k/k$ = 998.49

Table 3.15.4 Comparison of natural $UO_2$ Doppler effects in the Na-voided inner core plate of ZPPR assembly 2
(2-dimensional R-Z 1-st order perturbation calculation)

| Temperature (°K) | Doppler effect, $\Delta k/k \times 10^6$ | | | | | | |
|---|---|---|---|---|---|---|---|
| | Exp. | | | Calculation | | | |
| | | | | Plate-Homo | | Plate-Hetero | Homo/Hetero |
| | rod | plate | rod/plate | model-1 | model-2 | model-2 | model-2 |
| 300 | -64.52 | -70.1±0.22 | 0.920 | -75.57 (1.17) | -69.65 (1.08) | -70.98 (1.01) | 0.981 (1.07) |
| 500 | -1.546±0.12 | -1.632±0.10 | 0.947 | -1.203 (0.78) | -1.456 (0.94) | -1.626 (0.99) | 0.895 (0.95) |
| 800 | -3.121±0.12 | -3.296±0.13 | 0.947 | -2.413 (0.77) | -2.961 (0.95) | -3.335 (1.01) | 0.888 (0.94) |
| 1100 | -4.536±0.12 | -4.514±0.12 | 1.005 | -3.246 (0.72) | -4.022 (0.89) | -4.559 (1.01) | 0.882 (0.88) |

C/E values are presented in the parentheses.

# 4. Shielding

## 4.1 Preliminary Studies of Neutron Benchmark Experiments for One-dimensional Transport Calculation with an Iron Sphere[1)]

Y. Furuta, N. Sasamoto and S. Tanaka

Experimental Studies using an iron sphere were made to examine the possibility of the measurements of leakage neutron flux spectra, which may serve for verification of the one-dimensional discrete-ordinate transport calculations.

Two types of sources, D-T neutrons and the fission spectrum neutrons, were used and the possibility to obtain the angular flux spectra was suggested from the results of both cases by an NE213 detector for the neutron energy region from about 100 keV to 15 MeV. Several problems to be solved, however, still remain. It is intended, in near future, to overcome such problems and to obtain fine angular flux spectra which are suitable for the verification of one-dimensional transport calculation.

The same experiments using spheres other than iron are also planned in future.

Reference

1) Furuta, Y., Sasamoto, N. and Tanaka, S.: "Preliminary Studies of Neutron Benchmark Experiments for One-dimensional Transport Calculation," Presented for Specialists' Meeting on Sensitivity Studies and Shielding Benchmarks, Paris, Oct. 7-10, 1975.

## 4.2 Mockup Experiments on Shield Repair of MUTSU

J. Miita, M. Osanai*, S. Miyasaka, J. Miyakoshi*, T. Asaoka,
H. Suzuki, T. Fuse** and H. Takemoto*

From the investigations carried out by the MUTSU Radiation Shielding Technology Study Committee headed by Professer Y. Ando of University of Tokyo as chairman, it was concluded that the radiation leak in "MUTSU" was caused by fast neutrons which stream to upward and downward directions from void space between the pressure vessel and the primary shield[1),2)]. According to the conclusion of the committee, the shild repair of MUTSU has been planned by Japan Nuclear Ship Development Agency (JNSDA).

The main design modifications for the primary shield of MUTSU are as follows:

1) Replacement of mirror insulators in the gap between the pressure vessel and the primary shield by chrysotile asbestos, which is a kind of degenerated serpentine rock.
2) Addition of serpentine concrete contained $ZrH_x$ at the void space around the control rod mechanism above the pressure vessel.
3) Addition of polyethylene shield in the double bottom under the reactor container.
4) Replacement of the upper shield of ordinary concrete by serpentine concrete shield.

A series of shielding mockup experiments has been carried out to confirm the validity of basic calculational methods to be applied to the shield repair and to obtain useful design data and methods for complicated shield configulations. The mockup experiments were carried out on the above 4 items using JRR-4, a swimming pool type reactor, in collaboration with JAERI, JNSDA and Ship Research Institute, Ministry of Transport.

Figure 4.2.1 shows a schematic view of the experimental configuration for the upper part of the repaired primary shield.

Neutron and gamma-ray measurements were carried out by using threshold detectors, BF -counters, Bonner ball, proton-recoil counters and thermo-luminescence detectors. The analysis of the experiments is under way by

---

* Japan Nuclear Ship Development Agency

** Ship Research Institute, Ministry of Transport

using the $S_N$ codes, ANISN[3] and TWOTRAN[4], with basic nuclear data from the ENDF/B-IV and POPOP4[5] library. For processing basic nuclear data, a revised RADHEAT code system[6] is used which embraces detailed core physics treatments for resonance, thermal group and heterogeneity.

Preliminary results indicate that, for the experiment related to the addition of shielding materials above the pressure vessel, the calculated epithermal flux agrees with a factor of 5 with the obserbed value. The addition of chrysotile asbestos between the pressure vessel and the primary shield reduces the epithermal flux by three orders of magnitude, together with the effect of the addition of polyethylene and serpentine sand shield above the pressure vessel.

Reference

1) Hirota, J., E.: "Reactor Engineering Division Annual Report:, (4.1. 1974 ∿ 3.31.1975), JAERI-M, p.87 (1975).
2) Ando, Y., et al.: J. At. Energy Soc. 17, 57 (1975) (in Japanese).
3) Engle, W. W., Jr.: "A Users Manual for ANISN, A One Dimensional Discrete Ordinates Transport Code with Anisotropic Scattering", K-1693 (1967).
4) Lathrop, K. D., Brinkey, F. W.: "TWOTRAN-II, An Interfaced, Exportable Version of the TWOTRAN Code for Two-Dimensional Transport", LA-4848-MS, (1973).
5) Ford, W. E., III: "The POPOP 4 Library of Neutron-Induced Secondary Gamma-Ray Yield and Cross Section Data:, CTC-42, (1970).
6) Koyama, K., et al.: to be published.

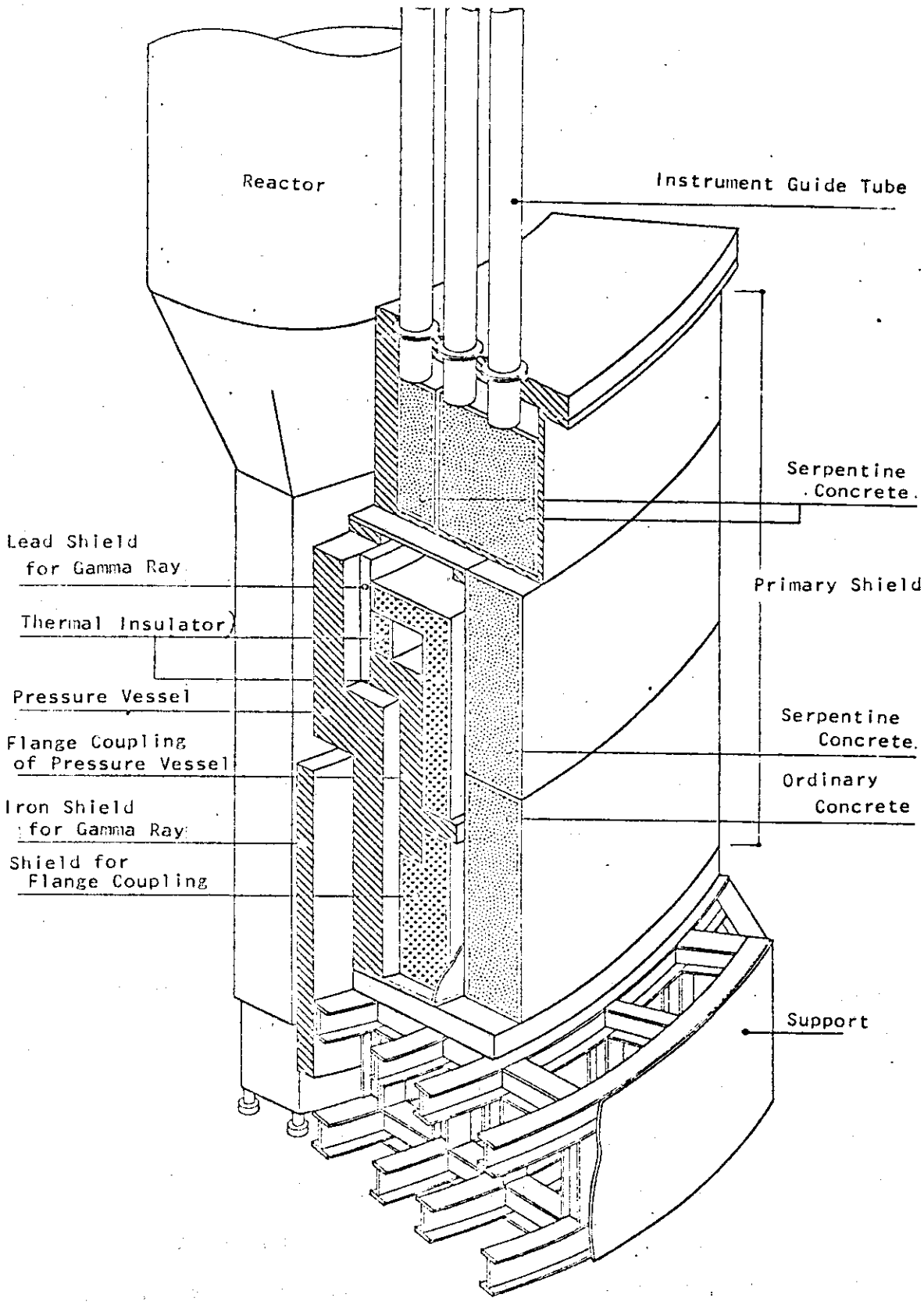


Fig. 4.2.1 A schematic view of the experimental configuration for the upper part of the repaired primary shield.

## 4.3 Neutron Energy-dependent Kerma Factors for Nuclides[1)]

S. Tanaka and K. Takeuchi*

Estimation of the radiation heating in various materials is important for the shielding and thermal design of reactor. The source of the radiation heating in reactor environments is mainly due to gamma rays and neutrons. The radiation heating in material, in general, is represented by the absorbed dose due to gamma rays and neutrons, and the absorbed dose for gamma rays and neutrons is given by the following equations, respectively,

$$D_\gamma = C \int_0^{E_{\gamma,max}} E_\gamma \, {}^m\mu_{en}(E_\gamma) \, \psi(E_\gamma) \, dE_\gamma \quad , \tag{1}$$

$$D_n = C \int_0^{E_{n,max}} K(E_n) \, \phi(E_n) \, dE_n \quad , \tag{2}$$

where

$D_\gamma$ : absorbed dose due to gamma rays (erg/g),

$D_n$ : absorbed dose due to neutrons (erg/g),

$E_\gamma$ : gamma-ray energy (MeV),

$E_n$ : neutron energy (MeV),

${}^m\mu_{en}(E_\gamma)$ : mass energy absorption coefficient ($cm^2/g$),

$K(E_n)$ : kerma factor per unit neutron fluence of energy $E_n$ (erg $g^{-1}$/neutron $cm^{-2}$),

$\psi(E_\gamma)$ : gamma-ray spectrum (photon/$cm^2$ MeV),

$\phi(E_n)$ : neutron spectrum (neutron/$cm^2$ MeV),

$C$ : energy conversion constant (erg/MeV).

Recently, the spectrum of gamma rays and neutrons in

---

* Ship Research Institute

materials can be calculated by a discrete ordinate code with good accuracy. Therefore, the absorbed dose of gamma rays and neutrons is easily obtained by knowing the mass energy absorption coefficient and kerma factor. The mass energy absorption coefficient for all nuclides has been obtained by Storm et al.[2] and Hubbell.[3] The kerma factor for neutrons has been calculated for some nuclides by Ritts et al.[4] and Abdou et al.[5], but these data are insufficient for calculating the absorbed dose of neutrons. In paticular, it is desired that the kerma factor is revised in accordance with the revise of the neutron cross section data, since the neutron cross sections are not still confirmed such as that of gamma rays.

In the present work, the kerma factors were obtained for 26 nuclides contained in fission and fusion reactor and thermo-luminescence dosimeters used for the absorbed dose measurements. As an example, the kerma factor for iron is shown in Fig.4.3.1. In this figure, the kerma factor is given for each component arizing from the different nuclear reactions as a function of the neutron energy.

References

1) Tanaka S., Takeuchi K. : "Neutron Energy-dependent Kerma Factors for Nuclides", JAERI-M 6348 (in Japanese) (1974)

2) Storm E., Harvey I. : "Photon Cross Sections from 0.001 to 100 MeV for Elements 1 through 100", LA-3753 (1967)

3) Hubbell J.H. : "Photon Cross Sections, Attenuation Coefficients, and Energy Absorption Coeeficients from 10 keV to 100 GeV", NSRDS-NBS 29 (1969)

4) Ritts J.J., Solomits M., Stevens P.H. : Nucl. Appl. Technol.

, 7, 89 (1969)

5) Abdou M.A., Maynard C.W. : Nucl. Sci. Eng., 56, 360 (1975)

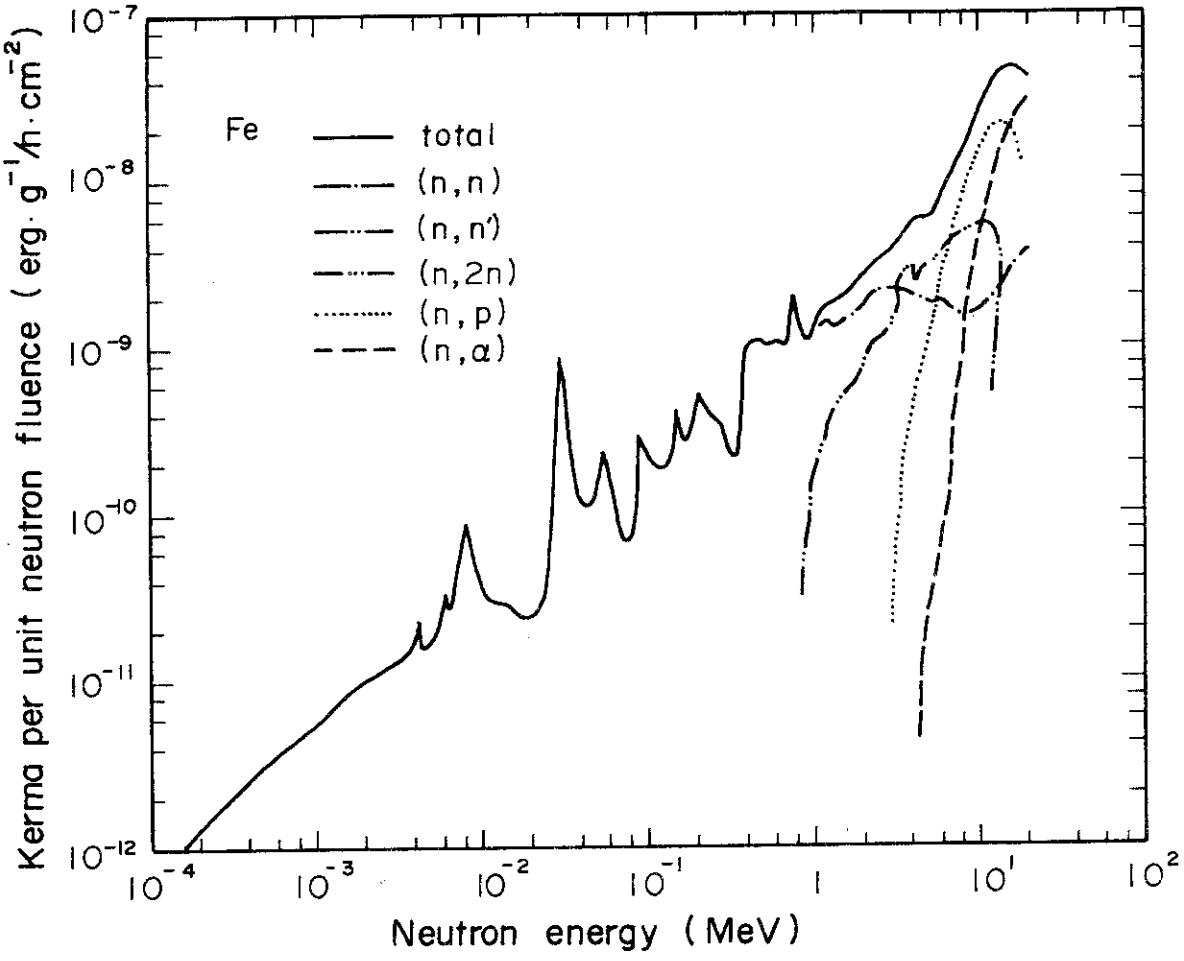


Fig.4.3.1 Kerma factor of iron per unit neutron fluence

## 4.4 Two-Dimensional Shield Calculations for JOYO

S. Miyasaka and T. Asaoka

Two-dimensional calculations for the primary shield system of JOYO have been performed and compared with the design calculations.[1] In the present calculations, special care is taken to deal with radiation streaming through the gap between the rotating plug and the heavy concrete pedestal. The two-dimensional transport code TWOTRAN-II[2] is adopted for the present calculations with a $S_6$ quardrature and $P_1$ scattering. Thirty-nine neutron group coupled nineteen gamma-ray group cross sections produced with the RADHEAT code system[3] were collaped into 7 neutron group coupled 3 gamma-ray group cross sections through the one-dimensional transport code ANISN[4].

Fig. 4.4.1 shows the overall geometry for the two-dimensional calculations. This system is so large that we divided this configuration into 5 subsections and treated it as a boot-strap problem.

Fig. 4.4.2 presents the typical results of isoflux curves of neutrons in the energy range between 1.4 MeV and 0.465 eV in the rotating plug and the pedestal. The results of two-dimensional calculation has shown that there is considerable upward streaming through the gap between the reactor vessel and the graphite shield. This streaming components raise the radiation level above the slot between the rotating plug and the pedestal. Neutron flux and gamma-ray dose above that position is higher by a factor of about $10^4$ compared to those at the center of the rotating plug. Nevertheless, the dose rate around the rotating plug obtained by the present analysis is estimated to be smaller than that of the previous design calculations.

Reference

1) Miyasaka, S., et al.: "Two-dimensional Shield Calculations for the Experimental Fast Reactor", (1975) (in Japanese).

2) Lathrop, K. D., Brinkey, F. W.: "TWOTRAN-II, An Interfaced, Exportable Version of the TWOTRAN Code for Two-Dimensional Transport", LA-4848-MS (1973).

3) Miyasaka, S., et al.: "Code System for the Radiation-Heating Analysis of a Nuclear Reactor, RADHEAT". JAERI-M 5794 (1974).

4) Engle, W. W., Jr.: "A Users Manual for ANISN, A One Dimensional Discrete Ordinates Transport Code with Anisotropic Scattering", K-1693 (1969).

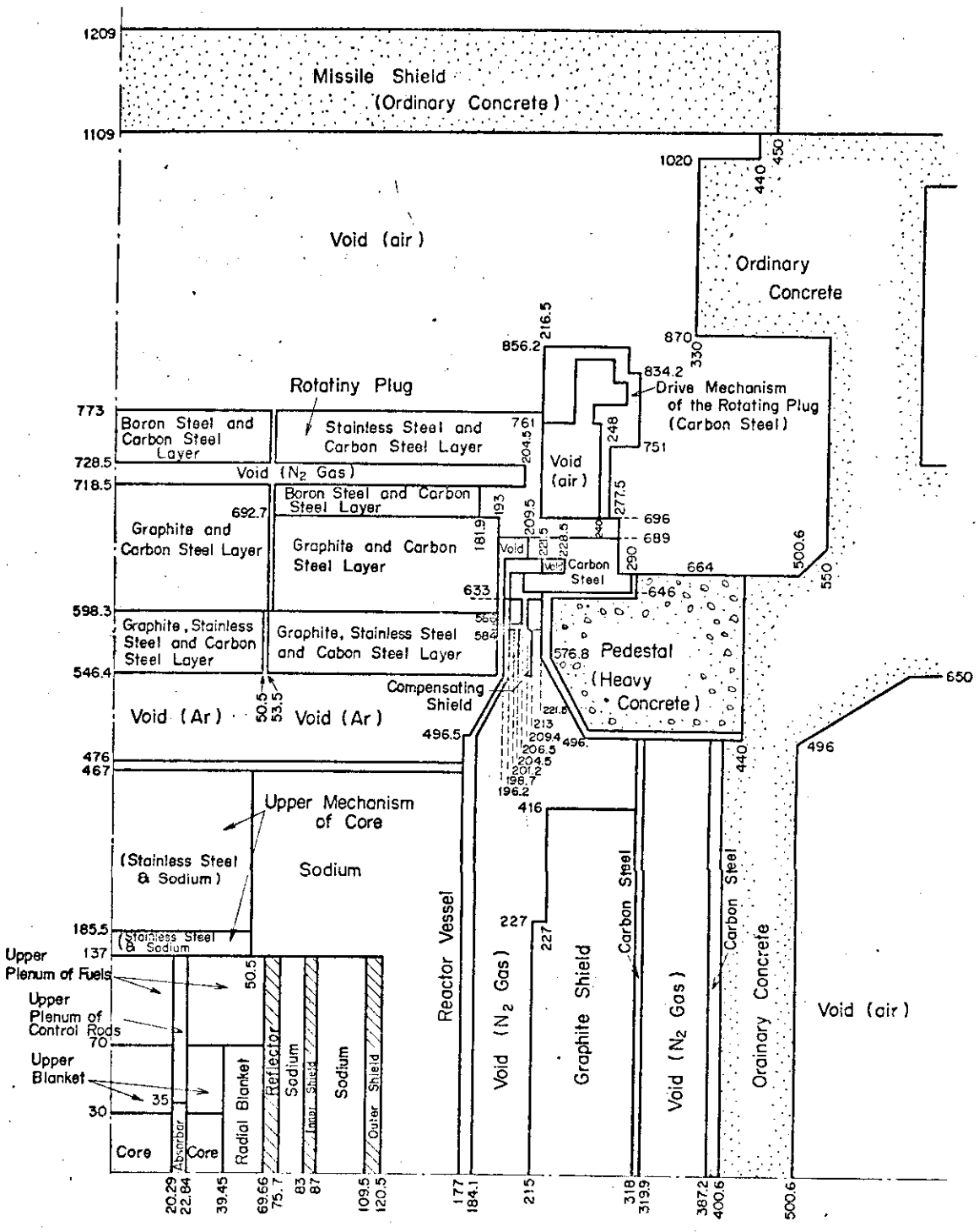


Fig. 4.4.1 Schematic vertical section of the primary shield of JOYO.

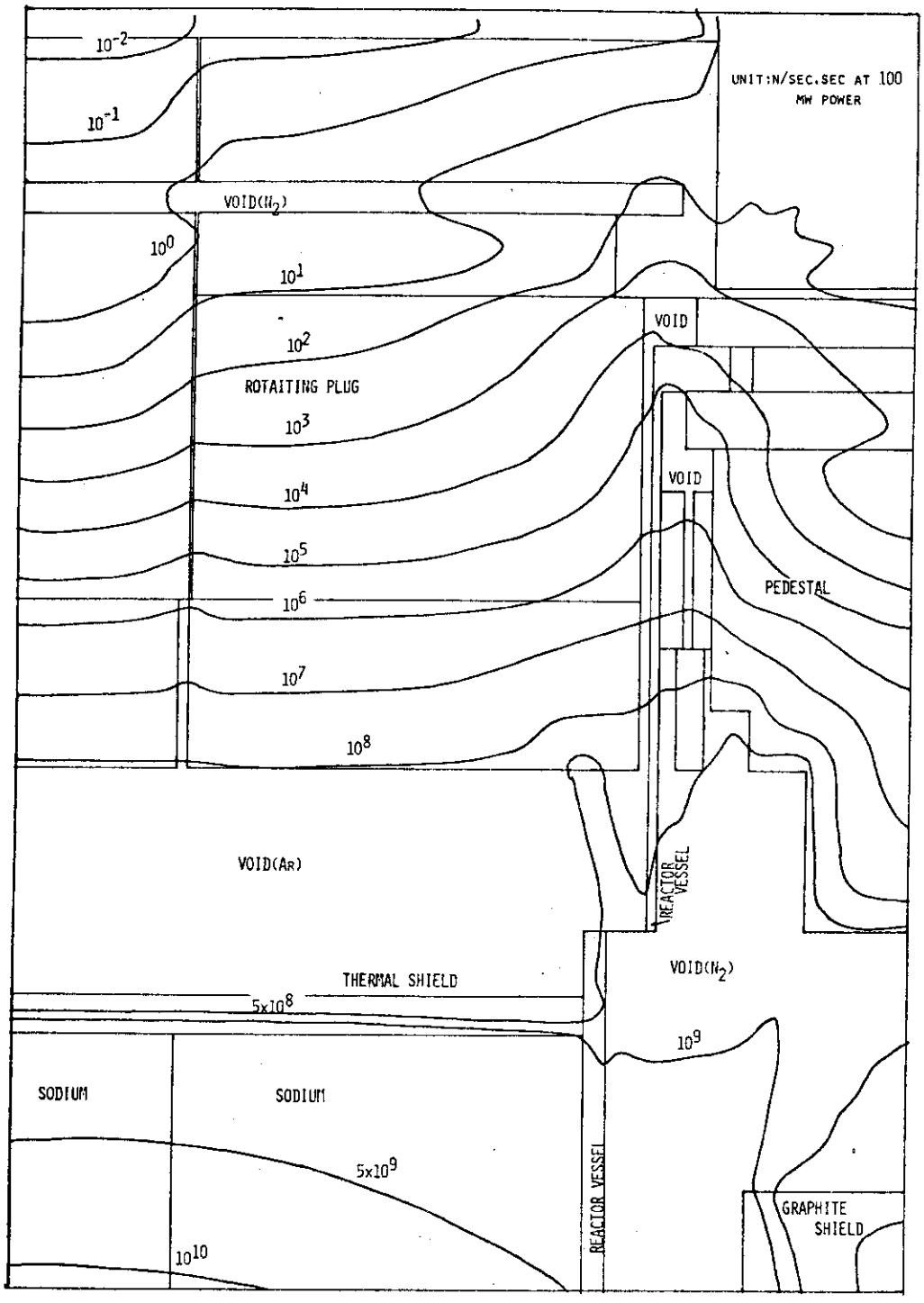


Fig. 4.4.2 Iso-flux curves of neutrons obtained by TWOTRAN-II in the rotating plug and the heavy concrete pedestal.

## 4.5 Evaluation of Shielding Computer Code DOT-3 through Experimental Results for Thick Sodium

T. Asaoka, S. Miyasaka, T. Tsutsui and T. Fujimura

A two-dimensional discrete ordinates transport code, DOT-III[1], has been modified to be equipped with the coarse-mesh rebalance acceleration for the convergence of iterative processes[2]. This modified code is tested through analyses of the ORNL benchmark experiment for neutron transport through sodium (see Fig. 4.5.1)[3]. The JAERI-Fast set[4)5)] of 70 energy-groups is adopted for neutron group constants. They are collapsed into five groups with the upper energies of 10.5 MeV, 1.4 MeV, 0.20 MeV, 4.65 keV and 21.5 eV, through the ANISN $S_N$ calculations for one-dimensional slab configurations.

The DOT-III calculations are then performed in the five-group model for two-dimensional cylindrical configurations. Figure 4.5.2 shows the Bonner ball count rates obtained with the $S_6$ calculations at a distance of 2 ft from the back of sodium of various thicknesses. The values calculated by taking account only of the attenuation due to solid angle are normalized to unity at a distance of 2 ft from the reactor beam port. As seen from Fig. 4.5.2, the calculated results agree with the measured values within a factor of 2 for all the cases. The relatively large discrepancy seen for thin sodium comes mainly from the fact that the $S_6$ approximation cannot represent well the collimated incident neutron beam.

Figure 4.5.3 shows the count rate distribution of 3-in. Bonner ball at a distance of 2 ft from the back of 15 ft sodium. The present calculated values are shown on the left side by labelling as S-6 with JAERI-FAST with impurities, which means that the calculations are performed in consideration of all Al tanks and impurities in Na. It is seen there that the calculation overestimates the counting rate by a factor of about 5. The use of the asymmetric $S_N$ quadrature combining $S_4$ in backward direction and $S_8$ in forward direction does not change the results so much. We therefore recalculate the values by using the group constants of Na based on the ENDF/B-IV instead of JAERI-Fast set. The results are given on the right side of Fig. 4.5.3. Since the calculation has neglected the presence of Al tanks and impurities in Na, for simplicity, we present also the results obtained with JAERI-Fast set by taking no account of the Al tanks and impurities on the right side of Fig. 4.5.3. It is seen that Na cross sections of ENDF/B-IV give the values smaller by a factor of 3 than those

obtained with JAERI-Fast set. Since the consideration of all Al tanks and impurities in Na reduces the values by about 40 % as seen from a comparison between the results with JAERI-Fast set shown on both the sides of Fig. 4.5.3, it shows that the present two-dimensional DOT calculation can represent accurately the deep penetration of neutrons.

References

1) Mynatt, F. R., et al.: "The DOT-III Two-Dimensional Discrete Ordinates Transport Code", ORNL-TM-4280 (1973).

2) Asaoka, T., Fujimura, T., Tsutsui, T.: "Acceleration of $S_N$ Transport Computations", in "Reactor Engineering Division Annual Report", 31, JAERI-M 6320 (1975).

3) Maerker, R. E., Muckenthaler, F. J., Clifford, C. E.: "The ORNL Benchmark Experiment for Neutron Transport in Thick Sodium", E-1, The Fourth International Conference on Reactor Shielding (1972).

4) Katsuragi, S., Tone, T., Hasegawa, A.: "JAERI Fast Reactor Group Constants Systems, Part I", JAERI 1195 (1970).

5) Katsuragi, S., et al.: "JAERI Fast Reactor Group Constants Systems, Part II-1", JAERI 1199 (1970).

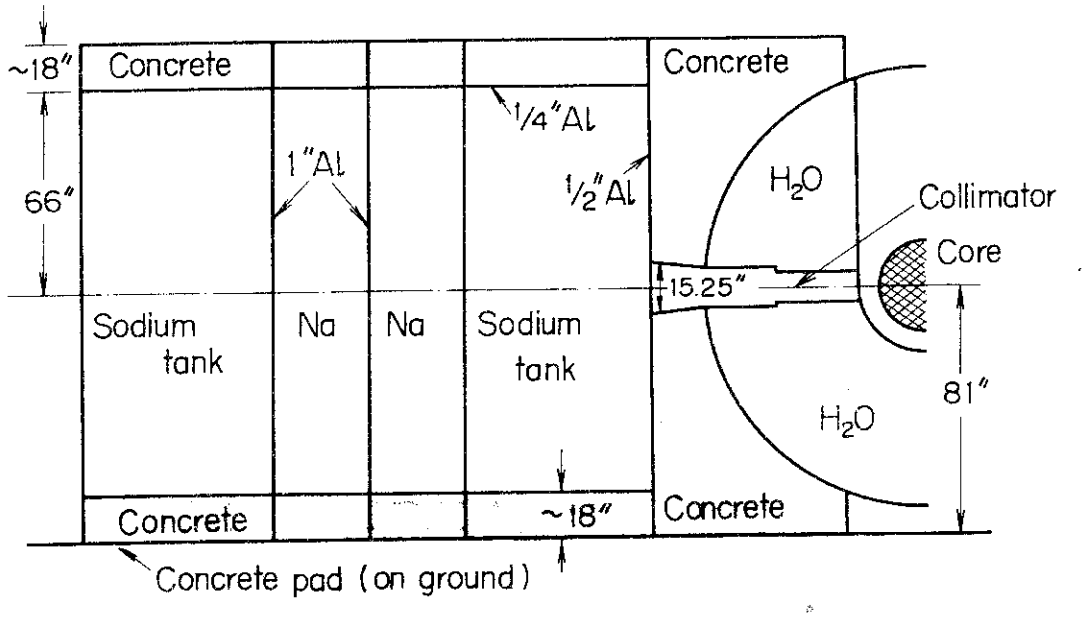


Fig. 4.5.1 ORNL-TSF configuration for neutron transport experiments in thick sodium

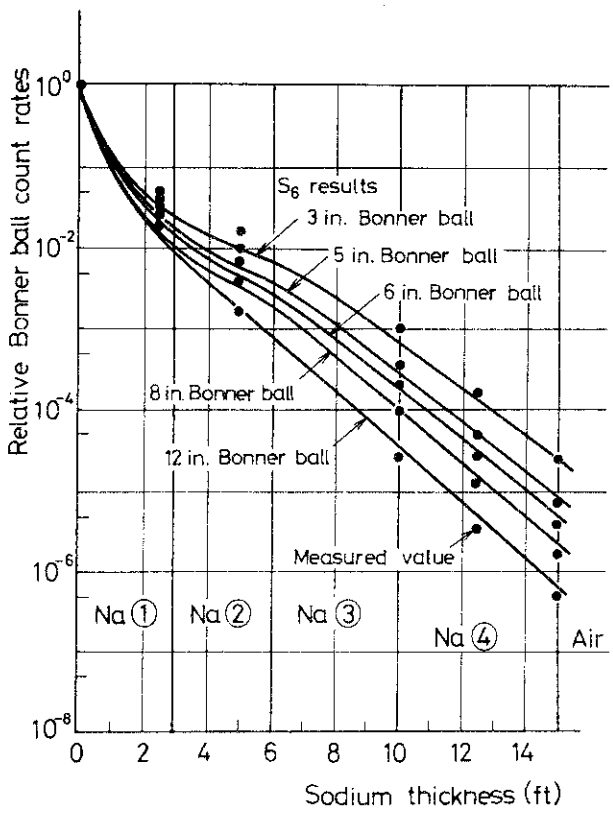


Fig. 4.5.2 Comparison of two-dimensional $S_N$ Bonner ball count rates with the measured values

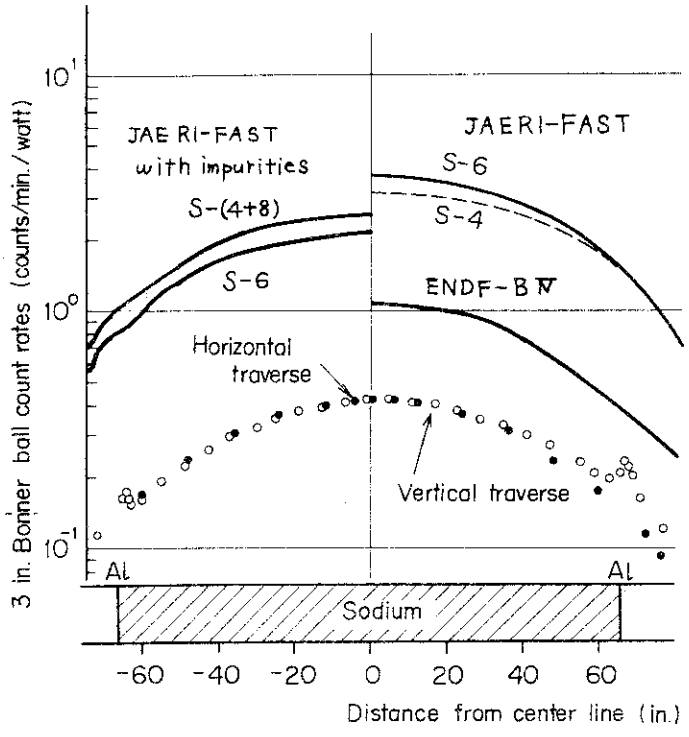


Fig. 4.5.3 Three-inches Bonner ball count rates at 24-in. behind 15 ft of sodium

# 5. Heat Transfer and Fluid Dynamics

## 5.1 Construction of High-Temperature Secondary Hydrogen Gas Loop

K. Sanokawa, M. Hishida, S. Nekoya, M. Ouchi, K. Emori, T. Takizuka, M. Ogawa, A. Miyazaki and Y. Okamoto

A high-temperature hydrogen gas loop is now under construction as a secondary loop of the high-temperature helium gas loop (HTGL). The whole system (the helium gas primary loop and the secondary hydrogen gas loop) simulates the reducing-gas heating system of the multi-purpose very high temperature gas reactor (VHTR).

The objectives of constructing the hydrogen gas loop are;

(1) to test hydrogen permeation and heat transfer characteristics of a high temperature helium gas/hydrogen gas heat exchanger,
(2) to test a hydrogen gas removing system in the primary helium gas loop
(3) to obtain useful informations for designing a reducing-gas heating system of VHTR,
(4) to get the experience on handling the high-temperature hydrogen gas facility.

The flow diagram of both the hydrogen and the helium gas loops is shown in Figure 5.1.1.

The hydrogen gas loop consists of main circulating line, purification equipment, nitrogen gas protection system, cooling system and measuring systems of temperature, pressure, flow rate and impurity gases.

The maximum temperature of hydrogen gas is 850°C at the outlet of a $He/H_2$ heat exchanger, and the maximum operating pressure is 42 $kg/cm^2 \cdot G$. The flow rate is up to 20 g/sec $\sim$ 30 g/sec.

Hydrogen gas is circulated by a double-acting compressor. The inlet temperature of a $He/H_2$ heat exchanger is controlled by electrical heater. The heater tube is made of TZM alloy metal and molybdenum. And this heat exchanger is a double tube type. Five double tubes, made of Incolloy-800, are inserted in a pressure tube of U-bend type. Helium gas, the inlet temperature of which is 950°C flows inside the inner tubes. Hydrogen gas flows in the annular space of the double tubes. Outer surface of the inner tubes are coated by calorizing process in order to reduce the hydrogen permeation rate through the tubes.

Thermal insulator is packed in the annular space between pressure tubes and heat resisting tubes of a heat exchanger, in order to reduce heat loss and prevent excess temperature of the pressure tubes. Heat resisting tubes are made of Incolloy-800, and pressure tubes are made of austenitic stainless steel.

The hydrogen gas removing system of the primary helium gas loop consists of two beds of CuO and molecular sieve. Figure 5.1.2 shows the test results of this system. Hydrogen gas in helium gas flow can be kept less than 5 p.p.m. at the outlet of the system. The hydrogen gas loop will be constructed by the end of September 1976.

Design Paramters of Hydrogen Gas Loop

| | |
|---|---|
| Maximum Operating Pressure ; 42 kg/cm$^2$g | Head of the Compressor ; 5kg/cm$^2$ |
| Maximum Operating Temperture ; 850°C | Heat Input ; 80 KW (30 KW at He/$H_2$ Heat Exchanger, 50 KW at Electrical Heater) |
| Flow rate ; ~30g/sec | Diamter of Main Pipe ; 6 or 8 inches (Pressure Pipe), 1 inch (Heat Resisting Pipe) |

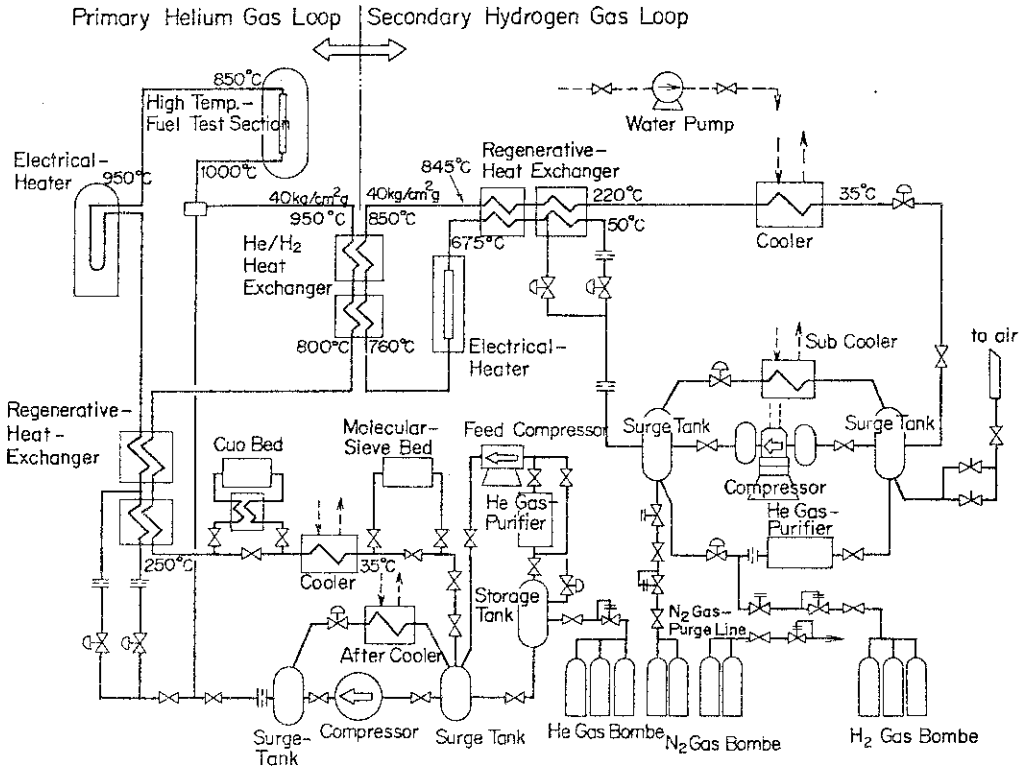


Fig. 5.1.1 Flow diagram of secondary hydrogen gas loop and primary helium gas loop.

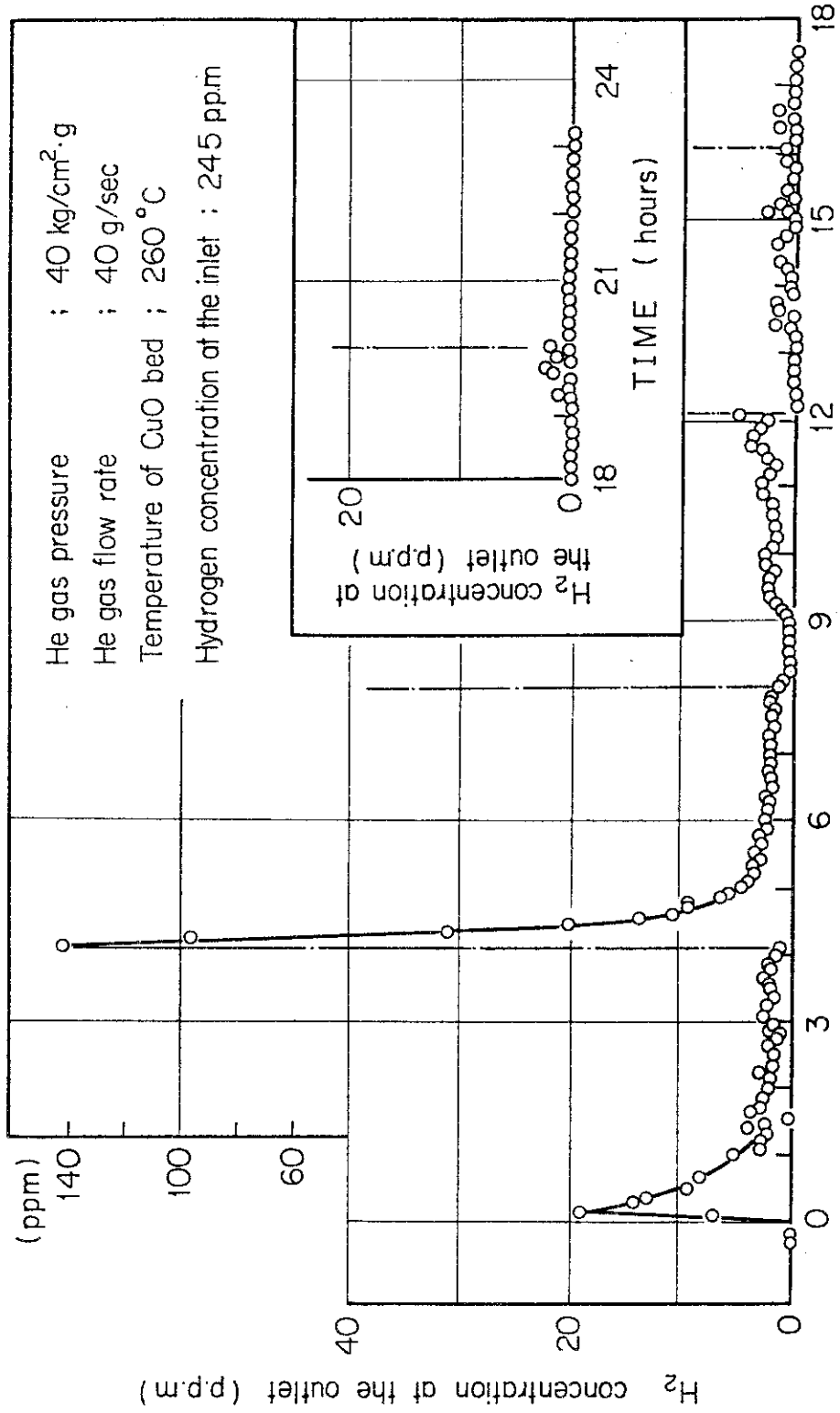


Fig. 5.1.2 Test result of hydrogen removing system

## 5.2 Heat Transfer Study of VHTR Fuel by Using High-Temperature Helium Gas Loop

N. Akino, S. Nekoya, Y. Shiina, M. Hishida, T. Takizuka, K. Emori, K. Sanokawa and Y. Okamoto

The Reynolds number of coolant in VHTR core is rather low, that is, between 3000 ∿ 6000, and is supposed to be in the range of transitional region where the flow conditions change laminar to turbulent. In the transitional region, heat transfer and pressure drop characteristics fall between turbulent value and laminar one, and sometimes very large oscillations are observed on account of intermittent behavior of flow. Moreover, another problems should be tested such as the change of surface condition by corrosion and errosion of graphite.

This study was planned to determine those characteristics of VHTR fuel by out-of-pile experiment under the same temperature (up to 1000°C) and pressure (up to 40 kg/cm$^2$·G) conditions by using High Temperature Helium Gas Loop (HTGL).[1)]

Fig. 5.2.1 shows a flow diagram of the loop. The cross-sectional drawing of this test section is shown in Fig. 5.2.2. This test section is designed to mock-up a single coolant channel and fuel rod of VHTR core according to the first conceptual design by JAERI (MARK-I)[2)]. Heated helium gas enters from HTGL through internally insulated pressure pipe and flows into upper mixing chamber. Then helium flows downward in the annular space composed of graphite outer channel tube (corresponding to the block of a fuel element) and electric heater (simulated to the fuel rod). Helium is heated up to 1000°C and heat transfer is measured. Then helium flows into lower mixing chamber before measuring the exit gas temperature and returns to HTGL through the high temperature pipe line.

Two types of heater are tested. One is composed of refractory metals. Heating section is made of tantulum pipe with 34 mmϕ O.D. and 2 mm thickness and installed with 6 W-Re type thermocouples on its inside surface[3)]. Electric current conductor is made of molibudenium. The heating section can be replaced by another graphite pipe, (34 mm O.D., 5 mm thickness) being equipped with 8 W-Re type thermocouples attached to the inner surface of graphite heater.

This test section surrounded with 3 layers of thermal insulation almost completely eliminate the heat-loss and guard heaters are axially divided into 7 segments including controllers respectively.

Experiments are conducted under the conditions shown below, covering the range of VHTR fuel:

| | |
|---|---|
| Reynolds number | 2000 ∿ 10000 |
| Inlet gas temperature | 200 ∿ 800 °C |
| Exit gas temperature | 400 ∿ 1000 °C |
| Pressure | 10 ∿ 40 kg/cm$^2$·G |
| Heat input | 30 ∿ 3000 W/cm |

Figure 5.2.3 shows an example of a temperature distribution of the highest temperature runs using a tantulum heater.

Figure 5.2.4 shows the results which represent the relation between Nusselt number and Reynolds number. Effects of variable gas properties and heat radiation are neglected, and all properties are supposed to be constant at the mean bulk gas temperature. In this Figure, almost all data are agree with previous heat transfer correlations[4∿6] even in the transitional region, except the data shown by a dark point.

The experimental conditions of the latter data are corresponding to the large heat flux and low inlet gas temperature run, so that the occurrence of laminarization can be anticipated. The experimental conditions are represented in the relation of inlet Reynolds number and non-dimensional heat flux $q_i^+$ as shown in Fig. 5.2.5. The lines in the figure show the critical value of $q_i^+$ for the occurrence of laminarization phenomena empirically determined by previous investigators[6,7]. Judging from this figure, the occurrence of laminarization in annular channel is very plausible. So, a new experiment is now planning to clarify the laminarization phenomena in annular channels by using the small helium gas loop, the pressure of which is nearly 1 kg/cm$^2$·G.

Graphite heater was tested during 6 days under the nearly same condition of tantulm heater and completed with success.

References

1) Shimomura, H., et al.: "Thermal and Hydraulic Performance of High Temperature Helium Gas Loop." ASME Paper 74-WA/HT-3 (1974).

2) JAERI-M 6141 (1975).

3) Kawamura, H., et al.: "High Temperature Thermometry of a High Temperature Helium Gas Loop", Proc. International Colloquium on High Temperature in-pile Thermometry, p.641, 12 ∿ 13th. Dec. 1974, JRC Petten, Netherlands.

4) Dalle-Donne, M., et al.: "Heat Transfer and Friction Coefficients for Turbulent Flow of Air in Smooth Annuli at High Temperature", Int. J. Heat Mass Transfer, vol.16, p.787 (1973).

5) Kawamura, H.: "On the Heat Transfer Coefficient of Annuli", Proc. 9th. Japanese Heat Transfer Symposium, p.273 (1972).

6) Hatton, A. P., et al.: "Heat Transfer in the Thermal Entry Length with Laminar Flow in an Annulus", Int. J. Heat Mass Transfer, vol.5, p.973 (1962).

7) Bankston, C. A.: "The Transition from Turbulent to Laminar Gas Flow in a Heated Pipe", J. Heat Transfer, Trans. ASME, vol.92, p.569 (1970).

8) Coon, C. W., et al.: "Transition from the Turbulent to the Laminar Regime for Internal Convective Flow with Large Property Variation", ibid, vol.92, p.506 (1970).

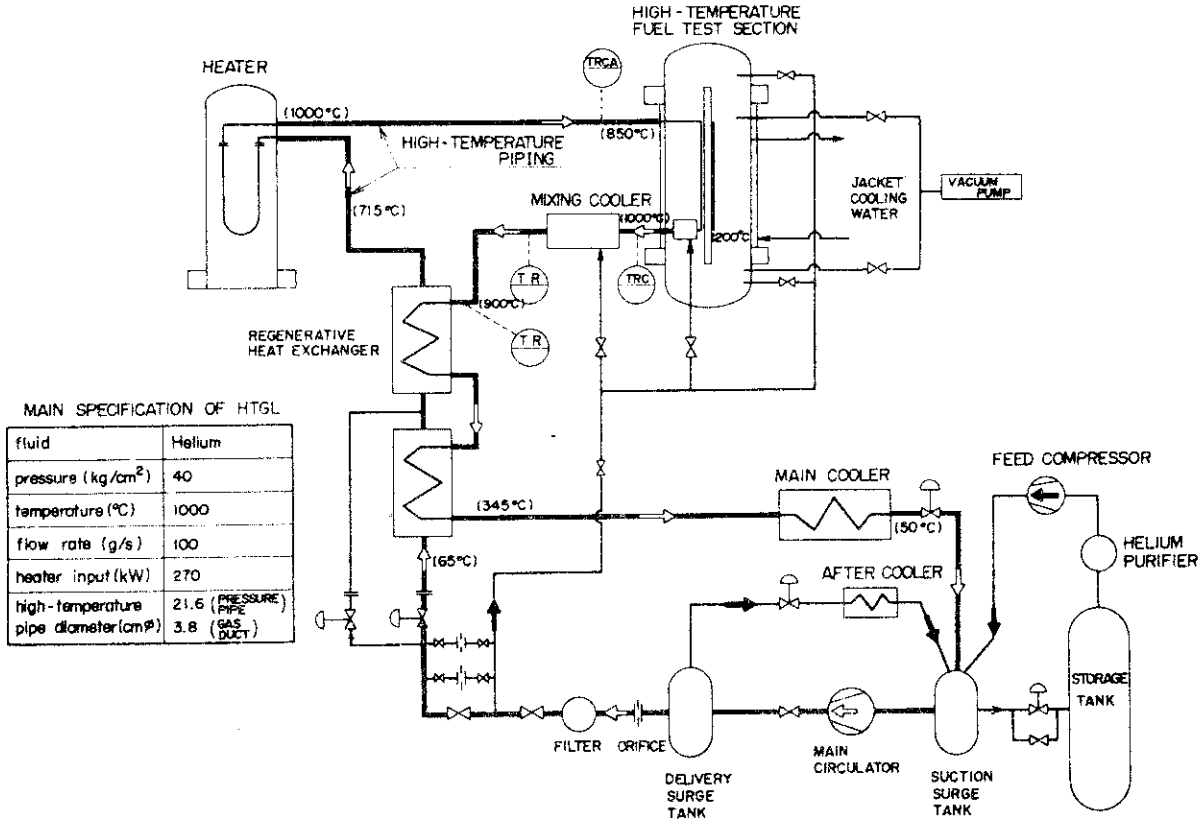


Fig. 5.2.1 Flowdiagram of the high temperature helium gas loop (HTGL) after the modification for this study.

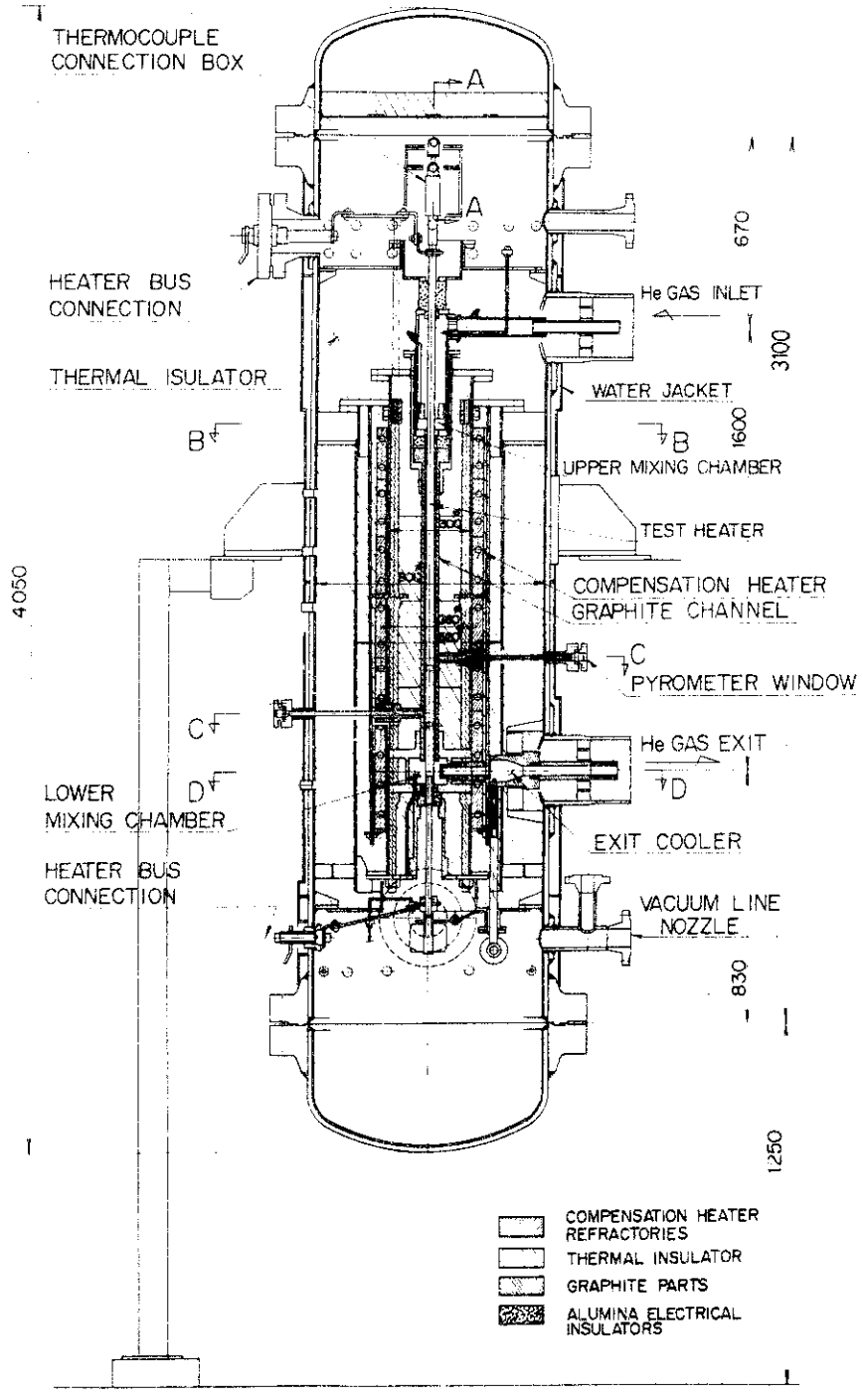


Fig. 5.2.2 High temperature fuel test section

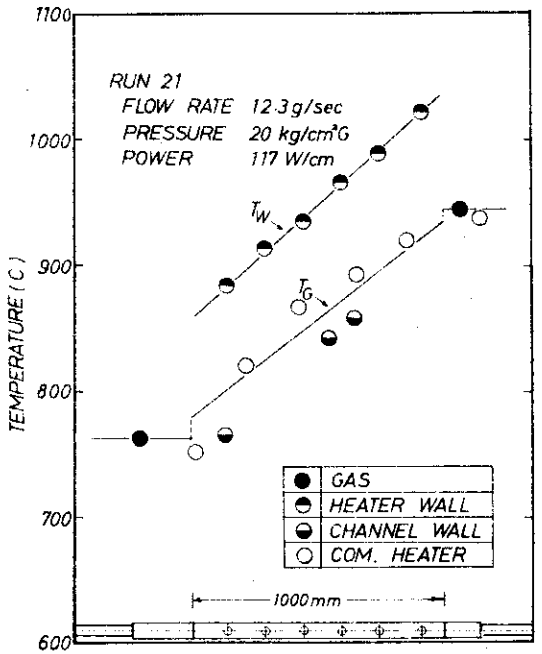


Fig. 5.2.3 An example of temperature distribution in the test section and Ta heater.

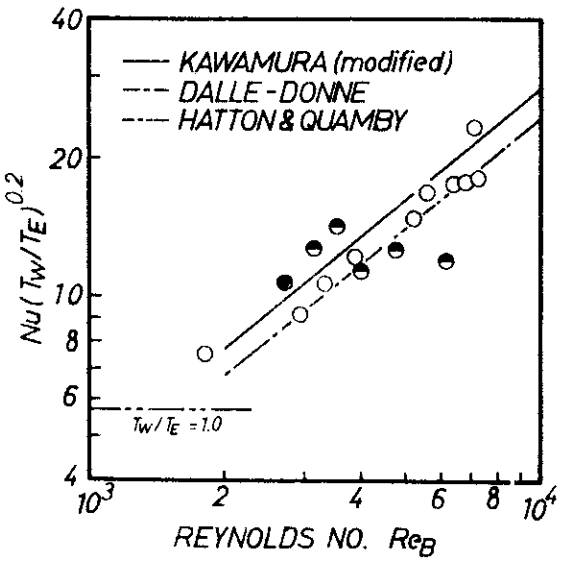


Fig. 5.2.4 Heat transfer correlation measured by Ta heater.

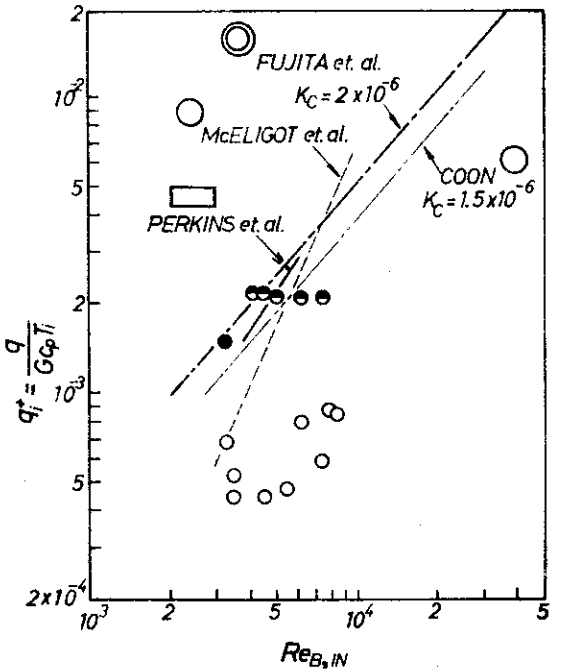


Fig. 5.2.5 The criterion for the occurence of the relaminarization phenomena.

## 5.3 Flow Visualization around Turbulence Promoters

Y. Shiina, T. Takizuka, M. Hishida, Y. Okamoto and N. Akino

Turbulence promoter is being used to improve heat transfer of nuclear fuel elements and industrial heat exchangers. However, we had found the deterioration of heat transfer rate compared with heat transfer of laminar flow at Re < 1000 when turbulence promoters were attached to the heated surface and the ratio of channel width to the diameter of promoter was 3[1]. We had examined the characteristics of the heat transfer by visualization technique of flow pattern around cylinder type turbulence promoters. We had explained that unstable and shedding vortices augumented the heat transfer at Reynolds number over 900, while stable and confined vortices at Re < 800 caused the deterioration of heat transfer[2].

In this experiment we observed the flow pattern around turbulence promoters at Reynolds number 100 to 3600 using Spinox oil as a fluid and aluminum powder as a tracer. The shape of turbulence promoter and channel width were varied. The experimental apparatus and the shape of turbulence promoter are shown in Fig. 5.3.1 and Fig. 5.3.2. The oil is circulated in the open oil circuit. Test section is 48 mm in width and 1200 mm in length.

The results are shown in Fig. 5.3.3. It has been observed that unstable and shedding vortices cannot exist below a certain value of Reynolds number which is defined by channel width as a characteristic length. Table 5.3.1 shows the critical Reynolds number when the flow around a promoter changes stable or confined vortices to unstable or shedding vortices. The subscript d denotes the diameter of a promoter as a characteristic length. The critical Reynolds number $Re_d$ in almost constant although critical Reynolds number $Re_w$ depends upon a channel width. The intensity of vortices around a promoter in the region of $Re_w$ above a critical Reynolds number depends on the shape of a promoter as is shown in Fig. 5.3.3. The vortices formed by a promoter of Fig. 5.3.2 (a),(g),(e) are stronger than those formed by (b).

References

1) Hishida, M., Okamoto, Y., Kawamura, H., Hanawa, J.: "Enhanced Heat Transfer of Fuel at Low Reynolds Number," European Nuclear Conference 1975.

2) Shiina, Y., Takizuka, T., Hishida, M., Akino, N., Okamoto, Y.: "Experimental Observation of Flow Effects on Heat Transfer of Wired

Turbulence Promoters at Low Reynolds Number", 3rd Symposium on Flow Visualization 1975.

Table 5.3.1 Comparison between critical $Re_w$ and critical $Re_d$ with w/d as a parameter

| w/d | $Re_w$ | $Re_d$ |
|---|---|---|
| 2 | 800~900 | 200~225 |
| 3 | 1000 | 170 |
| 4 | 1500~1600 | 190~200 |
| 5 | 1700~1900 | 170~190 |

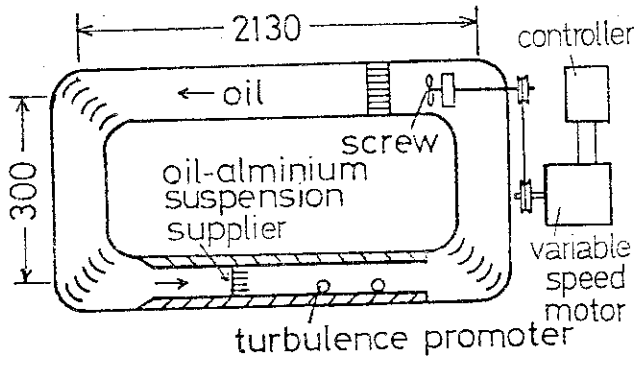


Fig.5.3.1 Test section

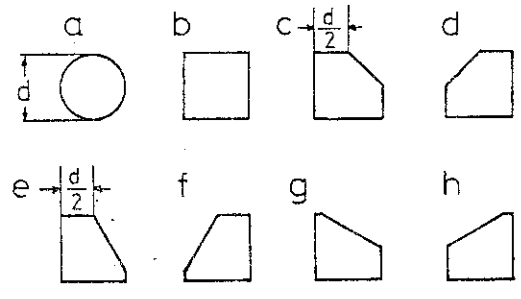


Fig.5.3.2 Shape of promoters

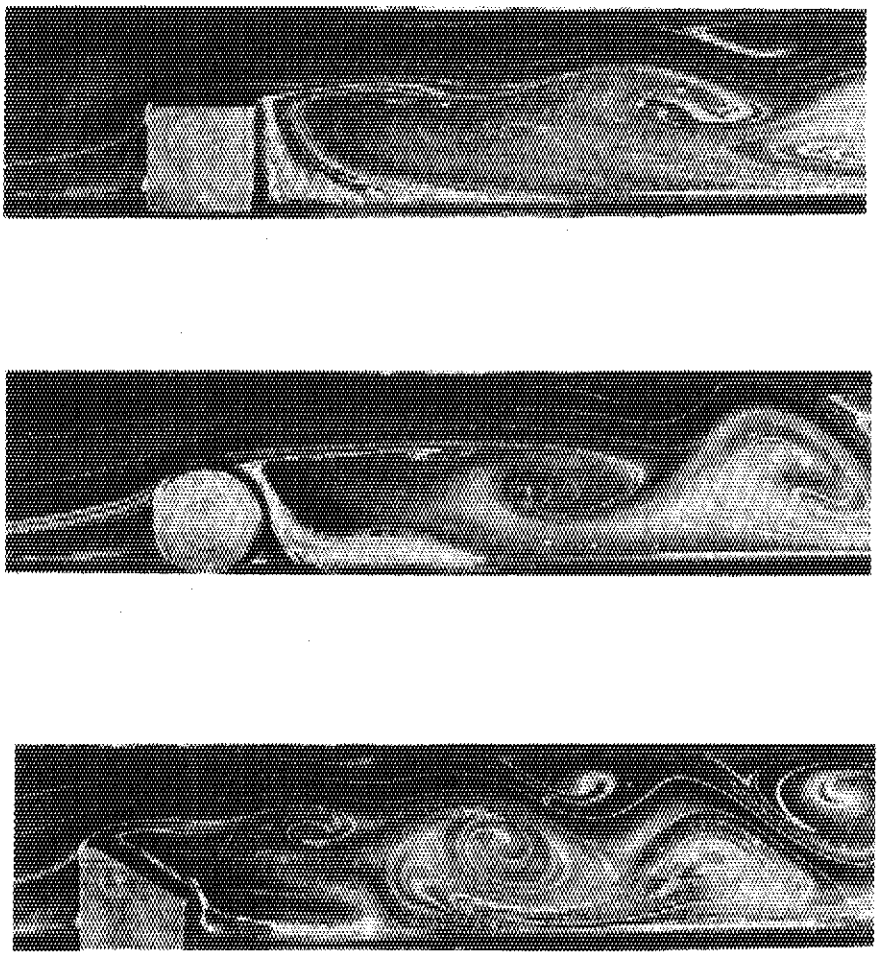

Fig. 5.3.3 Flow pattern around the promoters
( w/d = 2 , Re = 900 )

## 5.4 Transient Temperature and Thermal Stress of GCFR Fuel Elements

M. Hishida, T. Takizuka, Y. Shiina, Y. Okamoto, K. Miya*,
M. Hashimoto* and S. An*

Roughened surface is very effective to increase the heat transfer rate of fuel elements of gas cooled nuclear reactors. Roughened fuel elements or partially roughened fuel elements are supposed to be used in GCFR.

From a safety viewpoint of GCFR fuel elements, it is very important to analyse transient temperature and thermal stress of fuel elements in reactor accidents.

Transient temperature and thermal stress of GCFR fuel elements were calculated for stepwise and rampwise change of heat flux, heat transfer coefficient and coolant gas temperature.

The schematic model of GCFR fuel element and parameters, employed in the calculations, are represented in Table 5.4.1. Equations of transient heat conduction and thermal stress were numerically solved for roughened fuel element, and analytically solved for smooth part of the partially roughened fuel element.

Analytical solutions of transient temperature and thermal stress are listed in Table 1 of ref. (1).

Figure 5.4.2 shows the transient temperature and thermal stress of the roughened can for stepwise change of gas temperature. $\sigma_{\theta 1}$, the circumferential stress at the front tip of a rib, shows the highest thermal stress. Calculated temperature and thermal stresses for rampwise change of heat flux and heat transfer coefficient are shown in Figures 5.4.3 and 5.4.4. Circular symbols represent the temperature and thermal stress calculated from the steady state equations.

Calculated results for stepwise and rampwise changes of heat flux, heat transfer coefficient and gas temperature are summarized in the followings.

(1) Transient thermal stress is not so large as to impact the design of GCFR fuel elements.

(2) Time constant of transient thermal stress and temperature for stepwise changes is less than 1 sec, except the case when heat transfer coefficient is much smaller than the value at normal operation.

* University of Tokyo

(3) Transient thermal stress for stepwise changes of heat transfer coefficient and gas temperature has a maximum or minimum value.

(4) Transient temperature and thermal stress for rampwise changes can be assumed as quasi-static, unless the heat transfer coefficient is much smaller than the value at normal operation, because of rather slow change of heat flux, heat transfer coefficient and gas temperature in case of GCFR accidents.

Reference

1) Hishida, M., et al.: "Transient Temperature and Thermal Stress of GCFR Fuel Elements', NEA GCFR Meeting Tokyo (1976).

INPUT PARAMETER IN CALCULATIONS

| | | |
|---|---|---|
| material of the can | | SUS 316 |
| thermal conductivity of SUS 316 | (k) | 17.2 kcal/m hr °C (at 500 °C) |
| Poisson's ratio of SUS 316 | ($\nu$) | 0.308 (at 500 °C) |
| mean coefficient of thermal expansion | ($\alpha$) | $1.8 \times 10^{-5}$ 1/°C (at 500 °C) |
| elastic modulus of SUS 316 | (E) | 16,400 kg/mm (at 500 °C) |
| rib height | (e) | 0.1 mm |
| rib width | (w) | 0.2 mm |
| rib pitch | (p) | 0.7 mm |
| outer diameter of can tube | (Do) | 7.5 mm |
| inner diameter of can tube | (Di) | 6.8 mm |

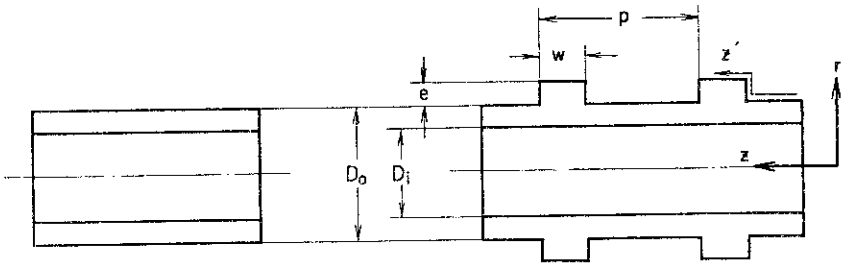


(a) swooth part of partialey roughened can (b) roughened can

Fig. 5.4.1 SCHEMATIC DIAGRAM OF GCFR FUEL CAN

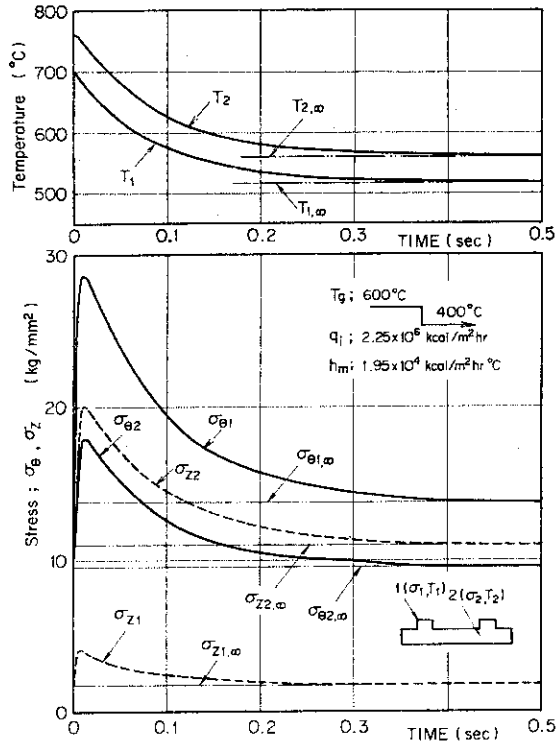


Fig. 5.4.2 TRANSIENT TEMPERATURE AND THERMAL STRESS OF THE CAN
( STEPWISE CHANGE OF GAS TEMPERATURE ; $T_g$ = 600°C → $T_g$ = 400°C ; $q_i$ = 2.25x10⁶ kcal/m²hr ; $h_m$ = 1.95x10⁴ kcal/m²hr °C )

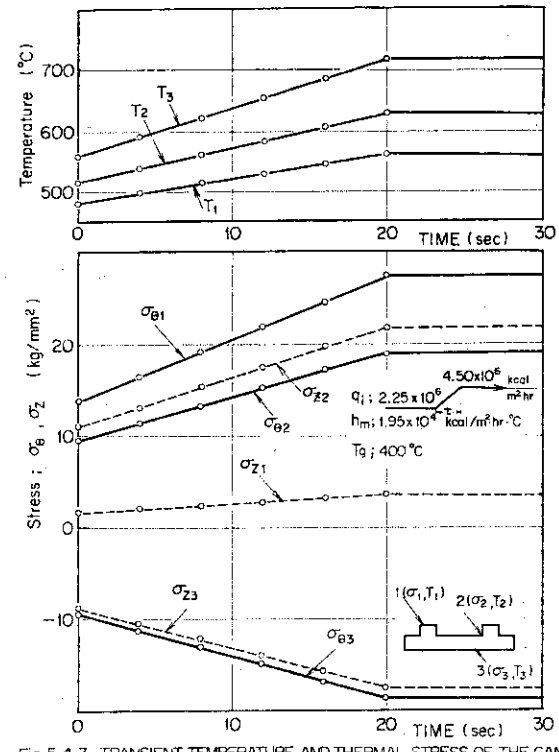


Fig 5.4.3 TRANSIENT TEMPERATURE AND THERMAL STRESS OF THE CAN
( RAMPWISE CHANGE OF HEAT FLUX ; $q_i$ = 2.25x10⁶ kcal/m²hr → $q_i$ = 4.50x10⁶ kcal/m²hr ; $\Delta\tau$ = 20 sec ; $h_m$ = 1.95x10⁴ kcal/m²hr °C ; $T_g$ = 400°C)

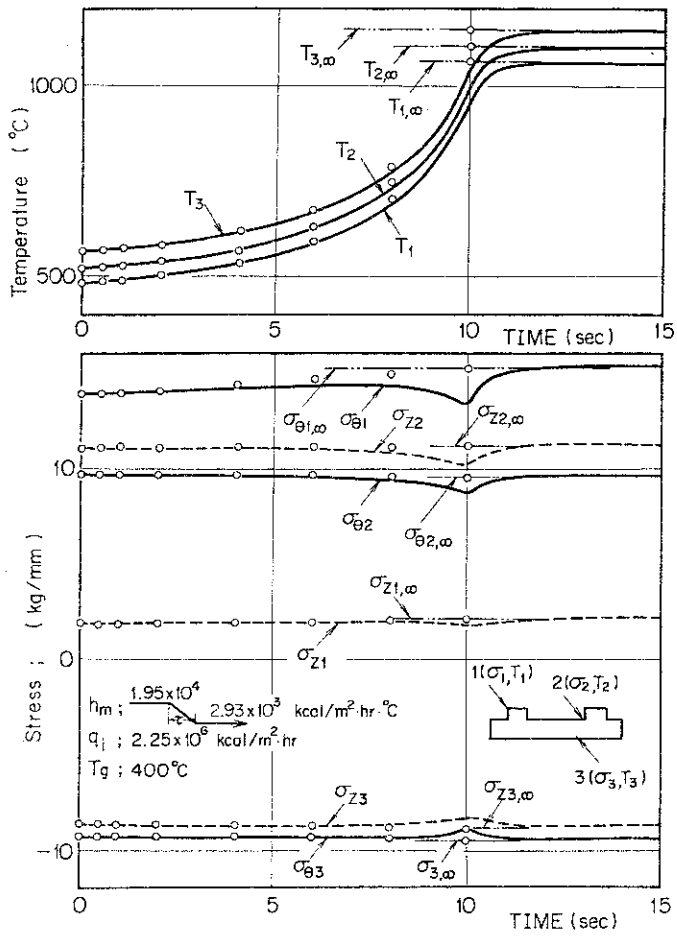


Fig.5.4.4 TRANSIENT TEMPERATURE AND THERMAL STRESS OF THE CAN
(RAMPWISE CHANGE OF HEAT TRANSFER COEFFICIENT :
$h_m = 1.95\times10^4$ kcal/m² hr °C → $h_m = 2.93\times10^3$ kcal/m² hr °C ;
$\Delta\tau = 10$ sec ; $q_i = 2.25\times10^6$ kcal/m² hr ; Tg = 400°C)

## 5.5 Tribology Study on VHTR Components

Y. Okamoto

The VHTR if planned to be constructed in JAERI. The outlet temperature is 1000°C, and the materials of components are exposed to high temperature helium environments. There is a large temperature difference between outer and inner parts of the components.

Then, thermal expansion of two parts, caused by the temperature difference of several hundred degrees, must be compensated by expansion and sliding joints. These parts should be operated at high temperature. But, contacting surfaces of these sliding parts are adhesive, corrosive at high-temperature condition.

These parts cause several troubles at high-temperature operation such as adhesion, corrosion, stick-friction and wear.

Tribology problem of VHTR components in high-temperature high-pressure helium environment has been surveyed and studied. Especially, tribology behavior in high-temperature helium is not clear and unknown from the viewpoint of reactor design.

Figure 5.5.1 shows the high-temperature dry contact mechanism for the purpose of VHTR reactors. The key point of the VHTR tribology is now concentrated on the several specified cases of high-temperature components, as shown in the followings,

(1) Reactor components

fuel rod + fuel block ∿ graphite + graphites

control rod + fuel block ∿ graphite + graphite

support plate + fuel block ∿ graphite + Hastelloy X

(2) Heat exchanger, reformer

heat transfer tube + supporter

∿ Hastelloy X, HK40 + HX, HK40 Incolloy 800

piping + Insulator ∿ Incolloy 800, HX + Ceramic pressure vessel + support plate

∿ Incolloy 800, HX + 2 1/4 Cr-Mo, SUS 304

Adhesion phenomena become troubles at the sliding part of both surfaces. Adhesion temperature is thought to be approximatelly (0.3∿0.4) × Tm(melting temperature).

The effect on adhesion force between contacing surface is influenced by the parameters of solubility, temperature, pressure, hardness, rougheness,

absorbed gas and contact speed. The available systematic data in helium environment are very few.

The friction and wear are also important on evaluating of feasibility of high-temperature thermal structure. The effects on temperature, pressure, contact speed, vibration, irradiation and helium impurity have been surveyed and studied. In order to avoid the wear and ahesion at dry contact surface, some lubricants, such as $MoS_2$, $WS_2$, TeSe, CaF, BaF, are successfully used in VHTR components. Techniques of slide lubricants for the VHTR are surveyed and analysed for system application. The proof of VHTR contact parts are proposed and planned, by using of coating and inserting material with self-solid lubricancy.

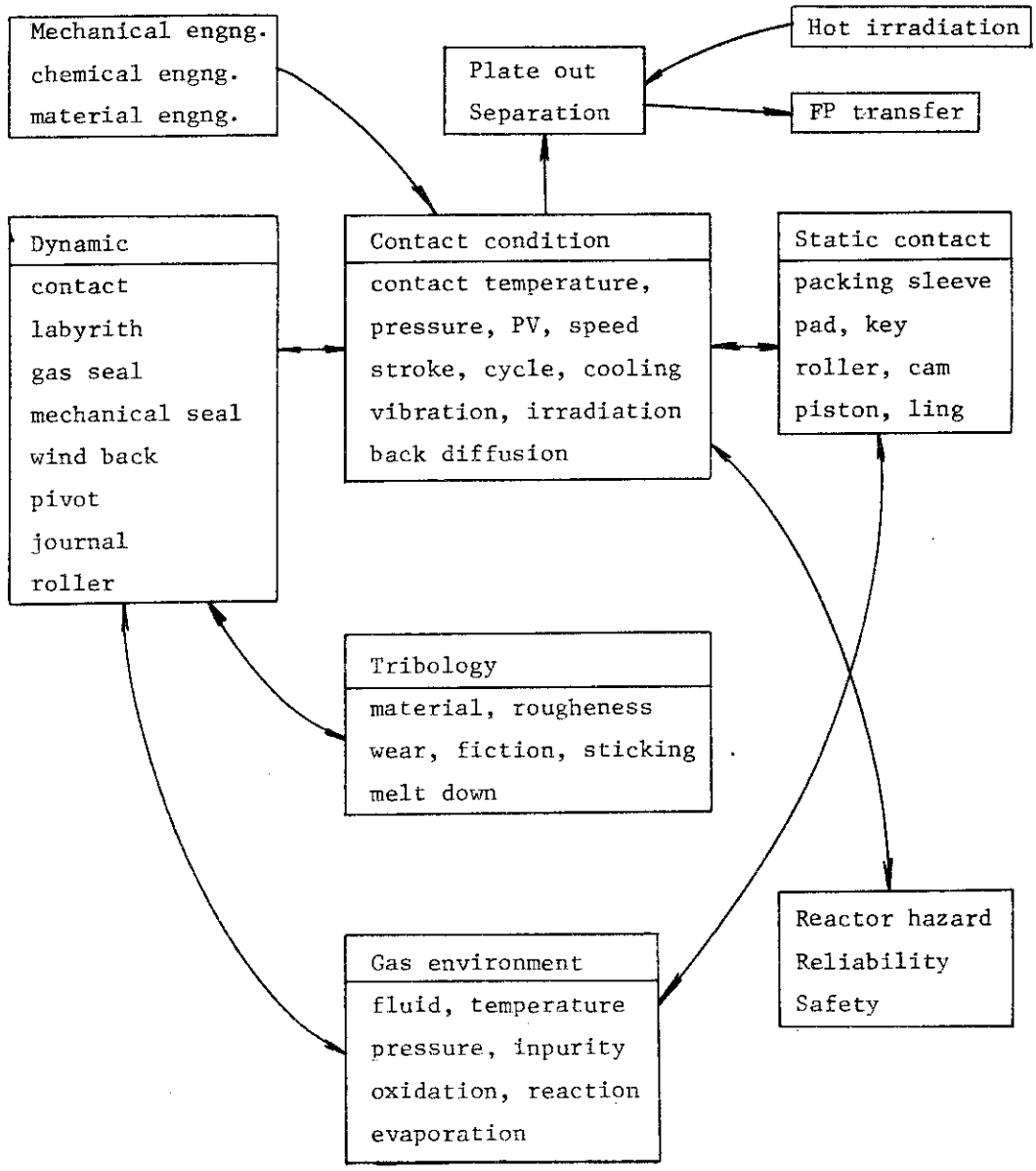


Fig. 5.5.1 Mechanism of High Temperature Dry Contact

# 6. Reactor and Nuclear Instrumentation

## 6.1 Fuel Elongation Detectors for NSRR High-Temperature Water Capsule —— Prototype Differential Transformer and the Tests ——

K. Ara and M. Yamada

The prototype of differential transformer for measuring the transient elongations of fuel clad and fuel stack in the NSRR high-temperature water capsule was constructed, and various tests were carried out[1]. The purpose was to examine its performance characteristics at high-frequency excitation condition in connection with the practical transient elongation detection, involving the optimal design of transformer.

The constructed transformer is shown in Fig. 6.1.1. The number of turns in each coil is 190, and a ceramic-insulated nickel-clad copper wire with the diameter of 0.15 mm is used for the coil. Figure 6.1.2 illustrates how the transformers are set up around the test fuel in the capsule. The magnetic core for fuel clad elongation measurement (C.E.M.) is placed at an end of the clad, and that for fuel stack elongation measurement (S.E.M.) is in the fuel clad, pressed against the end pellet with a spring.

Experiments and tests with the transformer produced several interesting results and suggestions for future works; the points of these are as follows.

One problem for solving in the experiment was how high the frequency could be in exciting the transformer without losing the sensitivity, since the desired response time was so fast that the excitation by a high frequency was inevitable. The experimental results indicated that the excitation by 7 kHz must be used for both the cases of C.E.M. and S.E.M., because the excitation by over 7kHz reduced sensitivity of the transformer rapidly in the latter case while it increased the sensitivity in the former case.

Excitation by such a high-frequency, however, induced much eddy current in the transformer body and the magnetic core. Experimental results showed that the eddy current lowered not only the sensitivity but the linear measuring range, and also the effectiveness of self-compensation where the ordinary differential output was devided by the sum of outputs of the two secondary coils to compensate for sensitivity changes due to variations of excitation condition and ambient temperature[2]. Longitudinal ditches along the magnetic core were useful in reducing the eddy current in the core and its effects.

Although the perfectness of self-compensation was reduced by the eddy current under a high-frequency excitation condition, experimental results showed that the self-compensation treatment was still effective, as compared with the ordinary differential treatment.

Figure 6.1.3 shows the calibration curves of the transformer. Each curve has been measured with the magnetic core having the optimum length where the maximum linear measuring range is obtained. The linear measuring range in the C.E.M. condition is about 16 mm, and that in the S.E.M. condition is about 10 mm. These are slightly small as compared with the desired ones. In the next stage of development, modification of coil arrangement will, therefore, be made; that is, changing the ratio in coil length between the primary and secondary.

Transient responses or step response times were not examined in the experiments, because the transient test equipment has not been prepared. However, the approximate estimates may be made from the excitation frequency. The excitation by 7 kHz presents fourteen samplings during the required response time of 1 msec, and this seems to be sufficient for obtaining the response time of 1 msec with an acceptable measuring accuracy.

The effect of eddy current induction on the transient response is not known; this will be studied in the future.

References

1) Ara, K., Yamada, M.: JAERI-M 6352, (1975).

2) Ara, K., IEEE Trans. on Instrum. and Meas., IM-21, 249 (1972).

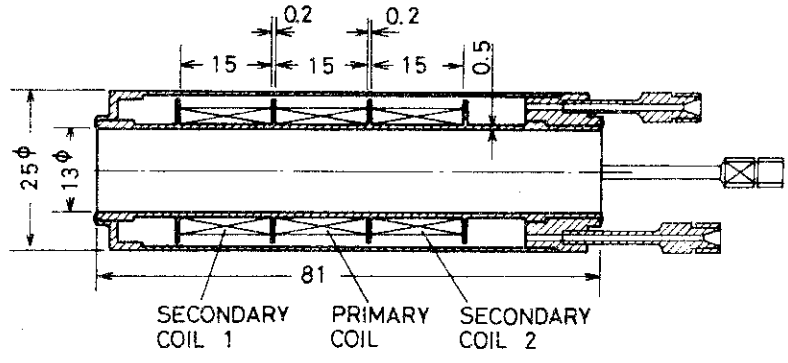


Fig. 6.1.1 Cross section of prototype differential transformer with its dimension

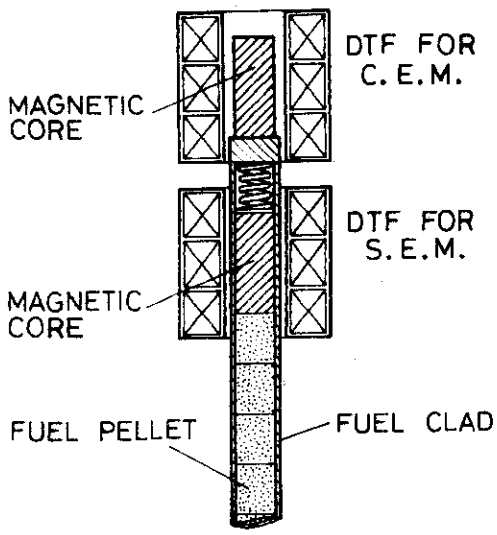


Fig. 6.1.2 Setting-up of differential transformers for fuel elongation measurements in NSRR high-temperature water capsule

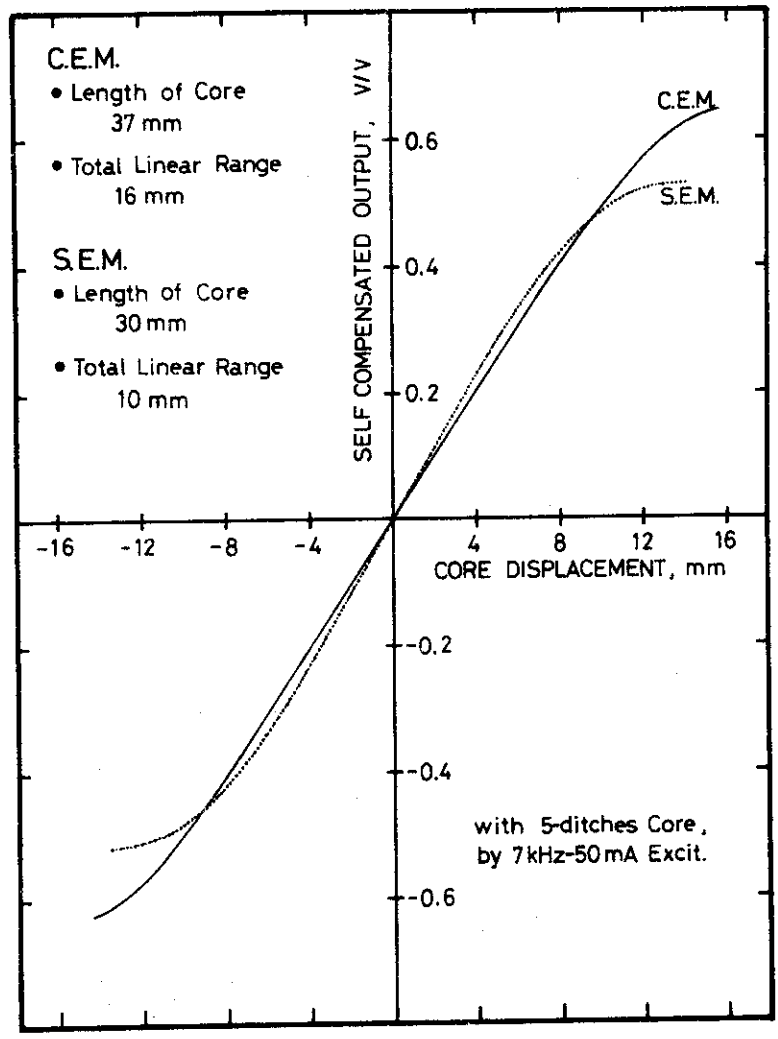


Fig. 6.1.3 Calibration curves of prototype differential transformer at the conditions of fuel clad and fuel stack elongation measurements

## 6.2 Study of Fast Response Nuclear Instrumentation Systems and Measurement of Nuclear Transient Characteristics of a Pulse Reactor NSRR

N. Wakayama, H. Yamagishi, T. Iida*, N. Ohnishi** and S. Ohtomo**

Fast response LogN-period-reactivity meters and Linear-N amplifiers were produced based on the results of developmental studies in 1974 and 1975[1][2] and nuclear transient characteristics in pulse operation of a pulse reactor NSRR were measured.

Fig. 6.2.1 shows block diagram of a instrumentation system used for nuclear transient measurement of NSRR.

Since the propagation speed of gamma-ray is faster than of neutrons, the gamma-chambers were used for measurement of reactor period and insertion reactivity.

For linear peak power measurement, a neutron chamber was used because peak power calibration against reactor power in steady state operation was very difficult when gamma chamber was used for this purpose. This difficulty is due to a change of the ratio of prompt gamma-ray current to delayed gamma-ray current depending on setting position of the chamber. (Fig. 6.2.2)

When neutron chamber is used for this purpose, big problems on pulse peak measurement are (1) widening of neutron pulse width and decreasing of peak pulse amplitude caused by neutron diffusion in water and (2) decreasing of neutrons-to-gamma-ray ratio caused by difference of attenuation factor in water.

In order to solve these problems, a micro-fission-chamber, of which neutron sensitivity is low, was used and positioned in a experimental hole (void) penetrating core center. (Fig. 6.2.3)

Some examples of the measuring results of transient characteristics of pulse reactor NSRR are shown in Fig. 6.2.4 (Oscilloscope display) and Fig. 6.2.5 (Computer display) as a function of time.

Some considerations necessary on these measurement is shown in reference (2).

As delayed neutron term in reactor kinetic equation can be neglected for short period pulse reactors, a one point, one group kinetic equation can be therefore written down as follows,

$$\frac{d\,n(t)}{dt} = \frac{\rho(t)-\beta}{\ell}\,n(t) \qquad \text{----------(1)}$$

therefore,

$$\rho(t)_{\$} = \frac{\ell}{\beta}\,\frac{1}{n(t)}\,\frac{d\,n(t)}{dt} + 1 = \frac{\ell}{\beta}\,\frac{d}{dt}\log n(t) + 1 \quad \text{---(2)}$$

As $\frac{d}{dt}\log n(t)$ is given as output of period amplifier, insertion reactivity is easily obtained as a function of time using a analogue circuits to calculate AX(t) + B.

Fig. 6.2.6 shows a measured results of pulse operation characteristics of NSRR.

References

1) Wakayama, N. and Iida, T.: "Fast Response Nuclear Instrumentation System for Pulse Reactors", JAERI-M 5955, pp. 127-130.

2) Wakayama, N., et al.: "Fast Response Nuclear Instrumentation for Pulse Reactors", JAERI-M 6320, pp. 122-124.

---

* Visiting student, Dept. of Nucear Eng., Faculty of Eng., Osaka Univ.

** Division of Reactor Safety

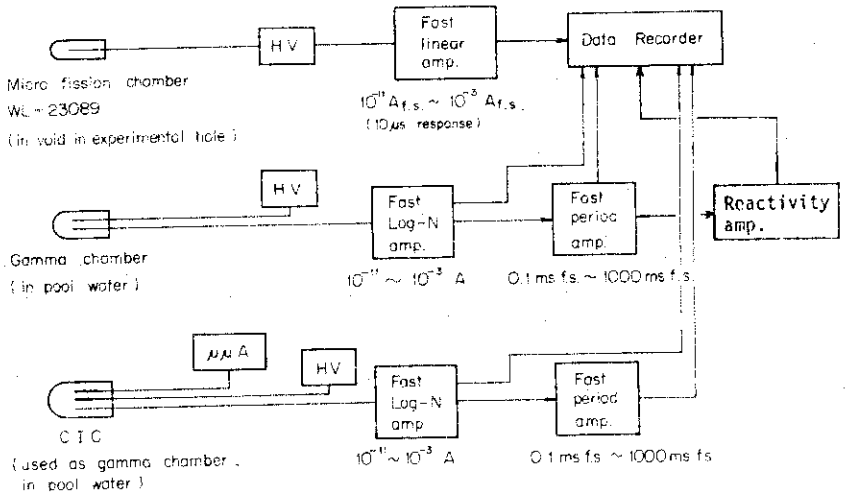


Fig. 6.2.1 Block diagram of measuring system

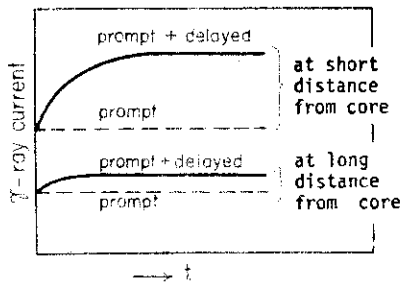


Fig. 6.2.2

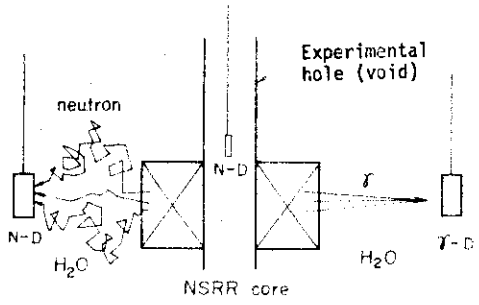


Fig. 6.2.3

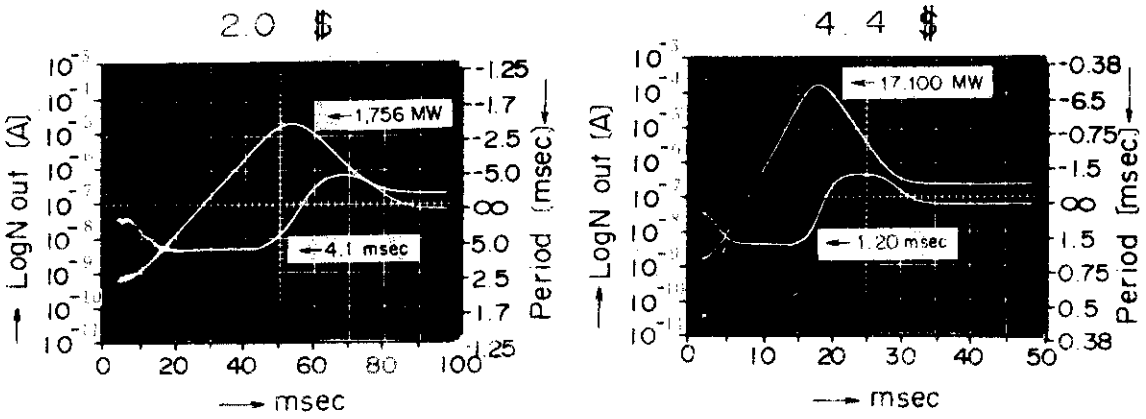


Fig. 6.2.4 Examples of oscillograph dispiay of output signals of LogN and period amplifiers in pulse operation of NSRR.

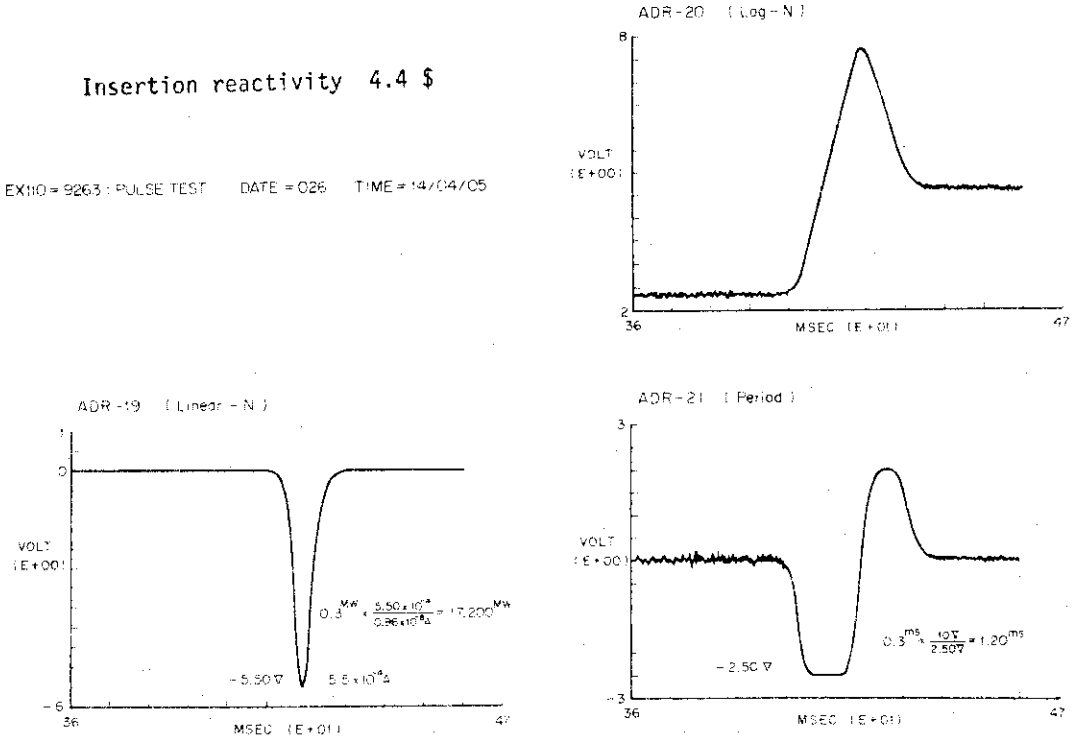


Fig. 6.2.5 An example of computer diaplay of transient characteristics of NSRR.

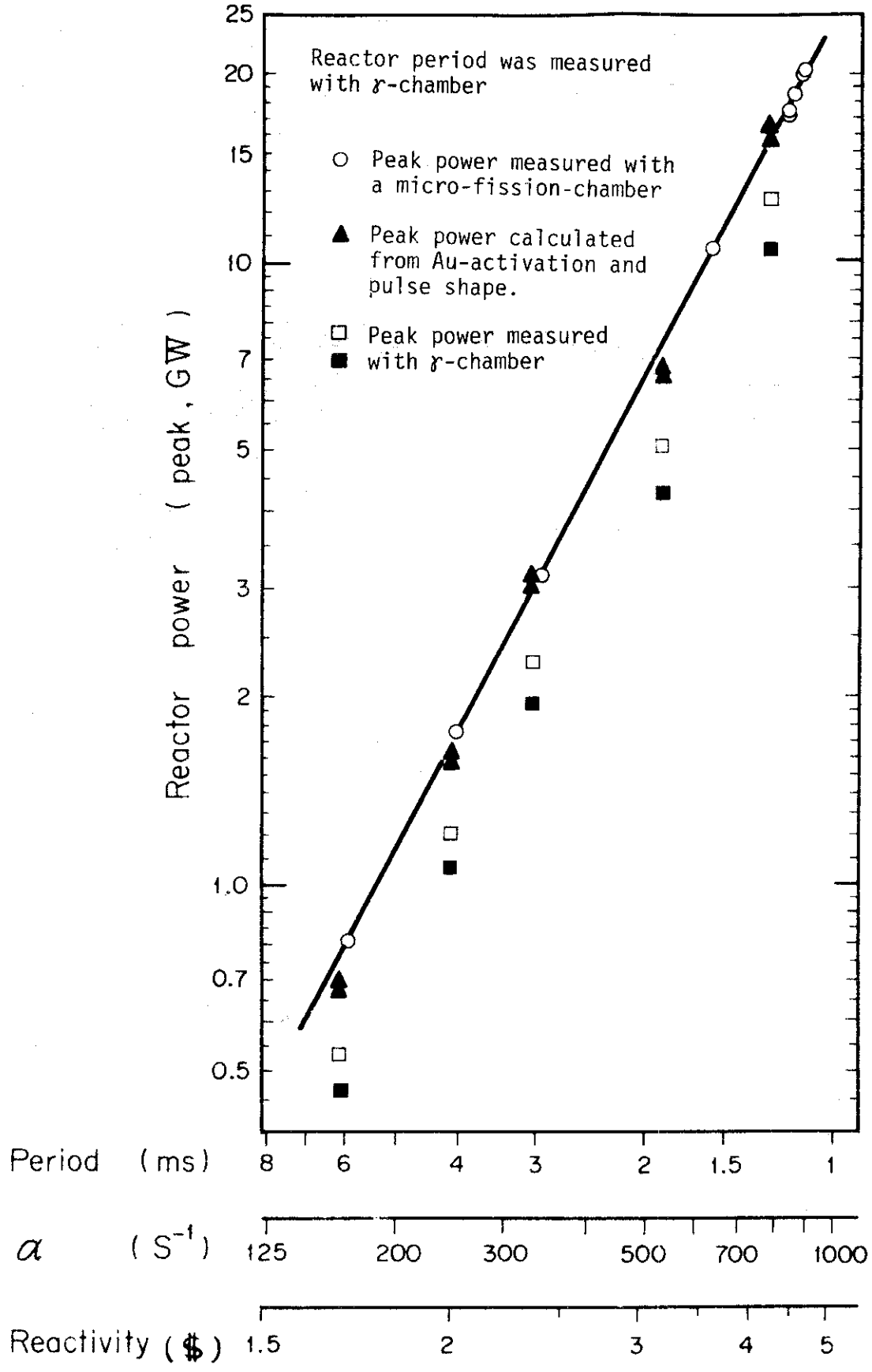


Fig. 6.2.6 Peak power, inserted reactivity and reactor period of NSRR.

## 6.3 High-Temperature-Resistant Neutron Detector Development

N. Wakayama, H. Yamagishi and T. Tomoda*

Irradiation test of high-temperature-resistant neutron counter-chamber FX-2 developed last year [1][2] was carried out with a material testing reactor JMTR in the period between May, 1975 and Jan., 1976.

FX-2 was inserted in a irradiation rig with heating elements and positioned in the reactor vessel. Ambient temperature of FX-2 in the rig was controlled between 600°C and 620°C during irradiation.

Total irradiation fluence of neutrons and gamma-rays during the period were $6.5 \times 10^{18}$ nvt and $7.2 \times 10^{10}$ R respectively.

Several times of characteristics measurements were made during the irradiation period on reactor power and in reactor shut-down period and, as a results of the measurements, it was confirmed that FX-2 was working without any trouble until end of irradiation period.

However decreasing of pulse breake down voltage of a MI-cable was observed at the end of the period. Although the PBD voltage did not reached to ordinary operating voltage, manufacturing techniques connecting with this part must be improved to increase the long term reliability.

Fig. 6.3.1 shows the effect of irradiation on integral bias curve of FX-2 during the 33rd operating period of JMTR.

References

1) Wakayama, N. et al. "High Temperature Neutron Detector Development" JAERI-M 5955 p.131 - 134.

2) Wakayama, N. et al. "High Temperature Neutron Detector Development" JAERI-M 6320 p.125 - 127.

---

* Central Laboratory, Mitsubishi Electric Corporation

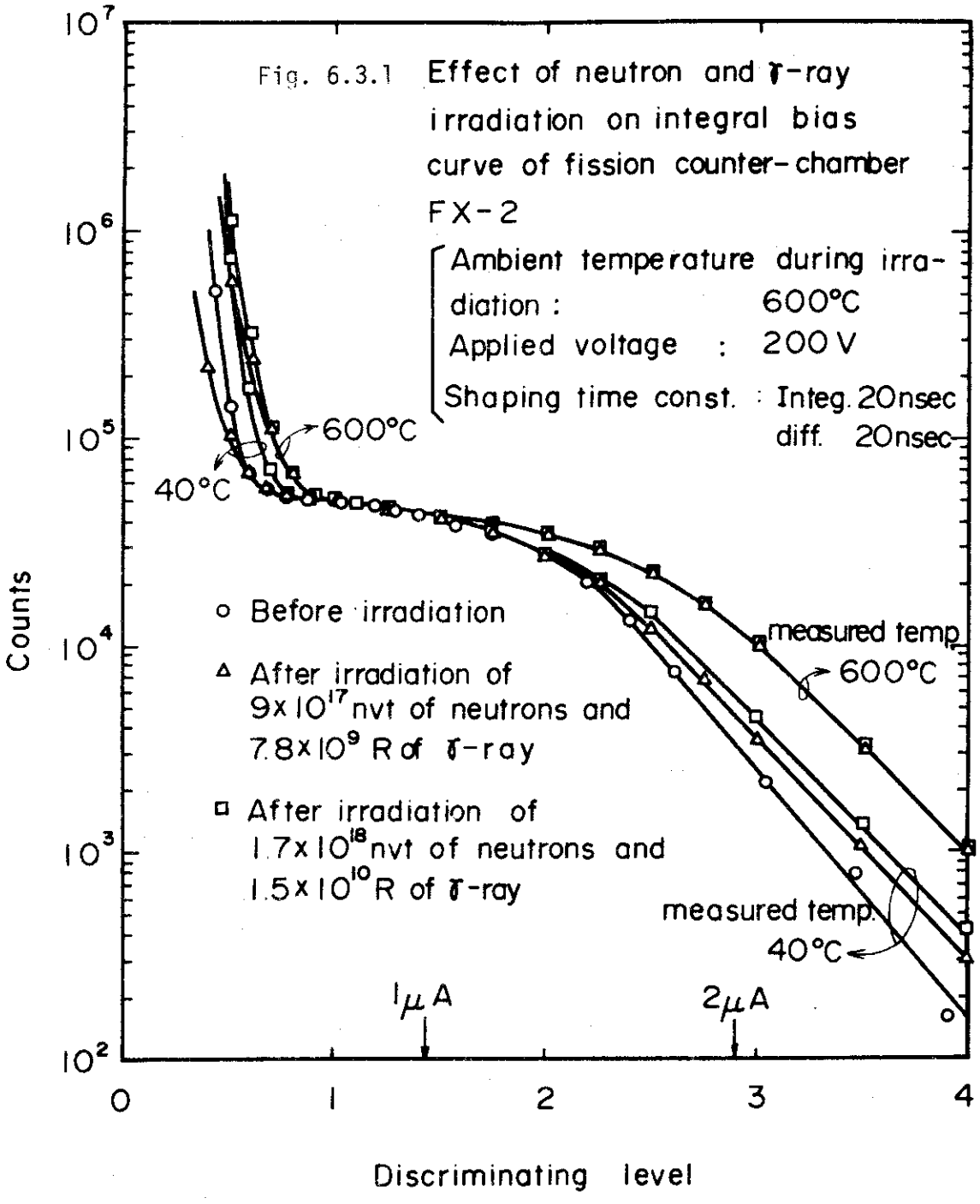
Fig. 6.3.1 Effect of neutron and γ-ray irradiation on integral bias curve of fission counter-chamber FX-2
Ambient temperature during irradiation : 600°C
Applied voltage : 200 V
Shaping time const. : Integ. 20nsec diff. 20nsec
600°C
40°C
○ Before irradiation
△ After irradiation of 9×10^17 nvt of neutrons and 7.8×10^9 R of γ-ray
□ After irradiation of 1.7×10^18 nvt of neutrons and 1.5×10^10 R of γ-ray
measured temp. 600°C
measured temp. 40°C
1μA
2μA
Counts
Discriminating level
10^7
10^6
10^5
10^4
10^3
10^2
0
1
2
3
4

## 6.4 In-Situ Measurement of Environmental Gamma-Rays Using Ge(Li) Spectrometers

E.Sakai, H.Terada, M.Katagiri, H.Yoshida and H.Itoh

A portable 73cm$^3$ closed-end coaxial Ge(Li) gamma-ray spectrometer was made and the in-situ measurement of environmental gamma-rays has been carried out. The detector has 17.5% peak detection efficiency and 2.5keV FWHM energy resolution for 1333keV gamma-rays at a source-to-detector distance of 25cm. The peak counting rate per unit flux of 662keV gamma-rays was 3.62 cps/photon/cm$^2$sec and FWHM was 2.1keV. Peak counting rate dependence on incident direction of parallel beam of gamma-rays was measured to find correction factors for in-situ data analysis. From the in-situ measurements, the concentrations of U-238, Th-232, K-40 and Cs-137 in the soil and their contributions to the total exposure rate at the detector were induced following the method developed by H.L.Beck,et al( HASL-258 (1972)), and shown in Tables 6.4.1 and 6.4.2. These results are compared with those of low level Ge(Li) spectrometer measurement of soil samples and with those of in-situ measurement using a 3" x 3" NaI(Tl)detector spectrum-to-dose conversion operator method( S.Moriuchi: JAERI-1209(1971)(in Japanese)). The agreement is not too bad when the surroundings of the in-situ measurement point are considered.

A lead shielding consisting of three lead rings( 40cm dia., 5cm thick, 6cm deep) stacked together on a 5cm thick lead bottom plate was made to suppress gamma-rays from the soil and to detect only gamma-rays from plumes. The shield was fitted to a vertical dip-stick type Ge(Li)detector and reduced the peak counting rates of gamma-rays from the soil to less than 1/3. The detection of a smaller amount of Ar-41 can be expected by the shielded detector.

Sequential variation in environmental gamma-ray spectrum was measured using Ge(Li)detectors. The increase in the peak counting rates of gamma-rays from Bi-214 was clearly observed during the rain, and the counting rates decayed within one hour after the rain had left over.

Summaries of the studies were presented at various meeting[1)-4)] and published in IEEE Transactions on Nuclear Science[5)6)].

References

1) Sakai,E., Terada,H., Katagiri,M., Itoh,H.: " In-situ measurement of

fallout Cs-137 using a portable Ge(Li) gamma-ray spectrometer ", The 12th Annual Meeting on Radioisotopes in the Physical Sciences and Industries, ( May 18, 1975, Tokyo )

2) Terada,H., Sakai,E., Katagiri,M., Itoh,H.: " In-situ measurement of environmental gamma-rays using Ge(Li)detectors ", 1975 Autumn Meeting on Health Physics of Atomic Energy Society of Japan, G-55( November 6, 1975, Osaka )

3) Sakai,E., Terada,H., Katagiri,M., Yoshida,H., Itoh,H.: " Ge(Li) detector measurement of gamma-rays from plumes ",1976 Annual Meeting on Health Physics of Atomic Energy Society of Japan, F8 ( March 25, 1976, Tokai University )

4) Sakai,E., Terada,H., Katagiri,M., Yoshida,H., Itoh,H.: " Ge(Li) detector measurement of sequential variation in environmental gamma-ray spectrum ", ibid, F9 ( March 25, 1976, Tokai University )

5) Sakai,E., Terada,H., Katagiri,M.: " In-situ gamma-ray measurement using Ge(Li) detectors ", IEEE Trans., NS-23(1), 726-733 ( 1976 )

6) Sakai,E., Terada,H., Katagiri,M.: " In-situ measurement of the environmental gamma-rays by portable Ge(Li) detectors ", JAERI-M 6498 ( 1976 )

Table 6.4.1 Concentrations of activities in the soil obtained by in-situ analysis and sampling method
In-situ measurement point: Lawn between Machin Shop and Storehouse, JAERI

| Nuclide | In-situ Ge(Li) 14:00 - 16:00 October 26, 1975 | Soil sampling method average of 5 sampled points | |
|---|---|---|---|
| | | Surface | 30 cm depth |
| Bi-214 | 0.29 pCi/g | 0.154 pCi/g | 0.245 pCi/g |
| Tl-208 | 0.48 pCi/g | 0.421 pCi/g+ | 0.459 pCi/g |
| K-40 | 9.37 pCi/g | 3.85 pCi/g | 14.8 pCi/g |
| Cs-137 | 69.47 mCi/km$^2$* | 77.7 mCi/km$^2$ | |

+ Average of two points
* $\alpha/\rho$ = 0.461 cm$^2$/g

Table 6.4.2 Total exposure rates obtained by in-situ Ge(Li) spectrometry and 3"×3"NaI(Tl) spectrometry on the lawn between Machine Shop and Storehouse, JAERI

| Nuclide | In-situ Ge(Li) 14:00 ∿ 14:00 October 26, 1975 | In-situ 3"×3" NaI(Tl) 15:05 - 17:05 September 16, 1975 |
|---|---|---|
| U-238+daughters | 0.523 (μR/h) | S. Moriuchi's method of dose evaluation by spectrum-dose conversion operator (JAERI-1209(1971) |
| Th-232+daughters | 1.405 (μR/h) | |
| K-40 | 1.677 (μR/h) | |
| Cs-137 | 0.391 (μR/h)* | |
| Total | 3.996 (μR/h) | 4.641 (μR/h) |

* $\alpha/\rho$ = 0.461 cm$^2$/g

## 6.5 Spectrum-to-Exposure Dose Rate Conversion Operator Value Function of a Ge(Li) In-Situ Environmental Gamma-Ray Spectrometer

H. Terada, E. Sakai and M. Katagiri

A spectrum-to-exposure dose rate conversion operator value function, G(E), was determined[1] for a 73.2cm$^3$ closed-end coaxial Ge(Li) in-situ gamma-ray spectrometer to calculate the total exposure rate at the detector position from the in-situ Ge(Li) gamma-ray spectrometry without any knowledge of source distributions.

The function G(E) is represented by a polynomial expression[1,2]

$$G(E) = \sum_{K=1}^{KMAX} A_K \cdot \{\log_{10}E\}^{K-m-1}$$

where E; gamma-ray energy

K; term number of a polynomial ( K=1,2,$\cdots\cdots$,KMAX )

KMAX; maximum number of terms

m; constant ( m=0,1,2,3 )

$A_k$; coefficient of each term

The coefficients $A_k$, thus G(E), are to be determined. From the standard pulse height distributions, $N_{ij}$, measured using several standard sources and the irradiation exposure rates, $D_j$, at the detector position calculated from the radioactivities of the standard sources, $A_k$ can be determined by solving the equations

$$D_j = \sum_{K=1}^{KMAX} N_{ij} \cdot G(E) \ , \ (j=1,2,\cdots\cdots,JMAX)$$

with the least square fitting where j designates the number of the standard sources used.

Fig. 6.5.1 shows the G(E) functions obtained for the 73.2cm$^3$ closed-end coaxial Ge(Li) detector; Curve 0° was obtained using the standard sources($\sim$ 100μCi) placed at 1m below the detector($\theta$=0°), and Curve 90° at 1m on a horizontal line drawn through the detector center($\theta$=90°), as also illustrated in the figure. Both the curves differ considerably for gamma-rays less than 300keV. This is caused by the dependence of detection characteristics on incident direction of low energy gamma-rays. Statistics of the standard pulse height distributions also affect G(E) functions.

Table 6.5.1 shows the total exposure rates obtained by applying three different G(E) functions to the same pulse height distribution of environmental gamma-rays. Those G(E) fonctions were obtained by using the standard

sources(∿100μCi) placed at 1m at θ = 0°,90°, and the other sources(∿10μCi) at θ = 0°. These total exposure rates differ ∿5%; different shapes of G(E) functions especially for low energy gamma-rays, did not effect appreciably the total exposure rates. Since these small differences in the exposure rates were brought by the shape of the pulse height distribution of the environmental gamma-rays, it is a matter of course for desirable Ge(Li) detector to have little dependence on incident gamma-ray direction.

Table 6.5.2 shows a comparison of the total exposure rates obtained by the G(E) function method and the HASL method( H.L.Beck, et al; HASL-258 (1972)) using the same in-situ Ge(Li) pulse height distribution. The result obtained by the G(E) function method[2] applied to an in-situ 3"x3" NaI (Tl) pulse height distribution measured at the same place, but on different day, is also listed. These three exposure rates differ max. 16% each other.

References

1) Terada, H.,Sakai, E. and Katagiri, M.: "Spectrum-to-Dose Conversion Operator Value Function of a Ge(Li) In-Situ Environmental Gamma-Ray Spectrometer," 1976 Annual Meeting on Health Physics of Atomic Energy Society of Japan, Paper F 10/SDG 76034, at Tokai University, March 25, 1976 (in Japanese)

2) Moriuchi, S.: "A New Method of Dose Evaluation by Spectrum- Dose Conversion Operator and Determination of the Operator," JAERI-1209 (1971) (in Japanese)

Table 6.5.1 Exposure rates calculated by various G(E) operators with same spectrum

| Parameters of G(E) operator | | Calculated exposure rates with same spectrum |
|---|---|---|
| Source position | 0° | 4.58 μR/h(<3MeV) |
| | 90° | 4.77 " |
| Source intensity | ∿100μCi | 4.58 μR/h(<3MeV) |
| | ∿10μCi | 4.47 " |

Table 6.5.2 Comparison of exposure rates obtained by three methods
In-situ measurement point: On the lawn between Machine Shop and Storehouse

| Method | Detector | Exposure rate |
|---|---|---|
| G(E) | Ge(Li)detector | 4.35* μR/h |
| HASL | Ge(Li)detector | 4.00 " |
| G(E)+ | 3"x3" NaI(Tl) | 4.64* " |

* Contribution of cosmic rays(0.23μR/h) has been already subtracted.

\+ The day of measurement is different from upper two cases but measurement point is same.

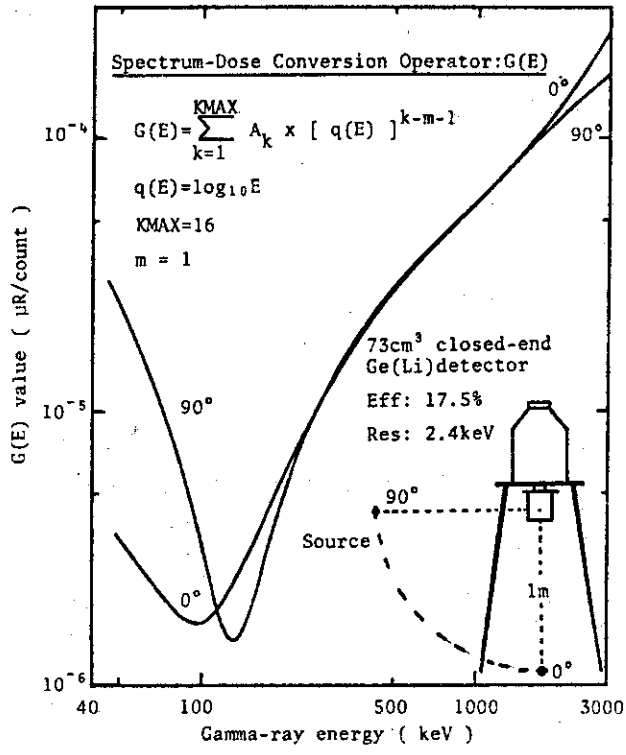


Fig. 6.5.1 Spectrum-to-exposure dose rate conversion operator value function G(E) for 73cm³ closed-end coaxial Ge(Li) gamma-ray spectrometer obtained by the measurement made using ∿100μCi standard sources placed at θ=0° and θ=90°

## 6.6 Pulse Height Dependence on Source Position in Ge(Li) Gamma-ray Spectrometer

K.Shizuma*, E.Sakai and M.Katagiri

The source position effect on peak center pulse height has been investigated in four Ge(Li) detectors (1.6 $cm^3$ and 1 $cm^3$ planar, 54.4 $cm^3$ true coaxial, and 73.2 $cm^3$ closed-end coaxial) for the gamma-rays of three different ranges of energies (300 keV, 500 keV, and 1 MeV). The experiments included the measurements of pulse height change as a function of source-to-detector distance obtained at different bias voltages, pulse height dependence on incident direction when the source was moved along a circle, and collimated gamma-ray beam scan. The peak center determination was made using Gaussian function least-square-fitted to the peak between lower side 1/2 Maximum and higher side 1/10 Maximum, and interpolating the peak center of the gamma-rays from the movable source between the two gamma-ray peaks from the fixed source. The precision of the peak center determimation was improved by increasing the numbers of the measurements.

Figure 6.6.1 shows the peak center pulse height dependence on Na-22 source position measured in a home-made 1.6 $cm^3$ planar Ge(Li) detector (14mm x 24.5mm x 6.5mm t). The peak center pulse height of 1274.511keV gamma-rays from the Na-22 source was measured as a function of the Na-22 source-to-the detector center distance by interpolating its energy between the two gamma-ray peaks (1173.226 keV, 1332.483 keV) from the Co-60 source placed at a fixed position 4.5 cm from the detector center on the $n^+$-layer side. The distance was moved between -20 cm (the $n^+$-layer side) and +20 cm (the p-layer side). The solid line shows the result obtained at 1000 V bias voltage (208 V/mm), and the dotted line at 500 V (104 V/mm). The both lines exhibited large pulse height for gamma-rays incident from the $p^+$-layer than those from the $n^+$-layer, and the difference in the pulse heights obtained at ±10 cm distance was ∿200 eV. Similar measurements gave the differences of ∿15 eV and ∿5 eV for the 511.861 keV gamma-ray

---

*Summer visiting student, July 21 to September 6, 1975; Ph. D. student (D2), Faculty of Science, Hiroshima University, Higashi-sendamachi, Hiroshima, Japan.

peaks from Ru-106 and for the 302.839 keV peaks from Ba-133, respectively. Another planar Ge(Li) detector, Ortec-made 1 $cm^3$(16 mm dia. 4.8 mm thick) exhibited almost the same results as the above, but the difference was ∿120 eV for 1274.511 keV gamma-ray peaks. The direction of the pulse height shift observed in the above two detectors can be explained by the "field increment effect" suggested by Gunnink(N.I.M. 65(1968) 26-30) and Heath(in Modern Trends in Activation Analysis (Ed. J.R.deVoe: NBS Special Publication 312(1968), vol. 2, p.959), but the amount of the shift depended on the detector. A simple calculation combining the charge collection characteristics of the 1.6$cm^3$ detector with the "field increment effect" could not explain the observed dependence on bias voltage. More experiments on Ge(Li) detectors having different charge collection characteristics are needed to complete the explanation.

The peak center pulse height of 1274.5 keV gamma-rays obtained by a home-made 54.4 $cm^3$ true coaxial Ge(Li) detector increased ∿15 eV as the Na-22 source got nearer to the detector on the detector on the detector axis, and decreased ∿60 eV as the source moved nearer on a line through the detector center perpendicular to the axis. The pulse height obtained for the source on the axis at a source-to-detector distance of 40 cm was ∿15 eV higher than that for the source on a line through the detector center perpendicular to the axis at the same source-to-detector distance.

The peak center pulse height of 1274.5 keV gamma-ray obtained by a home-made 73.2 $cm^3$ closed-end coaxial Ge(Li) detector decreased ∿20 eV as the Na-22 source came nearer to the detector on the detector axis, and decreased ∿80 eV as the source approached on a line perpendicular to the detector axis. These decrease of the peak center is an opposite direction to the "field increment effect". No attempt was made to explain these decrease of the peak center taking account of the charge collection characteristics since the situation is much complicated. The peak center pulse height was ∿40 eV lower for the source on the axis than for that on a line perpendicular to the axis.

As the above described, all the four Ge(Li) detectors exhibited the pulse height dependence on source position, and their dependence varied for each of detectors; this should be taken into consideration when the precise gamma-ray energy measurement is to be performed. It is desirable to place gamma-ray sources in the same position relative to the detector.

The summary of the above investigation was presented at the 31st Annal Meeting of Physical Society of Japan on April 4, 1976 at Nagoya University.[1] The detail was described in JAERI-M 6497(March 1976).[2]

References

1) Shizuma,K., Inoue,H., Yoshizawa,Y., Sakai,E., Katagiri,M.: "Source position effect on peak center variation in Ge(Li) spectrometers", the 31st Annual Meeting of Physical Society of Japan, 4p-D-10, April 4, 1976, Nagoya University.

2) Shizuma,K., Sakai,E., Katagiri,M.: "Pulse Height Dependence on Source Position in Ge(Li) Gamma-Ray Detectors", JAERI-M 6497(March 1976) (in Japanese)

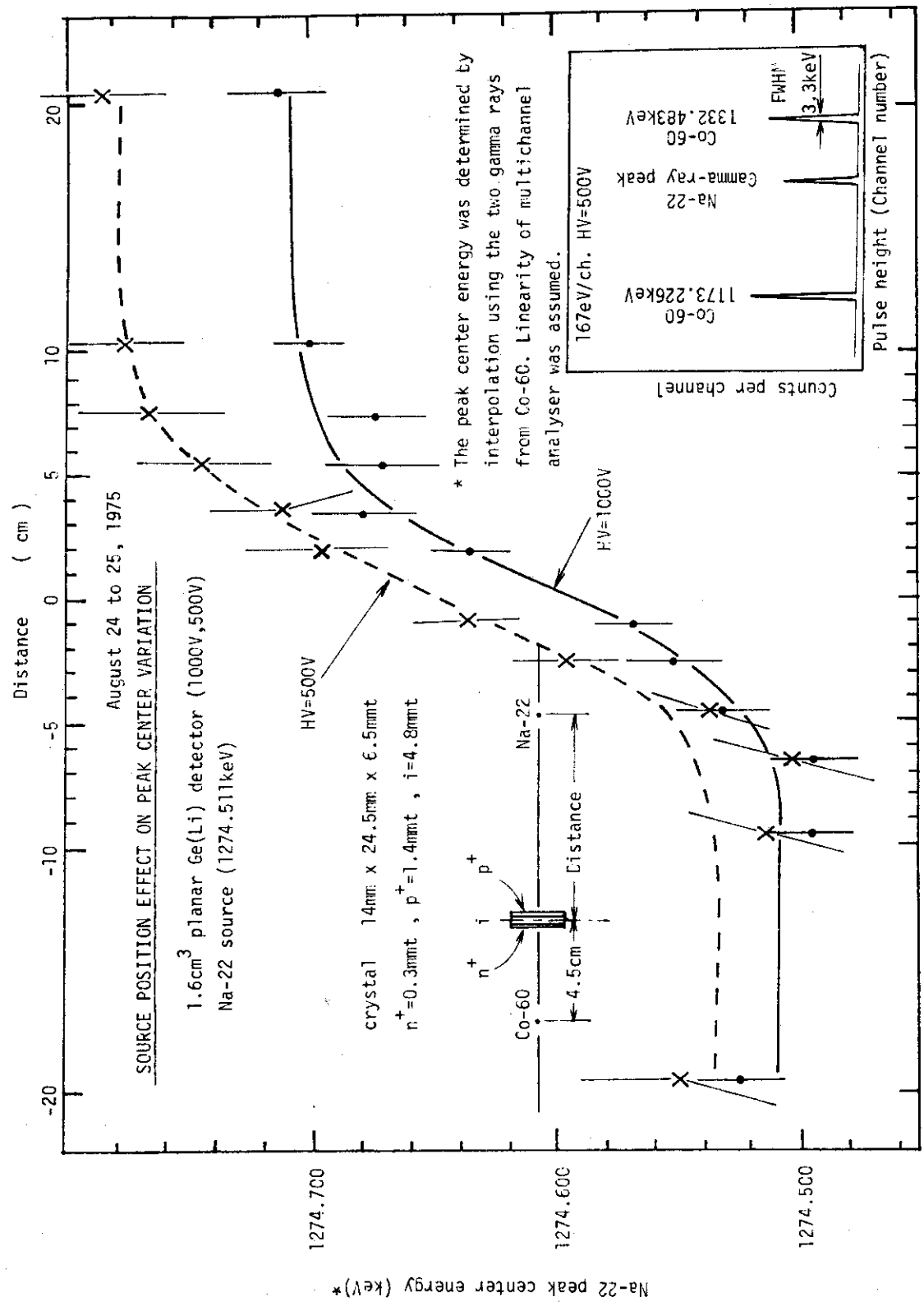


Fig.6.6.1 Na-22 source position effect on peak center variation measured in 1.6cm³ planar Ge(Li) detector.

## 6.7 Temperature Cycling Test of a Hyper-Pure Germanium Gamma-ray Detector

E.Sakai, H.Yoshida, H.Terada, M.Katagiri and H.Itoh

High-purity germanium detectors have been developed and become commercially available recently. But there still exists uncertainty whether they tolerate temperature cycling between 77K and room temperature or not. Also, there is very little published information on this matter. We have been continued this test for the last one year. Early stage of the work had been described in Sakai,E., et al: "Temperature Cycling Test of a Hyper-Pure Germanium Detector", JAERI-M5988(February 1975) (in Japanese).

The detector tested was one of the PHYGE(Passivated Hyper-pure Germanium) detector model 05005B(serial no. 100P5P3) manufactured by NRD (Nuclear Radiation Developments, 4401 Steeles Ave. W., Downsview, Ontario, Canada). The area of the entrance window for charged particle incidence and the thickness of the detector were 50mm$^2$ and 5mm, respectively.

Table 6.7.1 shows the time schedule of temperature cycling test. At the first time, at 10:00 on December 4, 1974, liquid nitrogen was filled into a common vacuum type cryostat in which the detector was mounted. Various performances of the detector such as leakage current, capacitance, gamma-ray detection efficiency, and energy resolution were measured at 77K. At 17:00 on December 12, 1974, liquid nitrogen was exhausted to warm up detector to room temperature. The detector had been at 77K for 208.0hr. After it had been left at room temperature in vacuum for 16.5hr, liquid nitrogen was filled again and the detector performance was measured. In the measurements after the 9th cycle, the detector was left in air at room temperature. The total duration of the detector at 77K until 17:22 on October 28, 1975 was 3506.5hr and the duration at room temperature become 4213.5hr(~6 months). The leakage current and the capacitance measured at 77K at a bias voltage of 600V were shown in the right columns in Table 6.7.1. They are also plotted in Fig. 6.7.1 as well as the peak detection efficiency and FWHM energy resolution for the 356keV gamma-rays from Ba-133 measured at a source-to-detector distance of 10cm. The leakage current varied between 9.3 and 33pA which was too small to affect the energy resolution. No change in the capacitance, efficiency, and resolution was observed during the 11 months test period. From the above result, one

can conclude the PHYGE detector tested was very stable against the temperature cycling between room temperature and 77K.

The summary of the study was presented at 1975 Autumn Meetings of the Atomic Energy Society of Japan[1], and KURRI-TR 142[2].

References

1) Sakai,E., Yoshida,H., Terada,H., Katagiri,M., Itoh,H.: "Temperature cycling test of a hyper-pure germanium detector(II)", 1975 Autumn Meeting on Reactor Physics and Engineering of Atomic Energy Society of Japan, C4(November 4, 1975, Osaka)

2) Sakai,E.: "Temperature cycling test of a planar hyper-pure germanium radiation detectors", KURRI-TR 142, 10-12(1976) (in Japanese)

Table 6.7.1 Time schedule of temperature cycling, leakage current and capacitance at 77°K

| No. of temperature cycling | Cooling cycle | | Duration (hr) | | Leakage current (pA) | Capacitance (pF) |
|---|---|---|---|---|---|---|
| | Start | Terminate | at 77°K | at room temperature | (at 600V) | (at 600V) |
| | (1974) | | | (Total) | | |
| Initial | 10.00 Dec. 4 | 17.00 Dec.12 | 208.0( 208.0) | (Total) 16.5( 16.5) | 9.2 | 9.0 |
| 1 | 9.30 Dec.13 | 16.30 Dec.14 | 31.0( 239.0) | 41.0( 57.5) | 9.3 | 9.0 |
| 2 | 9.30 Dec.16 | 18.30 Dec.16 | 9.0( 248.0) | 22.5( 80.0) | 9.3 | 9.5 |
| 3 | 17.00 Dec.17 | 18.00 Dec.19 | 49.0( 297.0) | 22.0( 102.0) | 11.95 | 8.7 |
| 4 | 16.00 Dec.20 | 14.00 Dec.21 | 20.0( 317.0) | 25.0( 127.0) | 13.0 | 9.4 |
| 5 | 15.00 Dec.22 | 14.30 Dec.23 | 23.5( 340.5) | 20.5( 147.5) | 14.2 | 8.5 |
| 6 | 11.00 Dec.24 | 10.00 Dec.27 | 71.0( 411.5) | 192.5(340.0) | 14.4 | 8.6 |
| | (1975) | | | | | |
| 7 | 10.30 Jan. 4 | 9.00 Jan.22 | 430.5( 842.0) | 893.5(1233.5) | 8.6 | 8.4 |
| 8 | 14.30 Feb.28 | 15.00 Mar. 8 | 192.5(1034.5) | 143.0(1367.5) | 15.8 | 9.1 |
| 9 | 14.00 Mar.14 | 12.00 Mar.22 | 190.0(1224.5) | 2620.0(3996.5) | 26.8 | 9.2 |
| 10 | 16.05 Jul. 9 | 18.40 Jul.28 | 485.5(1683.0) | 44.5(4041.0) | 18.0 | 8.9 |
| 11 | 15.00 Jul.30 | 13.20 Aug.12 | 313.5(1996.5) | 94.0(4135.0) | 31.0 | 8.5 |
| 12 | 11.30 Aug.16 | 16.32 Sep. 5 | 485.0(2481.5) | 19.0(4154.0) | (Not measured) | |
| 13 | 11.20 Sep. 6 | 11.28 Oct.20 | 816.0(3297.5) | 4.5(4158.5) | 18.0 | 9.4 |
| 14 | 16.04 Oct.20 | 9.22 Oct.21 | 17.0(3314.5) | 55.0(4213.5) | 33.0 | 8.8 |
| 15 | 16.33 Oct.23 | 17.22 Oct.28 | 192.0(3506.5) | | 20.0 | 8.8 |

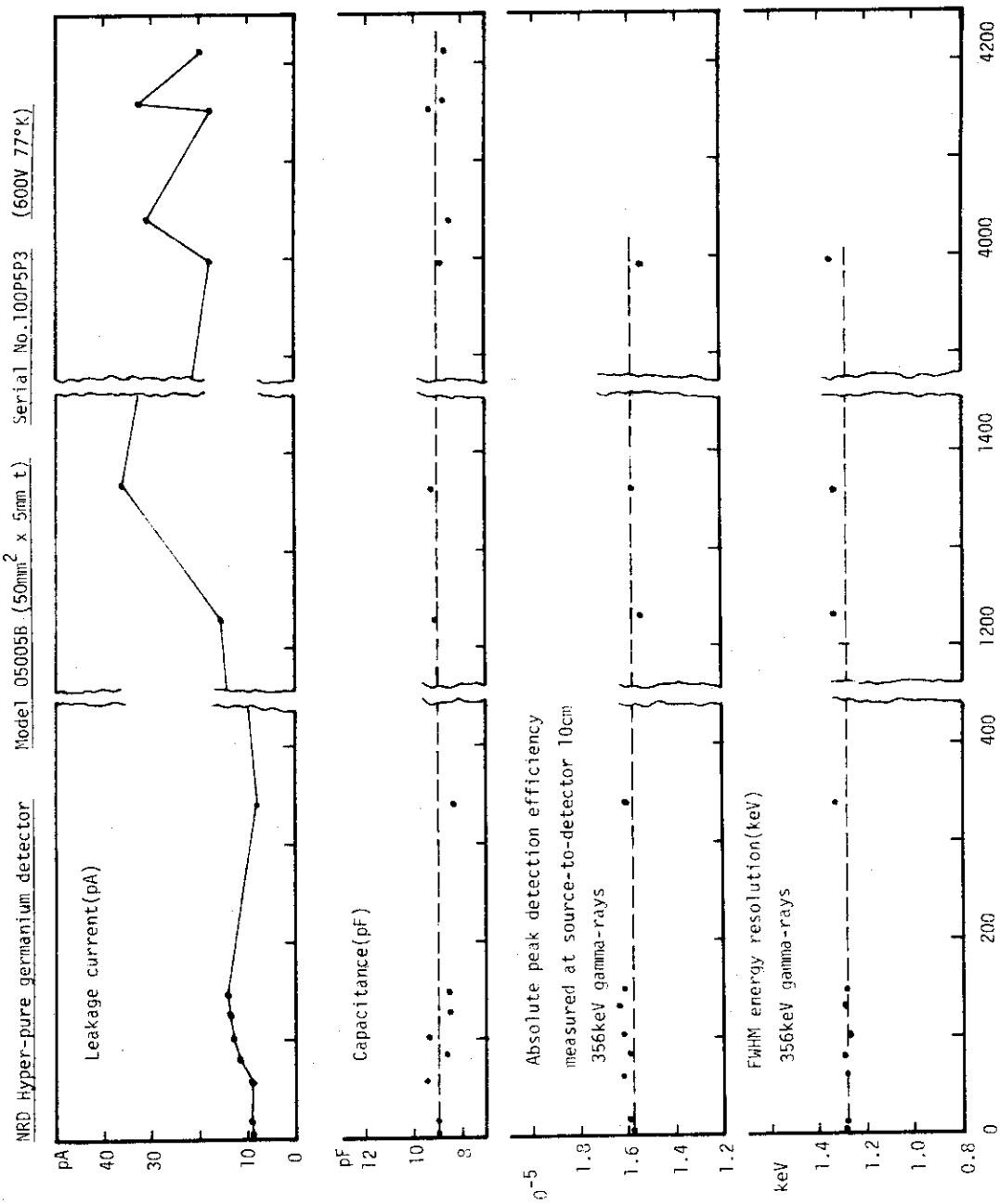


Fig.6.7.1 Characteristics variation vs. duration at room temperature.

## 6.8 Manufacturing of Silicon Detector by Ion-Implantation

M.Katagiri, H.Itoh and E.Sakai

The study of $N^+$ ion implantation into p-type silicon has been continued to make thin window radiation detectors. It was confirmed that the p-n junction could be produced by implanting 1.1MeV $N^+$ions of 2 x $10^{16}$ and 6 x $10^{16}/cm^2$ into boron-doped p-type silicon wafers( 200 ohm-cm ) in the experiments performed in FY 1974 ( in Sakai,E. et al.: " Progress Report Semiconductor Detector Group, April 1, 1974 to March 31, 1975 ", JAERI-M 6258 ( September 1975 ), also in " Reactor Engineering Division Annual Report ( April 1, 1974 - March 31, 1975 )", JAERI -M 6320 ( November 1975 )).

The effect of the energy and dose of the implanting $N^+$ions on the detector performance has been studied in FY 1975. Figure 6.8.1 shows the capacitance, and leakage current vs. bias voltage characteristics of the four silicon detectors made by the implantation of 0.55MeV and 1.1MeV $N^+$ ions at doses of 6.25 x $10^{16}$ and 6.24 x $10^{16}$ions/$cm^2$. The silicon wafers were of boron-doped p-type material and have a dimension of 25mm diameter and 1mm thickness. $N^+$ ions were implanted on an area of 0.5$cm^2$. From the figure, it is shown that the $N^+$ion energy, 0.55MeV or 1.1MeV, did not alter the leakage current and capacitance of the detectors, but the dose affected. Larger doses gave larger capacitance and leakage current. In order to understand this, the characteristics were measured of the 6.25 x $10^{15}$ 1.1 MeV $N^+$ions/$cm^2$ implanted silicon on which a layer of 50 microgram/$cm^2$ thick gold( 0.5$cm^2$) had been evaporated; the capacitance and leakage current increased and their values became almost as same as those of 6.24 x $10^{16}/cm^2$ implanted silicon, as shown in Fig.6.8.2. From this observation, one can conclude that the dose of 6.25 x $10^{15}/cm^2$ is not enough to make low-resistivity $n^+$-contact which results an equivalent circuit as shown in Fig.6.8.1, thus exhibiting lower capacitance and leakage current. The pulse height distribution of 5.37MeV alpha-particles obtained by the 6 x $10^{16}/cm^2$ implanted detector is shown in Fig.6.8.3. The FWHM energy resolution was 306 keV while pulser resolution was 229keV, which was resulted by too large leakage current. The alpha-peak height corresponds to 3.8MeV when the pulse height was compared with that obtained by a surface barrier silicon detector. This energy degradation corresponds to about 7 micrometer dead layer.

A summary of the study was presented at 1975 Autumn Meeting of Atomic Energy Society of Japan[1].

References

1) Katagiri,M., Itoh,H., Sakai,E.: " Manufacturing of p-n junction type silicon detector by use of $N^+$ ion implantation ", 1975 Autumn Meeting on Reactor Physics and Engineering of Atomic Energy Society of Japan, C 5 ( November 4, 1975, Osaka )

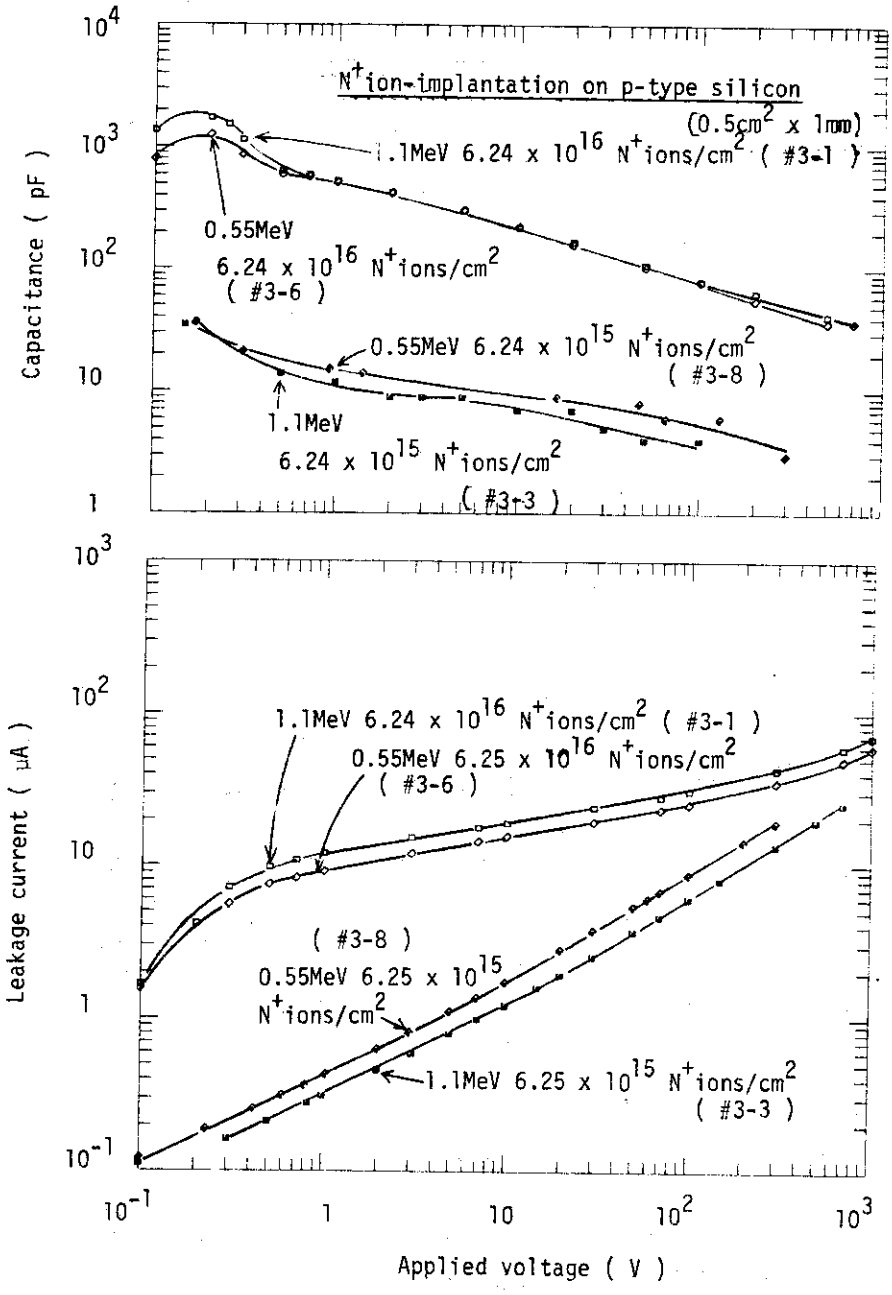


Fig.6.8.1 Effect of energy and dose on C-V and I-V characteristics of $N^+$ ion implanted silicon detector

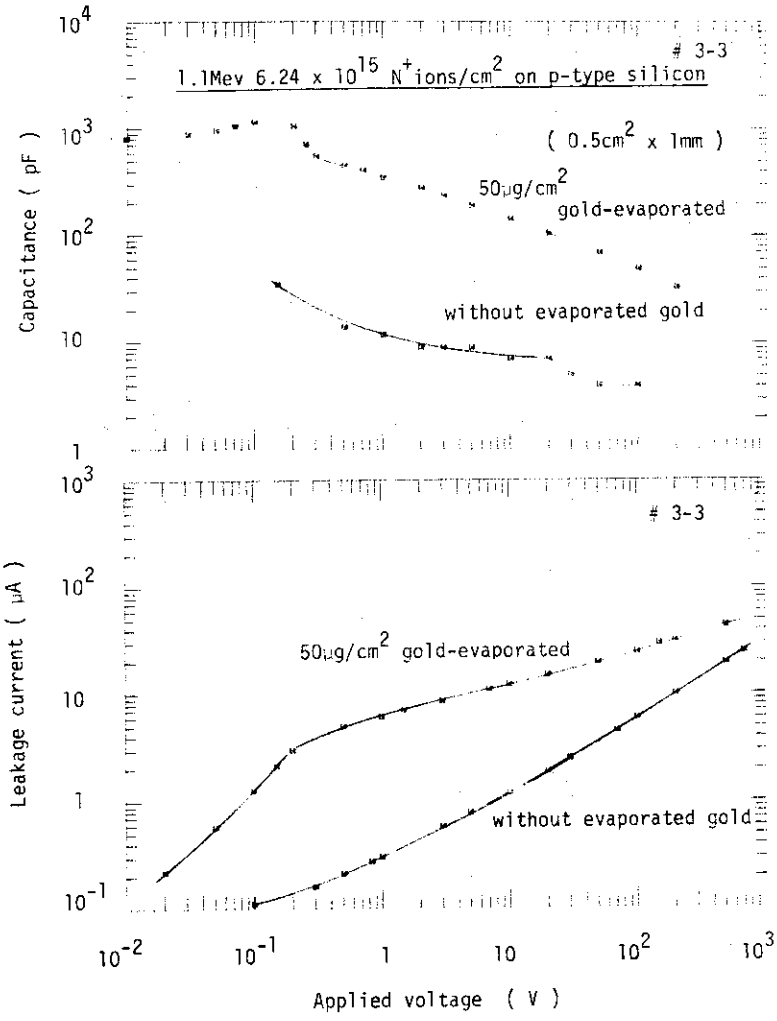


Fig.6.8.2 Effect of evaporated gold onto $n^+$-layer on C-V and I-V characteristics of $N^+$ ion implanted silicon detector

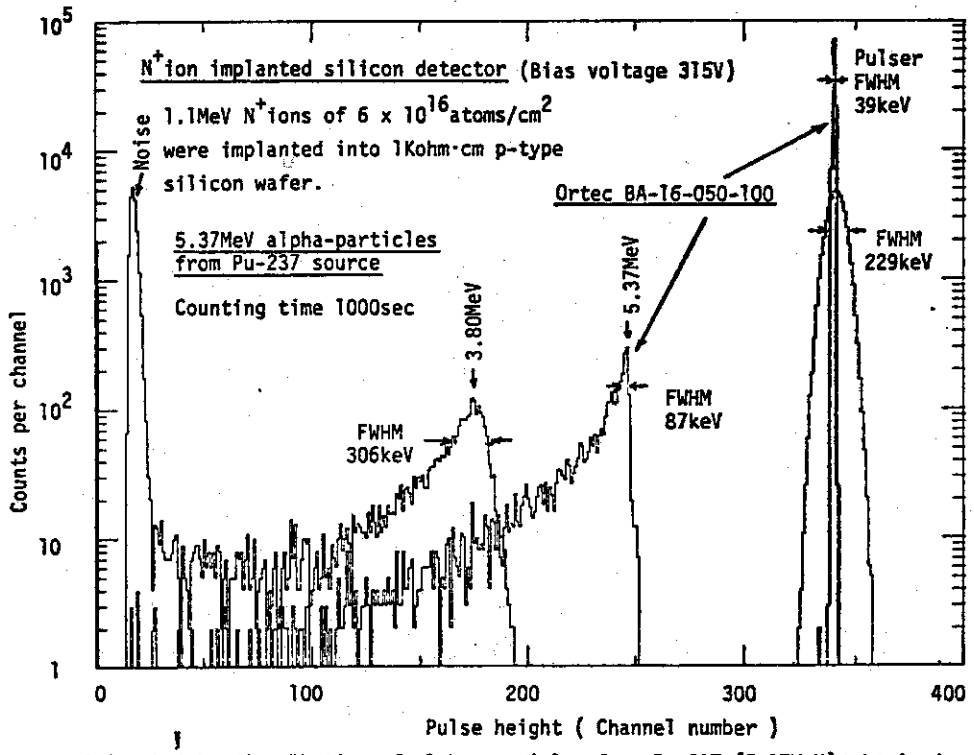


Fig.6.8.3 Pulse height distribution of alpha-particles from Pu-237 (5.37MeV) obtained by a $N^+$ ion implanted silicon detector

## 6.9 Fuel Failure Detector Study in Sodium In-Pile Loop

E.Sakai, M.Fujino*, H.Terada, M.Katagiri, H.Itoh and H.Yoshida

A study of performance of four different types of fuel failure detection systems using a sodium in-pile loop located in Japan Research Reactor 2 has been continued under the contract between Power Reactor and Nuclear Fuel Development Corporation and Japan Atomic Energy Research Institute. The work performed during the last three year periods were described in SJ 250 73-54/JAERI-memo 5287( 1973 ), SJ 250 74-12/JAERI-memo 5693( 1974 ), and SJ-250 75-04/JAERI-memo 6118 ( 1975 ), all in Japanese. The reactor which had a trouble of heavy water leakage has been under repair for the entire period of FY 1975 and no experiment using the sodium in-pile loop was performed. Only out-of-pile experiments were carried out.

A simulation experiment was made to obtain the neutron detection efficiency of the SIL graphite moderator - $BF_3$ combination. Am-Be and Ra-Be neutron source experiments on the simulated graphite moderator gave a neutron detection efficiency of $4 \times 10^{-4}$ count/n. The efficiency did not change even the sources were covered by different thicknesses of paraffin moderators.

Several modifications of the cover gas transport piping were made; a flow-adjusting valve for purge gas to the precipitator was added and the inlet and outlet valves were welded to the cover gas reservoir. An anti-Compton gamma-ray spectrometer consisting of a center high-purity germanium detector, a 10" by 10" NaI(Tl) annulus, and a lead shielding was designed to detect gamma-rays from fission products in cover gas with high peak-to-Compton ratios. One unit of Canberra 8100/Q multichannel analyzer system was prepared for analyzing gamma-ray peaks. A modified type of on-line digital subtract units was designed and tested.

The precipitator response curves obtained in the study performed in the last three years have been analyzed. In the calculation, sodium was devided into three regions and the cover gas between the sodium surface and the precipitator inlet devided into nine sections of equal volume. The concentrations of fission product rare gases were calculated for each of the

---

* Visiting scientist, from October 6, 1975 , on leave of absence from Atomic Energy Research Institute, Hitachi Ltd.( 1099 Gorodani, Ozenji, Tamaku, Kawasaki, Japan )

sections. The calculated response curves agreed with the measured when a release fraction of the fission product gases( Kr and Xe ) from the metallic uranium of $5.6 \times 10^{-3}$ and a rare gas transfer rate from sodium to He cover gas of 0.006/min were assumed.

The summaries of the studies were presented at the three meetings of Atomic Energy Society of Japan[1)-3)], and the results obtained in the study of the last three years was published in IEEE Transactions on Nuclear Science[4)].

References

1) Sakai,E., Katagiri,M., Terada,H., Itoh,H.: " Performance of on-line digital subtract unit ", 1975 Autumn Meeting on Reactor Physics and Engineering of Atomic Energy Society of Japan, C 17 ( November 4, 1975, Osaka )

2) Katagiri,M., Sakai,E., Terada,H., Itoh,H., Yoshida,H., Fujino,M.: " Performance of a gamma-ray peak counting rate measuring circuit ", 1976 Annual Meeting on Reactor Physics and Engineering of Atomic Energy Society of Japan, D 3 ( March 25, 1976, Tokai University )

3) Fujino,M., Sakai,E., Terada,H., Katagiri,M., Itoh,H., Yoshida,H.: " Precipitator time response analysis in sodium in-pile-loop ", ibid., D 14 ( March 25, 1976, Tokai University )

4) Sakai,E., Katagiri,M., Itoh,H.: " Sodium in-pile-loop experiment on delayed neutron detector-, precipitator-, and cover gas gamma-ray spectrometer-type fuel failure detection system ", IEEE Trans., NS-23(1), 363 - 374 ( 1976 )

## 6.10 Non-Destructive Measurement of Nuclear Material

H. Gotoh and H. Yagi

One hundred and forty $UO_2$ pellets and twelve $UO_2$ pins were manufactured as reference samples for non-destructive measurement of nuclear material in light-water moderated reactors[1]. The diameter and the height of pellets are about 9.3 mm and about 15.5 mm respectively. The weight is about 10.8 grams. Each pin contains 65 pellets and has a total length of about 1200 mm. The enrichment of these samples covers 2.0 through 3.4 weight percents in five steps.

A fuel pin container was produced[1]. The container is shielded with 2 mm thick lead sheet and can store ten fuel pins in locked state. The container can be carried by one person even when loaded full. A container stand was prepared. It is anchored to the floor and the container can be locked to it.

The authors had a chance to test two kinds of equipment for "passive gamma assay", an ORTEC Gamma-III system and a stabilized assay meter(SAM-2). These were tested for start-up characteristics and for the stability to ambient temperature change. The reproducibility of data was measured for both types using pellets and pins as radiation sources[2].

The authors also tackled with software making. The angular distribution of unscattered photons from a cylindrical $UO_2$ pellet, the center and the area of the total energy peak, the activation rate of a cylindrical sample irradiated with d-d neutrons and the self-activation rate of a cylindrical sample were treated. Here we introduce the result of the last item.

The self-activation rate of a cylindrical sample A(r,t) is given by

$$A(r,t) = \frac{2Nn\sigma}{\pi t^2}\left[\frac{t}{2r}\left\{\frac{t}{2r}\cdot\ln\left(\frac{\xi}{2}\right) + \frac{4}{3}\right\} - \frac{1}{8}\cdot\ln\left(\frac{\xi}{\xi-2}\right) - \frac{13}{48\xi^2}(4\xi+1)\right],$$

where r and t are the radius and the height of the cylinder respectively, N is the number of target nuclei contained in the sample, n is the total emission rate of radiation inducing activation, σ is the activation cross section, and

$$\xi = \{(\frac{2r}{t})^2 + 1\}^{1/2} + 1.$$

These soft-wares were all programmed for Hewlett-Packard model 65 calculators[3] and partly in the minicomputer language ORACL[4].

References

1) Gotoh, H., Yagi, H.: "Reference Pellets, Reference Pins and a Pin-Container for Non-Destructive Measurement of Nuclear Material", (to be published)

2) Yagi, H., Gotoh, H.: "Experience on Passive Gamma Assay", (to be published)

3) Gotoh, H., Yagi, H.: "A Program File for Non-Destructive Measurement of Nuclear Material(Hewlett-Packard model 65 Calculator)", (to be published)

4) Takeuchi, N., Yagi, H., Gotoh, H.: "An ORACL Program File for Acquisition, Storage and Analysis of Data in Radiation Measurement and in Non-Destructive Measurement of Nuclear Material", JAERI-M 6499(1976) (in Japanese)

## 6.11 Packet Exchange Unit for Computer Network

H. Yagi and K. Koyama

A Packet Exchange Unit (PEX) was developed for an inhouse computer network including the central host computer, various kinds of local host computer and terminals in Tokai Research Establishment.[1] The PEX is a network control computer of "store and forward message transfer" type and makes an "Intelligent Network".[2]

The PEX is composed of an 8-bits micro-processor, IC memories and Communication Adapters (CA, eight channels at maximum). There are two kinds of CAs, serial and parallel.

The serial CA is applied to the connections of PEX-to-PEX and PEX-to-Terminal. Figure 6.11.1 gives a simplified diagram of the serial CA. Message and command/status are transferred through four twisted pairs (message and command/status x send and receive). Serial CAs are isolated with photo couplers and can be separated up to 2 km.

Message transfer of serial CAs is done in 240k bps synchronous mode with a fixed word length of 256 bytes by a communication IC (COM 2601). Error check is performed by the method of "cyclic redundancy check" in 16-bits length. Any message is sent as a chain of message packets. A packet is composed of a packet header in 4 bytes, a message header in 12 bytes and a message part in 240 bytes, as shown in Fig. 6.11.2.

Command/status signals are periodically sent in 30k bps asynchronous mode with a fixed length of eight bits plus parity by a communication IC (TR 1602A). The command/status signal consists of three control command bits with three parameter bits and two status bits. The control command bits are used for communication between the PEX and an aimed PEX or Terminal. The status bits inform the condition of the PEX to neighbors.

The parallel CA is used as a PEX-to-Host Interface, and is a "full duplex" device that is logically devided into Host-to-PEX and PEX-to-Host transfer parts. Each part has an 8-bits data register with parity, an 8-bits command/status register with parity and three timing signals for data and command/status transfer. Hosts are connected to parallel CAs with 42 twisted triple cables of 7 m length.

References

1) Yagi, H., Koyama, K.: "Packet Exchange Unit for TOKAI Online System", (to be published)

2) Yagi, H., Koyama, K.: "Plan of JAERI TOKAI Online System and Design of PEX Network", (to be published)

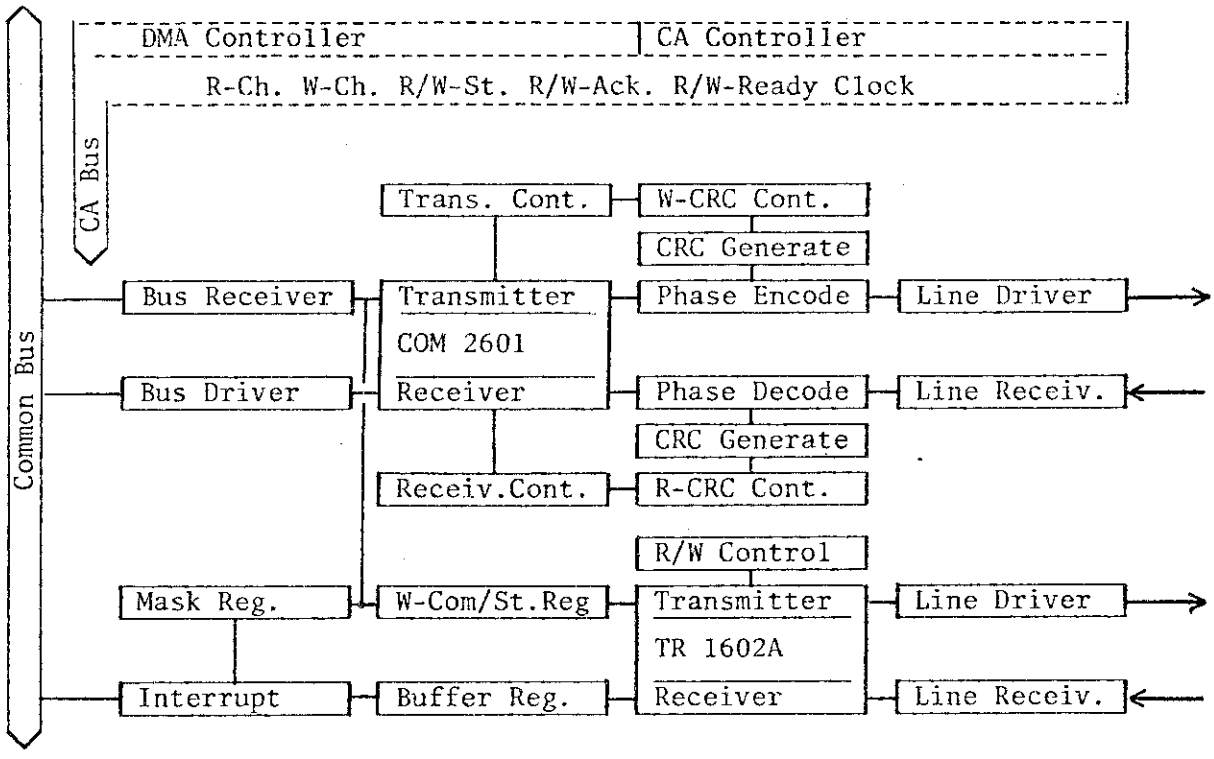


Fig. 6.11.1 Block diagram of a serial communicatiom adapter

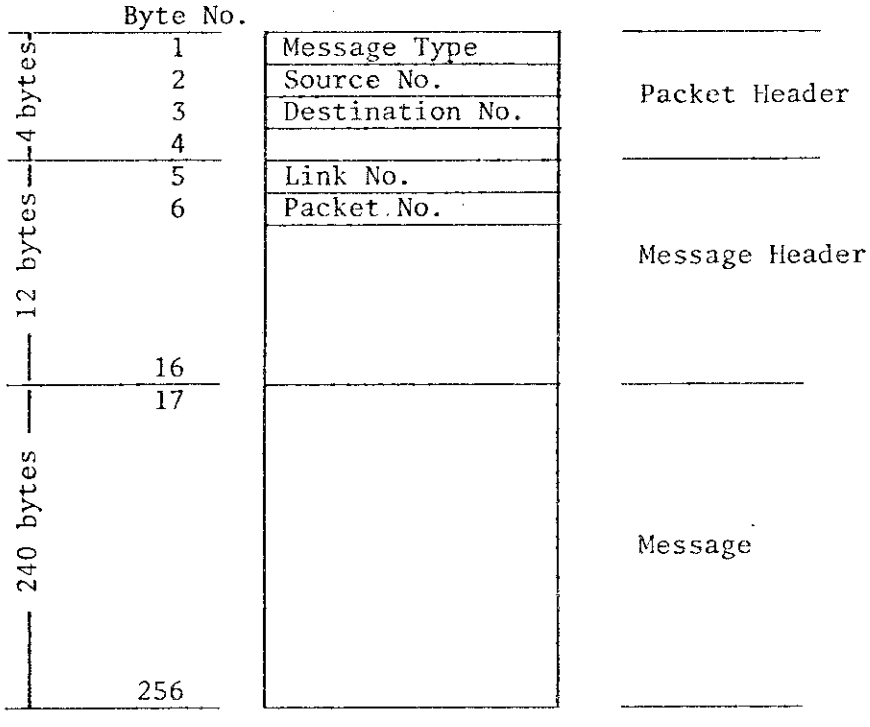


Fig. 6.11.2 Packet Format

## 6.12 An Interpolation Method for the Response Function of Radiations Obtained by Proton Recoil Type Scintillators[1)]

N. Sasamoto

A new method is proposed for obtaining the interpolated response function for any radiations measured by the proton recoil type scintillators. The energy response for monoenergetic radiation (response function) has the maximum pulse height (cutoff pulse height), beyond which the response is uniformly zero. As is evident from Fig.6.12.1, interpolations are impossible by an ordinary procedure at the region between the cutoff pulse height $p_{1,up}$ of the response $R_1(p)$ and $p_{2,up}$ of $R_2(p)$, because the $R_1(p)$ is kept zero in the region. So the following interpolation method is proposed.

At first, the response functions utilized for interpolation are all normalized so that their cutoff pulse heights agree to the common one (see Fig.6.12.2). Then the interpolation is made for obtaining $\tilde{R}_x(q)$ using the normalized response functions $\tilde{R}_1(q)$ and $\tilde{R}_2(q)$. The formula of interpolation used is the Lagrange's one. Finally the expected response function $R_x(p)$ is obtained by reversing the interpolated function $\tilde{R}_x(q)$ so that its cutoff takes the original value.

The usefulness of the method was verified by unfolding with the interpolated responses the pulse height distribution from Am-Be neutron source measured by the NE213 liquid scintillator.

Reference

1) Sasamoto, N. : "An Interpolation Method for the Response Function of Radiations Obtained by Proton Recoil Type Scintillators," JAERI-M 6536 (1976).

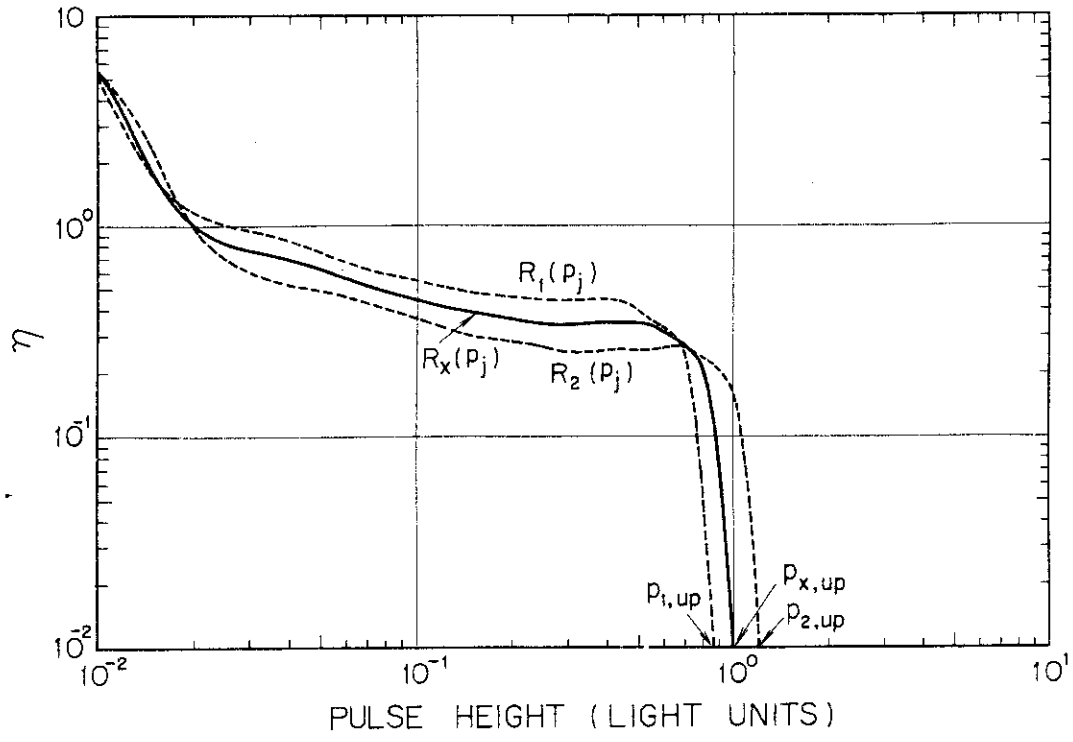


Fig.6.12.1 The response functions on the original pulse height axis

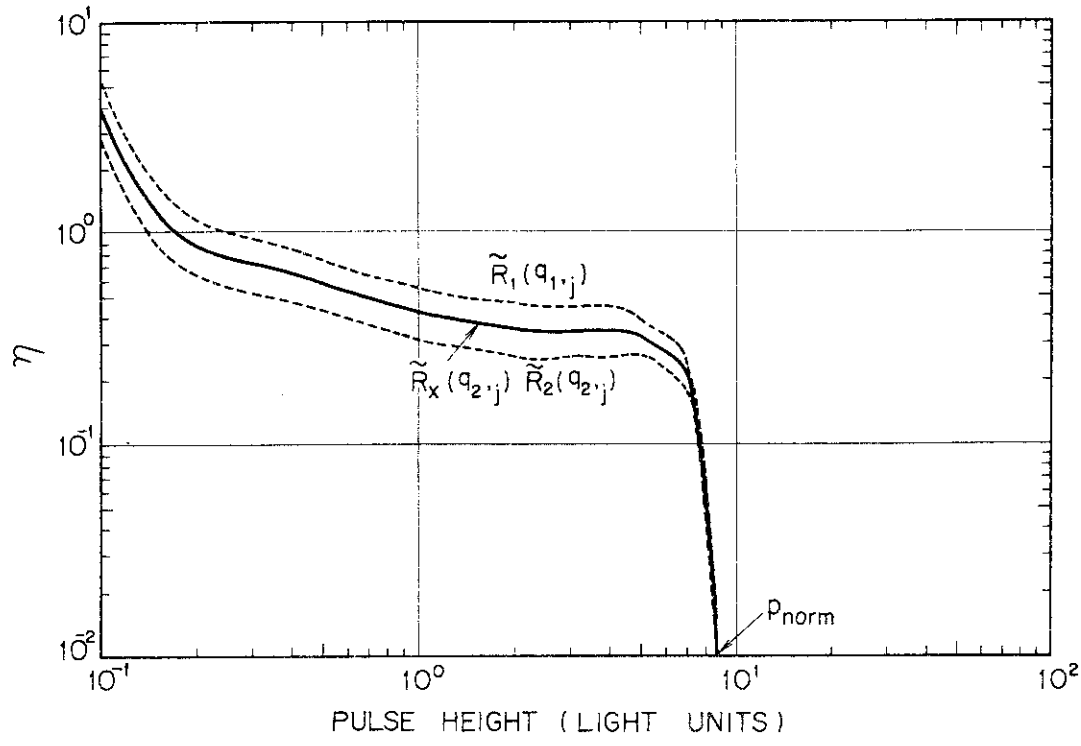


Fig.6.12.2 The response functions on the transposed pulse height axis

## 6.13 Usage of a Thermoluminescence Dosimeter as a Thermal Neutron Detector with High Sensitivity[1)]

S. Tanaka and Y. Furuta

Thermal neutron measurements by thermoluminescence dosimeters have been studied in paired $^{6}$LiF and $^{7}$LiF or UD-136N and UD-137N.

The results have a similar meaning to that of Au foils and the detectable minimum amount of thermal neutron fluence by the present method was about $10^{4}$ n/cm$^{2}$, which corresponds to a thermal neutron flux of several n/cm$^{2}$·s with one hour exposure.

The coefficients for obtaining the thermal neutron fluence from the difference in integral glow values of the Cd-covered and uncovered $^{6}$LiF and $^{7}$LiF, or UD-136N and UD-137N TLDs were $1.12(\pm 0.06)\times 10^{7}$ n cm$^{-2}$/R $^{60}$Co equivalence and $3.45(\pm 0.07)\times 10^{7}$ n cm$^{-2}$/R $^{60}$Co equivalence, respectively.

Reference

1) Tanaka, S., Furuta, Y.: "Usage of a Thermoluminescence Dosimeter as a Thermal Neutron Detector with High Sensitivity,"
Nucl. Instr. and Meth., 133, 495 (1976).

## 6.14 Application of Thermoluminescence Dosimeters for Nuclear Heating Measurements of Gamma Rays and Neutrons[1)]

S. Tanaka, K. Takeuchi* and Y. Furuta

The estimation of radiation heating in materials is necessary for reactor design and engineering. The radiation heating is caused to the absorbed energy due to gamma rays and neutrons, since the absorbed energy in material is thought to be converted entirely to thermal energy. In this report, a new method is presented to estimate gamma-ray absorbed dose by thermoluminescence dosimeters (TLDs) without any information of gamma-ray spectrum. In addition, an approach is also proposed to estimate the absorbed dose of neutrons in several materials by TLDs.

The absorbed dose, $D_M(E_\gamma)$, at a point in a material M for gamma rays of the energy $E_\gamma$ and the integral thermoluminescence, $G_{TLD}(E_\gamma)$, of a TLD placed at the same point are related as a following,

$$D_M(E_\gamma) = \frac{1}{\bar{\eta}(E_\gamma)} \frac{1}{\xi(E_\gamma)_{TLD-M}} \frac{m^{\mu}en(E_\gamma)_M}{m^{\mu}en(E_\gamma)_{TLD}} G_{TLD}(E_\gamma) \quad , \qquad (1)$$

where

$\bar{\eta}(E_\gamma)$ : the mean efficiency for obtaining the integral thermoluminescence from the absorbed dose ($R\ ^{60}Co$ equivalence/erg $g^{-1}$),

$\xi(E_\gamma)_{TLD-M}$ : the absorbed dose correction factor for obtaining the absorbed dose of TLD placed in the material M from the kerma,

$m^{\mu}en(E_\gamma)$ : mass energy absorption coefficient ($cm^2/g$),

---

* Ship Research Institute

$G_{TLD}(E_\gamma)$ : integral thermoluminescence of TLD calibrated by using $^{60}Co$ gamma rays (R $^{60}Co$ equivalence).

For gamma rays, the mean efficiency is independent on the energy, and the absorbed dose correction factor takes a value close to unity in the energy region lower than about $^{60}Co$ gamma-ray energy in any combination of TLD and material. Thus, eq.(1) is rewritten by using the mass energy absorption coefficient at $^{60}Co$ gamma-ray energy, as a following,

$$D_M(E_\gamma) = \frac{1}{\bar{\eta}(^{60}Co)} \frac{m\mu_{en}(^{60}Co)_M}{m\mu_{en}(^{60}Co)_{TLD}} G_{TLD}(E_\gamma) = f_\gamma G_{TLD}(E_\gamma). \quad (2)$$

The absorbed dose estimated by using the constant, $f_\gamma$, increases monotoneously with the effective atomic number of the TLD. Accordingly, the absorbed dose in the material can be estimated by interpolation or extrapolation using the measured values of various TLDs expressed as a function of the atomic number.

The absorbed dose in an iron sphere was measured by various TLDs for a $^{60}Co$ source placed at the center of the sphere, and the results were compared with that obtained by a transport code , PALLAS, to examine the accuracy of the present method. Fig.6.14.1 shows the experimental and calculated values of the absorbed dose at 10 and 15 cm from the center of the sphere, and the experimental values estimated by TLDs agreed with the calculated values within 5 percent.

On the other hand, neutron heating is considered to be important for fusion reactor. Its measurement, however, is not so easy. It is suggested that the absorbed dose in some materials due to neutrons may be estimated by a TLD, since the kerma factor represented as a function of the energy of some materials resemble the energy response of some TLDs.

Combinations of these materials and suitable TLDs are listed in Table 6.14.1. If the contribution of gamma rays to the integral thermoluminescence is known, the neutron heating in these materials may be estimated by the corresponding TLD listed in Table 6.14.1.

Reference

1) Tanaka S., Takeuchi K., Furuta Y. : "Application of Thermoluminescence Dosimeters for Nuclear Heating Measurement of Gamma Rays and Neutrons", presented for 1st ASTM-Euratom Symposium on Reactor Dosimetry, Petten, Sept. 22-26, 1975

Table 6.14.1 The combinations of material and TLD for estimating the neutron heating and the fitting factor, $f_n$,

| material | TLD | $f_n$ (erg $g^{-1}$/R $^{60}$Co equivalence) |
|---|---|---|
| borated graphite | $^{6}$LiF | $2.0 \times 10^{2}$ |
| sodium | UD-137N | $2.7 \times 10^{2}$ |
| aluminum | $^{7}$LiF | $1.0 \times 10^{2}$ |
| iron | UD-137N | $5.0 \times 10^{1}$ |

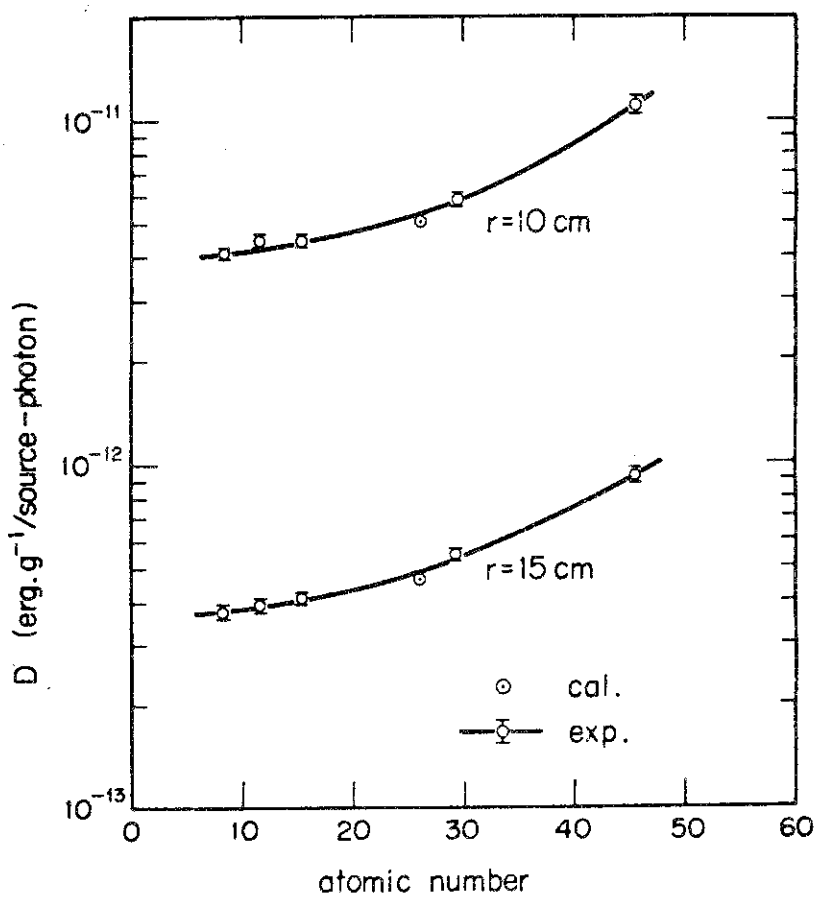


Fig. 6.14.1 Comparison of the experimental results with that of calculation of gamma-ray absorbed dose in an iron sphere

# 7. Dynamics Analysis and Control Method Development

## 7.1 Identification of System Dynamics of JPDR-II and its Application to Reactor Diagnostics

R. Oguma, K. Matsubara, M. Kitamura and Y. Fujii

A series of identification experiments and their data analyses were performed for 50 % power of JPDR-II (Japan Power Demonstration Reactor-II). These experiments and analyses are aimed to establish a statistical identification technique for the model building of a nuclear reactor and to show the effectiveness of this technique with regard to the system dynamics analysis (especially to the feedback loop analysis), at-power reactor noise analysis and reactor diagnostics.

The present report mainly describes some significant informations that were obtained through analyses using an identified dynamics model of JPDR-II.

A schematic diagram of JPDR-II is shown in Fig. 7.1.1. Identification experiments were carried out under the condition that the vessel pressure and the water level control loops were opened so that the reactor core was out of feedback control. Then, a bypass pressure regulator valve (BPR) and a master controller were used as the input. Thus, given a set of experimental data, identification is realized by the least squares fitting to the multidimensional autoregressive model (1). (A-R model)

$$X(k) = \sum_{m=1}^{M} A(m)X(k-m) + \sum_{m=1}^{M} B(m)U(k-m) + W(k) \qquad (1)$$

where X(k), U(k), W(k) are the multidimensional outputs, inputs and noise variables. A(m) and B(m) are system matrices.

The identified A-R model of JPDR-II is checked from various points of view. For example, the model fitness is checked by comparing the experimental data with their estimates derived from the identified model. The results are shown in Fig. 7.1.2.

After the goodness of the identified model is verified, step responses to inputs are computed using this model and compared with the theoretical ones. These results are shown in Fig. 7.1.3, where the parameters included in the theoretical model are evaluated according to their definitions. On the other hand, the results of parameter adjustment are shown in Fig. 7.1.4. In this case, the volume of the saturated water in riser was adjusted so that the step responses from the theoretical model became closer to the identified

ones.

Through the experiments and the analyses mentioned above, some significant informations are derived as described in the following:

1) The identified model appears to agree satisfactorily with the experimental data. This study has demonstrated that this identification technique is an efficient tool of reactor analysis.
2) The water circulation time in the recirculation loop is estimated using the identified model as shown in Fig. 3 and is verified to agree with the theoretical estimate.
3) The accurate evaluation of the volume of saturated water in riser turned out to be especially important for the theoretical model to provide a good result which agrees with the experimental data.

Reference

1) Matsubara, K., Oguma, R., Kitamura, M.: Identification of the System Dynamics of JPDR-II, Meeting of Research Committee on Application of Decision Making Techniques to Nuclear Engineering, Atomic Energy Society of Japan (1976).

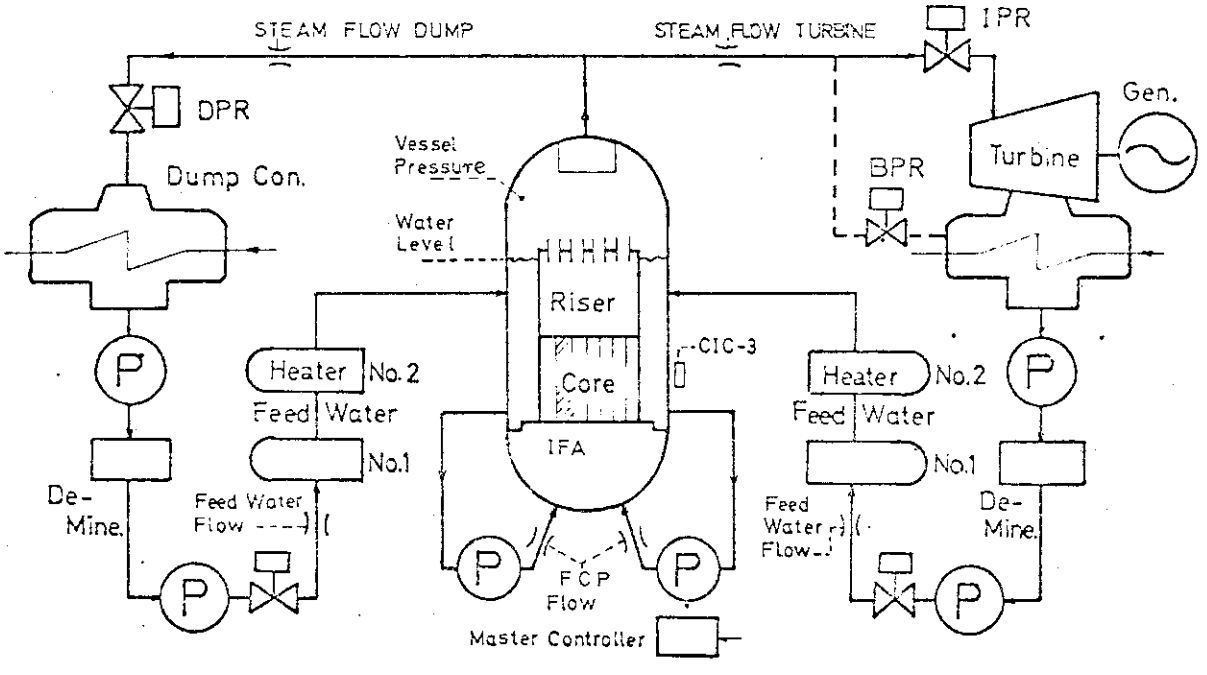


Fig. 7.1.1 Block diagram of JPDR-II plant.

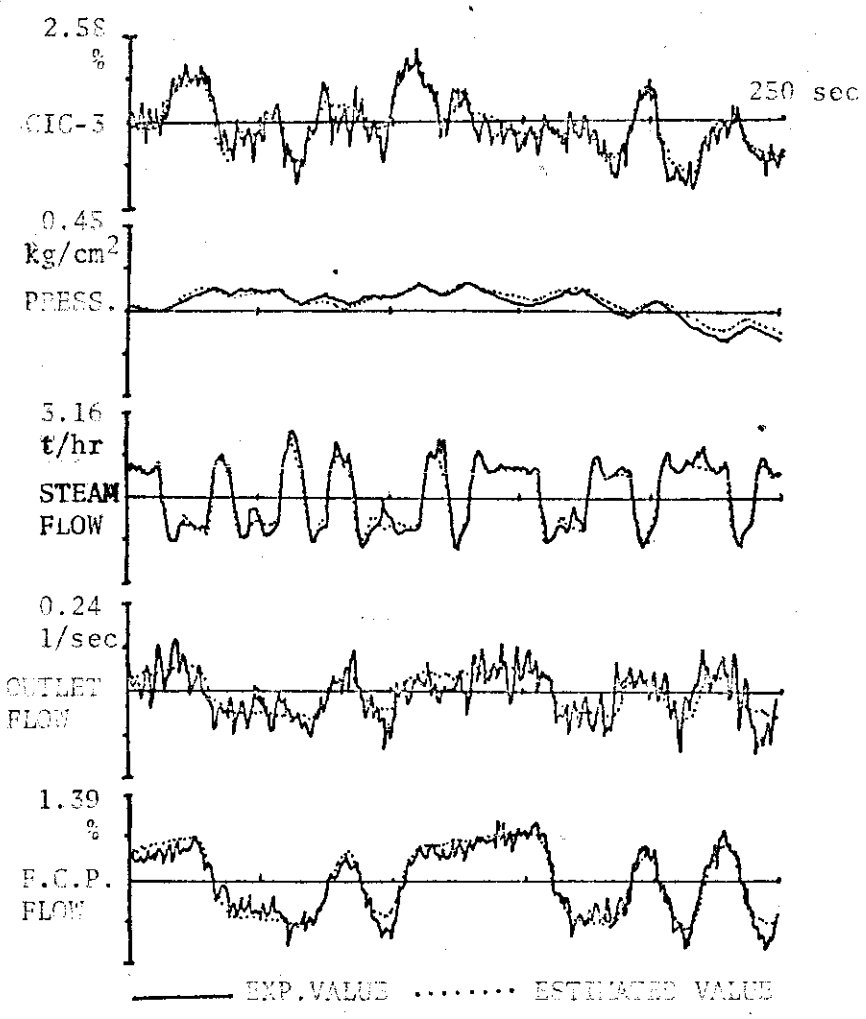


Fig. 7.1.2 Comparison between estimated outputs and experiment data.

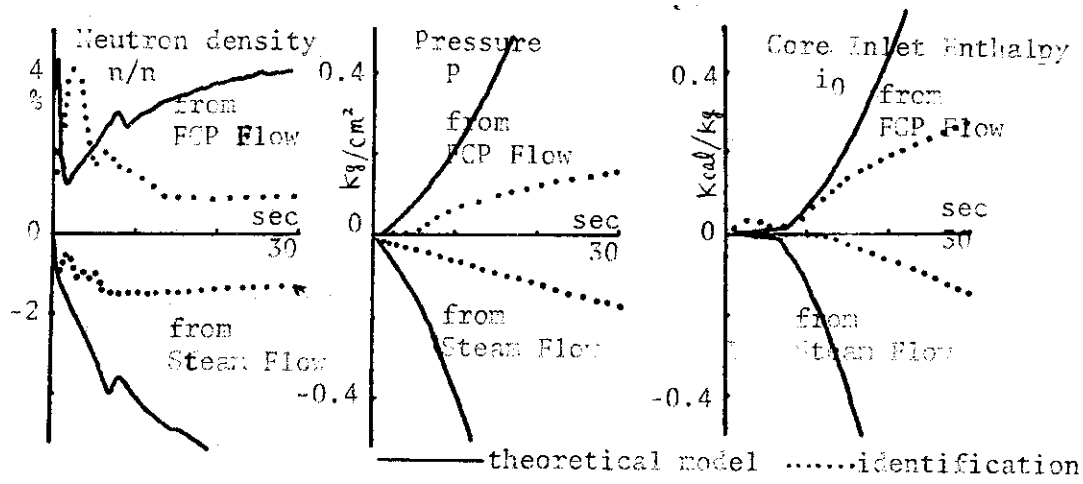


Fig. 7.1.3 Comparison of the step responses between identified results and computed ones by theoretical model.

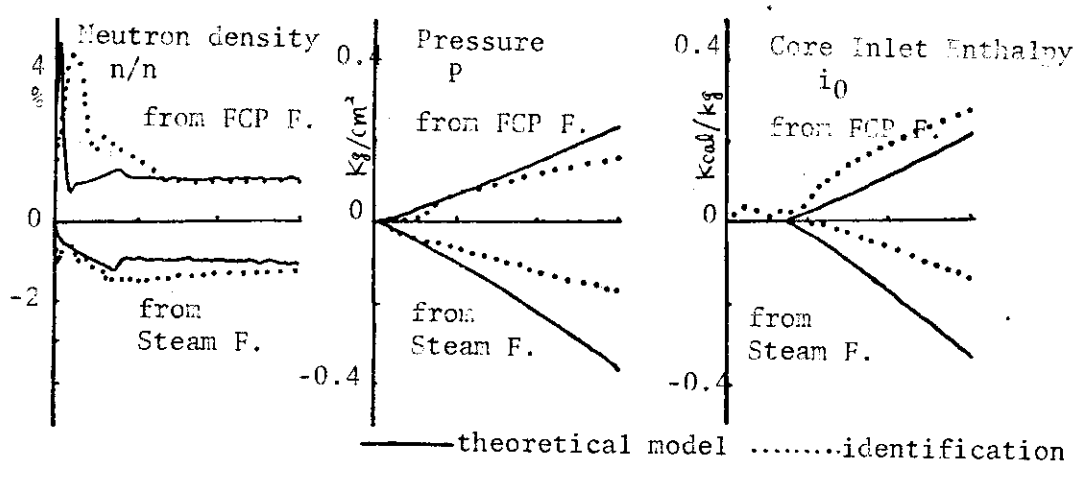


Fig. 7.1.4 The results of the parameter adjustment in the theoretical model so as to become closer to the identified results.

## 7.2 Hybrid Simulator of VHTR Dynamics—Development of Simulators of Plant Components—

K.Kudo*, H.Usui, Y.Fujii and M.Hara

A hybrid simulation of the VHTR(Very High Temperature Reactor) under conceptual design has been developed for the purpose of the stability and the control study.

One of the most effective application of hybrid operation is to solve partial differential equations quickly,hence a serial CSDT method is suitable for the transient analysis of the basic heat exchange model expressed in a set of hyperbolic types. Although the actual heat exchanger of helium gas is a once-through and helical tube type,the simulation is reduced to a straight counter flow and one dimensional model with the following assumptions. 1)helium gas is considered to be incompressible since the flow velocity is under 0.1Ma.,2)the pressure dependency of the gas density,the space dependency of the mass flowrate of the gas,and the work done by the pressure are neglected, 3)both of the heat transfer coefficient and the viscosity depend only on the temperature. As the results of parametric test operations on the CSDT paramenters, faily good performences were obtained in both accuracy and speed.

On the other side the development of time-dependent transport delay simulation has been carried out. Usually it makes use of an digital part of an analog-digital hybrid computer, which is not desirable in the point of the operation speed of the hybrid computer. So that a single perpose delay simulator is necessary. It uses a seperate digital computer (16bit,8kw)with analog input-output devices. Ten channels of process variables are equipped which are delayed within 0.1% distortion, and six channels are provided for the flowrate signals as variable time delay. The flowrate is simulated by the change of the shifting speed of data in the memory, and the relative change of time delay is up to 5o%. The excellent performance of the simulator will be made full use in the VHTR plant simulation as an "analog" type element.

References:

eg, Holland,F.A., "Heat Transfer", Heinemann Educational Books(1970), or Tachibana,F., et al: "Heat Transfer" Korona Co. (1965) (Japanese)

*Kyushu University

## 7.3 Application of Optimal Linear Regulator Technique to Reactor Plant Control

S. Mankin and Y. Shinohara

A synthesis technique which is partly based on the theory of linear optimal regulator with quadratic performance index has been studied in order to develop practical methods of controller design for multivariable nuclear power plants. The controlled plant used as an example is a direct cycle boiling water reactor with forced recirculation. Since the aim of the study is to investigate basic problems associated with the application of the linear regulator theory to nonlinear systems, a simplified dynamics model of the boiling water reactor plant was used.

The basic design procedure employed in this study is first to derive the optimal linear regulator for the linearized model of the nonlinear plant dynamics and then to modify the linear regulator thus obtained by adding appropriate integration-type actions. The first stage of the procedure is basically straightforward application of the optimal linear regulator theory, while the second stage is rather heuristical or trial-and-error application of the classical PID-type control concept.

Although the present method is not rigorous in mathematical sense, it is practical in engineering sense in that:

(1) Once the mathematical model is established for representing the controlled plant and the weighting matrices in the performance index, the optimal gain matrix of the linear regulator can be determined uniquely. This procedure is much simpler than that based on the classical frequency domain techniques if an appropriate computer code is once developed.

(2) The optimal linear regulator technique often reveals a control system structure that can not easily be synthesized by classical approach when the system becomes very complex.

(3) The integration-type control action can easily be introduced from considerations of the physical relationships existing between the control and the controlled variables with a view to compensating the biased disturbances and also to eliminating errors in the state variables of interest.

Reference

1) Mankin, S., Shinohara, Y.: J. Nucl. Sci. Technol., 12[12], pp.727 - 734 (1975).

## 7.4 Application of Hierarchical Control Concept to Reactor Plant

S.Mankin, Y.Fujii and M.Hara

In order to improve the control of an out of pile boiling water loop for testing fuel,a new type of hierarchical control system was developed. The control method consists of a hierarchical control system which has classical P.I.D.sub-loop controllers at the first level and a standard linear optimal regulator at the second level.The design procedure basically consists of two parts.One part is the formulation of the system model which is obtained from the identification experiments,where the system model is determined with the conventional sub-loop controllers included. The other is the design of 2nd level controllers which are constructed based on the standard technique of the linear optimal regulator applied to the system model. Synthesis and evaluation of the control system design have been tested using computer simulation.

The results of the simulation show that the hierarchical control scheme proposed has performed fairly well in comparison with the conventional one using sub-loop controllers only. We suggest that this control method will be useful for the improvement of the performance of nuclear power plant control and it is attractive because it makes use of conventional controllers and has safety advantages in the case of input-output system failure.

References;

1) Akaike,H.,et al: "Statistical Analysis and Control of Dynamic Systems" Science Co.(1972),(Japanese)

2) Mankin,S.,et al: "On the Application of Linear Optimal Technique to Control of Nuclear Power Plant" J.Nucl.Sci.Tech. 11,12 (1975),(Japanese)

# 8. Fusion Reactor Technology

## 8.1 Fission-Rate Distributions in Lithium and Hybride Fusion Blanket Assemblies

H. Maekawa and Y. Seki

In order to investigate the behavior of neutrons in fusion reactor blankets, a series of integral experiments on assemblies including lithium metal have been carried out[1),2),3)].

Absolute fission-rates of $^{235}U$, $^{237}Np$, $^{238}U$ and $^{232}Th$ are measured by micro-fission-chambers in four types of spherical blanket assemblies prepared by loading blocks of lithium and/or natural uranium and/or graphite on stainless steel structure. The four assemblies are named Li, Li-C, U-Li and U-Li-C Assemblies corresponding to their respective configurations. Source neutrons are generated at the center of the assemblies by a D-T reaction using a 300 kV Cockcroft-Walton type accelerator.

It is necessary for the absolute measurement to know the number of neutrons produced by an accelerator and the number of fissionable-atoms coated on the chambers. An α-monitor was set up on the accelerator to detect the associated α-particles of $T(d,n)^4He$ reaction. The neutron yield was estimated by the counts of the α-monitor. The fission chambers were calibrated by use of the same accelerator, assuming that the fission cross sections at 15 MeV referred are correct. The overall experimental errors were mostly less than 10 % and about 7 % on the average[4),5)].

The results of the measurement were compared with those of one-dimensional transport calculations employing 100-group neutron cross-sections obtained from ENDF/B-IV. The ratio of the calculated to experimental fission-rates of $^{238}U$ and $^{235}U$ in the four assemblies are shown in Figs. 8.1.1 and 8.1.2 respectively.

It was shown that the C/E's of $^{232}Th$, $^{238}U$ and $^{237}Np$ fission-rates decrease with the distance from the center. A large overestimation of $^{235}U$ fission-rate by calculation was observed in the graphite reflector region. One of main cause of the disagreement was found to be the incapability of the adopted multi-group cross-section production codes in taking account of angular distributions of the secondary neutrons from nonelastic reactions[6)].

References

1) Hiraoka, T., et al.: Nucl. Fusion Special Suppl., 1974, Proc. Symp. Fusion Reactor Design Problems, p.363, IAEA (1974).
2) Maekawa, H., et al.: Nucl. Sci. Eng., 57, 335-340 (1975).
3) Maekawa, H., Seki, Y.: "Preliminary Results of Integral Experiment on Fusion-Fission Hybrid Blanekt Assemblies", JAERI-M 6495 (1976).
4) Seki, Y., Maekawa, Y.: J. Nucl. Sci. Technol., 13, 272-275 (1976).
5) Maekawa, H., Seki, Y.: "Absolute Fission-Rate Distributions in Lithium and Hybrid Fusion Blanket Assemblies, I. Experimental Method and Results", to be published in J. Nucl. Sci. Technol.
6) Seki, Y., Maekawa, H.: ibid, II. Analysis and Evaluation.

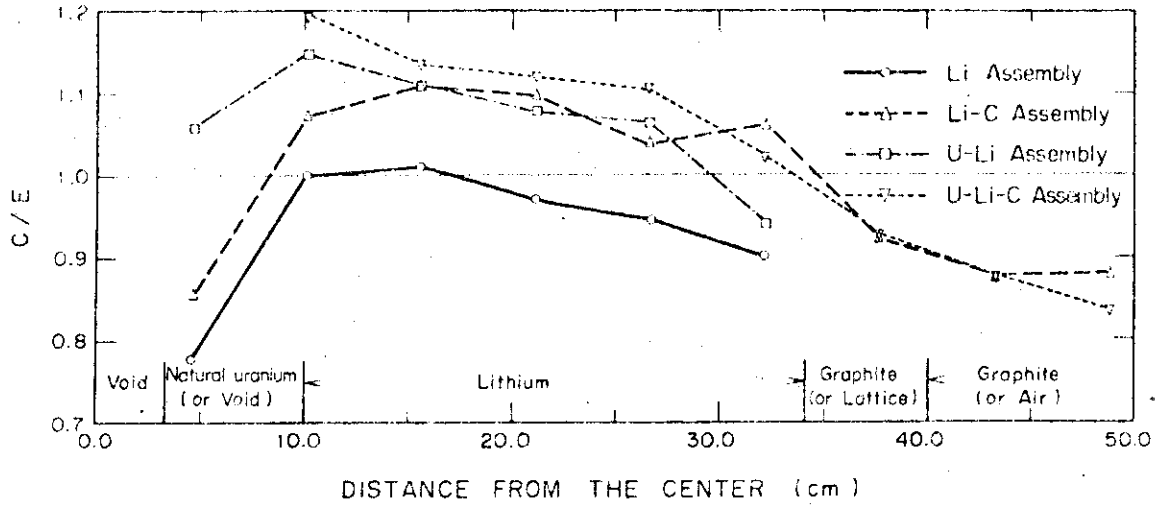


Fig. 8.1.1 C/E of $^{238}U$ fission-rate in four Assemblies

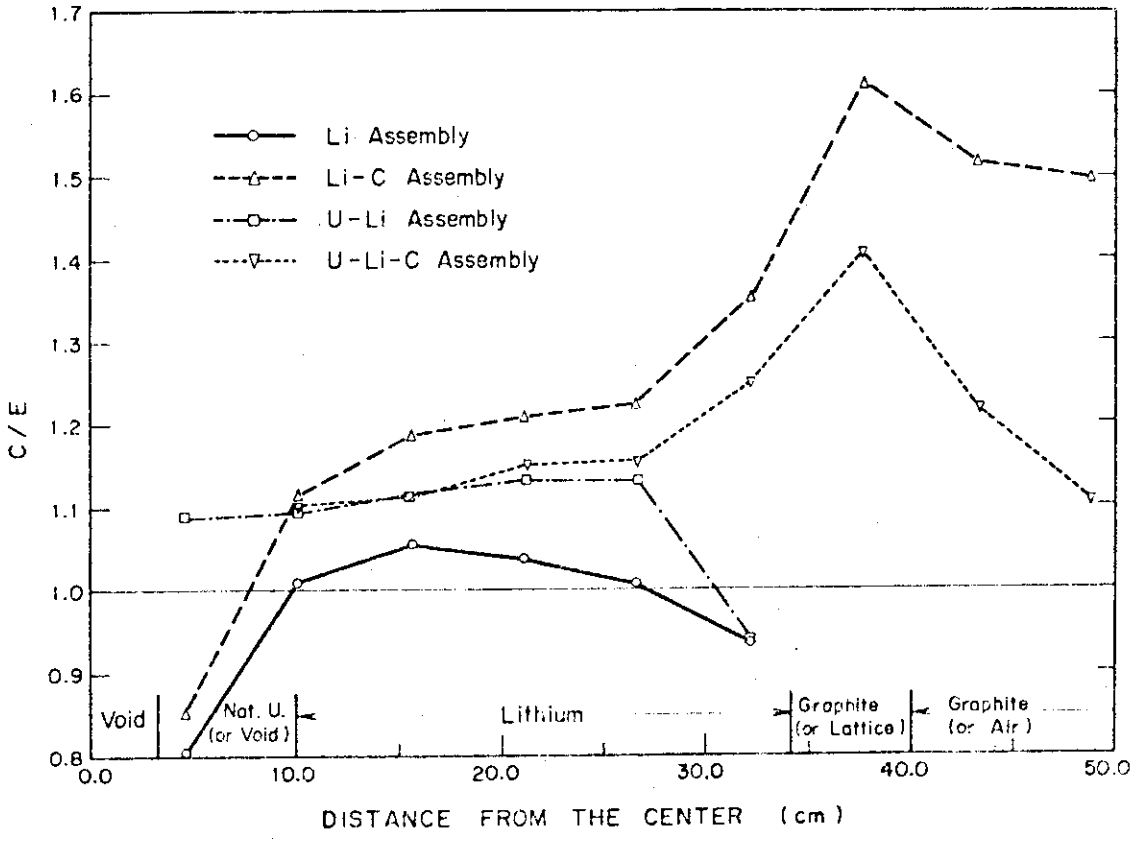


Fig. 8.1.2 C/E of $^{235}U$ fission-rate in four Assemblies

## 8.2 Response Distributions of $^{6}LiF$ and $^{7}LiF$ Thermoluminescence Dosimeters in Lithium Blanket Assemblies

H. Maekawa, J. Kusano and Y. Seki

Fusion energy is converted to thermal energy in the blanket region surrounding the plasma of a fusion reactor. The measurement of radiation heating-rate distribution in the blanket is equally important as the measurement of fission-rate distribution in a fission reactor. According to the neutronics calculation[1], heating rate due to gamma-rays in a blanket is about a third of that due to neutrons. At present, there is no direct means for measuring the radiation heating-rate distribution.

The reaction of $Li(n,\alpha)T$ and $Li(n,n'\alpha)T$ are the two major reactions contributing to heat deposition in a blanket with lithium. When TLD's of $^{6}LiF$ and $^{7}LiF$ are employed, the major portion of radiation heating rate by neutrons and gamma-rays in lithium may be measured. We have measured the responses* of $^{6}LiF$ and $^{7}LiF$ TLD's to the neutron and gamma-ray in pseudo-spherical lithium assemblies with and without a graphite reflector. They are same assemblies mentioned in 8.1.

The neutronics calculations are based on RADHEAT[2], the code system for calculating radiation heating-rate. The 42 group neutron transport cross-sections of up to $P_5$ Legendre terms are obrained by SUPERTOG from ENDF/B-III data file. The 21 group gamma-ray transport cross-sections are calculated by GAMLEG-JR. In order to calculate the total response of the TLD, the energy dependence of the TLD response to the neutrons and gamma-rays must be known respectively. The energy dependence of the response to gamma-ray are accurately known. As for energy dependence to the neutrons, the responses of $^{6}LiF$ and $^{7}LiF$ TLD's to various monoenergetic neutrons are measured by Y. Furuta and S. Tanaka, and they were shown to be in good agreement with the calculated values[3),4)].

The measured responses of $^{6}LiF$ and $^{7}LiF$ TLD's in Li and Li-C Assemblies are compared with calculated ones in Figs. 8.2.1 and 8.2.2, respectively[5]. Since both measured and calculated values are normalized to values per one source neutron, direct comparison of absolute values are possible.

---

* The unit value is the equivalent $^{60}Co$ gamma-ray exposure in roentgens.

Experimental error amounts to about 35 %.

In spite of all the uncertainties accompanying the present experiment and analysis, the measurement of the distribution of $^{6}LiF$ and $^{7}LiF$ TLD response in the fusion blanket mock-up assemblies is very promising as an effective means for obtaining the information on radiation heating-rate distribution.

References

1) Seki, Y.: "Evaluation of Shielding Design of Super Conducting Magnet (I)". JAERI-M 6046 (1975) (in Japanse).
2) Miyasaka, S., et al.: "Code System for the Radiation-Heating Analysis of a Nuclear Reactor RADHEAT", JAERI-M 5794 (1974).
3) Furuta, Y., Tanaka, S.: Nucl. Inst. Meth. 104, 365-374 (1972).
4) Furuta, Y., Tanaka, S.: "The Relation Between Light Conversion Efficiency and Stopping Power of Charged Particles in Thermoluminescence Dosimeter", International Symp. on Radiation Physics, Calculta (1974).
5) Maekawa, H., et al.: NEACRP-L-165 (1976); to be published in JAERI-M report.

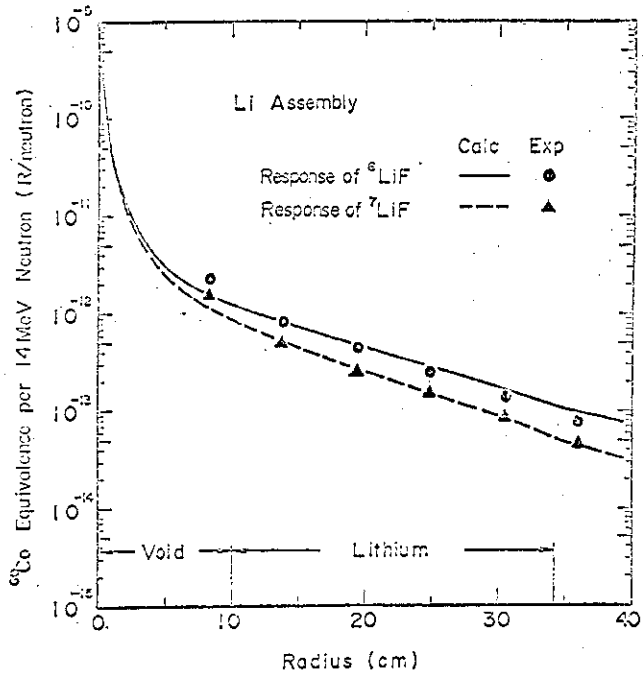


Fig. 8.2.1 Response Distributions of $^{6}$LiF and $^{7}$LiF TLD's in Li Assembly

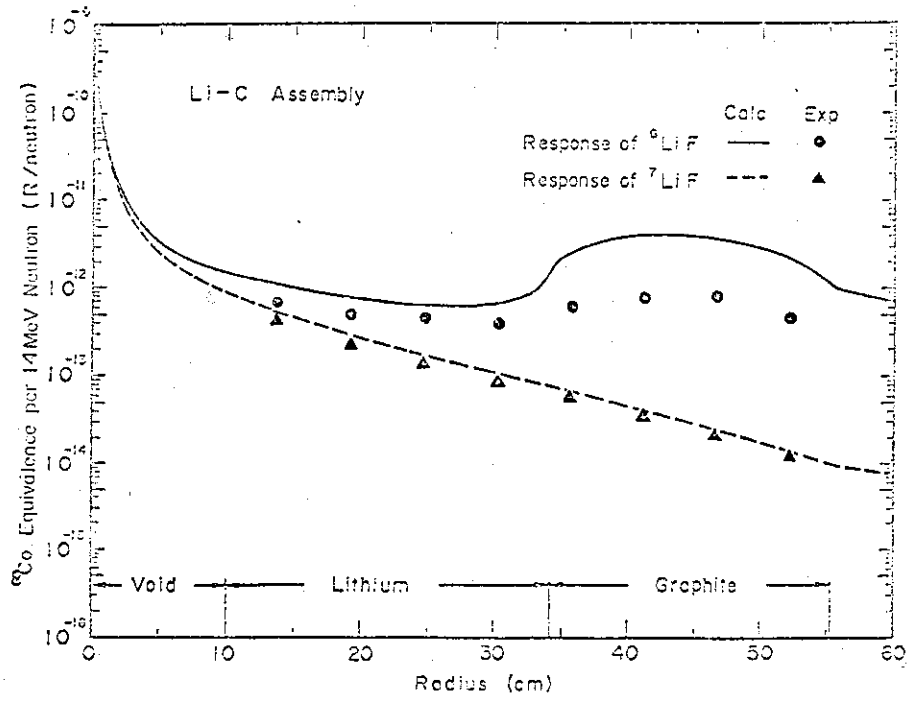


Fig. 8.2.2 Response Distributions of $^{6}$LiF and $^{7}$LiF TLD's in Li-C Assembly

## 8.3 Si(Li) X-Ray Spectrometry in JFT-2 Plasma

E.Sakai, M.Katagiri, H.Terada, N.Suzuki* and K.Maeno*

The measurement of X-ray spectrum in Japan Fusion Tokamak-2 plasma has been continued using a Si(Li) X-ray spectrometer. The electronics and the data analyzing system were described in progress reports( Sakai,E.,et al: " Progress Report Semiconductor Detector Group, April 1, 1974 to March 31, 1975", JAERI-M 6258( September, 1975 ), and in " Reactor Engineering Division Annual Report( April 1, 1974 - March 31, 1975 )", JAERI-M 6320( November, 1975 )).

The main progress made in the present period is as follows: As a result of an intense investigation of the high rate counting problem and absorber thickness effect, it was found that the electron temperatures induced from X-ray spectra became coincided with those from laser measurements when a 40 micrometer thick beryllium absorber was used in front of the detector whose counting rate was limited less than 30kcps and the slope of the spectrum was taken above 2.5keV. Electron temperatures as high as 1.7 keV were observed in the specific experiments.

Three-Si(Li)detectors in single cryostat was designed to make separate measurements of higher energy X-rays from lower energy X-rays with a high precision of statistics. One of the three detectors is to be used for measuring X-ray oscillation.

A surface barrier silicon detector was attempted to measure X-ray oscillation successfully. But, a problem of increasing leakage current was observed when the detector was placed in the JFT-2 vaccum. The presence of a small amount of $H_2$ might be one of the factors affecting the leakage current.

Summaries of the experiments were presented at the three meetings[1)-3)].

References

1) Suzuki,N., Maeno,K., Fujisawa,N., Sakai,E.,Katagiri,M.,Terada,H.: " Soft X-ray measurement in JFT-2 ", the 30th Annual Meeting of Physical Society of Japan, 2pC6 ( April 2, 1975, Kyoto University )

2) Suzuki,N., Sakai,E., Katagiri,M., Terada,H.: " Soft X-ray measurement in JFT-2 (II) ", 1975 Autumn Meeting of Physical Society of Japan, 10aR1 ( October 10, 1975 Koriyama )

* JFT-2 Group, Fusion Research Laboratory

3) Sakai,E., Katagiri,M., Terada,H., Suzuki,N., Maeno,K., Fujisawa,N.: " JFT-2 plasma X-ray spectrometry by use of Si(Li) detector ", 1975 Autumn Meeting on Reactor Physics and Engineering of Atomic Energy Society of Japan, C-6 ( November 4, 1975, Osaka )

## 8.4 Energy Transfer Rate of a Charged Particle as a Function of Injection Angle

T. Fujisawa

The rate of change of the energy which is transferred from a test particle to field particles through Coulomb collisions, has been calculated in early days by several authors[1-3], and recently, by Kammash and Galbraith [4], who assumed that the field particles have a symmetric Maxwellian velocity distribution. In this report, we present an expression of the energy transfer rate as a function of injection angle, on the assumption that the field particles have a shifted Maxwellian distribution, when we start from the equation given by Butler and Buckingham[1]. Although divergent integrals appear in the course of calculation, they are cancelled out, and the analytical expression of the energy transfer rate can be obtained.

Numerical evaluation of the expression shows that in the case of collisions of a beam deuteron with the bulk of deuterons in a plasma, the co-injection parallel to the plasma current is larger in energy transfer rate than the counter-injection. But the difference is not so significant. On the other hand, in the case of collisions of a beam deuteron with the bulk of electrons in the plasma, the energy transfer rate strongly depends on the injection angle. That is, in both cases, co-injection is more effective in energy transfer rate. For the perpendicular injection, the energy transfer rate approaches that of nondrift.

Finally, complete agreement with the expressions given in Refs[5-7] may be provided by averaging the result obtained here over $\vec{v}$ in a shifted Maxwellian distribution, and then by adding the energy change rate due to Ohmic heating.

References

1) Butler,S.T.,Buckingham,M.J.: Phys. Rev., 126, 1(1962).
2) Trubnikov,B.A.: Reviews of Plasma Physics 1, Consultants Bureau, New York, 105(1965).
3) Sivukhin,D.V.: Reviews of Plasma Physics 4, Consultants Bureau, New York, 93(1966).
4) Kammash,T., Galbraith,D.L.: Nuclear Fusion, 13, 133(1973).
5) Burgers, J.M.: Flow Equations for Composite Gases, Academic Press, 108

(1969).

6) Salat, A.: Plasma Physics, 17, 589(1975).

7) Braginskii, S.I.: see Ref. [2], 205.

## 8.5 Frequency Characteristics of the Horizontal Motion of a JT-60 Plasma Column

Y. Kambayashi

For the purpose of realizing the thermo-nuclear fusion, it is essential to have a long-lived confined plasma which may be obtained by employing the positional control of a plasma column. The extension of confining time of the plasma may depend largely on the functions provided for the control system, and so the system should be skillfully designed and its development can not be done without knowledge of the characteristics proper to the concerned apparatus.

We reported a kinetics model representing the horizontal displacement of a toroidal plasma column in JAERI-M-6292, in which we gave a numerical code "FLIC" which calculates the frequency characteristics. Now we applied the model to Japan Torus 60 and obtained frequency characteristics of the plasma column displacement to vertical field change and to terminal voltage change of one of the conductors, and also investigated influence of the uncertainty of design parameters, such as intrinsic time constant of the conductors, on these characteristics.

Concerning the characteristics to vertical field change, the uncertainty of design parameters does not much influence the characteristics in the control frequency range. Concerning the characteristics to terminal voltage change of the vertical field coil, the uncertainty of the intrinsic time constant of the coil affects the characteristics, but the uncertainty of other parameters brings not so much influence on the characteristics. The obtained frequency characteristics of the horizontal motion of a JT-60 plasma column are sufficiently presented in JAERI-M-6508.

References

1) Mukhovatov, V. S., Shafranov, V. D.: "Plasma Equilibrium in a Tokamak", Nuclear Fusion, 11 (1971).
2) Leontovich, M. A.: "Reviews of Plasma Physics 2", Translated from Russian by Lashinsky, H., Constants Bureau, New York (1966).
3) Hugill, J., Gibson, A.: "Servo Control of Plasma Position in CLEO-Tokamak", CLM-P 382 (1974).
4) Kambayashi, Y., Hara, M.: "A Kinetics Model for the Horizontal Displacement of a Toroidal Plasma Column", JAERI-M 6292 (1975).
5) Kambayashi, Y.: "Frequency characteristics of the Horizontal Motion of a JT-60 Plasma Column", JAERI-M 6508 (1976).

## 8.6 Analysis of Neutral Atom Transport in Troidal Plasma by the Monte Carlo Method

Y. Taji, S. Inoue, T. Suzuki, Y. Nakahara and T. Asaoka

Accurate analysis of the neutral atom transport in the troidal plasma has been performed by making use of the Monte Carlo method for the estimation of the ionizing rate of neutrals injected and also for the investigation of the energy distribution of plasma ions. The plasma has been assumed in an equilibrium or steady state.

The charge exchange reaction between neutrals and plasma ions is dealt as the energy transfer cross section:

$$\Sigma(\vec{r}:E'\to E,\vec{\Omega}\cdot\vec{\Omega}') = \int_{E}^{E+\Delta E} dE_i \int d\vec{\Omega}_i \frac{|\vec{v}_i-\vec{v}'|}{v'} \sigma_{cx}(|\vec{v}_i-\vec{v}'|)N_i(\vec{r},E_i,\vec{\Omega}_i)$$

where $\sigma_{cx}$ is the microscopic charge-exchange cross section, $N_i$ the distribution function of plasma ions and $\Delta E$ the group width of the neutral energy group. The multi-group transport code MORSE is used, which has been modified by introducing the TORUS GEOM[1]. In addition to this geometrical routine, statistical disposal and access routines have been prepared. Calculations have been performed for (1) the relation between the ionizing rate of neutrals and the direction of its injection, (2) the (r-θ) distribution (r is the minor radius) of the fast ions produced by neutral injection and (3) the relation between the energy distributions of plasma ions and of neutrals emitted from the troidal plasma. Though the last item is rather subtle, the calculation is performed through the following steps: a) select profiles of the energy distribution of plasma ions, b) produce the macroscopic cross section sets by using the profiles as a weighting function c) calculate the energy distribution of neutrals emitted from the troidal plasma and d) compare the energy distributions of neutrals obtained by calculations and experiments.

The maximum ionization of injected neutrals has been observed to occur for injection directed approximately to the middle point between the inner boundary of the plasma torus and its axis. It has been also revealed that the average temperature of neutrals emitted in the direction parallel with the minor axis is higher by about 10 % than that in the perpendicular direction. This fact was observed in experiments in ORMAC[3]. The difference calculated here is caused by the fact that the mean free path of neutrals is comparable with the minor radius of plasma. It may be also caused partially from the anisotropy of plasmas.

References

1) Inoue, S.: to be published (1976).

2) Suzuki, T., Taji, Y., Nakahara, Y.: "Macroscopic Cross Sections for Analyzing the Transport of Neutral Particles in Plasmas", JAERI-M 6119 (1975).

3) Berry, L. A., et al.: "Neutral Beam Injection Experiments in ORMAK", IAEA-CN-33/A5-2 (1975).

## 8.7 A Direct Method for Numerical Solution of Semi-linear Partial Differential Equations in Plasma Physics

Y. Nakahara

A non-iterative direct numerical method[1] developed for volterra integro-differential equations with quadratic nonlinearity has been applied to semi-linear partial differential equations*) in plasma physics. Most of important phenomena in interacting plasmas can be described with this type of equations, such as

a) a particle continuity equation for burning plasma in a axisymmetric fusion reactor[2]:

$$\frac{\partial}{\partial t} n(r,t) = \frac{1}{r}\frac{\partial}{\partial r}\left(Dr \frac{\partial}{\partial r} n\right) + S - Qn^2 \quad , \tag{1}$$

b) the Kampaneets equation for spectrally narrow radiation interacting with electrons[3]:

$$\frac{\partial}{\partial t} n(x,t) = \frac{1}{x^2}\frac{\partial}{\partial x} x^4\left(\frac{\partial n}{\partial x} + n + n^2\right) + B[(1+n) - ne^x], \tag{2}$$

where the Compton and bremsstrahlung processes are taken into consideration.

c) the Al'terkop's hydrodynamics equation for the time development of ion-sound instability in a fully ionized plasma[4]:

$$\frac{\partial^2 v}{\partial t^2} - c^2 \frac{\partial^2 v}{\partial x^2} = -f \frac{\partial v}{\partial x} + g \frac{\partial^3 v}{\partial^2 x \partial t} - \frac{\partial^2 v^2}{\partial x \partial t} \quad . \tag{3}$$

In Eqs. (1), (2) and (3) D, S, Q, B, c, f and g are constants.

We show here an outline of the direct method by taking Eq. (1) as an example. Since the degree of time derivative is one, the weighted step function method can be used for the time interval. Thus, the integration of Eq. (1) over a time interval $[t_i, t_{k+1}]$ and subregion $[r_j, r_{j+1}]$ with the aid of the interpolation:

$$n(r,t) = \theta n_{i+1}(r) + (1-\theta) n_i(r), \quad \theta \varepsilon [0,1] \tag{4}$$

gives

$$\int_{r_j}^{r_{i+1}} [n_{i+1}(r) - n_i(r)]rdr = \Delta t_i\{[\theta Dr \frac{\partial}{\partial r} n_{i+1}(r) + (1-\theta)Dr \frac{\partial}{\partial r} n_i(r)]_{r_j}^{r_{i+1}}$$

$$+ \frac{1}{2}(r_j+r_{j+1})\Delta r_j S - Q \int_{r_j}^{r_{j+1}} [\theta n_{i+1}(r) + (1-\theta)n_i(r)]^2 rdr\} . \qquad (5)$$

As can be seen from Eq. (5), the presence of the spatial derivative doesn't allow the use of the weighted step function for the spatial interval. One of the lowest possible degree is the linear interpolation:

$$n_{i+1}(r) = \frac{1}{\Delta r_i}[(r-r_j)n_{i+1,j+1} + (r_{j+1}-r)n_{i+1,j}]. \qquad (6)$$

Substituting Eq. (6) in Eq. (5) and performing elementary integrations and some tendious arithmetic exercises, we finally get an algebraic quadratic equation for $n_{i+1,j+1}$, i.e.,

$$A_j(n_{i+1,j+1})^2 + B_{ij}n_{i+1,j+1} + C_j = 0 , \qquad (7)$$

where $A_j$, $B_{ij}$ and $C_j$ contain only parameters already known. Thus, the unknown $n_{i+1,j+1}$ can be determined directly as a positive root of Eq. (7).

Although Eqs. (2) and (3) are more complicated, the direct method algorithms can be formulated also for them by using some intuitions and following procedures similar to that explained above.

References

1) Nakahara, Y., Ise, T. Kobayashi, K., Itoh, Y.: "A Direct Method for Numerical Solution of a Class of Nonlinear Volterra Integro-Differential Equations and its Application to the Nonlinear Fission and Fusion Reactor Kinetics", JAERI-M 6351 (1975).
2) Stacey, W. M. Jr.: Nucl. Fusion, 15, 163 (1975).
3) Kampaneets, A. S.: Soviet Physics JETP, 4, 730 (1957).
4) Al'terkop, B. A.: Soviet Physics JETP, 35, 915 (1972).

*) The partial differential equations with quadratic nonlinearity are called to be semi- or quasi-linear by mathematicians.

## 8.8 Heat Transfer of Liquid Metals in a Magnetic Field

K. Sanokawa, H. Kawamura, M. Seki and Y. Shiina

### 1. Experimental study on natural convection of mercury in a magnetic field

An experiment was carried out to investigate the effect of a magnetic field on the laminer natural convection of mercury from a vertical flat plate when a field was applied parallel to a heating surface.

Figure 8.8.1 shows the temperature time traces. The heat flux is 80 - 82 $W/cm^2$. A top curve represents heater surface temperature and a bottom curve shows mercury temperature measured by the travelling thermocouple at the position 1 mm apart from the surface. The surface temperature was getting higher with increasing magnetic field. It began to oscillate when the magnetic field exceeded 0.1 Tesla.

The amplitude became maximum at 0.48 T. The temperature of the mercury showed severe oscillation by the influence of magnetic field. The amplitude reached as high as 20 K when the magnetic field was 0.25 - 0.61 T.

Figure 8.8.2 shows temperature profile obtained by the travelling thermocouple. Heat flux was 105 $W/cm^2$. The profile changed clearly with application of the magnetic field.

Figure 8.8.3 shows the relation between $Nu_x$ and $Gr_x$. The height to the center of the heating surface (1 cm) was taken for characteristic length.

$Nu_x$ was decreased with increasing magnetic field. The effect of the magnetic field was more prominent for $Gr_x \lesssim 10^8$.

### 2. Numerical analysis of natural convection in a magnetic field

The differential equations of the laminer natural convection in a rectangular cavity were analysed numerically taking into account the Lorentz force induced by the applied magnetic field.

Typical results are shown in Figs. 8.8.4 and 8.8.5.

The velocity is surpressed by the application of magnetic field and a broad stagnation region is formed in the central part of the cavity.

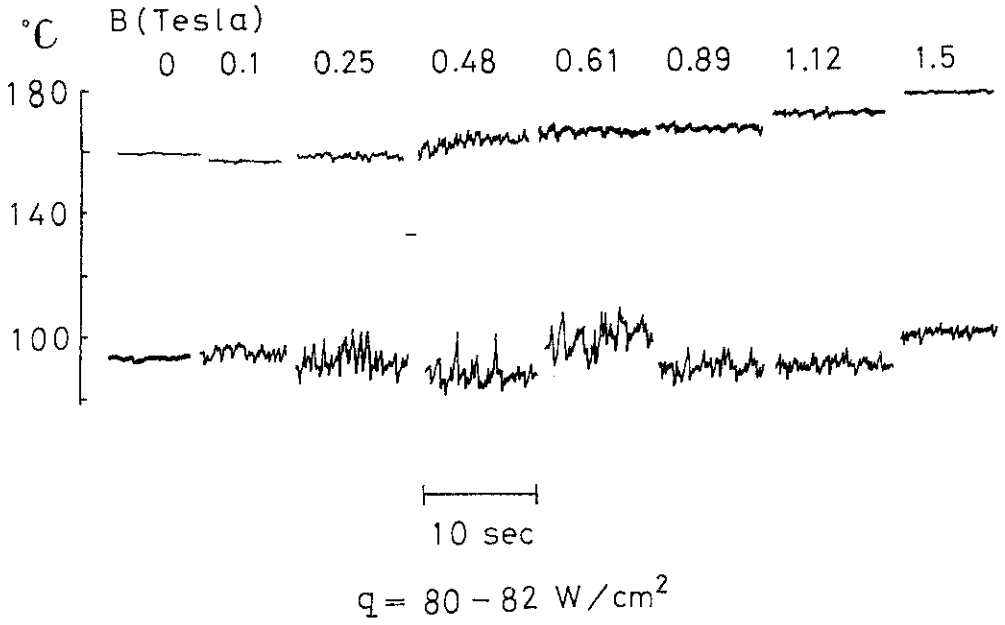


Fig.8.8.1 Effect of magnetic field strength on temperature fluctuation (Experimental).

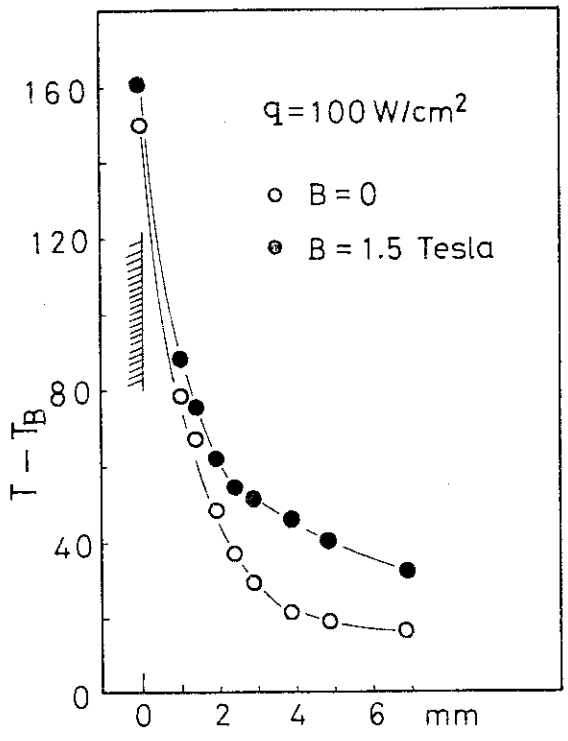


Fig.8.8.2 Temperature profile in mercury (Experimental).

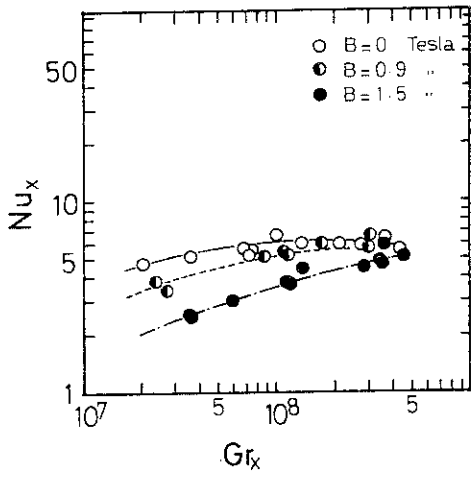


Fig.8.8.3 Effect of magnetic field strength on Nusselt number (Experimental).

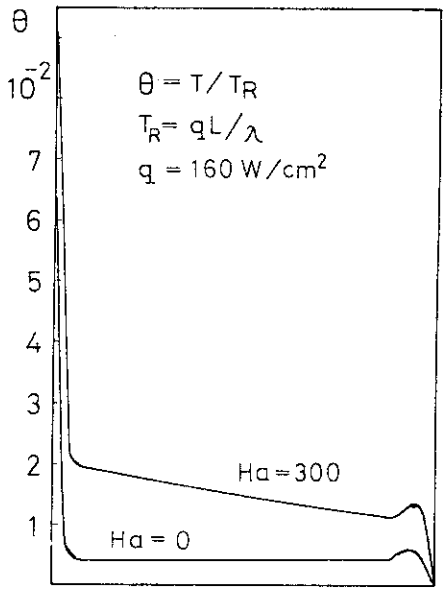


Fig.8.8.4 Effect of magnetic field strength on temperature profile in mercury (Numerical).

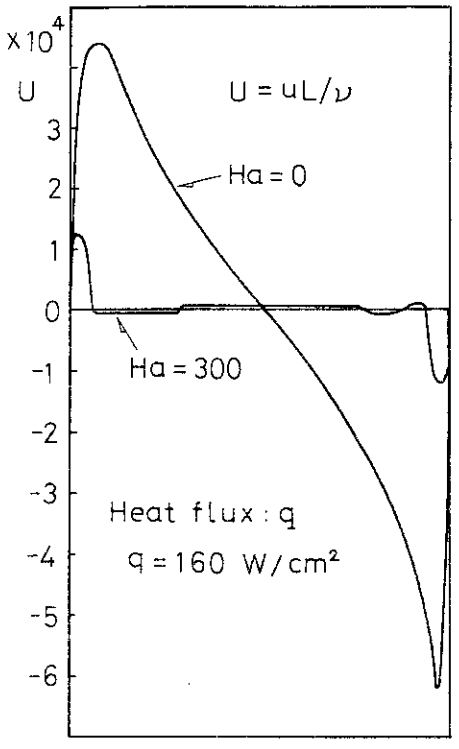


Fig.8.8.5 Effect of magnetic field strength on velocity profile in mercury (Numerical).

## 8.9 Self-Similar Analysis of Spherical Implosion Process

Y. Ishiguro and S. Katsuragi

Studies have been made for the spherical implosion process induced by laser-heated ablation by means of the self-similarity analysis[1]. Particular attention has been paid to the possibility of the existence of the self-similar solution which reproduces the implosion process revealed by hydrodynamic computer codes[2),3),4)].

The gas compression by a single shock was analysed by assuming its dynamics as a self-similar motion[5)]. A gas compression beyond the compression ratio of about 10 was shown to be impossible by a single shock, before the instant when shock wave arrives at the center of symmetry.

Investigations have been made into the possibility that a self-similar motion can reproduce the gas motion accompanied by extremely high compression. The following conclusions have been drawn:

(1) The implosion process accompanied by a sequence of the shocks can not be represented by a self-similar motion under the assumption of the uniform initial gas state and the extremely strong shock.

(2) The gas motion followed by a homogeneous isentropic compression[6)] can be reproduced by a self-similar motion with $k = 0$, $s = 0$ and $\delta = \frac{1}{2}$, in the Sedov's notation, at the final stage of compression.

Further studies will be needed for the following two cases from the standpoint of the self-similarity analysis:

(1) The first is the case where the shocks proceed in the unperturbed gas with a spatial dependence of density, $\rho \propto r^{2/\delta-2}$. This case can be proven to be a self-similar motion for the whole stage of implosion process[1)].

(2) The second is the homogeneous isentropic compression which has not completely been treated in the present study.

References

1) Ishiguro, Y., Katsuragi, S.: "Self-Similar Analysis of Spherical Implosion Process", JAERI-M 6616 (1976).
2) Goldman, E. B.: Plasma Phys., 15, 289 (1972).
3) Brueckner, K., Jorna, S.: Rev. Mod. Phys., 46, 325 (1974).
4) Mason, R. J., Morse, R. L.: Phys. Fluid, 18, 814 (1975).

5) Sedov, L. I.: "Similarity and Dimensional Method in Mechanics", Academic Press, New York (1959).

6) Kidder, R. E.: Nucl. Fusion, 14, 53 (1974) and 14, 814 (1974).

# 9. Activities of the Committee on Reactor Physics

## 9.1 Activities Related to the NEA Committee on Reactor Physics

J. Hirota

The objectives of the Committee on Reactor Physics are to review the existing state of knowledge in selected areas of reactor physics, to identify discrepancies and gaps in this knowledge and to promote the programmes of research to fill the gaps, having relation to the NEA Committee on Reactor Physics (NEACRP). During the past one year period, the Committee held the Meeting three times and continued to make efforts for the objectives.

The Committee held the 21st meeting in May 1975, mainly for making the preparation to the 18th meeting of the NEACRP. The research activities in Japan during the period from June 1974 to May 1975 were discussed preparing the review paper[1] to be presented at the 18th meeting. The items cover fast reactor physics, thermal reactor physics, fusion and shielding studies. As for the topics of the 18th meeting, an analysis of fission rate distributions in spherical lithium metal assembly with a graphite reflector and experiments on neutron streaming along void channel were reported and discussed.

The Committee held the 22nd meeting in December to discuss the highlights of the following Specialists' Meeting or Seminar recommended by the NEACRP:

(1) Specialists' Meeting on New Development in Three-Dimensional Neutron Kinetics and Review of Kinetic Benchmark Calculations (January 1975).

(2) Seminar on $^{238}U$ Resonance Capture (March 1975).

(3) Specialists' Meeting on Sensitivity Studies and Shielding Benchmarks (October 1975). Discussions were also made about the Specialists' Meeting on Control Rod Measurement Techniques: Reactivity Worth and Power Distribution (April 1976).

In March 1976, the Committee held the 23rd meeting. Preparatory discussions were made about the topics of the 19th

meeting of the NEACRP, especially reactor physics problems related to LMFBR safety. In addition, the existing state of reactor physics on transformation of actinides was reviewed. Transformation of actinides by neutron irradiation is one of the important topics which were discussed at the 18th meeting and will be moreover discussed at the near future meeting of the NEACRP.

Reference

1) Hirota, J.: "Reactor Physics Activities in Japan-Period June 1974 to May 1975", NEACRP-L-120 (Japan).

## 9.2 Activities of the Subcommittee on Thermal Reactor Physics

Y. Gotoh

The Subcommittee member consist of the representatives of universities, industries and research institutes in Japan. The main object is to promote the communication among the researchers in various groups, and their collaboration on the common objectives. The Subcommittee held the meetings quarterly. The following reports based on their work were presented and discussed.

(1) Method of solution of diffusion equation by the finite Fourier transformation.
(2) Measurement of the Doppler coefficient of fuel rod in DCA.
(3) Analysis of the Doppler coefficient of fuel rod in DCA.
(4) A code system for PWR-core analysis.
(5) Recent advance in the fuel management.
(6) Estimation of irradiation history of spent fuel by Gamma-ray spectroscopy.
(7) Burnup analysis of JPDR.
(8) Measurement of multiple control rods reactivity worth in semi-homogeneous critical assembly.
(9) Normalizing method of relative power in multi-regional core.

Concerning the fuel management, the code OPROD of HITACHI has been successfully operated for the control rod programming. The three-dimensional nuclear and thermo-hydraulic calculation code FLORA was developed. By using this code, the power distribution and the Burnup of JPDR were estimated, and compared with the data of Gamma scanning and of the Burnup measured by the destructive test. The measurement of fuel temperature coefficient in DCA was performed heating the central channel of the lattice by the hot helium-gas circulation. The heat loss through the surface of the central channel was estimated empirically.

## 9.3 Activities of the Subcommittee on Fast Reactor Physics

H. kuroi

The Subcommittee on Fast Reactor Physics held the 29th, 30th and 31st meeting during this period. The following topics were reported and discussed at these meetings:

(1) Discussion on sodium void coefficient, fission neutron spectrum and heterogeneous core concept relating to the topics of the 18th meeting of the NEACRP.

(2) Analysis of the measured sodium void coefficient in MOZART program.

(3) Reactivity insertion due to accidental core sodium voiding and related phenomena.

(4) Reactivity measurement in a far-subcritical fast system.

The following conclusions were obtained:

(1) Present accuracy in the prediction of sodium void coefficient is made clear and a further investigation of streaming effect is requested.

(2) Systematic discrepancy existed between far-subcriticalities measured by two different methods, statical and dynamical, is disappeared by introducing the detector efficiency.

(3) Reviewing the reports presented at the 18th meeting of the NEACRP, recent trends and problems in fast reactor physics have been summarized.

Publication List

1. Nuclear Data and Group Constants

(1) Takano, H., Ogawa, S.: "ARCFIT-1, -2 and -3: Codes for Revision of Group Constants for Heavy Nuclei of JAERI-Fast Set", JAERI-M 6372 (1976) (in Japanese)

(2) Kikuchi, Y.: "STAT, a Code for Analysis of Statistical Properties of Averaged Resonance Cross Sections", JAERI-M 6248 (1975) (in Japanese)

(3) Igarasi, S., Iijima, S., Kawai, M., Nakagawa, T., Kikuchi, Y., Maki, K., Matsunobu, S.: "Evaluation of Fission Product Nuclear Data for 28 Important Nuclides", Nuclear Cross Sections and Technology, Proceedings of a Conference, Washington, D.C., March 3 - 7, 1975, p. 320 (1975)

(4) Tasaka, K.: "Build-up and Decay of Fuel Actinides in the Fuel Cycle of Nuclear Reactors", JAERI-M 6541 (1976)

(5) Kim, J.D., Koyama, K., Kuroi, H.: "25-Group Constants of Tritium", JAERI-M 6494 (1975)

(6) Kuroi, H., Mitani, H.: "Adjustment to Cross Section Data to fit Integral Experiments by Least Squares Method", J. Nucl. Sci. Technol., 12 [11], 663 (1975)

2. Theoretical Method and Code Development

(1) Ise, T., Inabe, T., Nakahara, Y.: "Reactor Physics Characteristics of the NSRR", J. Atomic Energ. Soc. Japan, 17, 44 (1975) (in Japanese)

(2) Nishida, T., Horikami, K., Suzuki, T., Nakahara, Y., Taji, Y., Asaoka, T.: "Modification of the MORSE Code for Monte Carlo Eigenvalue Problems by Coarse Mesh Rebalance Acceleration", JAERI-M 6251 (1975)

(3) Ise, T., Horikami, K., Kobayashi, K.: "Present Status on Algorithms and Benchmark Tests for Numerical Solution of the Time-Dependent Neutron Transport Equation", JAERI-M 6373 (1975) (in Japanese)

(4) Ise, T., Inabe, T.: "Pulsed Thermal Reactor (Mainly on NSRR)", Report of Research Committee on Pile Neutron Technology, Atomic Energ. Soc. Japan, p. 116 (1976) (in Japanese)

(5) Ise, T.: "GURNET-2, Perturbation Theory Code in One-Dimensional Diffusion Approximation", JAERI-M 6491 (1976)

(6) Asaoka, T., Nakahara, Y., Horikami, K., Nishida, T., Suzuki, T., Taji, Y., Miyasaka, S., Hirota, J.: "Application of Coarse Mesh Rebalance Acceleration to Monte Carlo Eigenvalue Problems", Nucl. Sci. Eng., 59, 326 (1976)

(7) Nakahara, Y., Ise, T., Kobayashi, K., Itoh, Y.: "A Direct Method for Numerical Solution of a Class of Nonlinear Volterra Integro-Differential Equations and its Applications to the Nonlinear Fission and Fusion Reactor Kinetics", JAERI-M 6351 (1975)

(8) Asaoka, T., Watanabe, N.: "An Optimization Study of Peak Thermal Neutron Flux in Moderators of Advanced Repetitive Pulse Reactors", US/Japan Seminar on Fast Pulse Reactors, Tokai (1976)

(9) Ise, T., Nishida, T. Suzuki, T.: "Recent Computer Programs for Least-Squares Problems", J. Atomic Energ. Soc. Japan, 18, 33 (1976) (in Japanese)

(10) Suzuki, T.: "On I/O of the Optimization Code BESOM Based on the Hoffman Model", Report of Research Committee on Nucl. Power Systems, Atomic Energ. Soc. Japan (1976) (in Japanese)

(11) Kuroi, H., Tone, T.: "SP-2000; Program for Calculating Fine Group Neutron Spectrum in Multi-region Cell and Effective Broad Group Constants", JAERI-1240 (1975)

(12) Kuroi, H., Nakamura, Y., Onuma, Y., Koyama, K., Tone, T., Hirota, J.: "ARCADIA; A Comprehensive Semi-automated System for Cross Section Evaluation Utilizing Integral Measurements", JAERI-1241 (1975)

(13) Tasaka, K.: "Estimation of Irradiation History of a Spent Fuel by Gamma-Ray Spectroscopy", Nuclear Technology, 29, 239 (1976)

(14) Suzuki, T.: "Improvement of Coarse Mesh Difference Diffusion Scheme about Control Rod", J. Nucl. Sci. Technol. 12, 695 (1975)

(15) Kikuchi, Y., Katsuragi, S., Ogitsu, M., Suzuki, T.: "EXPANDA-75, One-Dimensional Diffusion Code for Multi-Region Plate Lattice Heterogeneous System", JAERI-1239 (1975)

(16) Gotoh, Y.: "Review of International Solutions to NEACRP Benchmark BWR Lattices Cell Problems", AEEW-R 1052 (1975)

3. Integral Experiment and Analysis

(1) Kaneko, Y., Akino, F., Yasuda, H., Kurokawa, R., Kitadate, K., Takeuchi, M.: "Measurement of Multiple Control Rods Reactivity Worths in Semi-Homogeneous Critical Assembly", Document for Specialist Meeting of NEACRP (1976)

(2) Kaneko, Y.: "Progress in Research of Reactor Neutron Spectra", J. Atomic Energy Society of Japan, 18, 77 (1976) (in Japanese)

(3) Nakano, M., et al.: "Reactivity Measurement in a Far-Subcritical Fast System (III), Source Jerk Method", JAERI-M 6496 (1976) (in Japanese)

(4) Nakano, M.: "A Method for Estimating Multiple-rod Worth by Single-rod Experiment", JAERI-M 6504 (in Japanese)

(5) Mitani, H.: "A New Experimental Method of Estimating Physics Parameters in Large Fast Reactors", J. Nucl. Sci. Technol., 13 [2], 58 (1976)

4. Shielding

(1) Furuta, Y., Sasamoto, N., Tanaka, S.: "Preliminary Studies of Neutron Benchmark Experiments for One-dimensional Transport Calculation with an Iron Sphere", Presented for Specialist Meeting on Sensitivity Studies and Shielding Benchmarks, Paris, Oct. 7 - 10 (1975)

(2) Tanaka, S., Takeuchi, K.: "Neutron Energy-dependent Kerma Factors for Nuclides", JAERI-M 6348 (1975)

5. Heat Transfer and Fluid Dynamics

(1) Hishida, M., Okamoto, Y.: "Enhanced Heat Transfer of Fuels at Low Reynolds Number", Trans ANS, 20, 756 (1975)

(2) Kawamura, H.: "Transient Heat Transfer in Turbulent Flow with Time-dependent Heat Input", Proc. US/Japan Seminar on Fast Pulse Reactors, V1 - 6, 383 (1976)

(3) Kawamura, H.: "Transient Hydraulics and Heat Transfer in a Turbulent Flow", KFK-2166, (1975)

6. Reactor and Nuclear Instrumentation

(1) Ara, K., Brakas, M.J.: "Inverse Magnetostrictive Sensitivity of Martensitic Stainless Steel AISI-410 and Its Application

to Pressure Measurements", IEEE Trans. on Magnetics, Mag-11, 1352 (1975)

(2) Ara, K., Yamada, M.: "Fuel Elongation Detectors for NSRR High-Temperature Water Capsule —— Prototype Differential Transformer and the Tests", JAERI-M 6352, (1975)

(3) Sakai, E., Terada, H., Katagiri, M.: "In-Situ Gamma-Ray Measurement Using Ge(Li) Detectors", IEEE Trans., NS-23(1), 726-733 (1976)

(4) Sakai, E., Katagiri, M., Itoh, H.: "Sodium In-Pile Loop Experiment on Delayed Neutron Detector-, Precipitator-, and Cover-Gas Gamma-Ray Spectrometer-Type Fuel Failure Detection Systems", IEEE Trans., NS-23(1), 363-374 (1976)

(5) Sakai, E.: "New Semiconductor Radiation Detector -$HgI_2$-", Hoshasen (Ionizing Radiation), 3(1), 15-25 (1976) (in Japanese)

(6) Shizuma, K., Sakai, E., Katagiri, M.: "Pulse Height Dependence on Source Position in Ge(Li) Gamma-Ray Detectors", JAERI-M 6497 (1976) (in Japanese)

(7) Sakai, E., Terada, H., Katagiri, M.: "In-Situ Measurement of the Environmental Gamma-Rays by Portable Ge(Li) Detectors", JAERI-M 6498 (1976) (in Japanese)

(8) Sakai, E.: "Present Status of Semiconductor Gamma-Ray Detectors", KURRI-TR 142, 8-9 (1976) (in Japanese)

(9) Sakai, E.: "Temperature Cycling Test of a Planar Hyper-Pure Germanium Radiation Detector", KURRI-TR 142, 10-12 (1976) (in Japanese)

(10) Katagiri, M.: "Data Analyzing Program for ND-50/50 Multichannel Pulse Height Analyzer", KURRI-TR 142, 23-24 (1976) (in Japanese)

(11) Takeuchi, N., Yagi, H., Gotoh, H.: "An ORACL Program File for Acquisition, Storage and Analysis of Data in Radiation Measurement and in Non-Destructive Measurement of Nuclear Material", JAERI-M 6499 (1976) (in Japanese)

(12) Tanaka, S., Takeuchi, K., Furuta, Y.: "Application of Thermoluminescence Dosimeters for Nuclear Heating Measurements of Gamma Rays and Neutrons", Presented for First ASTEM-Euratom Symposium on Reactor Dosimetry, Petten, Sept. 22 - 26 (1975)

(13) Tanaka, S., Furuta, Y.: "Usage of a Thermoluminescence Dosimeter as a Thermal Neutron Detector with High Sensitivity", Nucl. Instr. and Meth., 133, 495 (1976)
(14) Sasamoto, N.: "An Interpolation Method for the Response Function of Radiations Obtained by Proton Recoil Type Scintillators", JAERI-M 6536 (1976)
(15) Tasaka, K.: "Analysis of Gamma-Ray Spectrum by using a Standard Spectrum", JAERI-M 6145 (1975)
(16) Shirakata, K., Cho, M., Iijima, T.: "Development of a Double Scintillator Spectrometer", JAERI-M 6492 (1976)
(17) Ichimori, T., Obu, M., Shirakata, K.: "A High-Resolution Cylindrical Proportional Counter for Neutron Spectrum Measurements in a Fast Critical Assembly", Nucl. Inst. Method, 127, 571 (1975)

7. Dynamics Analysis and Control Method Development

(1) Mankin, S., Shinohara, Y.: "Application of Linear Optimal Regulator Technique to Control of a Nuclear Reactor Plant", J. Nucl. Sci. Technol., 12 [12], (1975)
(2) Oguma, R., et al.: "Computer Code MLCOSP for Multiple-Correlation and Spectrum Analysis with a Hybrid Computer", JAERI-M 6252 (1975)
(3) Kudo, K., Usui, H., Hara, M.: "Hybrid Computation of Basic Math Model of Heat Exchanger", JAERI-M to be published (in Japanese)
(4) Mankin, S., Fujii, Y., Hara, M.: "On the Application of Linear Optimal Technique to Control of Nuclear Power Plant", J. Atomic Energ. Soc. Japan, 17, 12 (1975) (in Japanese)

8. Fusion Reactor Technology

(1) Seki, Y., Maekawa, H.: "Analysis of Fission Ratio Distribution in Spherical Lithium Metal Assembly with a Graphite Reflector", JAERI-M 6220 (1975) (NEACRP-L-136)
(2) Maekawa, H., Seki, Y.: "Uranium-238 to Uranium-235 Fission-Ratio Distribution in Spherical Lithium-Metal Assemblies With and Without a Graphite Reflector", Nucl. Sci. Eng., 57, 253 (1975)

(3) Maekawa, H., Seki, Y.: "Preliminary Results of Integral Experiment on Fusion-Fission Hybrid Blanket Assemblies", JAERI-M 6495 (1976) (NEACRP-A-244)

(4) Kambayashi, Y., Hara, M.: "A Kinetics Model for the Horizontal Displacement of a Toroidal Plasma Column", JAERI-M 6292 (1975)

(5) Kambayashi, Y.: "Frequency Characteristics of the Horizontal Motion of a JT-60 Plasma Column", JAERI-M 6508 (1976)

(6) Fujisawa, T.: "Energy Transfer Rate of a Charged Particle as a Function of Injection Angle", Nuclear Fusion 16, 2 (1976), JAERI-M 6384 (1976)

(7) Suzuki, T., Taji, Y., Nakahara, Y.: "Macroscopic Cross Sections for Analyzing the Transport of Neutral Particles in Plasmas", JAERI-M 6119 (1975)

(8) Kawamura, H., Seki, M., Shiina, Y., Sanokawa, K.: "Experimental Studies on Heat Transfer by Natural Convection and Pool Boiling of Sodium in a Strong Magnetic Field", J. Nucl. Sci. Technol., 12, 280 (1975)

9. Activities of the Committee on Reactor Physics

(1) Hirota, J.: "Reactor Physics Activities in Japan —— Period June 1974 to May 1975", NEACRP-L-120 (1975)